MCR-79-1369
Contract 83-3638

SAND 80-8175

Final Report December 1979

Internally Insulated Thermal Storage System Development Program

MARTIN MARIETTA

Badger

Printed in the United States of America
Available from
National Technical Information Service
U. S. Department of Commerce
5285 Port Royal Road
Springfield, VA 22161
Price: Printed Copy $6.00 ; Microfiche $3.00

MCR-79-1369
Contract 83-3638

December 1979

FINAL REPORT

INTERNALLY INSULATED THERMAL STORAGE SYSTEM DEVELOPMENT PROGRAM

Work performed under contract to
Sandia Laboratories
Livermore, California 94550

Martin Marietta Aerospace
Denver Division
P.O. Box 179
Denver, Colorado 80201

FOREWORD

This report is submitted by Martin Marietta Aerospace, Denver Division, in accordance with Sandia Contract 83-3638. This satisfies the contractual requirement of the final report. A separate report will be issued on the salt safety evaluation. Acknowledgements are given to the manufacturers of products tested as they freely gave their products. Pittsburg Corning supplied and installed the Foamsil-12 in the thermal conductivity fixture and also evaluated their product after salt exposure. Kaiser Refractories spent a large amount of time and effort evaluating their material and their results greatly added to the confidence of the material test program.

TABLE OF CONTENTS

TABLE OF CONTENTS (continued)

FIGURES

FIGURES (continued)

FIGURES (continued)

TABLES

INTRODUCTION

Studies prior to this one have indicated that internally insulated molten salt storage tanks are more cost effective than externally insulated tanks for high-temperature applications. The internal insulation can either be wet with the molten salt or kept dry by using a sealed liner. Martin Marietta's *Advanced Central Receiver Power System, Phase I* final report (EG-77-C-03-1724) described a molten salt thermal storage system using wet internal insulation. This system has an estimated cost of storage of $8.20/kWhe. Another concept, offered as an alternative to the recommended system, used externally insulated stainless steel tanks and employed no new technology. Its cost of storage is $19.40/kWhe.

The biggest cost savings associated with internally insulated tanks is that they do not have to be constructed of stainless steel. Placing insulation on the inside of the tanks can reduce the temperature of the tank shell and permit the use of carbon steel. Since steel is stronger at lower temperatures, the tank walls can be thinner, eliminating postweld heat treatment. In a thermocline or cascade storage tank where the tank shell temperature is cycled daily, internal insulation also reduces the temperature excursions of the shell reducing the stress and fatiguing of the tank structure.

The purpose of this program was to define a cost effective thermal storage system for a solar central receiver power system using molten salt stored in internally insulated carbon steel tanks. The program was divided into six tasks--testing of internal insulation materials in molten salt; preliminary design of storage tanks, including insulation and liner installation; thermal analysis of internally insulated thermocline tanks; optimization of the storage configuration; and definition of a subsystem research experiment to demonstrate the system.

The sixth task, a safety study, is a document separate from this report that addresses the safety considerations of using molten salt. It is being evaluated by two utility companies and will include their responses when published.

II. EXECUTIVE SUMMARY AND CONCLUSIONS

The primary objective of this program is to define a cost effective thermal storage system for a solar central receiver power system using molten salt stored in internally insulated carbon steel tanks. This effort was divided into five tasks. The scope of these tasks were:

1) Task 1, internal insulation materials test program - Screening tests of candidate insulation materials were conducted by exposing them in 866 K (1100°F) molten salt for 500 hours. Materials selected from these tests were exposed to 866 K salt for up to 5000 hours. During this time the materials were examined and the salt chemistry determined. Other tests of the materials included temperature cycling, thermal conductivity, and mechanical wear tests;

2) Task 2, internally insulated thermocline storage tank analysis - A computer thermal model of internally insulated thermocline tanks was developed to predict thermocline behavior under various operational strategies. A thermocline tank is one that stores both hot and cold fluid in the same tank and relies on the temperature-dependent fluid density difference to prevent fluid mixing. The analytical model accounts for conduction, fluid circulation, and the effect of side wall heat capacity;

3) Task 3, storage tank design - A preliminary design study and optimization was made of both an externally insulated carbon steel tank for 561 K (550°F) molten salt and an internally/externally insulated carbon steel tank for 839 K (1050°F) molten salt. The study considered the constraints of the API and ASME Section VIII codes and included both the cylindrical and spherical tanks. Design of the tank foundation, insulation installation, and the internal liner were also examined. Costs were derived for the tanks as a function of size and geometry;

4) Task 4, storage system parametric analyses - A computer cost optimization was performed to find the optimum configuration for each of three different storage concepts--thermocline, dual-tank, and cascade systems. The analyses were done as a function of storage size and considered the following factors: tank geometry; number of tanks; insulation type, thickness, and cost; storage use rate; heat loss rate and its impact on upstream costs (heliostats, etc.); and others;

5) Task 5, storage subsystem research experiment (SRE) - Based on the conclusions of Tasks 1 through 4, a subsystem research experiment was proposed that would demonstrate both fabrication and performance of the major components of the recommended storage design. The price to perform the SRE was estimated and a schedule proposed.

A sixth task, a salt safety study, was also conducted and will be published as a separate report. The study addresses safety hazards, precautions, and procedures that should be considered in operating a salt central receiver solar system. It addresses both solid and molten salt mixtures. Extensive data were gathered through both a literature search and personal contact with industrial producers and users of salt. The safety report is being evaluated by two utilities and will include their responses when the report is published.

The material compatibility tests showed that all of the materials tested were attacked and are therefore unacceptable as internal tank insulation when in contact with the molten salt. Since a wide range of material types were tested, it is not likely that any currently available commercial insulation material will be compatible with the molten salt. Because internal insulation is extremely advantageous in reducing tank shell cost, a sealed metal liner is recommended to protect the internal insulation from the molten salt. It is also cost effective to use a liner because the thermal conductivity of dry insulation is much less than that of insulation wetted with salt. A thermal expansion liner made by Technigaz is recommended because of its unique design and exceptional reliability. It has been used extensively for about 15 years to line liquid natural gas tanks in ships such as the one shown in Figure 2-1. The stainless steel liner is orthogonally folded to allow for expansion due to pressure and thermal loads. The expansion folds can be seen in the foreground of the picture. The Technigaz liner has also been used in land-based and high-temperature applications. Technigaz is of several companies to have developed an internal liner for liquid natural gas tanks.

The computer analysis of the thermocline tank was a one-dimensional model that accounted for fluid circulation within the bulk fluid. The model was used to analyze a current French thermocline test for which empirical data were available. Temperature profiles from the model and the data were then compared to ensure that the analytical model was correct and to determine the amount of fluid circulation that should be used (this was a variable parameter in the program). It was found that the thickness of the transition zone between the hot and cold fluids was 2.6 m (8.6 ft) for a tank 40.4 m (132.5 ft) in diameter and 12.8 m (42.0 ft) high. This thickness increased with small tanks, large heat losses, and large heat capacity of the tank walls and insulation. Because of this, it is very difficult to scale thermocline tanks. The best way to limit the transition zone thickness is to outflow some of its fluid during charge and discharge.

Preliminary designs and cost estimates for both the cylindrical and spherical tanks were provided by Chicago Bridge and Iron (Boston). Both designs assumed a maximum soil bearing strength of 5000 psf and a maximum shell temperature of 588 K (600°F). The cylindrical tanks were designed to the API 650 code, and the spherical tanks were

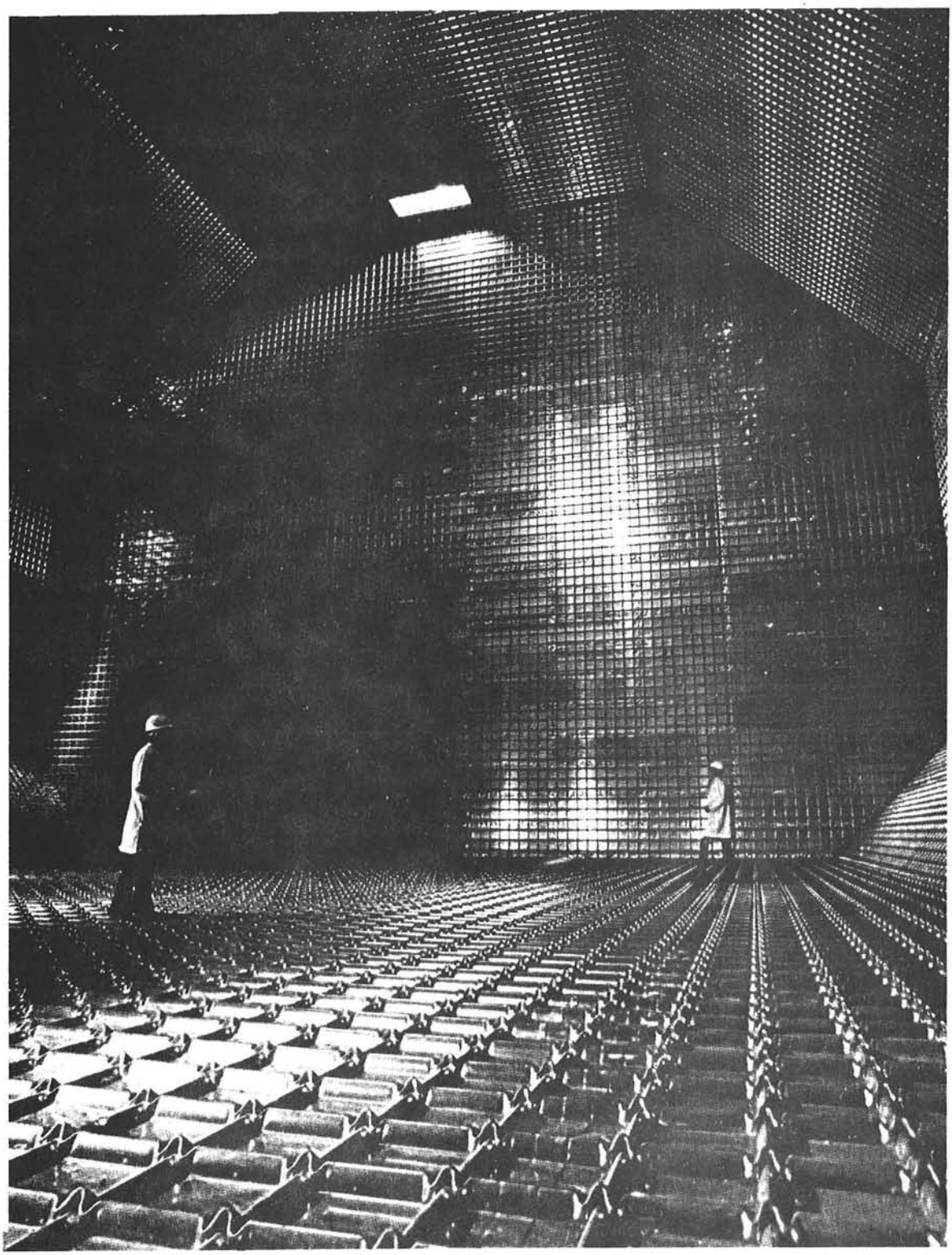

Figure 2-1 Technigaz Liner in Liquid Natural Gas Tanker

designed to the ASME Section VIII code, since this was the most applicable standard. The preliminary tank designs are shown in Figures 2-2 and 2-3.

Cost estimates for the tank shell, foundation, and insulation showed cylindrical tanks configurations to be less expensive than spherical tank configurations of the same volume.

The tank foundation design for the recommended cylindrical tank is a water-cooled concrete slab. This prevents the underlying soil from reaching the boiling point of water and eliminates the need for a stainless steel tank bottom. Placing the tank directly on the ground (whether insulated or not) would cause both the tank bottom and the ground to heat up gradually to the temperature of the molten salt. This is not recommended because very little is known about soil properties at elevated temperatures and boiling water trapped in the soil can produce unpredictable results.

Tanks storing hot salt [839 K (1050°F)] are internally insulated with a lightweight refractory brick on the sides and bottom and a fibrous insulation on the ceiling. This insulation is separated from the salt by the sealed steel liner. Cold salt tanks [561 K (550°F)] are not internally insulated. Both the hot and cold tanks are externally insulated with fibrous insulation on the sides and board insulation on the top, and are covered with aluminum jacketing for weather protection.

The three storage concepts studied in the storage system parametric analysis were the thermocline, dual-tank, and cascade systems (Fig. 2-4, 2-5, and 2-6). The thermocline system stores both the hot and cold fluids in the same tank and relies on the temperature-dependent fluid density difference to prevent fluid mixing. In the dual-tank system, the hot and cold fluid are stored in separate tanks. The cascade system is similar to a dual-tank system except that some of the tanks can be used interchangeably as either hot or cold tanks to reduce the total number of tanks.

The computer cost analysis of the various storage system parameters (insulation thickness, number of tanks, tank geometry, etc.) showed that (1) the most cost effective configuration has the fewest number of the largest practical cylindrical tanks, and (2) the optimum configuration is set by the mechanical constraints of the system, e.g., the maximum soil bearing strength and tank hoop stress, and not by the economics. Figure 2-7 shows a cost comparison of the three storage concepts for three representative storage sizes. Capital cost refers to the cost of the system components, while effective cost is the capital cost plus the compensation cost (i.e., the cost of the extra heliostats, etc., necessary to compensate for the storage system's energy losses). The cost of a drain tank is included in the thermocline systems.

DESIGN: ATMOSPHERIC PRESSURE
SHELL DESIGN TEMPERATURE: 589 K (600°F)
MATERIAL: SA-516, GR. 70
CORROSION ALLOWANCE: .003m (.125 in.)
CODE: API-650 CONSTRUCTION, NO STAMP.
MAX. SPECIFIC GRAVITY (COLD) 1.907
EARTHQUAKE: ZONE 3
X-RAY INSPECTION AS REQUIRED
STRESS RELIEVING: NOT REQUIRED

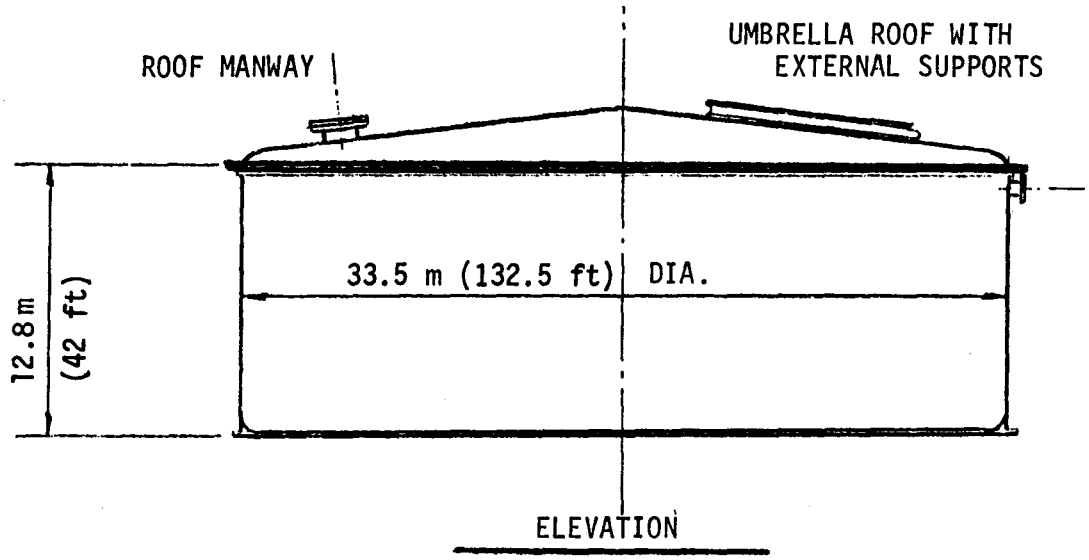

Figure 2-2 Cylindrical Tank Design

DESIGN: ATMOSPHERIC PRESSURE
SHELL DESIGN TEMPERATURE: 316 K (600°F)
MATERIAL: SA-516 GR. 70
CORROSION ALLOWANCE: 0.0 m
CODE: ASME SECTION VIII
MAX. SPECIFIC GRAVITY: 1.907
EARTHQUAKE: ZONE 3
STRESS RELIEVE: AS REQUIRED

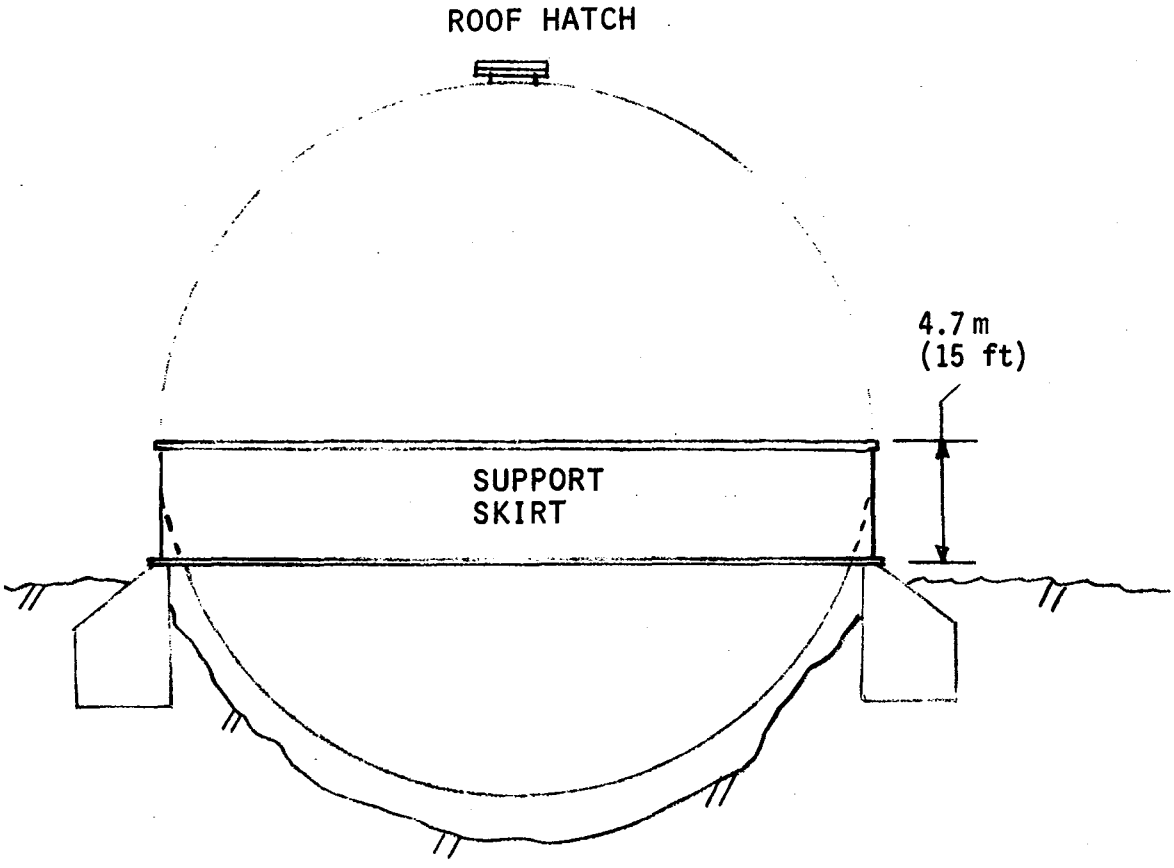

Figure 2-3 Spherical Tank Design

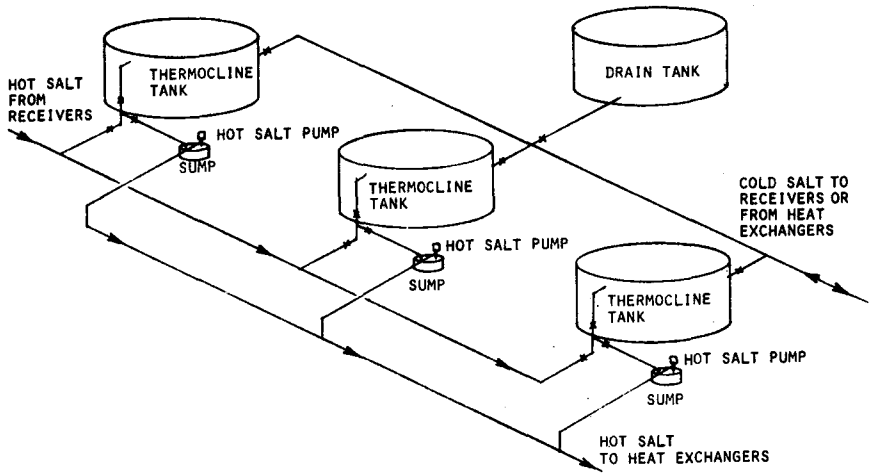

Figure 2-4 Thermocline Storage System Schematic

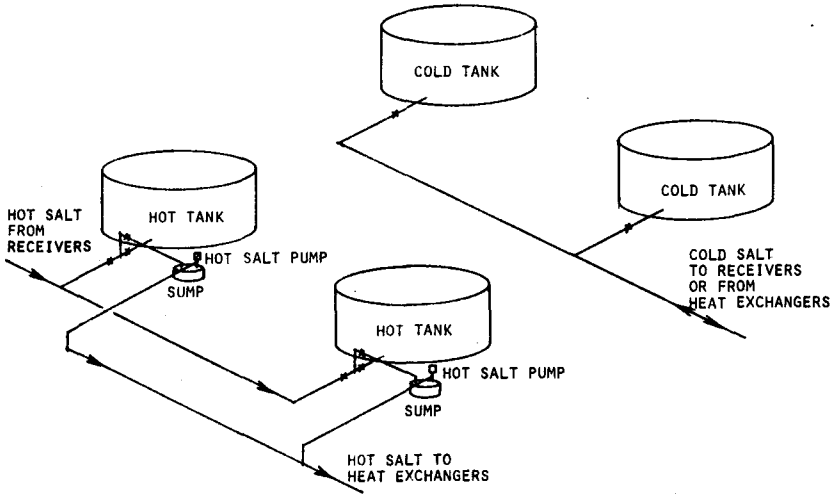

Figure 2-5 Dual Tank Storage System Schematic

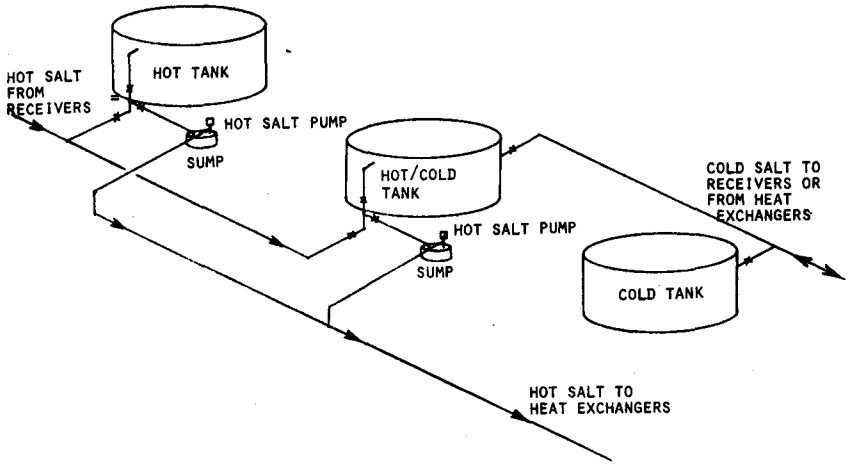

Figure 2-6 Cascade Storage System Schematic

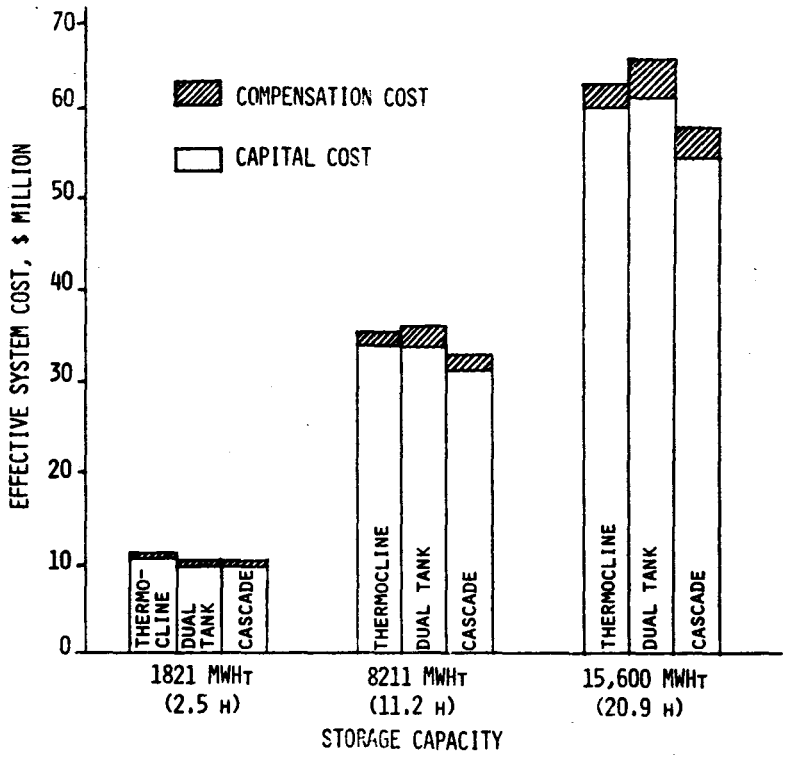

Figure 2-7 Effective Storage System Cost Vs Storage Size (300 MWe Plant)

Figure 2-8 shows the cost of storage for storage systems other than molten salt when coupled to their respective solar central receiver plants. It also shows the costs of molten salt storage for both internally and externally insulated tanks. (Storage costs for the nonmolten salt systems were taken from a storage system comparison done by Sandia Labs, Livermore.) It is important to note that this is a comparison of costs of storage for storage system/central receiver combinations that have been investigated in considerable detail. Although other combinations are possible, only those shown were available for comparison.

For small storage capacities where one tank can hold the entire quantity of salt (<2000 MWht), the dual-tank system is preferred because of its lower cost (Fig. 2-7). For larger storage capacities (about 8000 to 16,000 MWht), the dual-tank system is still recommended despite its greater cost. Refractories such as those used for internal insulation are typically brittle and have low conductivity. Cascade and thermocline tanks are temperature-cycled daily and this cycling induces stresses that can break up the refractory insulation. Industry tries to avoid thermal cycling of refractories whenever possible. Though it is difficult to quantify the technical risk, the cost of repairing the internal insulation would certainly more than offset the cost advantage of either of these two systems.

As Figure 2-8 shows, the greatest cost reduction for the least technical risk is made by switching from externally to internally insulated tanks. Using a cascade system instead of a dual-tank system yields only an additional 5% reduction in cost of storage at significantly greater technical risk. It is therefore not recommended.

The selected SRE design (shown schematically in Figure 2-9) is capable of demonstrating both the fabrication techniques and the operational characteristics of a full-scale storage system. It is a dual-tank system consisting of one hot (internally insulated and lined) tank and one cold (externally insulated) tank. Both tanks are 4.6 m (15 ft) in diameter and 4.6 m (15 ft) high and can simulate inflow and outflow of the molten salt. A heater and cooler are required to change the molten salt temperature between the tanks.

A schedule for the SRE is shown in Figure 2-10. The entire program, including a one-month initial test period, is completed in 13 months. Because this is such an ambitious program, procurement of such critical long-lead items as the cooler, liner material, valves, and pumps will have to be done very early. It is recommended that further testing be conducted beyond the initial one-month test.

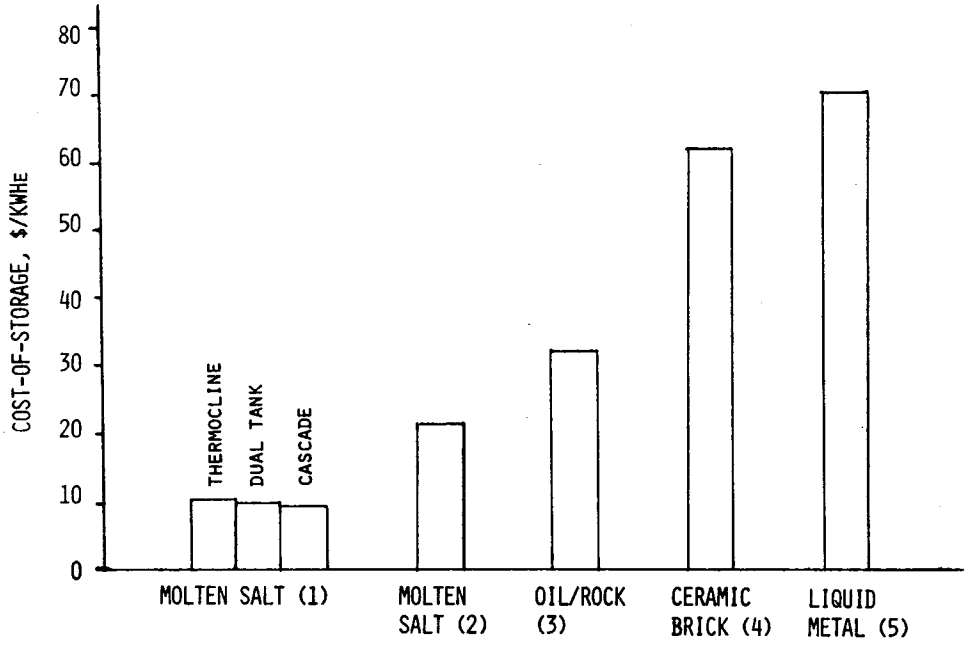

(1) MOLTEN SALT RECEIVER, 300 MWE PLANT, 11 HOURS STORAGE, INTERNALLY INSULATED TANKS
(2) MOLTEN SALT RECEIVER, 300 MWE PLANT, 11 HOURS STORAGE, EXTERNALLY INSULATED DUAL TANKS
(3) WATER/STEAM RECEIVER, 100 MWE PLANT, 6 HOURS STORAGE
(4) GAS COOLED RECEIVER, 100 MWE PLANT, 3 HOURS STORAGE, WELDED STEEL TANKS
(5) LIQUID METAL RECEIVER, 100 MWE PLANT, 3 HOURS STORAGE, EXTERNALLY INSULATED DUAL TANKS

STORAGE COSTS FOR (3), (4), AND (5) WERE SUPPLIED BY SANDIA LABORATORIES, LIVERMORE, FROM A STORAGE SYSTEM COST COMPARISON OF PROPOSED STORAGE SYSTEM/CENTRAL RECEIVER COMBINATIONS.

Figure 2-8 Cost of Storage for Various Storage Systems

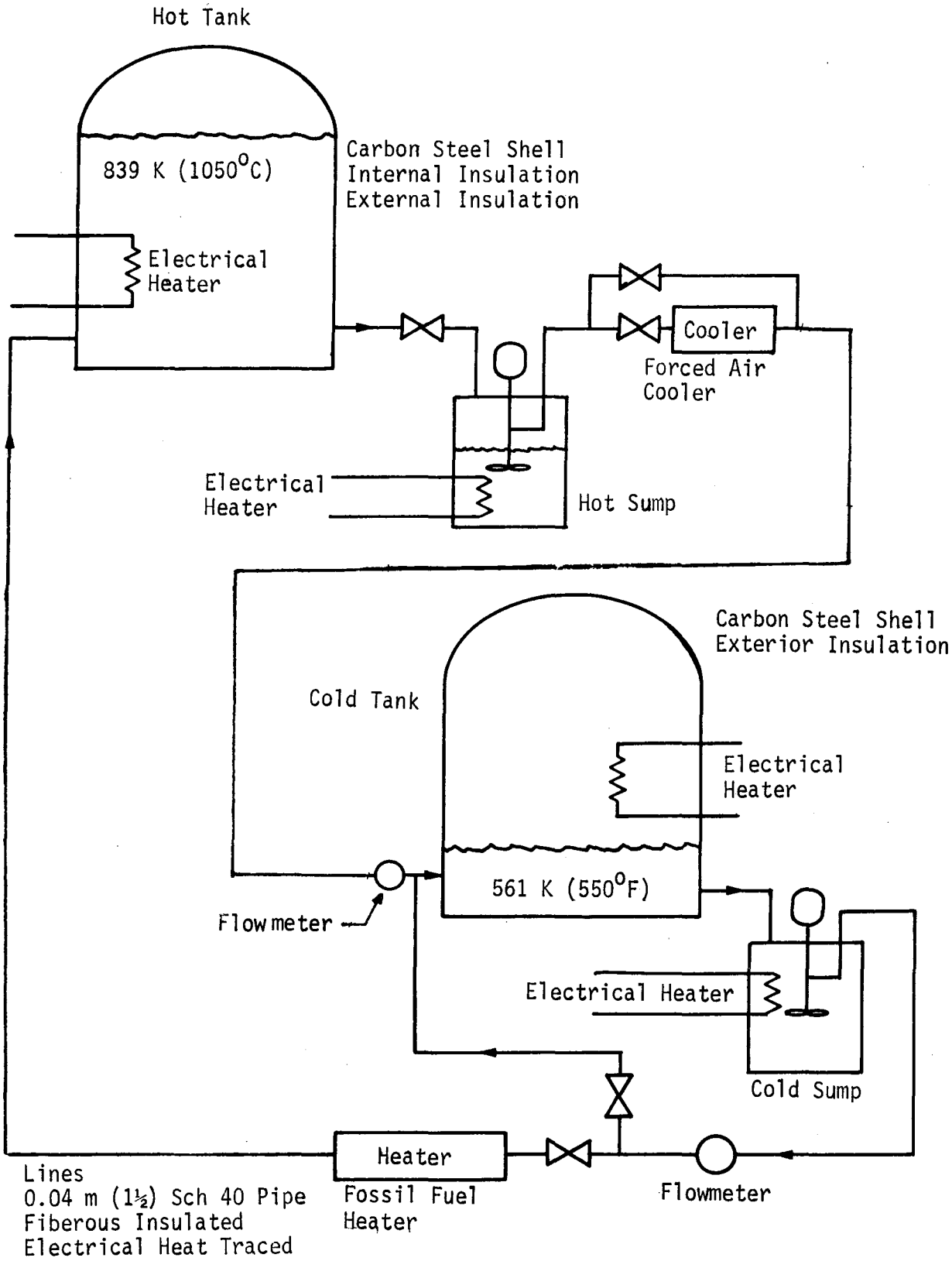

Figure 2-9 SRE Test Schematic

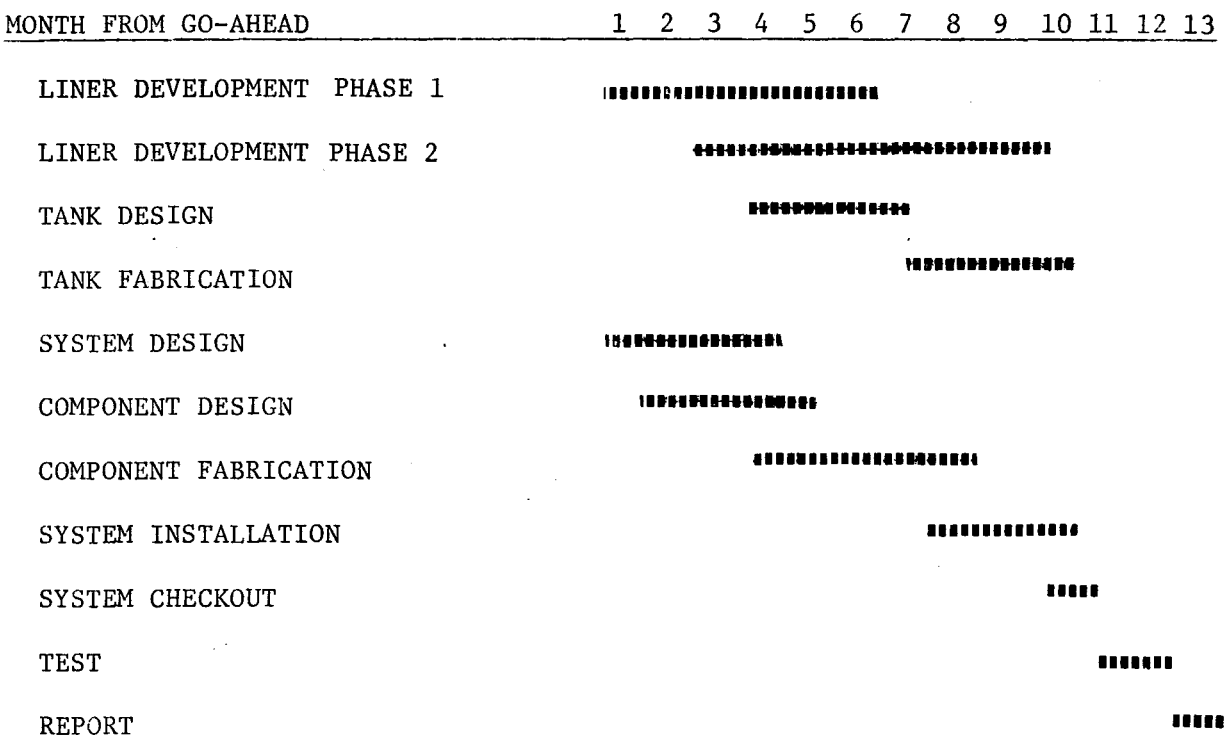

FIGURE 2-10 SRE PROGRAM SCHEDULE

III. MATERIAL TESTS

A. PURPOSE

The purpose of the material test program was to determine an insulation material compatible with the molten salt that could be used to insulate the storage tank wall from the hot draw salt 839 K (1050°F) . Previous studies had shown that the cost of a stainless steel tank at this temperature was much more expensive than an internally insulated carbon steel tank. The criteria for selecting the insulating material were:

1) Chemical compatibility with molten salt;
2) Mechanical compatibility with molten salt (both load bearing and temperature);
3) Ability to withstand thermal cycles and freeze-thaw cycles;
4) Ability to allow for thermal growth of tank walls;
5) Low thermal conductivity;
6) Low weight;
7) Low cost;
8) Ease of installation.

The design life of the tank system is 30 years at 839 K (1050°F).

B. MATERIAL COMPATIBILITY

1. Previous Test History

Previous programs and testing at Martin Marietta had limited the available candidates. The temperature requirement limited the materials to refractories. Table 3-1 lists the results of the previous tests. These tests were limited to visual observation and were not evaluated chemically or microscopically. The testing resulted in the candidate material charging from a lightweight ceramic fiber blanket to brick material. Ceramic fiber blankets were found to be mechanically unstable in molten salt and also allowed fluid convection to occur within the fibers thus creating a high effective thermal conductivity. The investigation of board materials showed that they mechanically broke apart in freeze-thaw cycles. Many castable materials were chemically attacked or broken during freeze-thaw cycles with the molten salt. Brick materials were the most stable in the molten salt.

2. Selected Material for Tests

The materials selected for test in this program are listed in Table 3-2. These materials are castable and brick except for a foamglass and

Table 3-1 Previous Tested Materials and Results

MATERIAL	MFR*	COMPOSITION	SOAK	TIME (WEEKS)	FREEZE-THAW	CYCLES**
			FELT			
DURABACK	CC	SiO_2 & Al_2O_3	UNSTABLE	4	--	--
DURABLANKET	CC	SiO_2 & Al_2O_3	UNSTABLE	4	--	--
DURABLANKET H	CC	SiO_2 & Al_2O_3	UNSTABLE	4	--	--
SAFFIL	CC	Al_2O_3	STABLE	17	--	--
			BOARD			
2300 M BOARD	BW	SiO_2 & Al_2O_3	STABLE	19	BROKEN	4
2600 BOARD	BW	SiO_2 & Al_2O_3	STABLE	19	BROKEN	4
2600 BOARD (SURFACE RIGIDIZED)	BW	SiO_2 & Al_2O_3	STABLE	19	BROKEN	3
3000 BOARD	BW	Al_2O_3	STABLE	19	BROKEN	4
DURABOARD	CC	SiO_2 & Al_2O_3	--	--	BROKEN	3
			CASTABLE			
CORELINE	KR	SiO_2 & Al_2O_3	STABLE	5	STABLE	20
IRC 24LI	KR	SiO_2 & Al_2O_3	STABLE		BROKEN	7
KOA-TAB 95	BW	Al_2O_3	STABLE		BROKEN	10
KOALITE 3300	BW	Al_2O_3	UNSTABLE	1	--	--
CORLOK	SE	K SiO_2	UNSTABLE	1	--	--
PLENCHLOR	SE	$NaSiO_2$	UNSTABLE	6	BROKEN	10
FST BRICK	SE	FUSED Si	UNSTABLE	5	BROKEN	14
			BRICK			
SR99	BW	Al_2O_3	STABLE	22	STABLE	20
VISIL	SE	VITREOUS SILICA	STABLE	7	STABLE	25
MODIFIED PUROTAB COARSE	KR	SiO_2 & Al_2O_3	STABLE	5	STABLE	20
SEMACID	SE	SiO_2 & Al_2O_3	STABLE	7	STABLE	15
CORDIERITE	CG	SiO_2 EXTRUSION	UNSTABLE	1	--	--

*CC = CORBORUMDUN CO. SE = STEBBINS ENGINEERING
BW = BABCOCK & WILCOS CG = CORNING GLASS
KR = KAISER REFRACTORY

**CYCLE FROM AMBIENT TEMPERATURE INTO 846K (1000°F) SALT

Table 3-2 Tested Material

MANUFACTURER AND MATERIAL		DENSITY lb/ft³	DENSITY gm/cm³	COMPOSITION PRODUCTS IN PERCENT Al_2O_3	SiO_2	Fe_2O_3	TiO_2	CaO	MgO	ALKALIES $Na_2O;B_2O_3$ K_2O	OTHERS
Brick											
*Maximul	KR	142-146	2.27-2.34	42.76	53.15	1.07	1.11	0.47	0.57	0.87	
Lo Erode	KR	135-143	2.16-2.29	57.94	32.06	0.91	1.29	6.67	0.22	0.59	
Hi Strength	KR	126-133	2.02-2.13	43.64	38.31	3.68	1.06	11.11	0.41	1.39	
*Krilite 30	KR	30	.48	55.5	38.2	1.6	1.4	2.2	0.2	1.2	
Krilite 60	KR	60	.96	55.5	38.2	1.6	1.4	2.2	0.2	1.2	
K-30	B&W	51	.82	46.0	52.0	0.9	1.4	0.5	0.1	0.4	
Firebrick 80-D	B&W	151	2.42	45.0	52.0	1.4	1.7	0.1	+	0.3	
*Visil	HW	116-120	1.86-1.92	0.5	98.9	0.3	0.02	0.02	0.1	0.2	
Krimax CS-124	KR	150-154	2.40-2.47	46.2	49.7	1.6	1.9	0.06	0.17	0.23	
Semacid	SE	137	2.2	36.30[3]	57.88	2.74		0.82	0.54	1.38	
Castable											
IRC 24LI	KR	56-58	.90-.93	40.55	36.15	1.65	1.30	16.39	0.37	1.93	
Coreline	KR	176	2.82	87.1	6.2	0.4	0.2	0.1	0.2	6.2[4]	
*Firelite 2100	KM	65	1.04	38.4	31.2	4.8	1.5	22.4	0.5	0.2	
*Firecrete 2800	JM	123	1.97	50.3	39.3	4.0	2.0	4.0			0.4
KAO TAB 95	B&W	166	2.66	95.0	0.1	0.1	+[2]	4.6	+	0.1	
Foamglass											
*Foamsil-12	PC	25	.40	4.0	88.0					8.9[1]	0.1
Fibreous Board											
Duraboard	CC	28-30	.45-.48	43.5	45.6	0.9		1.4		0.3	
Other											
T-Bond KT	KR	194.5	3.12	0.2	0.6	0.2		1.9	97.1		

Manufacturer

KR - Kaiser Refractories
B&W - Babcock & Wilcox
HW - Harbison-Walker Refractories
SE - Stebbins Engineering
JM - Johns-Manville
PC - Pttsburgh Corning
CC - Carborundum Co.

[1] B_2O_3 7.0
K_2O 1.0
Sb_2O_3 0.2
Na_2O_7 0.4-0.7

[2] + = Trace

[3] Includes a small amount of TiO_2

[4] Na_2O 0.2
K_2O 0.1
P_2O_5 5.9

a fibrous board. A cross section of products from seven companies was used, with alumina and silica percentages ranging from one extreme to the other. Alumina and silica are the only major components of refractories. The various forms of these compounds were not known. The compatibility of the products were not known by the manufacturer so they supplied various samples which they considered would best survive the molten salt environment. The one unique product tested was a tar-bonded magnesium oxide brick. However, this brick was quickly attacked by the salt.

3. Test Configuration and Conditions

The materials were tested in a commercial grade draw salt, Partherm 430 from Park Chemical Company. The analysis of trace elements in the Partherm 430 are listed in Table 3-3. The materials were tested for 500 hours at 866 K (1100°F), identified as the prescreening test, and evaluated. Seven of the samples were selected as the best candidates and placed in test at 839 K (1050°F) for a 5000-hour duration. This was identified as the longevity test. These samples were Krilite 30, Duraboard, JM 2800, JM 2100, PC-12 (foamglass), Maximul and Visil and they are noted in Table 3-2 by an asterisk. They were evaluated at 500, 1000, 3000, and 5000 hours.

The samples were tested in the oven shown in Figure 3-1. Six pieces of each sample material were placed into a tray. Thus one piece of each sample material could be removed at each evaluation time. Extra pieces were included for other evaluations that might have added to the program.

4. Technical Approach and Evaluation Techniques

Since most of the refractories are for high-temperature applications in excess of 866 K (1050°F), the primary concern during the testing was to evaluate general corrosion and internal chemical attack by the salt.

General corrosion was defined as the attack of salt on the exterior surfaces such as flaking, burning, pitting, surface cracking, etc. If the refractories exhibited any surface degradation in a short-time exposure test, their long-term application was seriously questioned.

Because of the inherent porosity of the refractory structure and the transport properties of the salt, impregnation of most of the refractories with salt was likely. The intruding salt may chemcially attack the bond structure, weakening the refractories and rendering them susceptible to intergranular or bondline failure. Salt may also react with the refractory base composition and alter the matrix by forming new chemcial compounds that could have possibly strengthened the material. Surface and/or internal cracking may be caused by the thermal stresses generated by the freezing and thawing of the salt inside the refractory matrix.

The material evaluation procedure was modified during the program. The results of the 1000-hour longevity test showed that the material was being significantly attacked. Analysis of the material by petrographic and SEM methods was eliminated and only the salt chemical test was performed for the 3000- and 5000-hour data points.

TABLE 3-3 ANALYSIS OF PARTHERM 430

	ANALYSIS 1	ANALYSIS 2
OXIDE	.005	.032
CARBONATE	.052	.034
NITRITE	.03	0.51
NITRATE	66.69	
SODIUM	16.0	
POTASSIUM	15.6	
INSOLUABLE RESIDUES	0.139	0.09
$NaNO_3$	59.4	
$K NO_3$	40.6	
SILICON (ppm)		41
ALUMINUM (ppm)		1.4
CALCIUM (ppm)		36

Partherm 430 is normally mixed in portions of 1600 pounds potassium nitrate and 2400 pounds sodium nitrate (40% KNo_3, 60% $NaNO_3$).

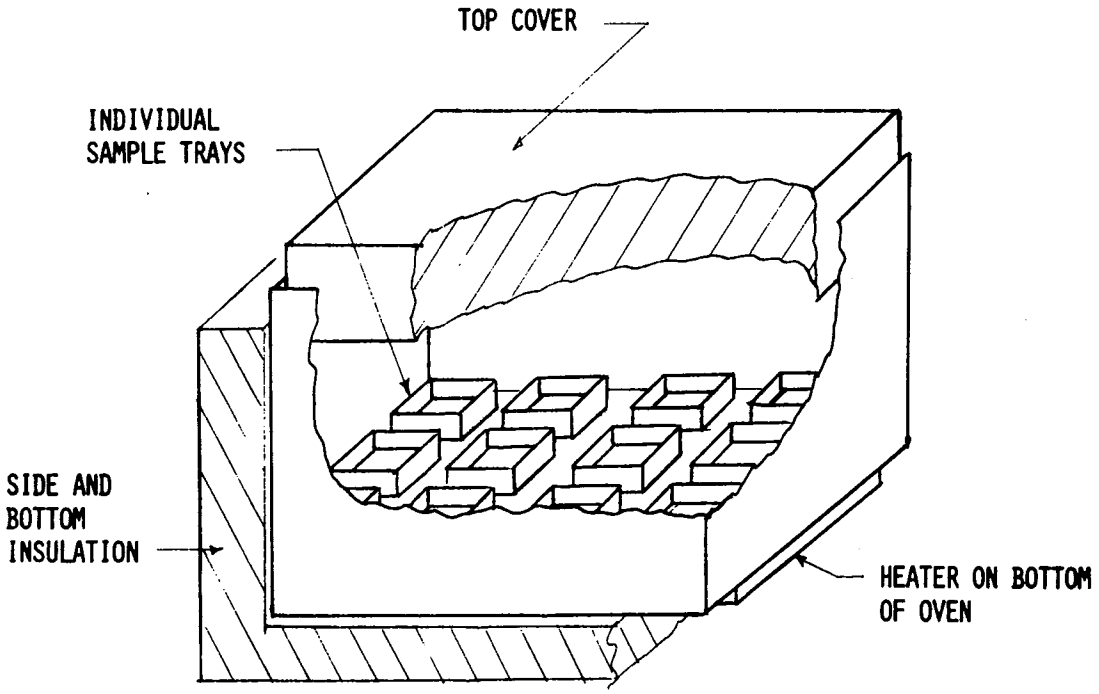

Figure 3-1 Test Oven Configuration

The evaluation techniques used are described in more detail in the following paragraphs.

a. Visual Inspection (General Corrosion) - The samples were examined after salt exposure at 10X magnification. The exposed surface was compared with an unexposed specimen. Surface cracks were examined at higher magnification to verify whether the cracks were filled with salt. If the cracks were filled with salt, they must have formed at higher temperatures where molten salt could fill the cracks.

   Absence of salt in the cracks resulted when the crack formed when the salt was frozen. The low-temperature cracking is defined in this report as thermal cracking. The high-temperature cracking could possibly be due to the corrosive attack of the salt.

b. Scanning Electron Microscope (SEM) Studies (Internal Chemical Attack) - The intruding salt may attack the internal structure and particularly the bond strength. When the bond strength is weakened the refractory is susceptible to an intergranular type of failure. The susceptibility of refractory to bondline failure was determined by examining the fracture surfaces under scanning electron microscope. The fracture surfaces were cracked by impact, fracturing the specimens as shown in Figure 3-2. The fracture modes of both unexposed and exposed specimens were compared to evaluate the salt attack. Elemental analysis using the Kevex-ray attachment to the SEM was used to determine the salt penetration into the refractories. The detection of sodium and potassium inside the exposed specimen when compared to the unexposed specimen was indication of salt impregnation.

c. Mechanical Wear Test - The mechanical wear test was conducted to determine the degradation of bond strength. A comparison was made between an unexposed and an exposed specimen. The sample with the weaker bond strength will wear faster. The wear test fixture is shown in Figure 3-3. Both unexposed and exposed specimens were subjected to the wear test and the results compared to evaluate the salt attack on the bond strength. The specimens were pressed at a normal load of 20 pounds against a steel disk rotating at 180 rpm. The test duration was 6 minutes for each specimen. The specimens were weighed before and after the wear test to determine the weight loss during the test. Observations were also made regarding the size of the particles generated.

d. Salt Chemical Analysis - Any chemical attack of the materials by the molten salt will form new compounds. These compounds may or may not be soluble in the molten salt. A chemical analysis was made of the salt in which each sample was submerged. The samples selected for the longevity test were exposed to a salt chemistry analysis. If elements of the material were detected in the salt, it established that the material was attacked by the salt. Figure 3-1 shows the arrangement of the material samples in the oven.

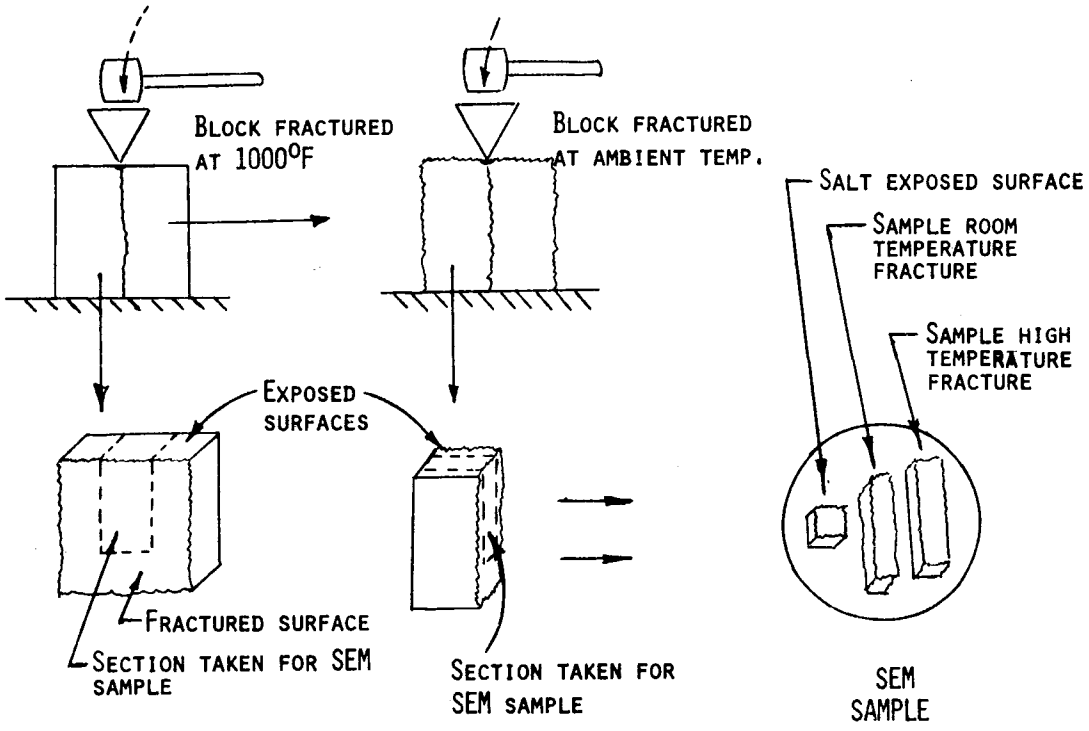

Figure 3-2 Specimen Preparation for SEM

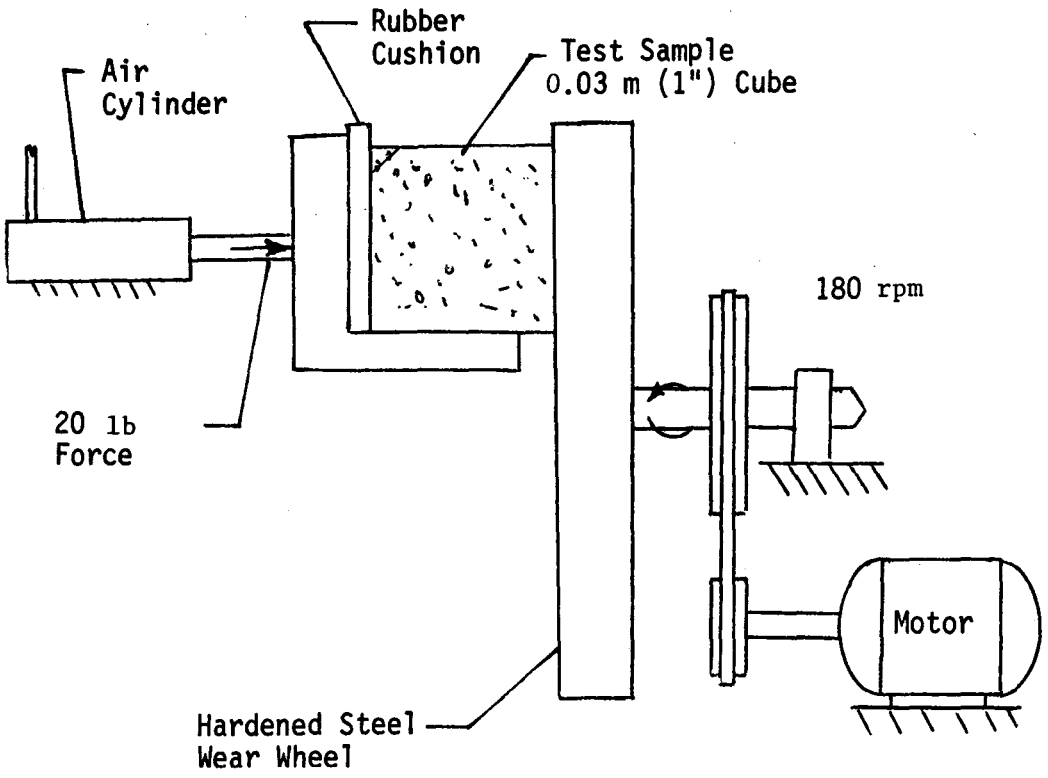

Figure 3-3 Mechanical Wear Test Apparatus

Over a period of time the salt "creeps" out of the tray into the bottom of the oven. Thus, salt had to be added to the trays to keep the samples submerged. Adding salt resulted in diluting the concentration of dissolved compounds from the material. Therefore new containers were made of 0.06-m (2.5-in.) diameter pipe 0.14-m (5.5-in.) long, making it unnecessary to add makeup salt throughout the test.

5. Results and Discussion (Visual and SEM Inspection)

The results of the visual inspection and SEM studies are summarized in Tables 3-4 and 3-5 respectively. Photographs of the materials evaluated and discussed here are given in Appendix A.

a. Krilite 30 - This lightweight insulating brick is porous and consists of what is called "bubble" structure. After a 500-hour immersion in salt, the bubble structure was to be filled with salt as shown in Figure A-1.

Fracture of the unexposed brick showed primarily pore or bubble wall rupturing (Fig. A-2). However, after exposure to salt, the room-temperatures fractures (Fig. A-3b and A-7a) showed a total absence of the bubble wall rupturing; a transgranular fracture mode with some cleavage facets was evident. This indicated that salt had filled the bubble wall structure during exposure and strengthened the brick matrix at room temperature. Kevex-ray elemental analysis (Fig. A-2 through A-5) confirmed the salt penetration throughout the brick cross section.

The room-temperature transgranular fracture was assumed to be due to the frozen salt, which does not characterize the effect of molten salt on the brick bond strength at 839 K (1050°F). Therefore the exposed brick was reheated to 811 K (1000°F) and fractured at this temperature. The high-temperature fracture reverts back to bubble wall rupturing (Fig. A-5) as was observed for the unexposed sample (Fig. A-2). The Kevex-ray analysis still showed the presence of salt (sodium potossium) on the fracture surface (Fig. A-5b).

It appears that at room temperature the frozen salt reinforces the bubble structure of Krilite 30 and strengthens the matrix. At high temperatures the molten salt did not seem to adversely affect the brick bond structure.

b. Duraboard - Duraboard is a fiberboard with a loose and light fibrous matrix as shown in Fig. A-6. There is no visible effect of salt exposure except weight gain, which also helps in tighter bonding of the fiber matrix. The fracture characteristic of the standard unexposed board is featureless and fracture appears to be due to separation of fibers (Fig. A-7a). After 500 hours of exposure to molten salt the duraboard matrix was filled with salt and the room-temperature fracture shows a definite cleavage pattern

Table 3-4 Material Visual Inspection Results

MATERIAL	UNEXPOSED SAMPLE	EXPOSED SAMPLE (500 Hrs)	EXPOSED SAMPLE (1000 Hrs)
*KRILITE 30 (INSULATING BRICK)	VERY POROUS SURFACE. FINE CRACKS	PORES FILLED WITH SALT. NO DISCOLORATION. NO CRACKING.	NO CHANGE
*DURABOARD (FIBERBOARD)	FIBROUS SURFACE TEXTURE. FINE POROSITY	SAME SURFACE TEXTURE. NO CRACKING OR DISCOLORATION.	NO CHANGE
*JM 2800 (MEDIUM DENSE CASTABLE)	FINE SURFACE POROSITY. MICROCRACKS AT SURFACE.	PORES FILLED WITH SALT. BURNT HOLES. SOME CRACKS WIDENED. COLOR DARKENED.	NO CHANGE
*JM 2100 (INSULATING CASTABLE)	FINE SURFACE POROSITY. SOME LARGE VOIDS. MICROCRACKS AT SURFACE.	PORES FILLED WITH SALT. BURNT HOLES. SOME CRACKS WIDENED. COLOR DARKENED.	NO CHANGE
*PC-12 (FOAM GLASS)	OPEN HONEYCOMB TYPE STRUCTURE.	SURFACE PORES FILLED WITH SALT. NO DISCOLORATION. NO CRACKING.	SALT PENETRATION 1/4 INCH.
*MAXIMUL (DENSE BRICK)	SMOOTH FINE TEXTURE. SMALL FINE CRACKS.	COLOR BLEACHED. EXTENSIVE SURFACE CRACKING.	NO CHANGE.
IRC-24LI (INSULATING CASTABLE)	POROUS, FINE CRACKS.	CRACKS WIDENED. NEW CRACKS (THERMAL).	
HI STRENGTH (DENSE BRICK)	FINE POROSITY. CRYSTALLINE SURFACE TEXTURE.	SURFACE CRACKING. DISCOLORATION.	
KRILITE 60 (INSULATING CASTABLE)	VERY POROUS SURFACE. EXTREMELY FINE CRACKS.	PORES FILLED WITH SALT. NO DISCOLORATION. NO ADDITIONAL CRACKING.	
K-30 (INSULATING BRICK)	VERY COARSE CRYSTALLINE STRUCTURE.	WIDE CRACKS. SURFACE EXTREMELY CRUMBLY.	
D-80 (DENSE BRICK)	FINE SMOOTH SURFACE TEXTURE.	NO DIFFERENCE.	
CORLINE (FIRED CASTABLE)	FINE SMOOTH SURFACE. TEXTURE. FINE CRACKING NEAR SECOND PHASE PARTICLES.	EXTENSIVE CRACKING. WIDER CRACKING AROUND SECOND PHASE PARTICLES. COLOR CHANGE FROM LIGHT BROWN TO PINK.	
LO ERODE (DENSE BRICK)	SMOOTH SURFACE TEXTURE. NO SIGNIFICANT POROSITY OR CRACKING.	COLOR BLEACHED. EXTENSIVE CRACKING AROUND SECOND PHASE PARTICLES. DEEPER BURNT HOLES.	
KOA TAB 95 (DENSE CASTABLE)	AMORPHOUS	SAME SURFACE TEXTURE. BIG WIDE CRACK IN CENTER (THERMAL).	
*VISIL (DENSE BRICK)	SMOOTH CRYSTALLINE.	SAME SURFACE TEXTURE. LIGHT DISCOLORATION. LONG LINEAR CRACKS.	NO CHANGE.
CS 124 (DENSE BRICK)	POROUS, FINE CRACKS.	PORES FILLED WITH SALT CRACKS WIDENED.	

Table 3-5 Scanning Electron Microscope Results

MATERIAL	UNEXPOSED SAMPLE	EXPOSED SAMPLE
*KRILITE 30 (INSULATING BRICK)	IMPACT/OVERLOAD TYPE FRACTURE. RUPTURE OF PORE WALLS.	SALT PENETRATION THROUGHOUT. TRANSGRANULAR OVERLOAD FRACTURE.
*DURABOARD (FIBERBOARD)	FEATURELESS FRACTURE.	MATRIX STRENGTHENED BY SALT. SOME OVERLOAD FEATURES.
*JM 2800 (MEDIUM DENSE CASTABLE)	IMPACT/OVERLOAD FRACTURE.	SAME FRACTURE MODE. UNIFORM COMPOUND FORMATION THROUGHOUT THE CROSS SECTION.
*JM 2100 (INSULATING CASTABLE)	RUPTURING AROUND LARGE VOIDS.	NO VOIDS. IMPACT/OVERLOAD TYPE FRACTURE. SURFACE COVERED WITH SALT. COMPOUND FORMATION IN CENTER.
*PC-12 (FOAM GLASS)	PORE RUPTURING.	IMPACT/OVERLOAD TYPE FRACTURE NEAR SURFACE. PORE RUPTURING. LITTLE SALT PENETRATION.
IRC 24LI (INSULATING CASTABLE)	IMPACT OVERLOAD.	ELONGATED CLEAVAGE PLATELETS. LARGE VOID FORMATION. SALT PENETRATION THROUGHOUT (NA, AL, SI, K, CA) COMPOUND FORMATION.
HI STRENGTH (DENSE BRICK)	TYPICAL TRANSGRANULAR IMPACT/OVERLOAD FRACTURE.	INTERGRANULAR FRACTURE NEAR SURFACE. FEATURELESS FRACTURE NEAR CENTER. SALT PENETRATION ENTIRE CROSS SECTION.
CORLINE (FIRED CASTABLE)	OVERLOAD TYPE FRACTURE. RUPTURING OF THE PORES. SOME SECONDARY CRACKING.	SIMILAR FRACTURE MODE WITH MORE UNDERLYING CRACKING.
D-80 (DENSE BRICK)	SOME AREAS DEEP INTERGRANULAR CRACKING. MOST AREAS FLAT FEATURELESS FRACTURE.	"CA" LEACHED OUT. HEAVY INTERGRANULAR CRACKING AT THE CENTER.
*VISIL (DENSE BRICK)	IMPACT/OVERLOAD TYPE FRACTURE.	SAME FRACTURE MODE. NOT MUCH SALT PENETRATION.
CS-124 (DENSE BRICK)	PORE WALLS RUPTURED. INTERGRANULAR CRACKING.	SAME FRACTURE MODE. PORES FILLED WITH SALT SO NO PORE RUPTURING. SALT PENETRATION THROUGHOUT. "CA" LEACHED OUT FROM NEAR THE SURFACE.
SEMIACID (DENSE BRICK)	OVERLOAD TYPE FAILURE. SOME PORE RUPTURING.	SAME FRACTURE MODE. VERY LITTLE SALT PENETRATION.

(Fig. A-7b) indicating a tighter bonding of the fiber matrix instead of loose fiber separation. After 1000 hours of exposure the room-temperature fracture appeared to be a stress-corrosion type (Fig. A-7c), apparently due to an increased amount of salt and probably a completely new matrix formation. Both cleavage- and stress-corrosion-type fracture characterisitics indicate higher strength for the salt-exposed samples as compared to the loose fiber separation fracture of the unexposed sample.

The Kevex-ray analyses (Fig. A-8) shows the salt penetration (sodium and potassium) throughout the sample cross section. To evaluate the effect of molten salt at higher temperature, one of the exposed specimen was reheated to 811 K (1000°F) and fractured at elevated temperature. The fracture appearance was very similar to that obtained for room-temperature fracture (Fig. A-9), confirming the original fibrous matrix transformation to a new matrix because of the frozen salt.

c. JM 2100 - JM 2100 is an insulating castable showing fine surface porosity, some large voids and extensive surface microcracking in the unexposed specimen (Fig. A-10). After 500 hours of immersion in molten salt, the surface porosity appeared to be completely filled with salt; however, deeper and wider cracks are observed with additional burnt holes as shown in Fig. A-10. The color was also changed probably due to the reaction of the salt with the sample matrix.

The room-temperature fracture Fig. A-11a was primarily due to the rupturing of pores. After 500 hours of immersion in salt when salt apparently has filled the porous matrix, the fracture mode (Fig. A-11b) has changed to intergranular with many small cleavage facets, indicating strengthening of the matrix in the presence of frozen salt.

Fig. A-12 shows the penetration of salt throughout the specimen cross section. After a 1000-hour exposure the fracture appearance, shown in Fig. A-13a, is typical of a stress-corrosion product. Again, the high-temperature fracture (Fig. A-13b) is similar to the room-temperature fracture showing alteration of the original matrix.

d. JM 2800 - This material is a medium-dense castable insulation. JM 2800 appears more dense and less porous than JM 2100. The room-temperature fracture (Fig. A-14a) exhibits large areas of impact overload and small areas of pore rupturing as compared to the fracture for JM 2100 (Fig. A-11) This indicates the greater strength of JM 2800. The salt-exposed specimen shows intergranular-type failure with some cleavage facets. As evident from Fig. A-15 the salt penetration is throughout the specimen cross section and probably the complete matrix has been chemically changed. Fig. A-16 shows both the room- and elevated-temperature fracture surfaces after 1000 hours of exposure. The fracture is similar to

the stress-corrosion-type fracture with the surface covered with corrosion product. The fracture modes of both the room-temperature fracture and the elevated-temperature fracture present a strong possibility of a chemical or a bondline change from the original material.

e. PC-12 (Foamglass) - The standard unexposed sample is a closed cell glass foam as shown in Fig. A-17a. The cells are more clearly seen in Fig. A-19. Fig. A-17b shows the surface after salt exposure during prescreening test. Some of the cells have been enlarged, presumably due to the attack of the salt on cell walls. Fig. A-17c shows the prescreening sample sectioned 0.01-m (0.25-in.) below the surface. Only minor salt penetration at the sample surface was seen.

The salt penetration of the 500-hour sample was investigated using an electron microprobe diffraction pattern. Fig. A-18 presents the electron microprobe results. While sodium and potossium are detected at the salt-exposed surface and 50 microns below the exposed surface, no sodium or potassium are observed 2000 microns below the salt-exposed surface (Fig. A-18d). Therefore salt does not penetrate PC-12 like other refractory materials.

Even the small amounts of salts in PC-12 have a definite effect on the fracture characteristics. The unexposed specimen primarily fractures because of pore rupturing (Fig. A-19a). Fig. A-19b shows the room-temperature fracture mode of both salt-impregnated and salt-free areas. Salt-impregnated areas fractured when frozen exhibit a tougher transgranular fracture mode as compared to a weak pore rupturing.

A lower temperature and less expensive foamglass, PC-28, was immersed in 714 K (825°F) molten salt for 3000 hours. The sample showed no visual degradation and left no visual precipitates in the salt.

To eliminate the possible strengthening effects of frozen salt, the specimen exposed for 1000 hours was fractured at 811 K (1000°F). Both the elevated- and room-temperature fractures (Fig. A-20) show the tougher transgranular mode, indicating strengthening of the PC-12 matrix and the new compound or bonding mechanism due to salt PC-12 interaction.

The depth of salt penetration into the PC-12 was variable. The prescreening sample had every little penetration whereas the longevity sample had salt penetration up to 0.01-m (0.25-in.). It was thought that cutting the 1-inch cube samples resulted in surface cracks, allowing salt penetration. In the thermal conductivity test it was found that salt penetration increased with time so the 0.025-m (1-in.) penetration occurred after 5000 hours.

f. Maximul - Maximul is a dense fired brick. The unexposed specimen has a fine smooth texture, fine cracks, and a light brown color with gray second-phase particles. After exposure to salt for 500 hours the color changed to dark yellow (Fig. A-21). Extensive surface cracking, predominantly thermal, occurred around the second-phase particles. Salt penetration of specimen was confirmed by Kevex-ray analyses (Fig. A-22).

The fracture mechanics of the unexposed brick (Fig. A-23a) are mainly intergranular with some pore rupturing evident. The fracture of the salt-exposed specimen is primarily intergranular (Fig. A-23b); however, some deeper and wider intergranular cracks are clearly observed. These cracks are filled with salt indicating they were formed at molten salt temperature. Presumably the molten salt corrosively attacked the bond structure (grain boundary) of the brick and the intergranular cracks filled with salt. The color change due to salt penetration throughout the specimen strongly suggests a possible adverse interaction between the salt and the brick matrix. Kaiser Refractories' evaluation of this material showed salt impregnation of the brick structure. However, only minimal reaction or alteration of the original bond structure was evident in the 500-hour specimen. Fracture evaluation of the 1000-hour-exposed specimen indicates an increase in intergranular cracking and thermal cracking, which is considered detrimental for long-term applications.

g. IRC 24 LI - This material is a lightweight insulating castable. The exposed specimen exhibits many thermal cracks and widening of existing surface cracks, as shown in Figure A-24.

Figure A-25 presents the Kevex-ray elemental analysis results showing complete impregnation of the specimen by the salt. The fracture of the unexposed specimen was primarily due to pore rupturing with some fine cleavage facets (Fig. A-26a).

Fracture of the exposed specimen shows large void formations and fine elongated cleavage facets (Fig. A-26b). The large voids could be the result of severe corrosion attack. The fine elongated cleavage facets also suggest a change in the bonding system. Overall, the fracture study indicates the material was corrosively attacked by the high-temperature salt. The Kaiser Refractories' analysis basically confirms this conclusion.

h. Hi Strength - Hi Strength is a dense fired brick. The exposed specimen (Fig. A-27b) exhibits extensive thermal cracking and discoloration. The Kevex-ray analyses (Fig. A-28, A-29, and A-30) show the complete impregnation of the brick by salt. The fracture of the unexposed brick was a transgranular overload, wereas the fracture of the exposed specimen near the exposed surfaces was extensively intergranular (Fig. A-29a and A-29b), indicating salt attack on the brick bonding matrix. The fracture at the center of

the specimen presents an interesting situation. It was similar to a severe intergranular stress corrosion and the surface was completely covered with salt (Fig. A-30). It seems that salt had corrosively attacked the bonding system of the brick, promoting intergranular fracture. Kaiser Refractories' analysis agrees with the above conclusion.

i. Krilite 60 - The unexposed and exposed specimens of this insulating brick are shown in Figure A-31. No discoloration, cracking, or any other degradation can be visually observed except that the pores have been filled with salt. The Kevex-ray analysis (Fig. A-32) shows complete impregnation of the specimen by the salt. Fracture of the unexposed specimen (Fig. A-33a) was due to pore rupturing similar to Krilite 30 . After exposure to salt the specimen is impregnated with salt. The room-temperature fracture showed the matrix was strengthened as indicated by less pore rupturing (Fig. A-33b). The high temperature fracture (Fig. A-33c) showed a fracture mode similar to that of the unexposed specimen. Even though the salt completely impregnated the Krilite 60, the visual evaluation did not show any adverse effect.

j. Corline - This medium-density castable material was fired at 644 K (700°F). The exposed specimen showed extensive, wide thermal cracking. Also the color changed from light brown to rose pink (Fig. A-34). Kevex-ray analysis (Fig. A-35) showed complete impregnation of the specimen by the salt. The fracture characteristics of the exposed and unexposed specimens were similar as shown in Figure A-36, except for the exposed specimen that has thermal cracks.

The extensive thermal cracking was assumed to be detrimental to the Corline performance for long-time applications.

k. D-80 - D-80 is a dense high-service-duty brick. There was no visible effect of salt on the ouside exposed surface as shown in Figure A-37. The Kevex-ray elemental analysis showed surface impregnation of the brick by the salt, but the center of the specimen was void of salt as indicated by the absence of sodium and potassium peaks as seen in Figure A-38b.

Another interesting observation was the absence of a calcium peak from the exposed specimen. The calcium peak was clearly seen in the unexposed specimen. Calcium was leached from the specimen into the salt. The unexposed specimen fracture is intergranular (Fig. A-39a). The exposed specimen fracture was predominantly intergranular indicating corrosive attack of molten salt on the brick bonding system. The extensive intergranular cracking, combined with the leach of calcium from the brick matrix, was considered detrimental.

l. VISIL - The salt-exposed surfaces of this fired brick exhibited long line or thermal cracks as shown in Figure A-40. Kevex-ray analysis (Fig. A-41) did not show complete impregnation of the brick by the salt. Salt concentration was near the surface and negligible at the center. The unexposed fracture was intergranular with large cleavage facets (Fig. A-42). The type of fracture of the exposed specimen near the surface was stress corrosion indicating a corrosive attack of the molten salt on the brick's matrix and the bonding system. Similar fracture was observed at the center of the exposed specimen.

The susceptibility of VISIL to thermal cracking and extensive stress-corrosion cracking excluded VISIL from the possibility of long-term applications in the molten salt.

m. CS-124 - The visual inspection of CS-124, which is a dense fired brick, showed light discoloration and some fine long thermal cracks after salt exposure (Fig. A-43). The Kevex-ray analysis (Fig. A-44) showed complete impregnation of the brick by the salt and that there might also be some calcium leaching from the surface. The fracture surface of the unexposed specimen (Fig. A-45a) shows pore rupturing and some areas of intergranular cracking. The exposed specimen fracture surface (Fig. A-45b) does not show any pore rupturing, possibly due to the fact that the pores are filled with salt. The fracture is primarily intergranular with some large thermal cracks.

The fracture characterisitics of CS-124 dense brick is not adversely affected by the salt; however, the susceptibility of the brick to thermal cracking excludes the brick from a long-term application where possibly many freeze-thaw cycles may be experienced.

n. Semiacid - Figure A-46 presents the Kevex-ray analysis of the salt penetration of this dense brick. Very little or no salt penetration is evident from the analysis. The fracture modes of both unexposed and exposed specimens are similar (Fig. A-47) however, some thermal cracks can be observed on the exposed fracture surface. Semiacid was not selected for the longevity test because other products were more stable.

o. K-30 - K-30 is a lightweight insulating brick. The external surfaces after salt exposure were extremely crumbly. The particles could be rubbed out with finger pressure. There were no cracks or other effects as shown in Figure A-48. This refractory was not selected for further evaluation.

6. Results and Discussion (Mechanical Wear Test)

The test results of five refractory materials are presented in Table 3-6. The weight differences between the unexposed samples and the

samples exposed to salt and then boiled to remove the impregnated salt are shown. Specimens were originally placed in the wear test after salt exposure but it was found that no wear occurred. Even the Krilite 30, which lost 36.1% weight as an unexposed sample, lost nothing when exposed. To remove the salt from the samples they were boiled in water for 5 minutes and baked dry. The wear test of these specimens resulted in less weight percentage loss than the unexposed samples. Fracture analysis of the materials showed an increase in strength when the specimens were filled with frozen salt, probably because the salt remaining in the specimens increases their strength. The mechanical wear test was deleted from consideration since it did not give conclusive results.

Table 3-6 Mechanical Wear Test Results

Specimen	Initial Weight gms	Weight After Wear Test gms	% Weight Loss	Weight After Boiling & Dry gms	% Weight Loss	Weight After Second Wear Test	% Weight Loss	Remarks After Second Wear Test
Krilite 30								Gray-Black Shavings
Unexposed	11.9	7.6	36.1					from wear test,
Exposed (1)	42.2	42.2	0.0	19.5	53.8	18.1	7.2	black on work
Exposed (2)	34.3	34.3	0.0	15.6	54.5	15.5	0.6%	surface.
Duraboard								Specimen crumbled
Unexposed	12.8	10.8	15.6					upon application of
Exposed (1)	41.2	41.2	0.0	24.8	39.8	22.1		normal force, wear
Exposed (2)	46.2	46.0	0.4	31.1	32.4	29.5	5.1	test stopped.
JM 2800								
Unexposed	31.7	29.7	6.3					
Exposed (1)	35.9	35.8	0.3	32.5	9.2	32.3	0.6	
Exposed (2)	36.0	36.0	0.6	31.7	11.9	31.5	0.6	
JM 2100								
Unexposed	14.3	9.7	32.2					
Exposed (1)	36.9	36.8	0.3	34.7	5.7	34.6	0.3	
Exposed (2)	39.3	38.9	1.0	37.4	3.9	37.4	0.0	
PC 12								Turned Black After
Unexposed	7.5	7.35	2.0					Boiling, White
Exposed (1)	29.5	29.5	0.0	10.2	65.4	10.1	1.0	Particles acked
Exposed (2)	31.8	31.7	0.3	5.7	82.0	5.7	0.0	on surface.

(1) Sample saturated with salt

(2) Sample boiled in water to remove surface salt

7. Results and Discussion

The results of the chemical analysis of the salt in which the samples were tested are shown in Table 3-7. All the open tray had some amount of "makeup salt" added to replace the salt that "creeps" out of the trays. Makeup salt may have diluted the concentration of dissolved compounds. The cylindrical containers were made very deep to prevent the necessity of adding "makeup" salt.

The data were somewhat inconsistent as they did not show a constant increase of leached material with time. Also the results from the cylindrical containers were different from those of the open trays. The important item noted was that in all cases either aluminum or silica was leached from all materials into the salt. The amount of shaking or mixing that occurred while taking the salt sample probably affected the results because a precipitate-type material collected at the bottom of the trays. The presence of precipitate-type materials indicated that the test samples were being attacked by the molten salt. The molten salt attack of the castable materials (JM 2100 and JM 2800) and the Duraboard is readily seen in Table 3-7 by the large values of aluminum or silicon in the salt. The greater attack of these three materials was expected.

The other four test materials showed attack but of a lesser magnitude. The rate of attack was questionable but, sufficient attack had occurred in several months of tests to show material incompatibility. The considered opinion of Kaiser Refractories Inc., was that the byproducts formed between the material and the salt can be soluble in the salt at 830 K (1050°F) but will precipitate before the salt cools to 561 K (550°F). Cooling the salt would occur in the heat exchanger, which may result in fouling of the heat exchanger.

8. Material Compatibility Summary

When testing was begun we realized that the method of evaluating the results was not absolute. To evaluate a material for a 30-year life from a relative short exposure is difficult. The materials were totally wetted by the salt. The attack by the salt could form compounds that were not salt-soluble or compounds that were mechanically stronger or weaker than they were originally.

The evaluation methods used by refractory companies were discussed with Kaiser Refractories, Inc., who evaluated their own products after exposure. Their products are Maximul, CS-124, Krilite 30, Krilite 60, Lo Erode, Hi Strength, and IRC24LI. The effort by Kaiser Refractories was considered significant because they have carefully logged and maintained all their material service history. Their method of evaluation involved petrography, knowledge of materials and identification by X-ray diffraction. Their reports are given in Appendix B. They evaluated specimens exposed for 500 hours at 867 K (1100°F). Their conclusion was that all their products were being

TABLE 3-7 SALT CHEMISTRY ANALYSIS

	TRAY SAMPLES			CYLINDRICAL CONTAINERS		
HOURS	1000	3000	5000	500	1000	2750
MATERIAL						
JM2100						
Al (ppm)	37.4	41.5	22.1	6.0	17.9	292.3
Si (ppm)	35	38	≤12	18	≤12	≤12
Insol. (%)*	0.58	1.54	0.68	0.01	0.31	1.28
JM2800						
Al (ppm)	4.0	29.1	80.6	7.3	6.4	29.6
Si (ppm)	195	25	≤12	17	13	≤12
Insol. (%)*	0.55	1.21	0.88	1.08	0.18	0.47
DURABOARD						
Al (ppm)	15.4	4.1	12.1	6.8	2.3	6.6
Si (ppm)	126	173	99	25	12	1918
Insol. (%)*	0.88	0.95	1.78	0.30	0.49	0.64
KRILITE 30						
Al (ppm)	2.0	1.2	8.1	7.1	2.3	5.1
Si (ppm)	24	56	≤12	25	12	≤12
Insol. (%)*	0.36	0.99	0.55	0.73	0.76	0.22
FOAMSIL-12						
Al (ppm)	3.8	1.0	6.9	5.7	4.5	6.6
Si (ppm)	76	59	13	22	15	8
Insol. (%)*	0.31	1.53	0.12	0.13	0.16	0.38
MAXIMUL						
Al (ppm)	6.0	1.1	14.1	3.9	1.1	6.7
Si (ppm)	170	161	64	31	38	27
Insol. (%)*	0.63	2.31	1.47	0.20	0.70	0.68
VISIL						
Al (ppm)		1.1	5.2	5.2	1.2	8.1
Si (ppm)		93	72	19	13	≤12
Insol. (%)*		0.34	1.29	0.75	0.26	0.29

*Insoluable percent by weight in water during analysis

attacked at various rates, and that none of their products would survive a 5-year usage. Byproducts formed between the material and the salt could be precipitated in the system heat exchanger, resulting in fouling.

The chemistry evaluation of the salt showed that all products were attacked. The visual and microanalysis showed the products being altered. It was concluded that refractory products tested will not be usable for molten salt storage when saturated with molten salt. Also since a very wide selection base of products was used, it is unlikely that any currently available product will be compatible with molten salt. The products that will survive the greatest duration are dense high-service-duty fired bricks. Foamglass also appears to be attacked, although at a slow rate. The castable products are more readily attacked due to their cement binding.

C. THERMAL CONDUCTIVITY TEST

1. Test Configuration and Conditions

The determination of thermal conductivity of the insulation materials when saturated with molten salt was needed to optimize the tank system. Test fixtures were designed so representative tank temperatures could be simulated and thermal conductivity could be measured. Standard fixtures for measuring thermal conductivity could not be used because the material had to be submerged in molten salt. The test fixture shown in Figure 3-4 was used for castable, foamglass, and board types of insulation. The exterior of the canister was instrumented with thermocouples and sheath thermocouples measured the molten salt temperature. Using the power measurement into the electrical heater made it possible to calculate the thermal conductivity of the material by using the temperature difference across the insulation.

Figure 3-5 shows the test configuration used with bricks. Heat was added to the molten salt covering the bricks and the salt was heated to 811 to 839 K (1000 to 1050°F). The temperature was maintained at 811 to 839 K. A test was also performed with the Krilite insulating brick wet with salt but not immersed in the salt. During this test a second heating element was added to limit the heating element temperature and obtain a more even heat flux for the test sample.

2. Thermal Conductivity Test Results

The thermal conductivities of insulation material saturated with molten salt are listed in Table 3-8, including test data obtained prior to this study. These previous data was obtained by the same method with identical fixtures. Testing of M-Board 224 kg/m^3 (14 lb/ft^3) showed that bulk convection was occurring within this low-density material. Convection increased the heat loss through the insulation. Convection within the insulation is geometry-sensitive and would increase with large tanks.

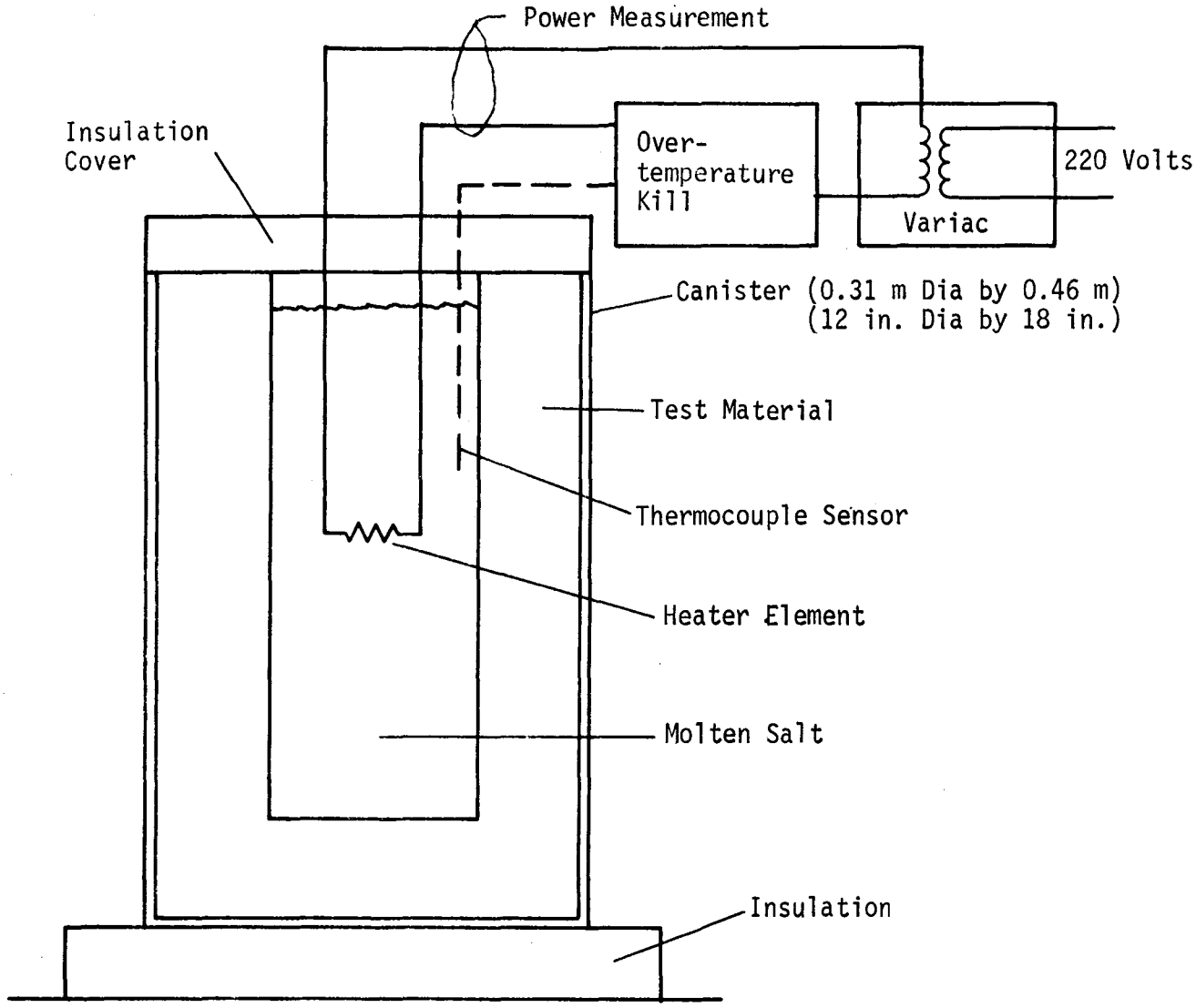

Figure 3-4 Thermal Conductivity Test Schematic

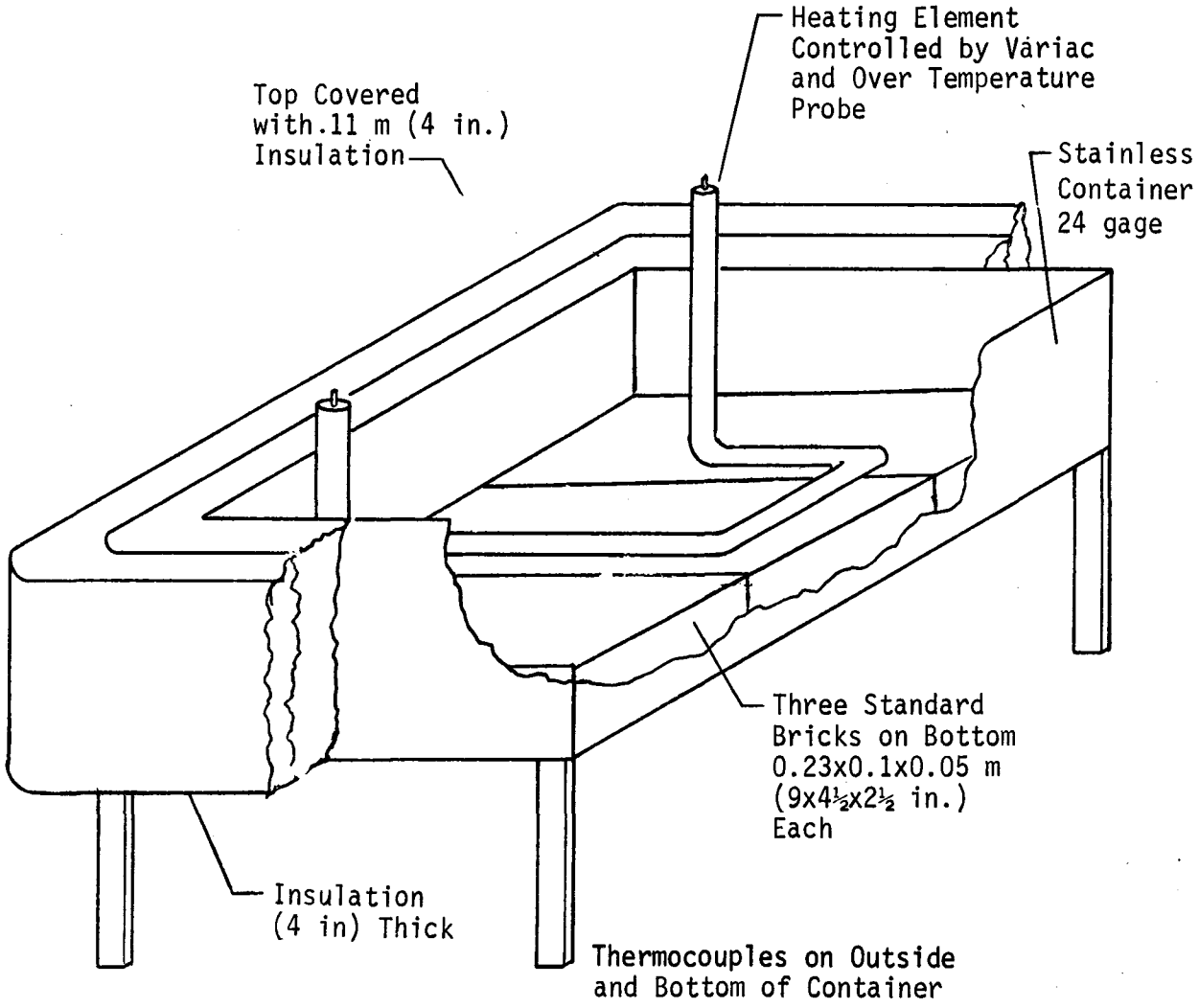

Figure 3-5 Thermal Conductivity Test for Bricks

Table 3-8 Thermal Conductivity Results

	THERMAL CONDUCTIVITY		
	WET		DRY (ADVERTIZED)
	W/M-K	BTU/HR-FT-°F	W/M-K
FOAMSIL 12 (FOAMGLASS)	.24	.14	.24
DURABOARD (GLASSBOARD)	.66	.38	.09
△ M BOARD* (GLASSBOARD)	1.59	.92	.06
FIRECRETE 2800 (MEDIUM DENSE CASTABLE)	1.99	1.15	.59
△ IRC 24LI (INSULATING CASTABLE)	.59	.34	.24
KRILITE 30** (INSULATING BRICK)	1.02	.59	.24
△ KAO TAB-95 (DENSE CASTABLE)	2.68	1.55	1.89

△ - PREVIOUS DATA.
* - CONVECTION WITHIN MATERIAL
** - BRICK SUBMERSED IN SALT; ALSO BRICK SATURATED BUT NOT SUBMERSED

With Duraboard 400 kg/m3 (25 lb/ft 3) convection was eliminated within the material, indicating the effect of material density. The initial testing of foamglass (PC-12) had the same thermal conductivity as advertised because the material did not absorb the salt. All other material had an increase in thermal conductivity. In general the lower density materials had a greater increase in thermal conductivity.

The effect of time on the thermal conductivity is not known. With the material being chemically attacked, the thermal conductivity may increase with time. The foamglass initially had the lowest thermal conductivity of any material tested when immersed in molten salt. The thermal conductivity of foamglass increased from 0.24 W/m-K initially to 0.36 W/m-K after 5000 hours of testing. Salt had penetrated 0.025-m (1-in.) into the surface.

D. THERMAL CYCLING TEST

A thermal cycle test was initiated to evaluate the effect of thermal cycling and freeze-thaw cycling on the material when saturated with molten salt. The test fixture shown in Figure 3-5 was used with the materials selected for the longevity test. The materials were Duraboard, Krilite 30, JM 2800, JM 2100, Visil, and Foamglass and were all in the same test. The molten salt was cycled from 839 to 561 K (1150 to 550°F), which caused the outside surface of the materials to range from 572 to 450 K (570 to 350°F). The freezing temperature of the draw salt is 494 K (430°F). Thus the outside surfaces of the materials went through a freeze-thaw cycle. A 12-hour cycle was used in which linear ramps of 4 hours with 2-hour holds at the hot and cold temperatures were maintained.

When the results from the material test showed that chemical attack was occurring with all materials, the cycling test was terminated after eighty cycles.

IV. THERMOCLINE TANK ANALYSIS

A. GENERAL

A "thermocline storage tank" is one that stores both the hot and cold fluid in the same tank and relies on the temperature-dependent fluid density difference to prevent fluid mixing. The thickness of the transition zone between the hot and cold fluids over which the temperature gradient occurs and the rate at which it grows or shrinks is a function of the fluid properties, the heat capacity of the tank sidewalls, the inflow/outflow characteristics, and other variables. A computer thermal model was made of a thermocline tank to analyze the effects of these variables on storage system performance.

The reports listed in the bibliography (Appendix C) were reviewed for methods of analyzing thermocline tanks and for test data that could be compared with results from the analytical model to verify its accuracy. The only published test data used to confirm the model was that from a French thermocline test that used oil as a working fluid (Ref 2). There are some thermocline test systems in the United States, but the available test data are insufficient for a comparison.

B. THERMAL MODEL

The analytical models in literature were not considered appropriate to this program. Detail models which calculate stream flows and isotherms are too costly to use for long transient conditions. It was necessary to consider the effect of fluid circulation on the transition zone. Since the scope and funding of this program would not permit such an analysis, a simplified two-dimensional model was developed in which the wall nodal system was two-dimensional but the fluid nodal system was one-dimensional. A separate subroutine accounted for fluid circulation parametrically at each iteration.

The thermocline tanks were analyzed by a generalized finite difference thermal analytical computer program called MITAS (Martin Marietta Interactive Thermal Analysis System). The analytical technique used for this transient problem was the central differencing method, which is generally more stable than the forward differencing method. MITAS allows for user-defined operations on the thermal model at each iteration. Thus it was possible to account for fluid inflow/outflow from the tank as well as parametric treatment of the fluid circulation.

Figure 4-1 shows the nodal system and the conduction network used for the computer analysis. The liner, internal insulation, and the tank

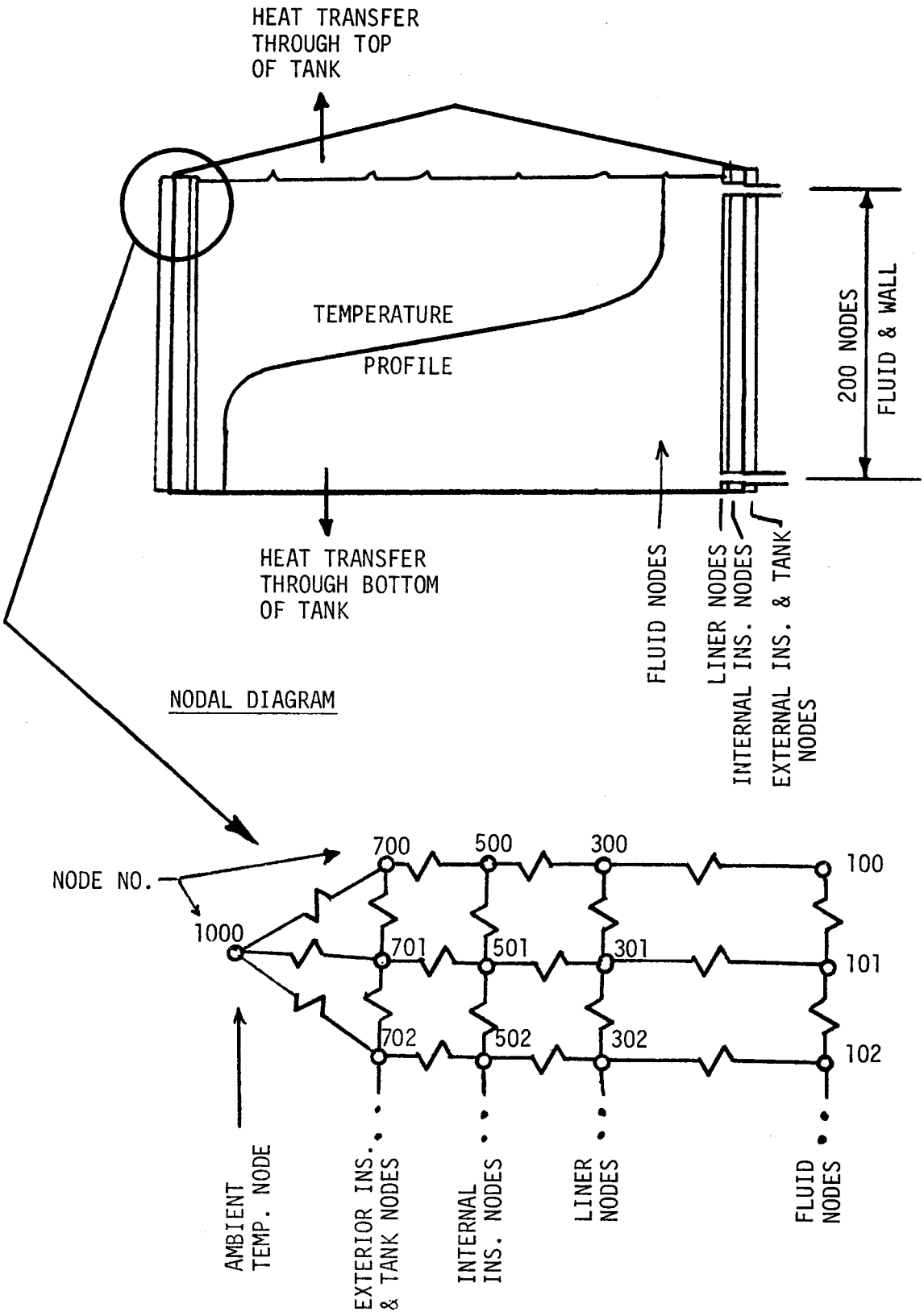

NODES HAVE HEAT CAPACITY

FIGURE 4-1 THERMOCLINE CONDUCTION MODEL

shell, lumped with the external insulation, were each divided into 200 vertical nodes representing the full height of the tank. The fluid was also divided into 200 vertical nodes, but was considered to be isothermal radially (horizontally). Each node had a heat capacity. The values of the thermal conductances between nodes and the heat capacity of each node were dictated by the tank dimensions and the matertials used. The model also accounted for heat loss through the top and bottom of the tank.

Figure 4-2 shows the fluid circulation loops in the thermocline tank. Above the transition zone, the bulk fluid is hotter than the adjacent wall so the fluid loses heat and flows "down" the wall. The fluid gains heat at the center of the tank and flows "up." It is also possible to have fluid circulation below the transition zone as it moves up the tank during storage discharge. In this case the wall is hotter than the fluid and the loop is driven in the opposite direction. These flow patterns are seen in the literature in detailed analyses and test observations.

To account for fluid circulation, the analytical model modified the energy distribution of the heat transfer between the fluid nodes and the wall nodes (Fig. 4-3). With no circulation, all heat loss through the wall nodes comes from the adjacent fluid nodes. With fluid circulation, only a specified percentage of the losses comes from the adjacent fluid nodes; the remaining energy comes from a fluid circulation loop that gets its energy from the bulk fluid nodes (although it does not receive an equal quantity from each node). The analysis was parametrized by the ratio "R."

$$R = \frac{\text{heat from bulk fluid}}{\text{heat loss into wall}} = \frac{\text{heat loss from fluid node i}}{\text{heat loss into wall node i}}$$

Thus R=1 indicates a no-circulation case and R=0.40 means that 40% of the wall heat losses comes from the adjacent fluid nodes and 60% comes from the fluid circulation loop.

The energy in the circulation loop comes from the bulk fluid nodes. As the circulating fluid flows up the center of the tank, it absorbs energy from each node as a result of the temperature difference between nodes. An energy balance is maintained in the circulation fluid by absorbing heat from all the bulk fluid nodes that is equal to the total energy lost at the wall.

During storage charge the transition zone moves down the tank. This is simulated at each iteration by assigning to each fluid node the temperature of the fluid node above it. Node 100 (the top of

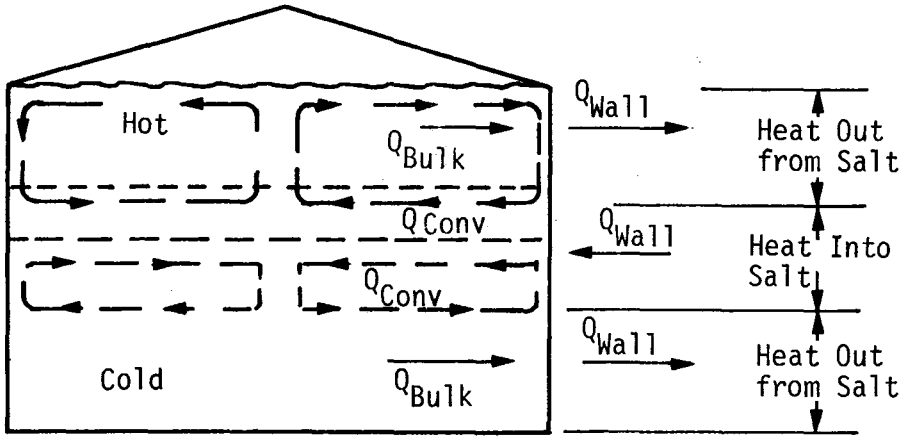

1. Heat loss at wall is divided between
   a. Adjacent salt
   b. Convection layer (which is redistributed into the bulk fluid)
2. Circulation is assumed to occur in
   a. The hot layer above the thermocline
   b. The layer below the thermocline when the wall is hotter than the fluid

Figure 4-2 Thermocline Circulation Model

the tank) is assigned a temperature of 839 K (1050°F) representing incoming hot salt. When the transition zone reaches the bottom of the tank, the temperature of node 299 (the fluid node at the bottom of the tank) begins to increase, simulating outflow of the fluid in the transition zone. The maximum temperature increase of the fluid allowed to outflow before flow is terminated is called the temperature "bite."

For example, assume the temperature of the cold fluid in the bottom of the thermocline tank is 561 K (550°F). As long as the transition zone is remote from the bottom of the tank, the outflowing cold fluid will have a temperature of 561 K (550°F). As outflow continues, the transition zone will approach the tank bottom. When it reaches the bottom, the temperature will begin to increase as the fluid in the transition zone is outflowed. If flow is stopped when the outflow temperature is 577 K (580°F) a temperature "bite" of 16 K (30°F) has been taken out of the bottom of the transition zone. Similarly, if the hot fluid temperature is 839 K (1050°F) and outflow of the hot fluid is terminated when the flow temperature has decreased to 823 K (1020°F), a temperature "bite" of 16 K (30°F) has been taken out of the top of the transition zone.

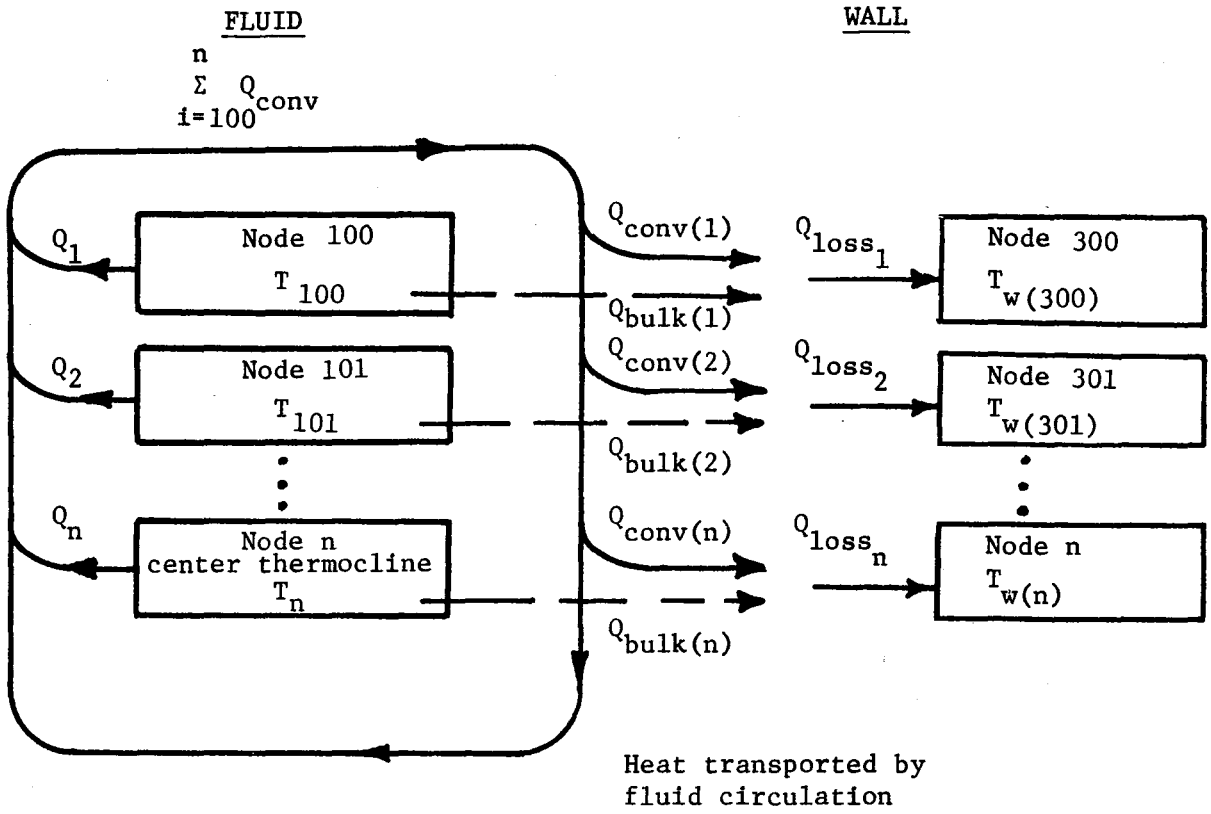

Q_{loss_i} is the heat loss due to the temperature difference between the fluid and wall and is calculated at node i

Q_{bulk} is a set ratio (R) of Q_{loss_i} at each node

Q_{conv} is the remainder (1-R) of Q_{loss_i} at each node

$\sum_{i=1}^{n} Q_{conv(i)}$ is sum of all heat at the wall from convection

Circulation flow rate is $\dot{\omega} = \frac{\Sigma Q_{conv}}{Cp \cdot (T_{100} - T_n)}$

Distribution of energy into circulation flow from bulk fluid is $Q_i = \dot{\omega} \cdot Cp \cdot (T_i - T_{i-1})$

Figure 4-3 Parametric Evaluation of Fluid Circulation

During storage discharge the transition zone moves up the tank from the bottom and the entire procedure is reversed. Each node is assigned the temperature of the node below it and node 299 is assigned a temperature of 561 K (550°F) to simulate incoming cold salt. Note this produces a step function in the transition zone temperature gradient because node 298 has a temperature of 577 K (580°F). This step function limits the thickness of the transition zone. As the temperature "bite" increases, the thickness of the transition zone decreases. What must be considered in setting the temperature "bites" for a storage system is the effect of the change in salt temperature on the rest of the power system. For example, the heat exchangers might not be able to accept salt with a temperature much below that of their normal inlet temperature, or the receiver might not be able to accept salt with a temperature much above that of its normal inlet temperature. This study made no effort to evaluate the effect of the temperature "bite" on other subsystems.

C. RESULTS

In an effort to validate the accuracy of the analytical model, results were compared with existing data. Martin Marietta had previously used a simplified analytical model to determine the effect of the temperature "bite" on the transition zone thickness. This simplified model had no wall effects and did not consider fluid circulation. Results of the present analytical model without wall effects and convection were compared with the previous simplified program as shown in Figure 4-4. There seems to be good agreement between the models. In the previous model, steady-state thickness was reached when the change in the temperature profile between cycles became small. The present computer model took too much computer time to run the 30 to 40 cycles necessary to obtain this type of temperature closure. Instead, steady-state conditions were determined by using initial temperature profiles that bounded the final result and running through charge/discharge cycles. This technique resulted in a better definition of the steady-state temperatures.

The only empirical data that could be obtained for comparison were those from the thermocline tank installed at the Centre National de la Recherche Scientifique (CNRS) facility in Odeillo, Font Romeu, France. This tank, shown in Figure 4-5, used oil as the working fluid. The test did not have continuous cycling so steady-state thermocline thickness could not be determined.

Figure 4-6 shows the temperature-time history of a hot charge of the French test tank. It seems that the flow rate was not constant and that some of the curves are not drawn consistently, but the data are sufficient for a comparison with the results of the analytical model.

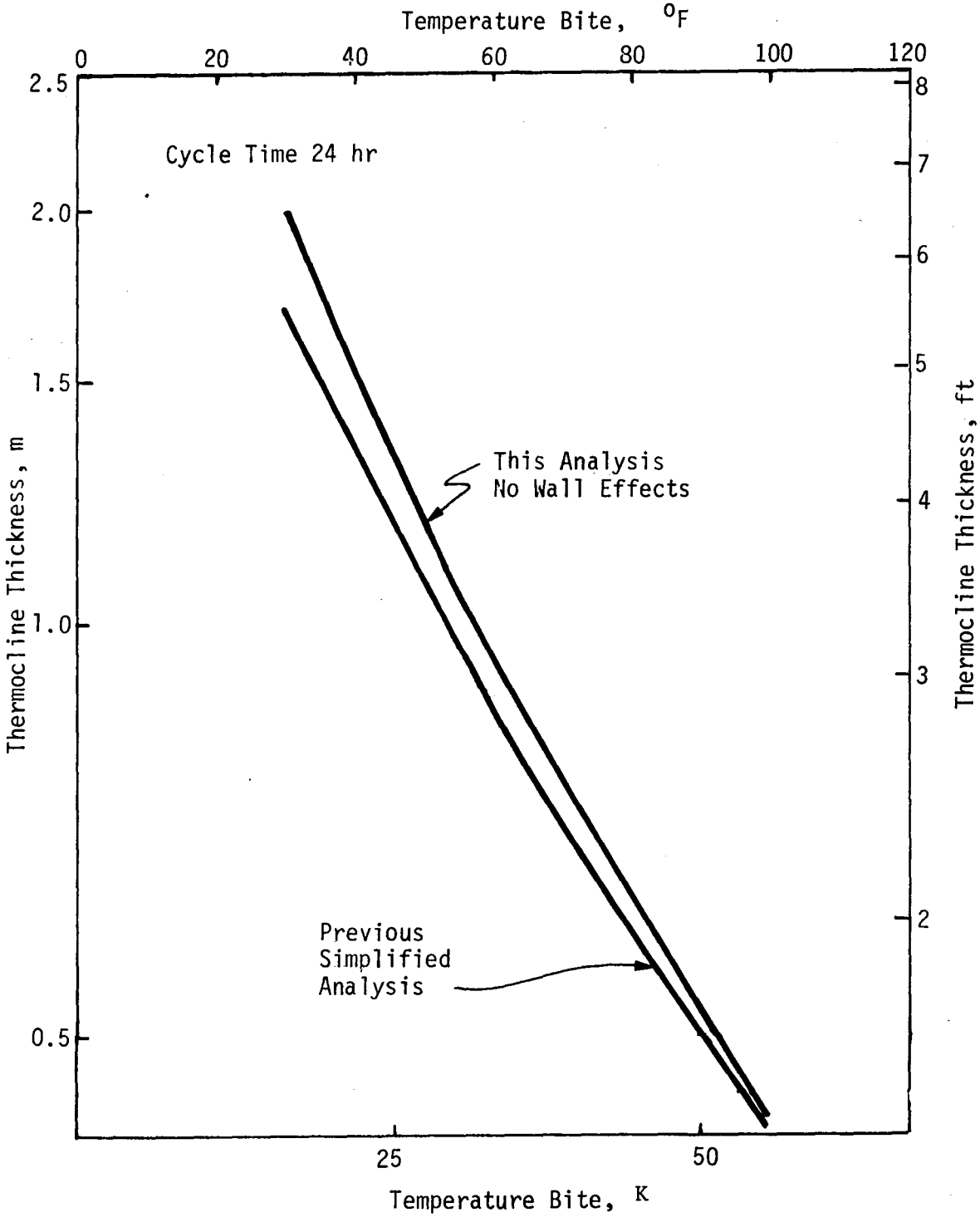

Figure 4-4 Comparison of Thermocline Models

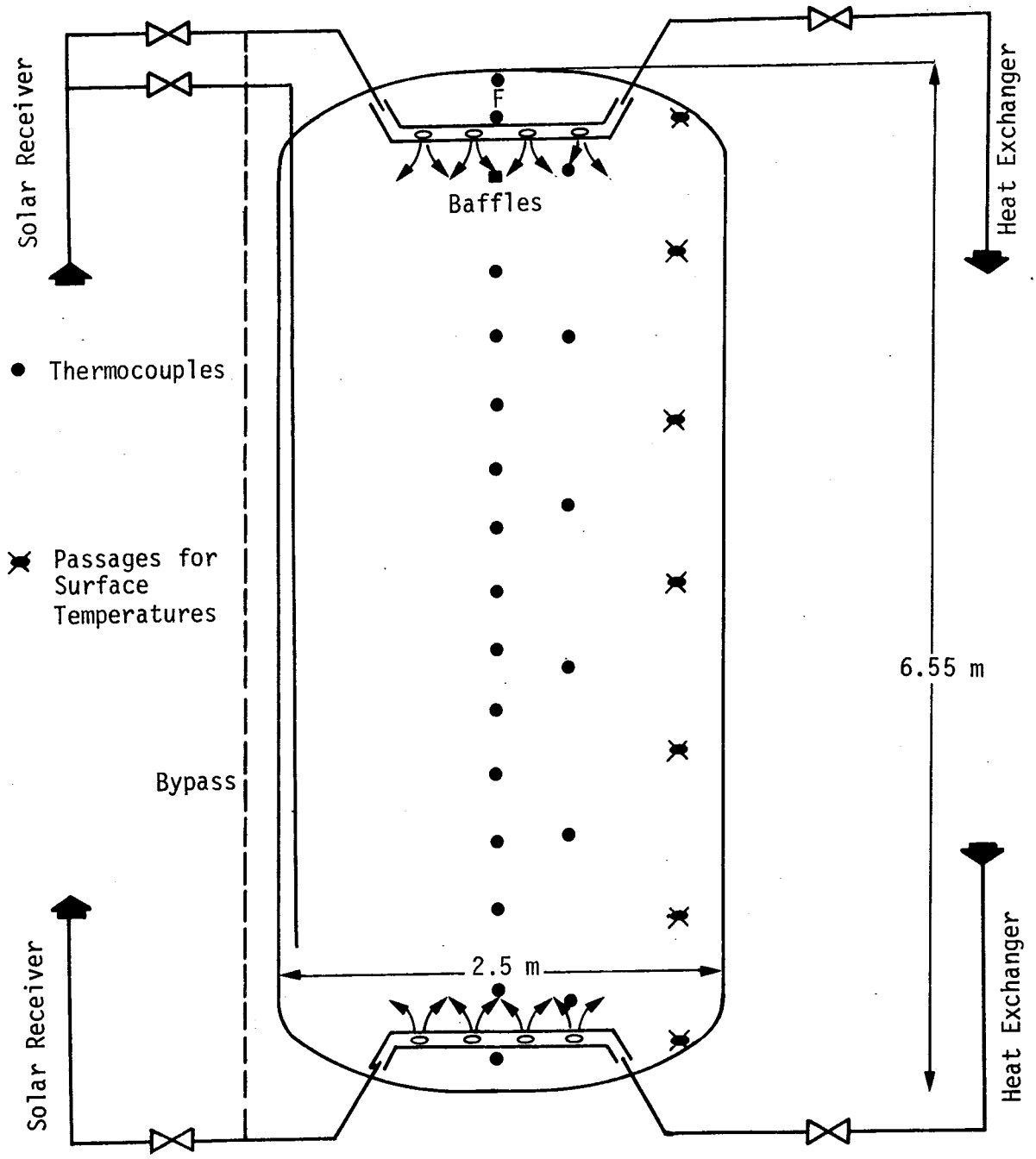

Figure 4-5 French Thermocline Tank

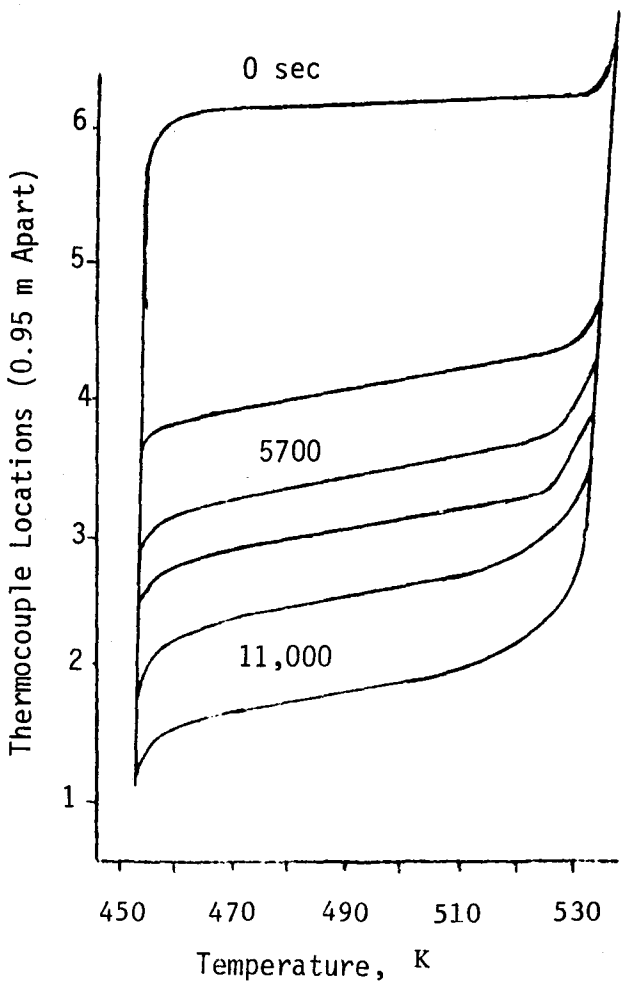

Figure 4-6 French Tank-Hot Charge

Figure 4-7 shows the high-temperature end of the 11,000-second temperature profile from the French test. It also shows the results of the analytical model of this test for different fluid circulation ratios, R. Figure 4-7 shows that as circulation increases (R decreases) the thickness of the transition zone decreases. From Figure 4-7 it was possible to determine that the best overall comparison of the data occurred with circulation ratios between 0.5 and 0.9. A ratio of 0.6 best matches the test data and was used as the baseline for the thermocline analysis of molten salt.

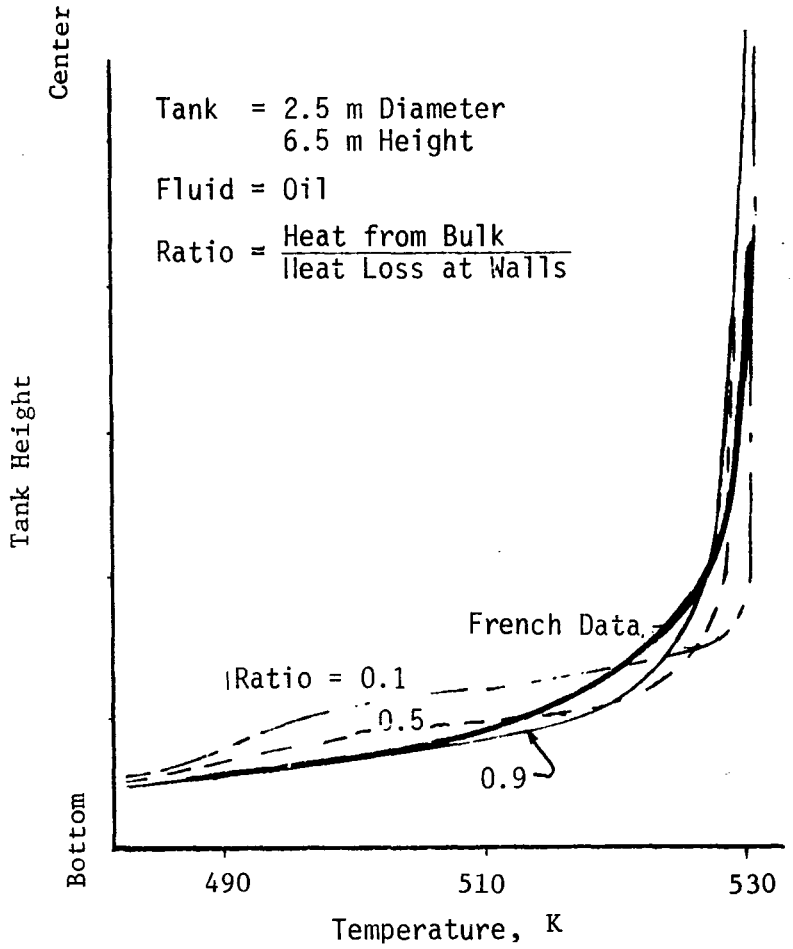

Figure 4-7 Analytical Comparison of French Tank

Analysis of a 45.7-m (150-ft) diameter tank 12.8-m (42-ft) high with molten salt at 839 to 561 K (1050 to 550°F) was made using a 12-hour charge with a 12-hour diacharge. The tank wall was constructed as shown in Figure 4-8, which is approximately the cost optimum configuration (as will be shown in Chapter VI). Figure 4-9 shows the effect of the temperature "bite" and circulation ratio on the thickness of the transition zone for this tank. Thickness is more sensitive to temperature "bite" than to circulation ratio. A transition zone thickness of 2.6 m (8.6 ft) was used for the system analyses. This assumed a circulation ratio of 0.6 and a temperature "bite" of 16.7 K (30°F), which is considered acceptable for a molten salt central receiver plant. If a metal liner is not used and the bricks are saturated with salt, the

greater heat loss and higher heat capacity of the walls results in a thickness of 8.9 m (29.2 ft). An 8-hour hold time with no inflow or outflow increases the transition zone thickness only 0.05 m (2 in).

Reducing the tank diameter to 22.9 m (75 ft) increased the thickness of the transition zone to 4.4 m (14.5 ft).

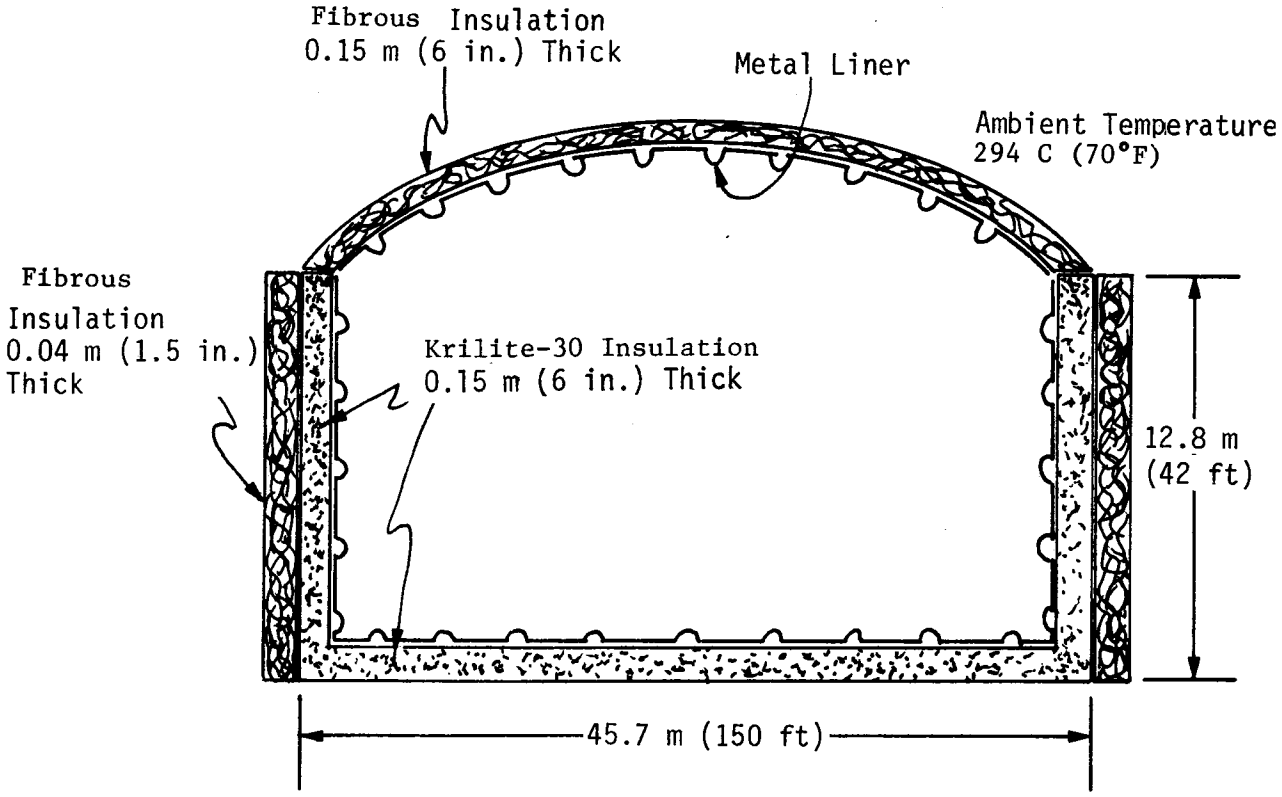

Figure 4-8 Tank Model Configuration

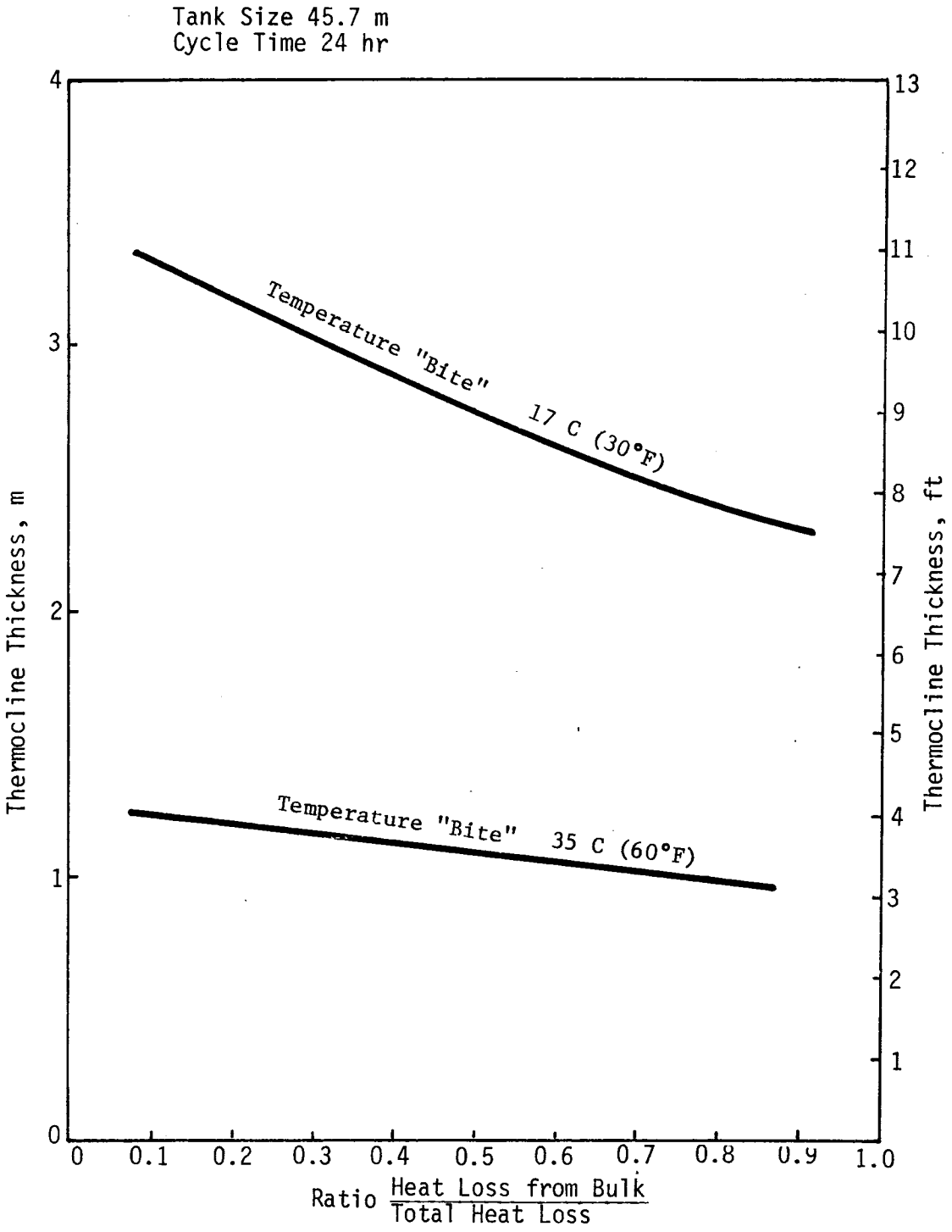

Figure 4-9 Thermocline Thickness vs Ratio and Bite

D. CONCLUSIONS

An increase in wall heat capacity significantly increases the thermocline thickness. Also the smaller the tank diameter, the greater the thermocline thickness. The most significant method of reducing the thermocline thickness is by using large temperature "bites." How the temperature "bites" affect the system operation or system efficiency was not evaluated in this program. Some temperature decrease to the turbine is permissible but the rate of change is important. An increase of salt temperature to the towers is permissible at off peak solar loads. It is obvious that changes in the control methods and temperature limits are necessary in a central receiver power system with thermocline storage. Quantitative evaluation of the effect on the system was not determined.

The most desirable condition for a thermocline tank is a large tank with wall insulation that has a low thermal conductance and low heat capacity. The largest temperature "bite" that is compatible with system operation should be used. The effect of thermocline thickness on storage system cost is discussed in Chapter VI.

This analysis indicated greater transition zone thickness than originally expected. It showed that scaling is not practical since the smaller tank greatly increases the thermocline thickness. To reduce the thermocline thickness, it would be necessary to take large temperature "bites" which would adversely affect the rest of the system.

It is also realized that thermal cycling of the wall will cause expansion and contraction of the tank shell and insulation attachment studs thus increasing the stress. This thermal cycling will also be detrimental to the internal insulation material. If a metal liner is not used and the bricks are saturated with salt, the greater heat loss and higher heat capacity of the walls result in a thickness of 8.9 m (29.2 ft). An 8-hour hold time with no inflow or outflow increases the transition zone thickness only 0.05 m (2 in.).

V. TANK DESIGN

A. DESIGN CONSTRAINTS

The tank structural material selected was A-516 grade 70 carbon steel, which is compatible with molten salt up to 572 K (750°F). The working stress of the material is 121,000 kPa (17,500 psi) between ambient temperature and 616 K (650°F). The cylindrical tanks were designed to the API 650 code and the spherical tanks were designed to the ASME pressure vessel code Section VIII. There are no codes that specifically apply to the design of hot, unpressurized vessels. However, since construction fabricators only design and build to codes, these tanks were designed to the most applicable codes. Since the API applies to unpressurized cylindrical tanks, it was used even though the design temperature exceeds by 28 K (50°F) the maximum permitted under the code. Because the API code does not apply to spherical tanks, they were designed to the ASME code even though the tanks are not pressurized.

To eliminate the need for ppostweld heat treatment, the cylindrical tanks could not exceed a maximum shell thickness of 0.478 m (1.75 in.) according to the API code, and the ASME code dictated a maximum of 0.410 m (1.50 in.).

One constraint used in the tank design was to set the maximum soil bearing load to 34.5 kPa (5000 lbf/ft^2). This limits the tank height to 12.8 m (42.0 ft). Since the tank site was not defined, this bearing strength was used because it is considered typical.

The feasibility of placing the hot tank on the ground was investigated. An extensive telephone survey was made of 18 companies, federal bureaus, and college professors. The conclusion was that this is a new area and that no data exist for soil properties or behavior at these elevated temperatures. As part of the evaluation process, a statement of work was issued to D'Appolonia Consulting Engineers, Inc.; Geomechanics, Inc.; Excavation Engineering and Earth Mechanics Institute, Colorado School of Mines; and Chen and Associates, Inc. From the response of each organization it was concluded that the following soil properties at elevated temperatures need to be determined before direct soil contact of the storage tanks can be considered:

1) Bearing load;
2) Thermal expansion;
3) Deformation;
4) Creep;
5) Cohesion;
6) Shear.

Another concern is that of water in the soil. If the water vapor pressure in the ground exceeds the lithostatic head of the soil, the soil will be lifted. The rate of heating of the soil and the rate at which the water is added to the hot soil are important. Experience has shown that rapid heating of loose soil with moisture in it can produce violent lifting of

the soil. If the hot tanks are placed on the ground, whether they are insulated on the bottom or not, a large volume of water beneath the tank will eventually exceed the boiling point. It is not known what happens to the initial moisture in the soil or what happens when water is added to surface or subsurface penetration.

Evaluation of existing hot tanks in current usage showed that phthalic anhydride tanks held at 422 K (300°F) are supported on vermiculite concrete set on ordinary concrete pads. Hot asphalt Exxon tanks maintained at 561 K (550°F) are insulated from the soil with coolant loops placed under the insulated tank bottom. Present-day practices place furnaces above the ground so they can be cooled. Heaving and cracking problems have occurred with older furnaces that have been placed on the ground.

Placing the tank on the ground also requires the tank bottom to be stainless steel because it will eventually reach the temperature of the molten salt. This creates problems with the thermal expansion difference between the tank bottom and sides.

It was concluded that although it may be possible to place the hot tank on the ground, the data available are not sufficient to engineer this type of foundation. This study therefore assumed the use of a cooled foundation.

B. TANK DESIGN

A tank design and cost estimate was provided by Chicago Bridge and Iron for both spherical and cylindrical tanks. The spheres were designed with the A 516 grade 70 carbon steel for temperatures to 588 K (600°F). Cold salt density (1906 kgf/m^3 (119 lb/ft^3)) was used for the design to allow for the possibility of filling the hot tank with cold salt (e.g., during repair of a cold tank). Although no ullage pressure was assumed in the vessels, the tanks were designed to the ASME pressure vessel code Section VIII since this was the most applicable standard. Figure 5-1 shows the spherical tank with the support skirt design. The skirt height is limited to 4.7 m (15 ft) to prevent overturn moment in a zone 3 earthquake. Costs for two tank sizes are tabulated below. They are for the shell cost and do not include insulation, walkway, painting, or corrosion allowance, but do include fabrication, radiographic inspection, and postweld heat treatment, as required.

No. Tanks	Spherical Tank Diameter, m (ft)	Total Volume, m^3	Total Cost
1	33.5 (110)	19,734	$4,575,000
2	26.5 (87)	19,527	$3,565,000

The cost of the large tank is a million dollars greater because of the need to postheat-treat the welds. This is necessary because the tank walls exceed 0.041 m (1.5 in.) in thickness. This cost should be

DESIGN: ATMOSPHERIC PRESSURE
SHELL DESIGN TEMPERATURE: 316 K (600°F)
MATERIAL: SA-516 GR. 70
CORROSION ALLOWANCE: 0.0 m
CODE: ASME SECTION VIII
MAX. SPECIFIC GRAVITY: 1.907
EARTHQUAKE: ZONE 3
STRESS RELIEVE: AS REQUIRED

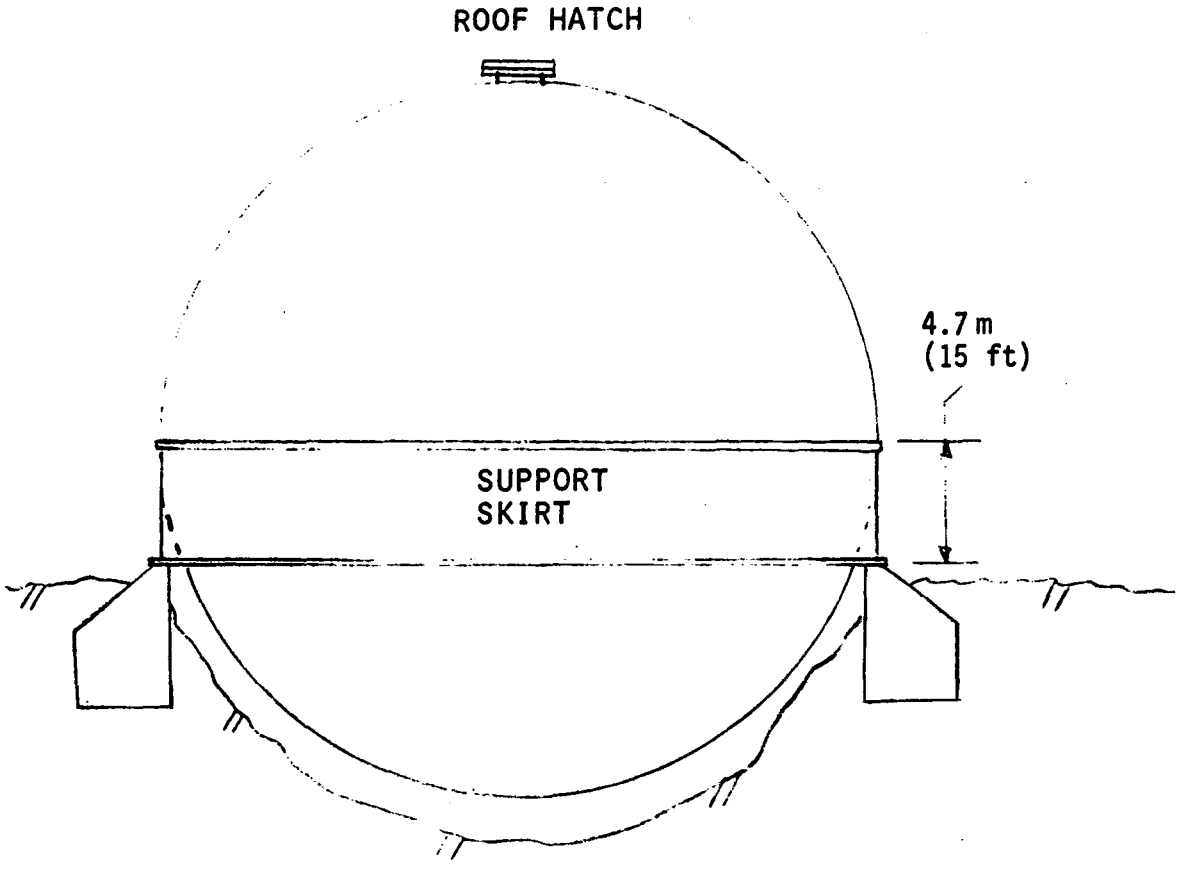

Figure 5-1 Spherical Tank Design

contrasted with that of a 316 stainless steel tank 33.5 m (110 ft) in diameter constructed for 839 K (1050°F) service, or $23,000,000. Most of the additional cost for the stainless steel tank is for fabrication and stress relief of the walls, which are approximately 0.1 m (4 in.) thick.

Two sizes of cylindrical tanks were designed using the API-650 Appendix D code without the cost of code inspection.

No. Tanks	Cylindrical Tank Dimensions	Total Volume m^3	Total Cost
1	40.4 m dia x 12.8 m high (132.5 ft x 42 ft)	16,399	$1,000,000
2	28.4 dia x 12.8 m high (94 ft x 42 ft)	16,507	$1,080,000

These two tank configurations have approximately the same volume as the spherical tanks but are much less expensive. The general design of the cylindrical tank is shown in Figure 5-2.

Cylindrical and spherical tank costs as a function of size are discussed in Chapter VI (Storage System Parametric Analysis).

The knuckle between the tank wall and floor shown in Figure 5-3 was designed to reduce the stresses at this junction caused by thermal expansions. The maximum permissible thermal gradient across the knuckle is 39 K (70°F) when the tank is filled with salt. The only time a gradient would occur across the knuckle is during initial tank filling. However, without the hydrostatic pressure of a full tank of molten salt this does not present a problem.

The tank design by Badger Energy Inc. is shown in Figure 5-4. This cylindrical tank design has the insulation and liner necessary for a hot 839 K (1050°F) tank. Internal and external insulation is used to maintain the tank shell temperature at 589 K (600°F).

The internal wall insulation is 0.23 m (9 in.) insulating fire brick and the external insulation is 0.08 m (3 in.) fibrous insulation with lagging. The roof has 0.15 m (6-in.) fibrous insulation on top of the liner and 0.15-m (6-in.) block insulation on top of the tank. The internal floor insulation is 0.25 m (10 in.) of insulating brick.

It should be noted that the tank shell temperature should be uniform throughout the roof, wall, and floor. If the tank were placed on the ground without cooling, the temperature of the shell floor would increase to the salt temperature. This would require the floor to be constructed of stainless steel with special expansion joints to accomodate the large thermal expansion of the tank floor and would complicate tank design and increase tank cost.

DESIGN: ATMOSPHERIC PRESSURE

SHELL DESIGN TEMPERATURE: 589 K (600°F)

MATERIAL: SA-516, GR. 70

CORROSION ALLOWANCE: .003m (.125 in.)

CODE: API-650 CONSTRUCTION, NO STAMP.

MAX. SPECIFIC GRAVITY (COLD) 1.907

EARTHQUAKE: ZONE 3

X-RAY INSPECTION AS REQUIRED

STRESS RELIEVING: NOT REQUIRED

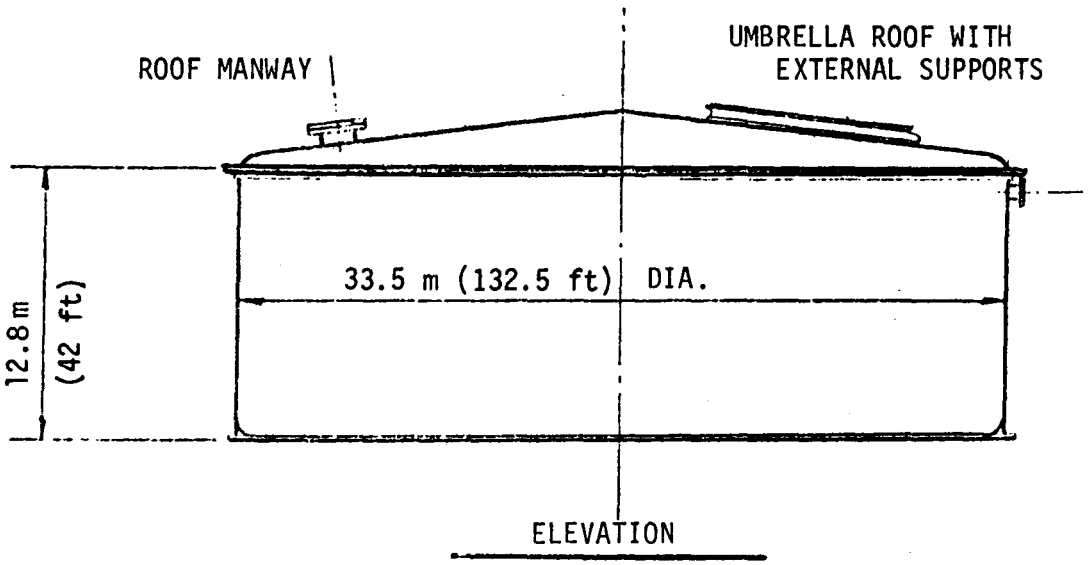

Figure 5-2 Cylindrical Tank Design

NOTE: THIS CONFIGURATION ALLOWS FOR EXPANSION AND RELIEVES DISCONTINUITY STRESSES.

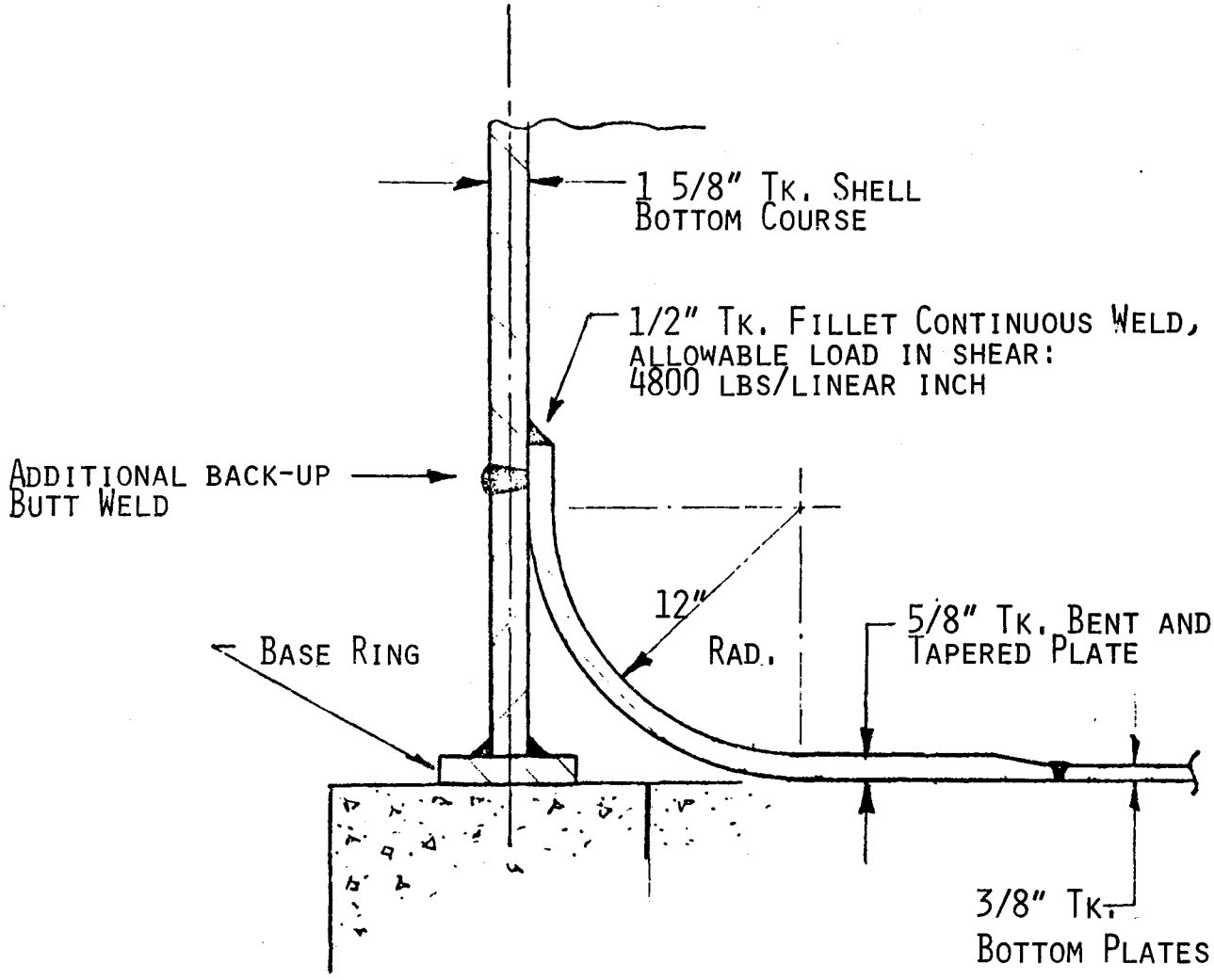

Figure 5-3 Knuckle Design

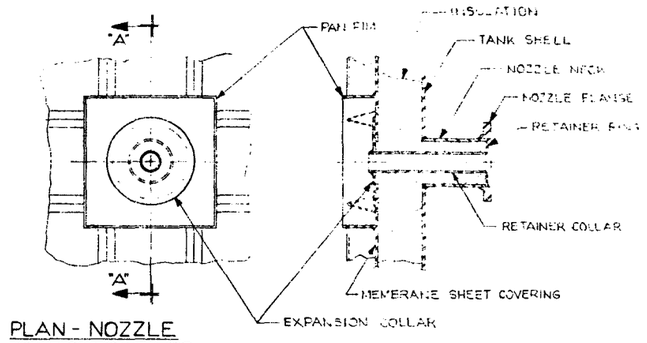

PLAN - NOZZLE ATTACHMENT TO MEMBRANE SHEET

SECTION "A-A"

HOT STORAGE TANK ONLY

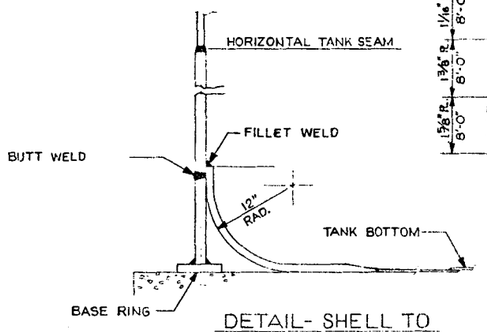

DETAIL - SHELL TO BOTTOM JUNCTION

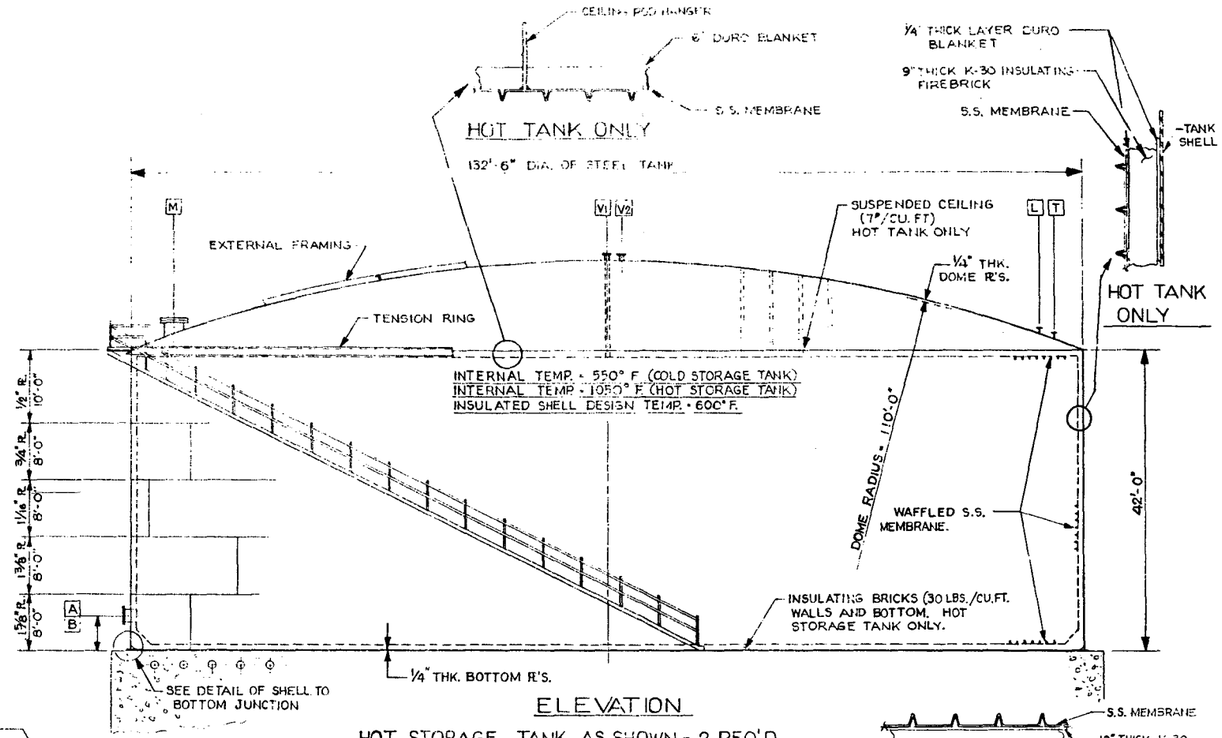

ELEVATION

HOT STORAGE TANK AS SHOWN - 2 REQ'D.
COLD STORAGE TANK AS SHOWN, BUT WITHOUT INTERNAL REFRACTORY AND S.S. MEMBRANE

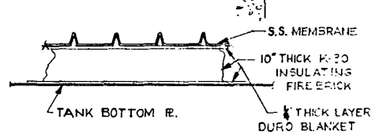

HOT TANK ONLY

MATERIALS

SHELL		SA-515 GR. 70
HEADS		SA-515 GR. 70
CLAD OR LINING		NONE
SUPPORT FOUNDATION		CONCRETE W/ COOLING WATER PIPES
NOZZLES	FLANGES	SA-105 OR SA-181 GR. I OR II
	NECKS	SA-106 GR. B
MANHOLES AND/OR HANDHOLES	FLANGES	SA-283 GR. C
	NECKS	SA-106 GR. B
	COVERS	SA-283 GR. C
GASKETS	NOZZLES	
	MANHOLES	1/8" THK. COMPRESSED ASBESTOS
	INTERNALS	
BOLTING INTERNAL	BOLTS	
	NUTS	
BOLTING EXTERNAL	BOLTS	SA-307 GR. B
	NUTS	SA-307 GR. B
INTERNALS	PIPE	SA-106 GR. B
	PLATE	SA-[illegible] TYPE 316 (WELDMATE)
	STRUCT	
EXTERNALS	PLATE	SA-283 GR. C
	STRUCT	SA-36
REINFORCING PADS		SA-515 GR. 70

DESIGN DATA

ZONE		DESIGN PRESSURE	DESIGN TEMP	OPERATING PRESSURE	OPERATING TEMP	
		ATMOS	600°F	ATMOS	550°F	
SEISMIC ZONE		0		SEISM. COEFF.		
WIND PRESSURES	ZONE					
	ROUND	30		25		
	FLAT	35		30		
MAWP(INT) AT DESIGN TEMP & CORR		—		LIMITED BY	—	
MAWP(EXT) AT DESIGN TEMP & CORR		—		LIMITED BY	—	
MAWP (NEW & COLD)		—		LIMITED BY	—	
CORR. ALLOW	SHELL, HEADS & CONNECTIONS	NONE				
	INTERNALS - FIXED					
	INTERNALS - REMOVABLE					
RADIOGRAPHING		SPOT				
JOINT EFFICIENCY		85%				
POST WELD HEAT TREATMENT		NOT REQ'D				
ALLOWABLE STRESS (DESIGN TEMP.)				V2	1	CYCLE VENT
ALLOWABLE STRESS (NEW & COLD)				V1	1	CYCLE VENT
CONSTRUCTION		AS STAMPED ON NAMEPLATE				
CODE STAMPING				T	1	CYCLE TEMPERATURE
INSPECTION BY		[illegible] AND STATE OF WISCONSIN				
PAINTING		[illegible]				
INSULATION		[illegible]				
SHIPPING WEIGHT	SHELL, HEADS ETC			M	1	[illegible]
	REMOVABLE INTERNALS			L	1	[illegible]
OPERATING WEIGHT						
SPECIFIC GRAV. [illegible]						
SPECIFIC GRAV. [illegible]						
MAX. LOAD ON FOUNDATION				B		
				A		
HYDROSTATIC TEST (BASED ON WATER HEAD THICKNESS IN S.T.M.)	PRESSURE	PRESS. REMAINED ON	WITNESSED BY	CONN.	SIZE	REMARKS
HOR. ZONTAL						
VERTICAL						

LEVEL OF CONNECTIONS

GENERAL NOTES

1. HEADS TO BE DOME OR 110'-0"
2. NOZZLE BOLT HOLES TO STRADDLE NATURAL ℄ OF VESSEL UNLESS OTHERWISE NOTED ON DRAWING
3. CONNECTIONS TO BE PROTECTED FOR SHIPMENT WITH COVER PLATES OR PIPE PLUGS
4. NOZZLES SHALL BE REINFORCED FOR TOTAL THICKNESS INCLUDING CORR. ALLOW AT LIMITING PRESS. AND TEST TEMP. OR FOR CORR. THICKNESS AT DESIGN CONDITIONS, WHICHEVER GOVERNS
5. PROJECTIONS ARE FROM OUTSIDE OF SHELL TO FINISHED FACE OF FLANGE. FOR HEAD CONNECTIONS THE PROJECTIONS ARE FROM THE TANGENT LINE
6. TO BE USED BY BADGER'S MODEL SHOP.
7. RADIAL PROJECTIONS ARE MEASURED FROM CENTER OF VESSEL. FOR HEAD CONNECTIONS THE PROJECTIONS ARE FROM THE TANGENT LINE
8. ALL ELEVATIONS ARE FROM GRADE AT ——— ———
9. MANHOLE COMPLETE WITH AND BLIND FLANGE, GASKET, BOLTING AND DAVIT

Figure 5-4 Tank Design

c. FOUNDATION DESIGN

Two methods of cooling the foundation were considered. One concept was to support the tank above the ground to allow natural convection. The second concept is to place the foundation on a water-cooled concrete slab. The cooling water available for the turbine steam condenser could be used for the tank cooling.

The foundation cooling using natural convection is shown in Figure 5-5. In this design the tank rests on insulating concrete supported by a 0.03-m (1-in.) thick steel plate. The plate is supported by W12 x 22 steel beams spaced on 0.76-m (30-in.) centers, which are supported on a concrete slab 0.76-m (30-in.) thick. This allows air to circulate underneath the tank (this is a passive system). In this configuration it may be necessary to add chimneys at the side of the tank to achieve adequate airflow. The cost of this foundation system is approximately $\$678/m^2$ ($\$63/ft^2$).

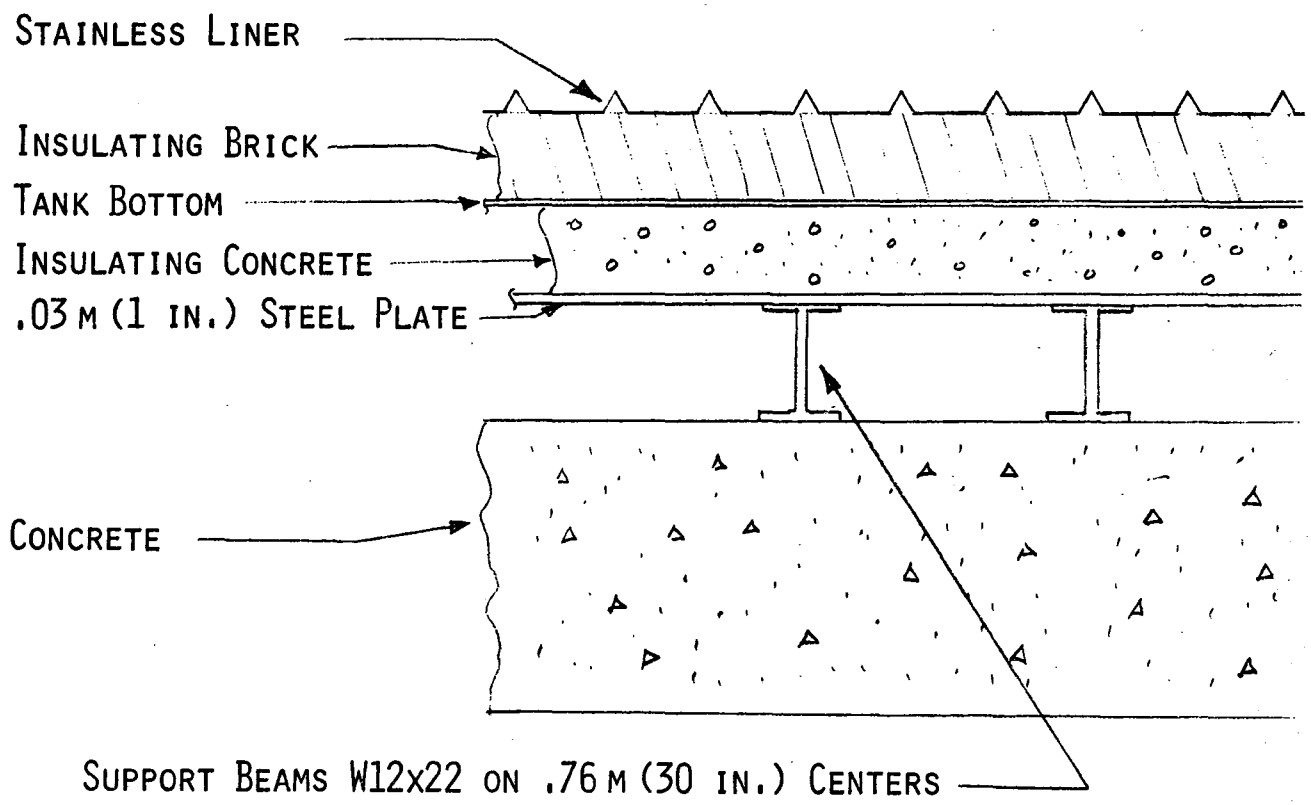

COST = $\$678/M^2$ ($\$63/FT^2$)

Figure 5-5 Foundation Design - Natural Convection

An active cooling system is achieved with cooling coils placed in the support concrete slab as shown in Figure 5-6. The thermal resistance of the internal insulating brick is balanced with the thermal resistance of the insulating concrete so the tank bottom has the same temperature as the walls.

The cooling coils are 0.08-m (3-in.) diameter pipes set on 0.30 m (12-in.) centers. The concrete slab is 0.30-m (12-in.) thick and has an 0.61-m (24-in.) ring wall under the tank wall. A sand base is used underneath the concrete slab. The cost of this foundation system is $312/m^2$ ($29/ft^2$) including cost of the pumps and water lines.

Selection of the active cooling system for the foundation was predicated on several factors. In addition to its lower cost, the active system is not sensitive to wind conditions as the passive system is. No empirical data are available to calculate the heat transfer coefficient for the passive configuration. It is also difficult to maintain a uniform temperature across the tank bottom, which is important to limiting the stress at the knuckle between the tank floor and wall.

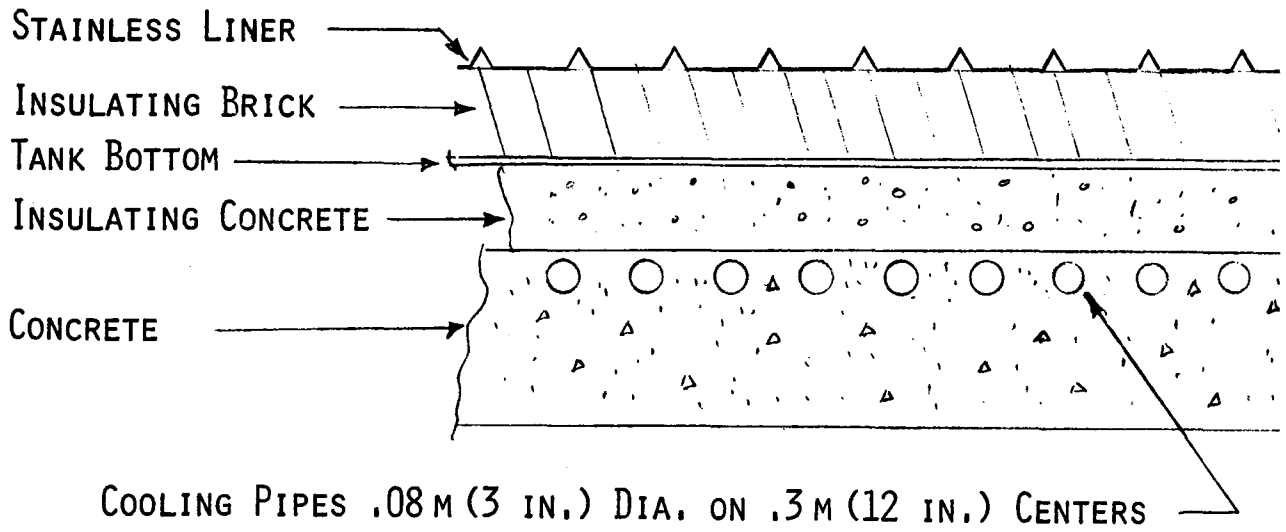

COST = $312/M^2$ ($29/FT^2$)

Figure 5-6 Foundation Design - Cooling Coils

D. INSULATION DESIGN

Since the material tests showed salt attack and degradation of all the insulation materials, it was deemed necessary to protect the internal insulation from the salt with a sealed metal liner. A commercially available thermal expansion liner made by Technigaz was selected because of its unique design and exceptional reliability. Technigaz has used the design extensively for about 15 years to line liquid natural gas (LNG) tanks (such as the one shown in Figure 5-7) in ships. The stainless steel liner is made of orthogonally folded sheets to permit the expansion and contraction caused by thermal and pressure loads. The expansion folds can be seen in the foreground. The sheets are welded to make a sealed membrane inside the tank. The cryogenic LNG tanks experience numerous thermal cycles in addition to the pressure cycling caused by sloshing of the liquid and flexing of the tanker. Despite this severe service, no leaks have ever been detected on any of the tankers. These liners have also been used in land-based applications up to 700 K (800°F) and 4000 kPa (580 psi). The only development required for molten salt applications is that needed to select a liner material and to optimize the design (e.g., to select the proper spacing of the expansion folds).

The decision to use a liner resulted not only from the necessity to protect the internal insulation but also from the cost optimization of the insulation material and the tank heat losses. Table 5-1 presents the optimum insulation cost for dry (not salt-saturated) insulation. The total cost includes the cost of the insulation material and installation, the cost of the liner, and the cost of the extra heliostats and larger receiver necessary to offset the heat loss through the insulation. Advertised values of material thermal conductivity were used. Insulation costs were provided by vendors, as was the liner material and installation cost of $293/m^2$ ($27.21/ft^2$). A heliostat cost of $0.73/watt ($0.21/Btu/h) was used and is based on the predicted performance of the 300-MWe Advanced Central Receiver Power System Phase I design (Martin Marietta final report EG-77-C-03-1724).

Table 5-2 shows the optimum insulation cost of various salt-saturated insulations. The thermal conductivity at the salt-saturated material was taken from actual measured data from the test program and from estimated values. The test program showed an increase in thermal conductivity that was somewhat dependent on the material's original density.

Note that the dry insulation costs, which include the added cost of a liner, are generally less than those of the wet insulation. This is because the thermal conductivity of the dry insulation is so much lower than that of the salt-saturated insulation that less insulation is needed and fewer heliostats must be added to compensate for the heat losses. Thus it is actually cost effective to use a liner.

The dry Duraboard fibrous board and the dry Krilite 30 insulating brick were the lease expensive of all the materials tested.

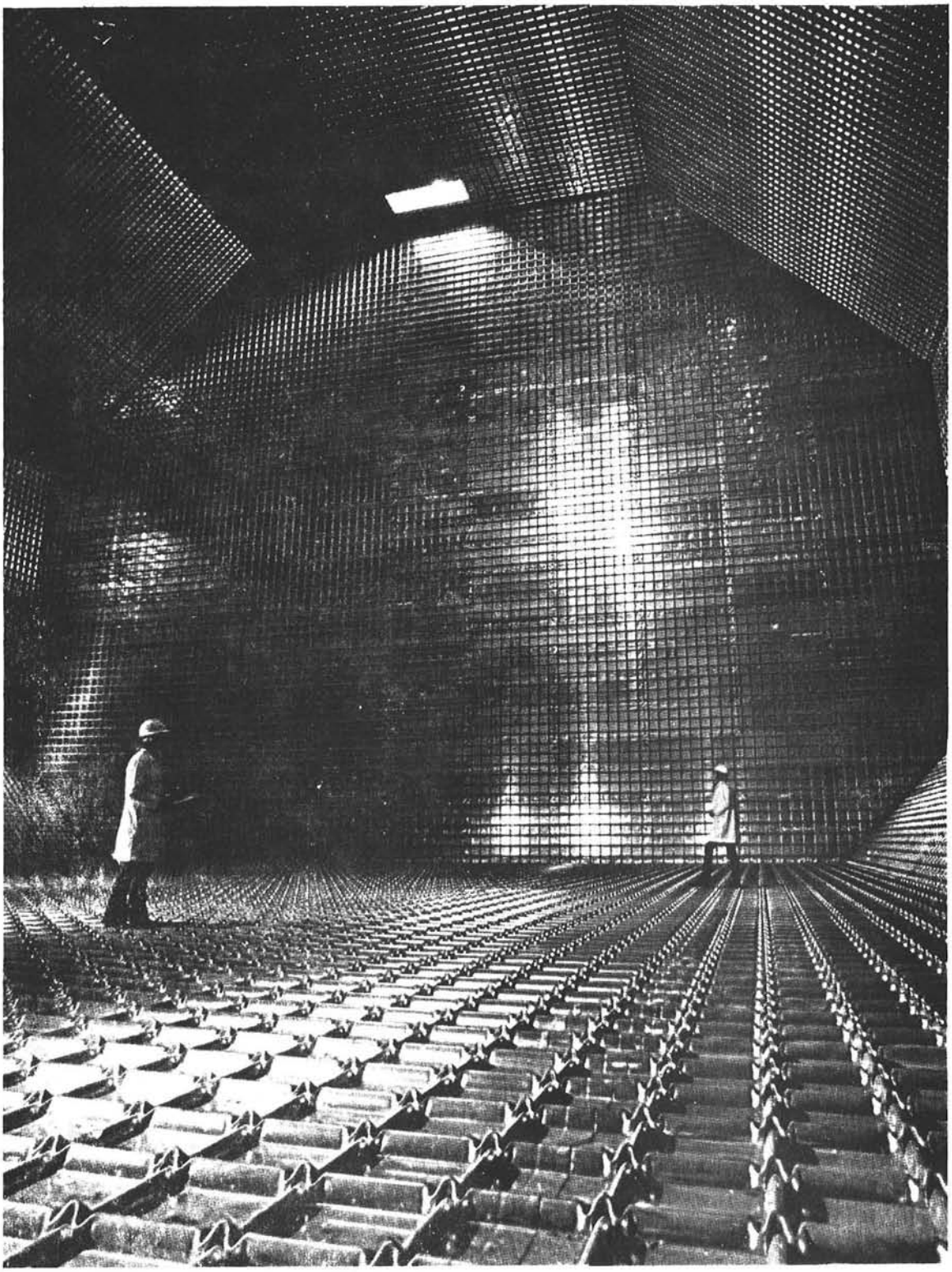

Figure 5-7 Technigaz Liner in Liquid Natural Gas Tanker

Table 5-1 Dry Insulation Cost Optimization

MATERIAL	THERMAL CONDUCTIVITY W/M-K	MATERIAL & INSTALLATION COST $/M^3	OPTIMUM THICKNESS M	HELIOSTAT COST $/M^2	TOTAL COST $/M^2
DURABOARD	.09	1404	.14	199	691
HI STRENGTH	.61	1375	.38	521	1335
IRC 24LI	.69	528	.65	346	984
JM-2100	.83	525	.72	378	1048
JM-2800	.59	840	.48	402	1096
K-30	.31	749	.37	256	844
KOA-TAB-95	1.90	2246	.53	1180	2654
KRILITE-30	.24	722	.33	239	771
KRILITE-60	.40	778	.41	318	928
KRIMAX	1.33	866	.71	613	1519
LO-ERODE	1.49	2572	.43	1117	2527
MAXIMUL	1.33	663	.81	537	1367
PC-12	.24	2329	.18	429	1151
VISIL	.93	1548	.44	687	1667
80-D	3.34	1125	.93	1049	2390

Table 5-2 Wet Insulation Cost Optimization

MATERIAL	THERMAL CONDUCTIVITY W/M-K	MATERIAL & INSTALLATION COST $/M^3	OPTIMUM THICKNESS M	HELIOSTAT COST $/M^2	TOTAL COST $/M^2
DURABOARD	1.30	1404	.55	771	1543
HI STRENGTH	2.08	1375	.70	964	1929
IRC 24LI	1.18	528	.85	451	902
JM-2100	2.25	525	1.18	621	1243
JM-2800	1.99	840	.88	739	1477
K-30	1.90	799	.91	682	1363
KOA-TAB-95	2.60	2246	.61	1379	2758
KRILITE-30	1.76	722	.89	646	1291
KRILITE-60	1.38	778	.76	592	1184
KRIMAX	1.82	866	.83	716	1432
LO-ERODE	2.25	2572	.53	1373	2747
MAXIMUL	1.82	663	.94	627	1254
PC-12	.24	2329	.18	429	1151
VISIL	2.08	1548	.66	1024	2049
80-D	4.12	1125	1.09	1230	2460

Another consideration in material selection was the material's performance if a leak occurred and the insulation saturated with salt. In this case the material can be selected according to the increased thermal conductivity, compatibility with molten salt, and cost. The compatibility of material with molten salt in decreasing order was firebrick, foamglass, insulating brick, castable and board material. It was not feasible to use the boards wet with salt because they lost their compressive strength.

An insulating brick and foamglass were selected as best satisfying all requirements. The insulating brick Krilite 30 was selected as the baseline for this study because of its cost and compatibility. The foamglass PC-12 offers a significantly better margin with a large salt leak since it does not wet and the salt attack is slow. It protects the carbon steel shell from a large temperature increase because its thermal conductivity increases slowly as the surface material is attacked. This material would, however, add to the system cost.

The external insulation and the internal roof insulation were of a glass fiber blanket material. Due to its low thermal conductivity and cost, glass fiber was a cost effective insulation. For the exterior of the roof, a load-bearing block insulation was selected to allow personnel access during construction and inspection.

For spherical tanks the foamglass was used for cost trade-offs since it is a material that can be readily attached to the internal surface. The spherical tanks were externally insulated with glass fiber insulations.

All external insulation is covered by aluminum jacketing for weatherproofing.

The method of attaching the internal insulation to the tank is shown in Figure 5.8. This is a conceptual design. The liner can be directly attached to the tank wall, which also supports the brick; or the liner can be attached to the bricks, which are attached to the wall. Since the brick insulation is attached to the wall it moves with the wall. Fibrous blanket insulation was placed on both sides of the internal insulation material to protect both the liner and tank wall from abrasion during thermal expansion, etc. The fibrous insulation is crushed to a thin layer. A metal shelf at the bottom of the wall supports the insulation bricks above the knuckle connecting the tank wall and floor. Fibrous insulation insulates the knuckle area below the shelf.

The roof liner is supported horizontally from the umbrella roof. Thus the liner design for the tank ceiling is identical to that of the floor.

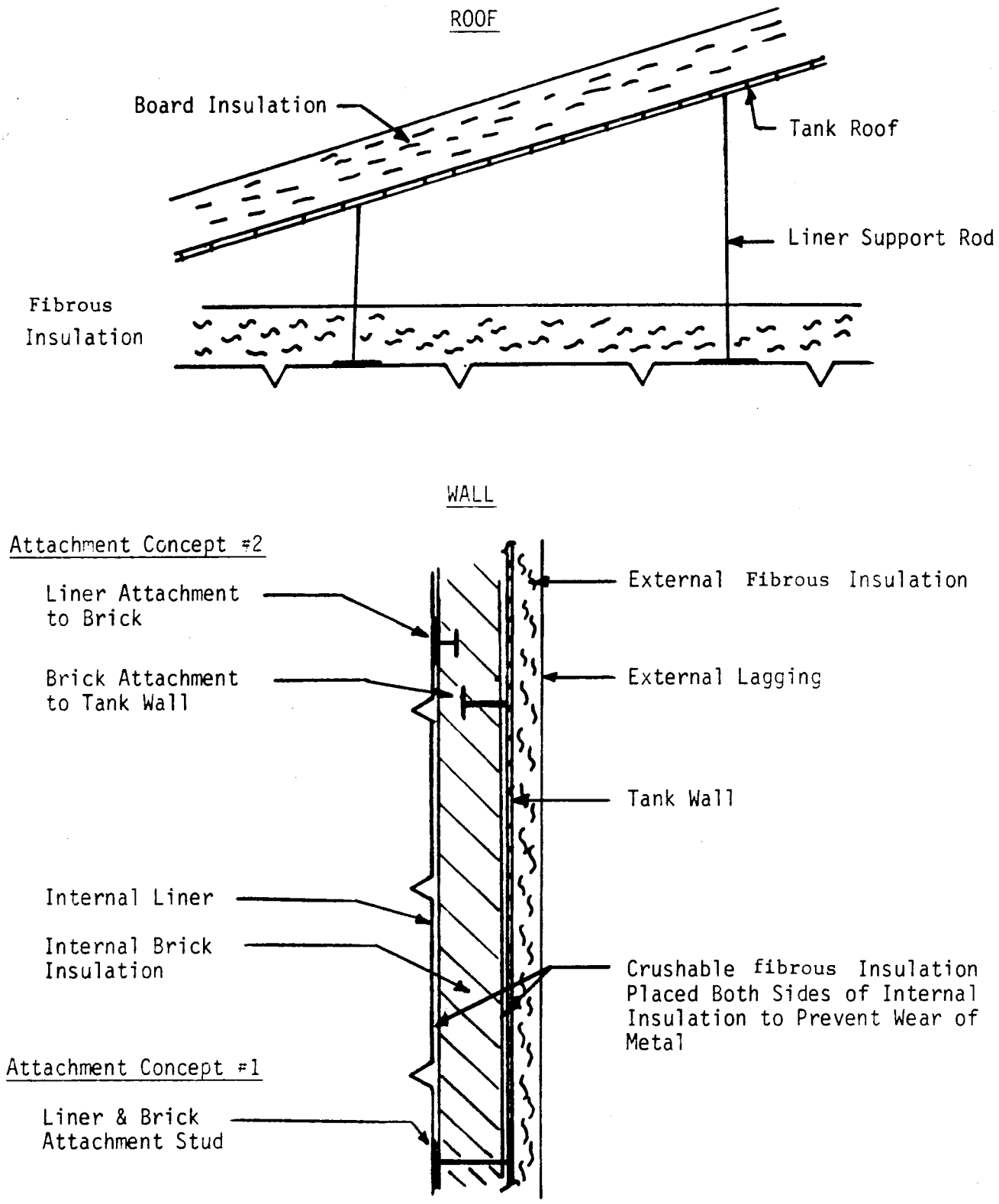

Figure 5-8 Insulation Attachment

VI. STORAGE SYSTEM OPTIMIZATION

A. STORAGE SYSTEM CONCEPTS

Three different concepts were considered for the molten salt storage system--thermocline, where the high- and low-temperature salts are stored stratified in the same tank; dual tank, where the hot and cold salts are stored in separate tanks; and cascade, where the tanks are used interchangeably as hot or cold tanks, with one tank volume always empty. These systems and their operation are described in more detail.

1. Thermocline

Figure 6-1 shows a typical thermocline storage system. Cold salt is pumped from the bottom of the storage tanks and heated up by the receivers. The hot salt can then be pumped into the tops of the storage tanks, or via the hot salt pump sumps to the salt/steam heat exchangers, or both. When the receivers are not operating, the hot salt is pumped from the tops of the tanks to the heat exchangers. Cold salt returning from the heat exchangers flows into the bottom of the tanks.

The thermocline storage tanks are always full; only the interface between the hot and cold salt (the transistion zone) moves up and down the tank. Thus the tank if full of hot salt when the interface is at the bottom and full of cold salt when it is at the top. Because of this, the thermocline system requires minimum storage tankage. However, it may also require an additional drain tank in case one of the storage tanks must be emptied for maintenance or repair. Since the drain tank does not have to be internally insulated, it can be relatively inexpensive.

There are two drawbacks to a thermocline storage system. First, because the hot/cold dividing line moves up and down the tank during charge and discharge, the refractory internal insulation is exposed to a large thermal shock twice a day. This cycling and shock could crack and disintegrate the relatively brittle refractory (this possibility would have to be investigated more closely before such a tank could be built). Second, the transition zone has a finite thickness and that thickness varies with the rate of storage usage. The additional salt needed (the transition zone salt is unusable) and the larger tanks needed to contain it increase the total system cost.

2. Dual Tank

The dual-tank system shown in Figure 6-2 operates essentially the same as the thermocline system except that the cold salt is pumped to and from separate cold tanks (not internally insulated) rather than from the bottoms of the thermocline tanks. Hot salt is pumped to and from the bottom of the hot tanks. Because hot and cold salt are stored in

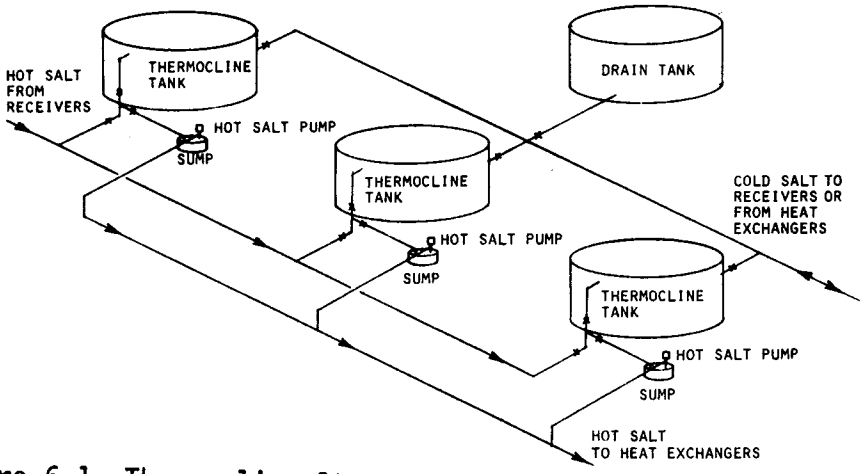

Figure 6-1 Thermocline Storage System Schematic

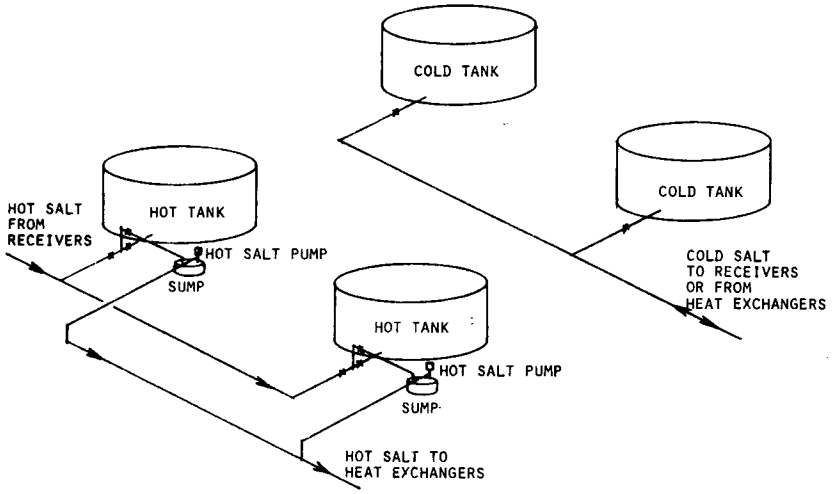

Figure 6-2 Dual Tank Storage System Schematic

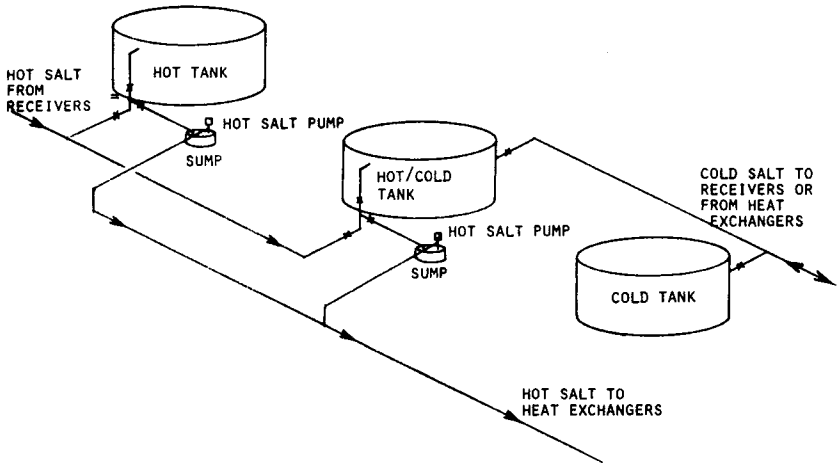

Figure 6-3 Cascade Storage System Schematic

separate tanks and because residual salt is left in each tank to maintain the tank temperature when it is "empty," this is the simplest of the three systems to design and build and the one with the least technical risk. The storage tank volume for a dual-tank system is nearly twice that of a thermocline system because both hot and cold tanks must each be able to hold the entire volume of salt. However, a drain tank is not required.

3. Cascade

A cascade system is essentially a dual-tank system with only one cold tank. Referring to Figure 6-3, storage charging begins with tank 1 empty and cold salt in tanks 2 and 3. Cold salt from tank 2 is pumped to the receiver(s), heated, then put into tank 1. When tank 1 is full, cold salt is pumped from tank 3, heated, then pumped into the now-empty tank 2. On discharging, hot salt from tank 2 is pumped to the heat exchangers and the returning cold salt goes into tank 3. Hot salt from tank 1 is cooled in the heat exchangers and pumped into the empty tank 2. Note that only tanks 1 and 2 ever contain hot salt and therefore need to be internally insulated. For larger storage volumes, (n) tanks could be used, the first one hot, the next (n-2) hot/cold (or cascade), the last one cold.

The advantages of the cascade system are that it requires a minimum of tankage and no additonal drain tank. The disadvantages are the same as those of the thermocline system--all the tanks but the first and last must see both hot and cold salt and are therefore both thermally shocked and thermally cycled. (Thermal shock in a cascade tank is also more severe than that in a thermocline tank because the temperature change is more sudden. The walls of a thermocline tank see a more gradual change as the finite thickness transition zone moves up or down the walls). A certain technical risk is therefore involved in going to either the cascade or thermocline storage system.

B. STORAGE PARAMETRIC ANALYSIS MODEL (SPAM)

1. Description

To aid in finding the most economic thermal storage configuration, the computer program SPAM was created. SPAM calculates the effective cost of storage systems defined by the user as well as the capital costs of its component parts (such as insulation, tank and foundation, salt, etc.). This effective cost is the capital cost of the storage system components themselves plus the cost of the extra heliostats and receiver components necessary to compensate for the energy losses from the system. While using less tank insulation may lower the capital cost of the system, the cost of the energy lost (i.e., the make-up heliostats) may actually make the system more expensive. The addition of this cost allows different storage configurations to be compared on the basis of equivalent annual performance.

To use SPAM, the user inputs the parameters shown in Table 6-1. Note that some of the variables allow multiple values so several different insulation thicknesses, for example, may be tried on the same run. Also some of the variables (such as the convective heat transfer coefficients and some of the costs) are constants for curve fits used in the program. The user may define, say, insulation cost/ft2 as $C_1 \exp(C_2 x)$ (where x = thickness) by inputting C_1, C_2, and an integer indicating that an exponential curve fit is desired.

Table 6-1 SPAM User Inputs

- Storage Type - Thermocline, Hot/Cold Tank, Cascade
- Tank Type - Cylindrical, Spherical
- Storage Capacity
- Storage Use Rate - indicates percentage of time tank is "hot"
- Number of Tanks (multiple entry)
- H/D Ratio (multiple entry)
- Parameters for each of Top, Side, Bottom Insulations:
  - Thickness (multiple entry)
  - Minimum thickness
  - Conductivity of internal insulation
  - Cost of internal insulation (curve fit)
  - Conductivity of external insulation
  - Cost of external insulation (curve fit)
- Convective Heat Transfer Coefficients for Top, Side, Bottom (curve fits)
- Ambient Air Temperature
- Maximum Tank Temperature
- Percent Ullage Volume
- Tank Cost (curve fit)
- Foundation Cost (curve fit)
- Internal Liner Cost
- "Per Tank" Costs (such as instrumentation, etc.)
- Cost of Compensation Heliostats
- *Percent Residual Salt
- *Thermocline Thickness
- *Maximum Tank Height
- *Maximum Tank Height x Diameter (for hoop stress)

*Program has default values for these parameters

A flow chart of the program is shown in Figure 6-4. SPAM first initializes constants for the particular storage system involved, then calculates the volume of salt that must be contained (both working salt and any residual salt). This is divided equally among the number of tanks and the tank dimensions are calculated for a given height-to-diameter (H/D) ratio.

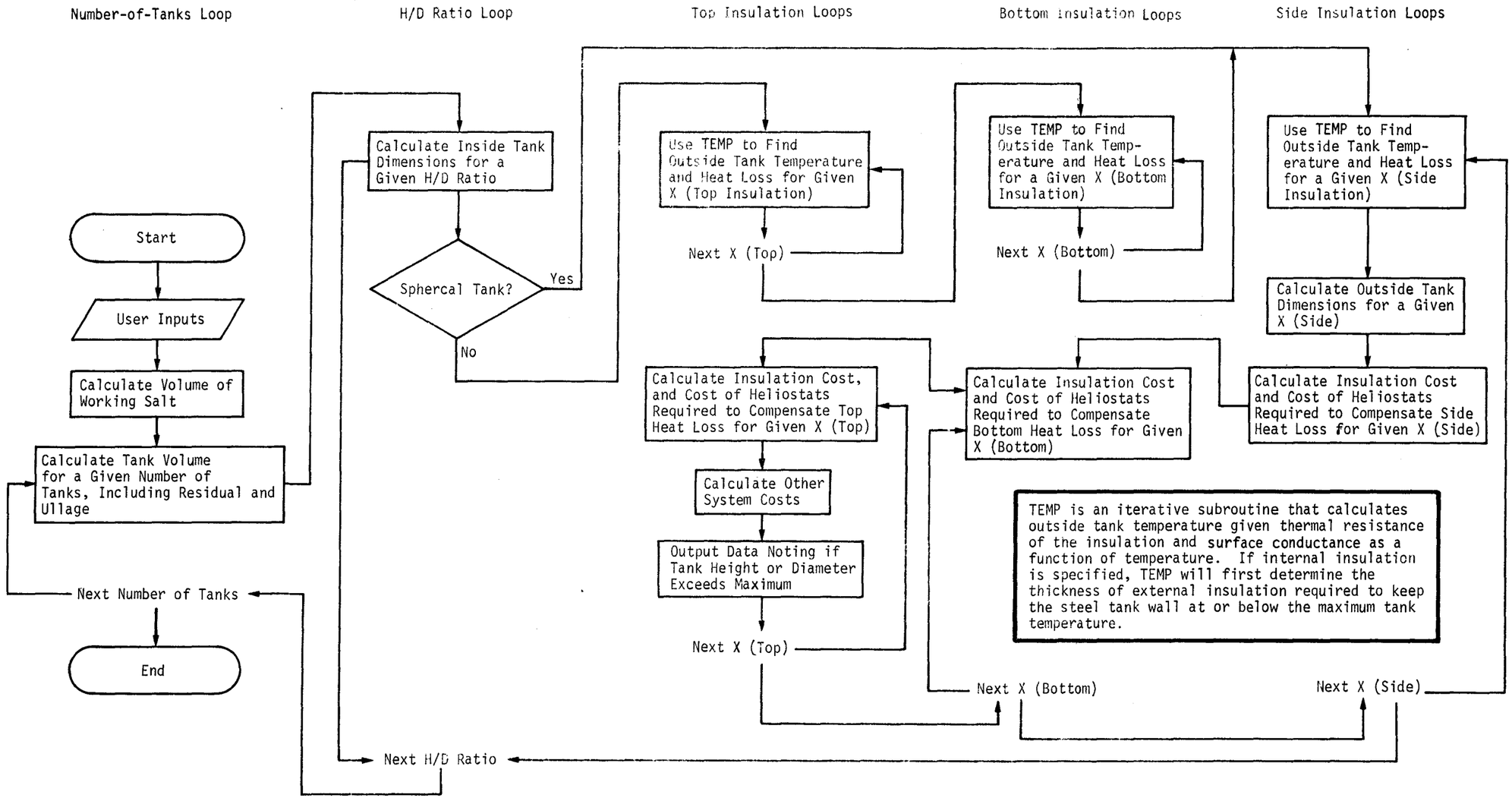

Figure 6-4 SPAM Flow Chart

There are three heat loss program loops, one each for the top, sides, and bottom of the tank (the top and bottom loops are skipped for a spherical tank). Where the tank is exposed to cold (561 K (550°F)) salt, SPAM calculates the outside surface temperature and the heat loss through the chosen thickness of external insulation. The cost of the extra heliostats needed to make up that heat loss is also calculated.

Where the tank is exposed to hot (839 K (1050°F)) salt, SPAM first determines the amount of external insulation necessary to limit the carbon steel tank to a temperature T_{max} for the chosen thickness of internal insulation. SPAM then calculates heat loss and outside surface temperature. If the internal insulation is not thick enough to allow for any external insulation while keeping the tank at T_{max}, the program prints an error message and proceeds with the next case.

After figuring the costs for the rest of the storage system, SPAM outputs values for the parameters listed in Table 6-2 for each combination of number of tanks, H/D ratio, and thicknesses of top, side, and bottom insulations. The user is flagged if either the soil bearing load is exceeded because the tank is too tall, or if the maximum tank hoop stress is exceeded because the diameter is too great for the height.

By examining the effective cost for each storage tank configuration, the user may determine the most cost effective storage system within the constraints set, as well as note the sensitivity of cost to any parameter.

Table 6-2 SPAM Output

ALL USER INPUTS ARE OUTPUT WITH LABELS

EACH LINE OF OUTPUT CONTAINS:

- NUMBER OF TANKS
- H/D RATIO
- TANK HEIGHT (FLAGGED IF EXCEEDS MAXIMUM)
- TANK DIAMETER (FLAGGED IF EXCEEDS MAXIMUM)
- INSULATION - TOP, SIDES, AND BOTTOM:
  - EXTERNAL INSULATION THICKNESS AND COST
  - INTERNAL INSULATION THICKNESS AND COST
  - COST OF HEAT LOSS COMPENSATION
  - TOTAL COST/SALT TANK AREA
  - OUTSIDE SURFACE TEMPERATURE
- LINER COST
- TANK COST
- FOUNDATION COST
- OTHER COSTS
- SALT COST
- TOTAL COST
- EFFECTIVE COST

2. Input Rationale

Tables 6-3 and 6-4 and Figure 6-5 summarize the inputs used for the parametric analyses discussed on the following pages.

Table 6-3 shows the insulation combinations used in the parametric analyses along with their cost and thermal performance. A 50-50 combination of PC12 and PC28 foamglass was chosen for the spherical tanks because it would be easier to form to the walls than the Krilite 30. The high-temperature PC12 would be used just outside the liner, and the PC28 would constitute a layer between the tank shell and the PC12. This lowers the insulation cost because the PC28 is much cheaper than the PC12. All other insulations were chosen for their ability to do the job at the lowest effective cost. All insulation, lagging, and liner costs were supplied by their respective manufacturers and include the cost of installation.

Figure 6-5 shows construction costs for carbon steel cylindrical tanks of the design described in Section V. These costs were generated by Badger Energy Inc. (Boston) for the tank only (no foundation, platforms, walkways, etc) constructed at the site to all applicable codes, and are based on 2nd quarter 1979 prices. Note that cost is shown as a function of volume; the H/D ratio has little effect on cost within the range considered (about 0.1 to 1.0).

Spherical tank costs are based on an estimate of $1,782,500 for a 26.5-m (87-ft) diameter tank needing no postweld heat treatment of the design described in Section V and are varied by volume to the 0.75 power. These costs apply up to a diameter of 26.5 m.

Table 6-4 summarizes other costs used in the SPAM program. Only the cooling coil foundation was considered in the parametric analyses because of its much lower cost. Of the two liner materials considered, the Incoloy 800 was used in the program. Since piping and valve costs vary little from system to system, they did not affect system optimization.

The heliostat compensation cost is the cost for the extra heliostats (and some of the receiver components) necessary to compensate for a constant 1-MWt heat loss from the storage tanks (8784 MWht per year). Heat loss was calculated separately for each section of the tanks (top, sides, bottom) using standard heat transfer equations for natural and forced convection and radiation.

- Tank losses vary as a function of ambient temperature and wind speed (and therefore time of day and day of year). They are also a function of both plant size and storage size. For example, a 300-MWe plant would discharge storage roughly three times as fast as a 100-MWe plant with an equivalent storage capacity. The tanks of the larger plant would then be empty, or "cold," for a greater part of the day and suffer less heat loss. (Note that this only holds true for cascade and

Storage Type / Tank Type	Thermocline Cylinder	Dual-Tank, Hot Cylinder	Cascade Cylinder	Dual-Tank, Cold Cylinder	Dual-Tank, Hot Sphere	Cascade Sphere	Dual-Tank, Cold Sphere
Top, external Type Conductivity Insulation cost Lagging cost	Mineral block with lagging load bearing boards k = 0.069 W/m-K (0.040 Btu/hr-ft-°F) $353.00/m³ ($10.00/ft³) $22.10/m² ($2.05/ft²)				(not applicable)		
Top, internal Type Conductivity Insulation cost Liner cost	Duroback with liner fiberglass blanket k = 0.109 W/m-K (0.063 Btu/hr-ft-°F) $237.00/m³ ($6.70/ft³) $292.90/m² ($27.21/ft²)			None			
Side, external Type Conductivity Insulation cost Lagging cost	Duroback with lagging fiberglass blanket k = 0.073 W/m-K (0.042 Btu/hr-ft-°F) $237.00/m³ ($6.70/ft³) $22.10/m² ($2.05/ft²)						
Side, internal Type Conductivity Insulation cost Liner cost	Krilite 30 with liner insulating brick k=0.242 W/m-K (0.140 Btu/hr-ft-°F) $715.70/m³ ($20.55/ft³) $292.90/m² ($27.21/ft²)	-OR-	PC12 & PC28 with liner foamed silicas k=0.237 W/m-K (0.137 Btu/hr-ft-°F) $1400.00/m³ ($40.00/ft³) $292.90/m² ($27.21/ft²)	None	PC12 & PC28 with liner foamed silicas k=0.237 W/m-K (0.137 Btu/hr-ft-°F) $1400.00/m³ ($40.00/ft³) $292.90/m² ($27.21/ft²)		None
Bottom, external Type Conductivity Insulation cost	Vermiculite concrete insulating concrete k = 0.087 W/m-K (0.050 Btu/hr-ft-°F) $530.00/m³ ($15.00/ft³)				(not applicable)		
Bottom, internal Type Conductivity Insulation cost Liner cost	Krilite 30 with liner insulating brick k=0.242 W/m-K (0.140 Btu/hr-ft-°F) $725,70/m³ ($20.55/ft³) $292.90/m² ($27.21/ft²)	-OR-	PC12 & PC28 with liner foamed silicas k=0.237 W/m-K (0.137 Btu/hr-ft-°F) $1400.00/m³ ($40.00/ft³) $292.90/m² (27.21/ft²)	None			

Table 6-3 SPAM Insulation Inputs

Table 6-4 Other SPAM Inputs

FOUNDATION (1)		
RAISED, AIR-COOLED FOUNDATION	$673.8/M^2 ($62.6/FT^2)	(INCLUDES INSTALLATION)
COOLING COIL FOUNDATION	$312.2/M^2 ($29.0/FT^2) *	
LINER (2)		
INCOLOY 800	$282.9/M^2 ($26.28/FT^2)	(INCLUDES $108/M^2 ($10.0/FT^2) FOR INSTALLATION)
316 STAINLESS STEEL	$230.7/M^2 ($21.43/FT^2)	
PER-TANK COSTS (3)		
INSTRUMENTATION	$16,000 PER TANK	
AIR PURGE SYSTEM	$30,000 PER TANK	
SALT COST (3)	$0.253 PER KG ($0.115 PER LBM)	
HELIOSTAT COMPENSATION COST (4)		
$75/M^2 ($7/FT^2) HELIOSTATS	$522,156/CONSTANT MWT LOSS FROM STORAGE	
$108/M^2 ($10/FT^2) HELIOSTATS	$708,503/CONSTANT MWT LOSS FROM STORAGE	
$140/M^2 ($13/FT^2) HELIOSTATS	$894,850/CONSTANT MWT LOSS FROM STORAGE	

*Includes cost of auxiliary power

Sources of Costs
(1) Badger Energy
(2) Technigaz
(3) Cost estimates made for Advanced Central Receiver Power System, Phase I (EG-77-C-03-1724)
(4) (see text)

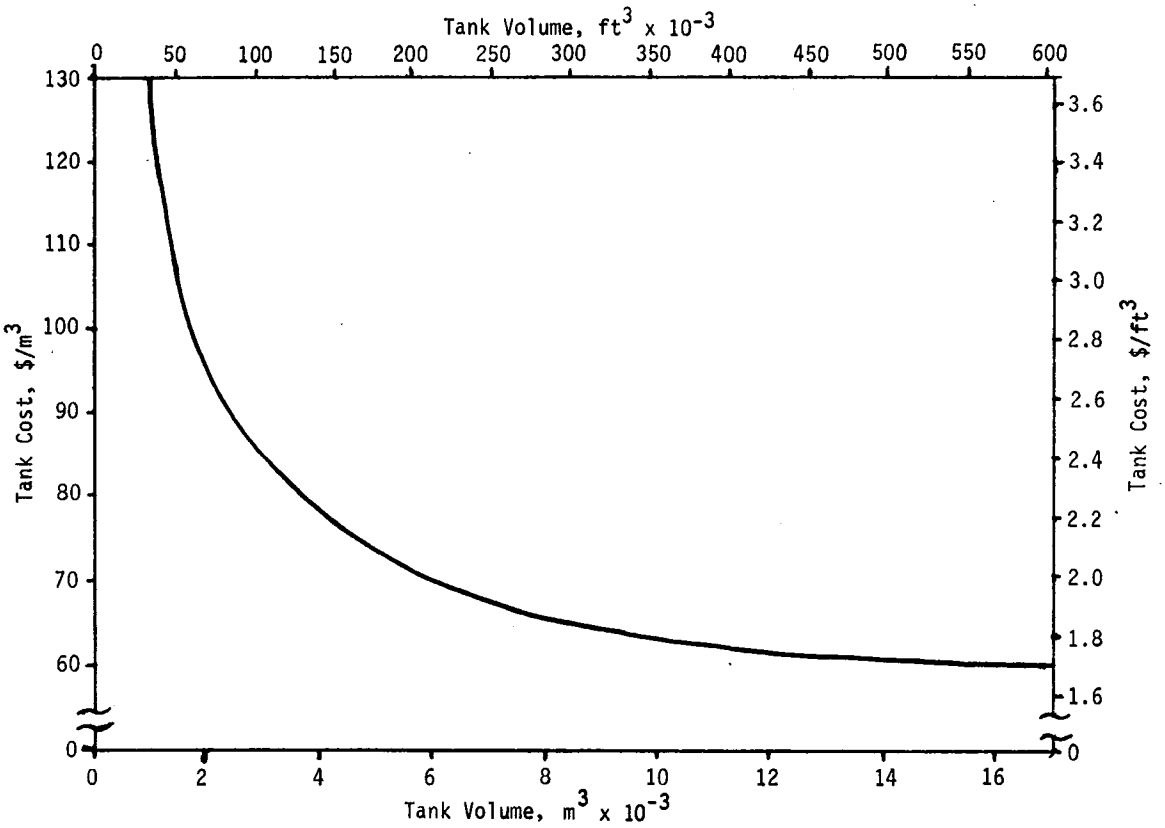

Figure 6-5 Cylindrical Tank Cost Vs Size

thermocline tanks. Hot and cold tanks maintain their internal temperature by retaining about a foot or so of residual salt even when "empty." The cascade and thermocline tanks actually contain cold salt when storage is "empty" and so will actually lose less heat). To calculate the heat loss on a yearly basis, two things had to be established--average ambient temperature and wind speed, and a charged/discharged storage profile for a given plant size and storage capacity.

Average ambient temperature and wind speed were taken to be 301 K (82°F) and 3.5 m/s (11.5 ft/s), respectively. These are the design point conditions for Barstow, California, 1976. The charged/discharged profile for a given plant was derived from STEAEC* computer runs that modeled that plant's annual performance using the Barstow, 1976 weather data tape. Output from the computer model indicated the percentage of time the storage was in a fully charged ("hot") state and this

*Solar Thermal Electric Annual Energy Calculator (Sandia Labs, Livermore).

percentage was input to SPAM. Heat losses were calculated by SPAM for both the "hot" and "cold" conditions and were appropriately ratioed.

The heliostat compensation cost input to SPAM is the capital cost of heliostats and most of the receiver components necessary to produce a constant 1 MWt of available power (i.e., 8784 MWht per year at the inlet of the storage tanks). For example, the STEAEC run for the 300-MWe 11-hour storage molten salt ACR plant showed a usable thermal output of 4.22×10^6 MWht per year. The estimated cost of the power-related items is \$340,378,230 if the heliostat cost is \$108/m^2 (\$10/ft^2). Assuming a linear relationship, it would therefore cost an additional \$708,503 to produce the 8784 MWht needed to make up for a constant 1-MWt storage loss (note that 1976 was a leap year and thus had 366 days = 8784 hours).

C. RESULTS AND CONSLUSIONS

1. Tank Parametric Analyses

The sensitivities to the following variables were investigated for each type of storage system tank--insulation thickness, compensation cost, number of tanks, H/D ratio of cylindrical tanks, soil bearing load, tank type, and storage size. The effect of thermocline thickness on system cost was also examined.

a. Insulation Thickness and Compensation Cost - The optimum insulation thickness is that thickness where the cost of the insulation (external and, if applicable, internal) plus the cost of the heat loss compensation is minimum. This optimum depends on the cost and conductivity of the insulation, cost of heliostat compensation, type of tank, and thermal conductance used at the tank surface; it is independent of the tank size. Optimum insulation thicknesses were found for each storage type for the insulation combinations listed in Table 6-3. Figures 6-6 through 6-12 show the sensitivity of effective cost to insulation thickness and heliostat cost for each type of storage. Note that the primary effect of raising heliostat cost is to increase the optimum thickness.

   The optimized thicknesses for the \$108/m2 (\$10/ft^2) heliostats were used for all the remaining parametric analyses because these heliostats are considered representative of those in a commercial plant.

b. Number of Tanks - Figures 6-13 to 6-16 show the results of the number of tanks, H/D ratio, and storage size analyses. The ordinate in the figures is the effective cost of the tank system, i.e., the cost of the tanks, foundations, insulation, liners, residual and thermocline salt, compensating heliostats, and anything else with a cost that is system-dependent. Also shown are the cut off points for 34.5-kPa (5000-psf) and 68.9-kPa (10,000-psf) soil bearing loads (dotted lines) and the points where the hoop stress is exceeded (shaded areas).

In almost all cases, the optimum number of tanks is the fewest possible within the constraints of hoop stress and soil bearing load. Thus a few large tanks tend to be more economical than several small ones. Note that this lower limit is set by the tank's mechanical constraints and not by the economics.

c. H/D Ratio - Figures 6-13 through 6-16 show that for the 34.5-kPa (5000-psf) soil limit the optimum H/D ratios are again set by the tanks' mechanical constraints and not by system economics. These optimums are in the vicinity of H/D = 0.3 for multitank systems and H/D = 0.4 for single-tank systems and are reasonably independent of storage type. For a maximum allowable soil pressure of 68.9 kPa (10,000 psf), the optimum H/D ratios are around 0.4 to 0.6 and are set by the hoop stress constraint alone.

d. Soil Bearing Load - As has been noted, both the optimum number of tanks and the optimum H/D ratio depend on the soil bearing load assumed. For the hot, cold, and cascade tanks, the effect of increasing the maximum allowable bearing load from 34.5 kPa (5000 psf) to 68.9 kPa (10,000 psf) is to increase the optimum number of tanks by one, increase the optimum H/D ratio to about 0.6, but decrease the cost by less than 10%. The cost advantage to a thermocline tank, however, is anywhere from 15 to 30% because a thermocline tank with a high H/D uses considerably less transition zone salt than one with a low H/D.

e. Tank Type - Figures 6-14 through 6-16 clearly show that cylindrical tanks are less expensive than spherical tanks. This is not only because a spherical tank costs more to build than a cylindrical tank of the same volume, but also because more tanks are required due to the hoop stress limitation.

f. Storage Size - Once storage size is large enough to require a multitank system, the optimum tank size does not change very much; larger storage just dictates a greater number of tanks.

g. Transition Zone Thickness - As discussed in Section IV, the transition zone thickness can be decreased by increasing the "bite" into the transition zone during charge and discharge. This decreases the amount of unusable salt needed and therefore the cost of the tanks as well. When the "bite" is increased from 17 K (30°F) to 33 K (60°F), the thickness of the transition zone is reduced from 2.6 m (8.6 ft) to 1.0 m (3.4 ft) and the optimization curves approach those of the hot and cascade tanks (Figures 6-14 and 6-16, respectively). However, the larger the "bite," the less efficiently the plant is likely to operate (because of turbine inlet conditions, etc). It is not clear at this time exactly how to evaluate the effect on cost and whether increasing the transition zone "bite" is truly advantageous from a total plant standpoint.

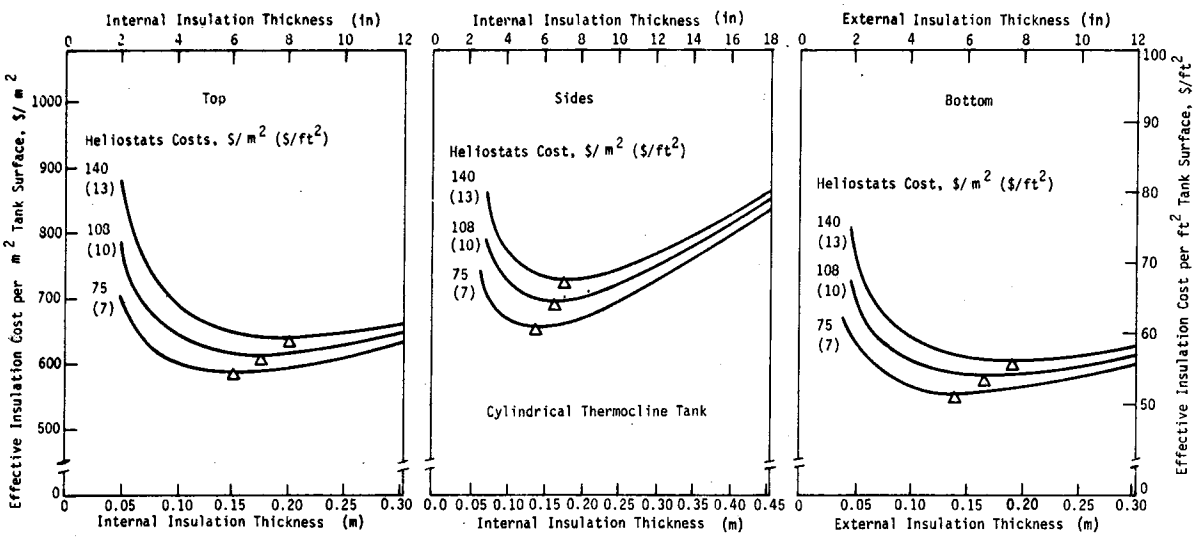

Figure 6-6 Insulation Optimization for Cylindrical Thermocline Tanks

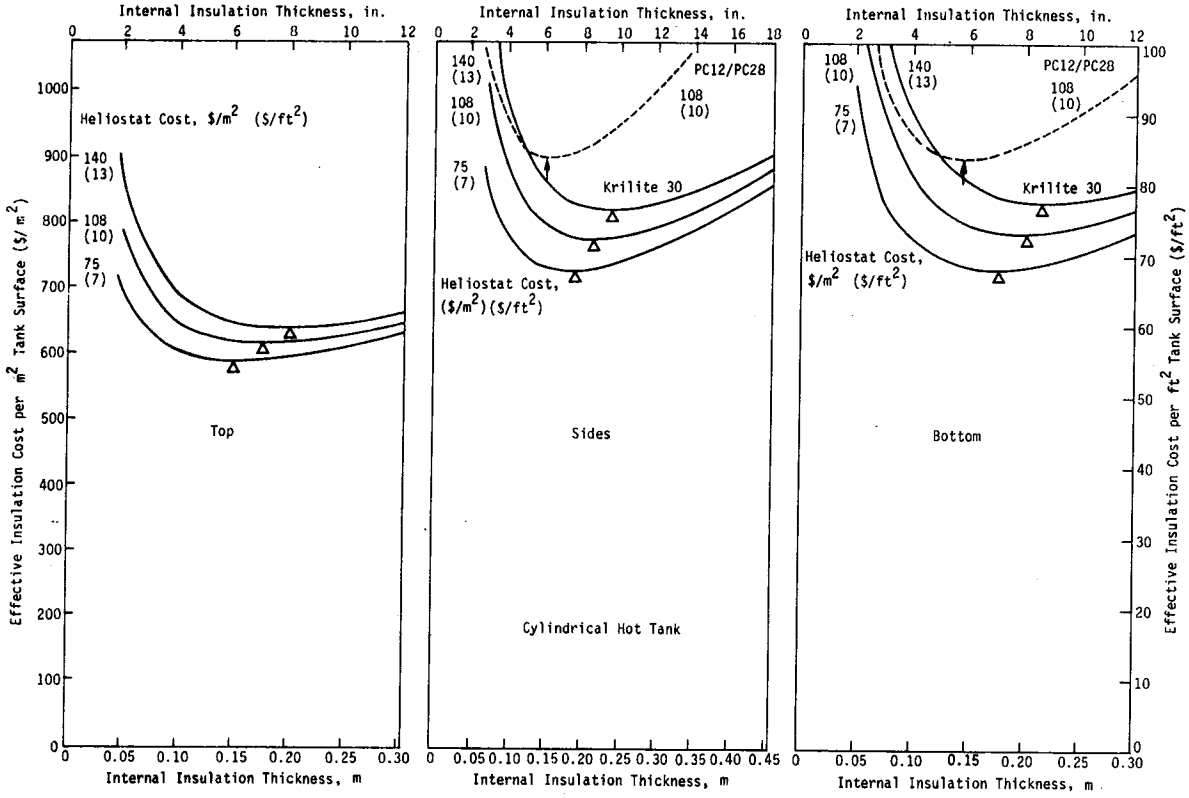

Figure 6-7 Insulation Optimization for Cylindrical Hot Tanks

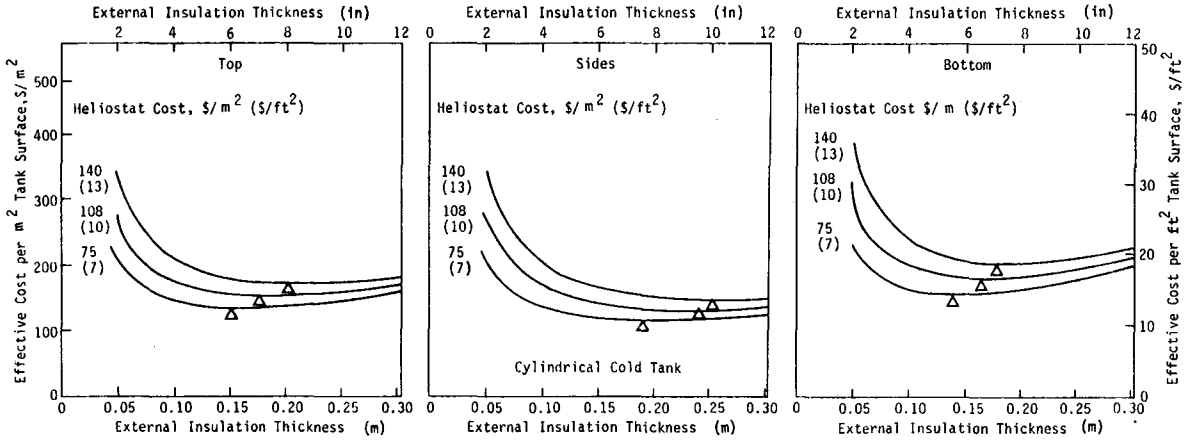

Figure 6-8 Insulation Optimization for Cylindrical Cold Tanks

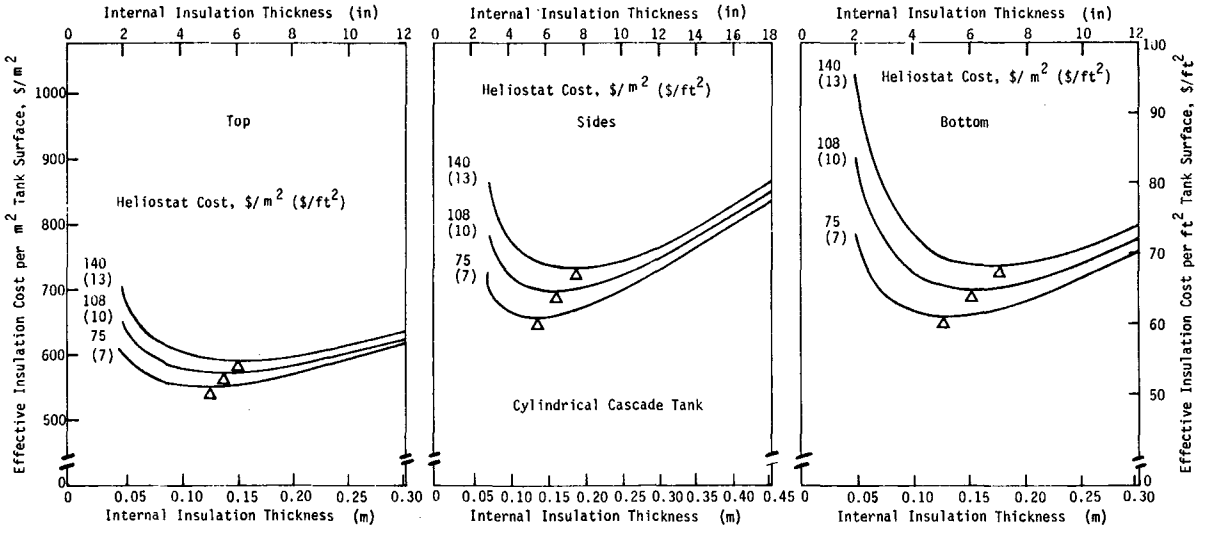

Figure 6-9 Insulation Optimization for Cylindrical Cascade Tanks

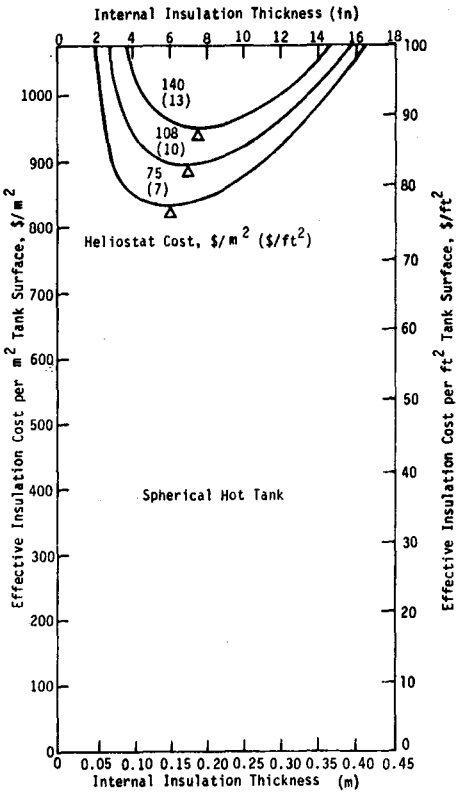

Figure 6-10 Insulation Optimization for Spherical Hot Tanks

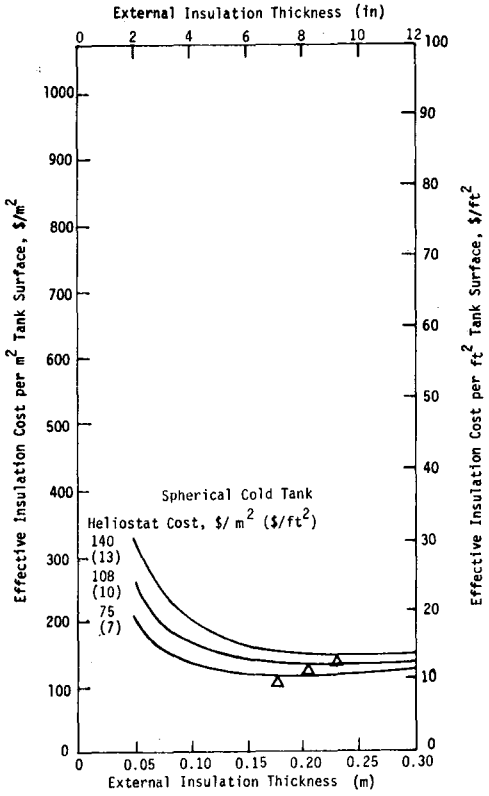

Figure 6-11 Insulation Optimization for Spherical Cold Tanks

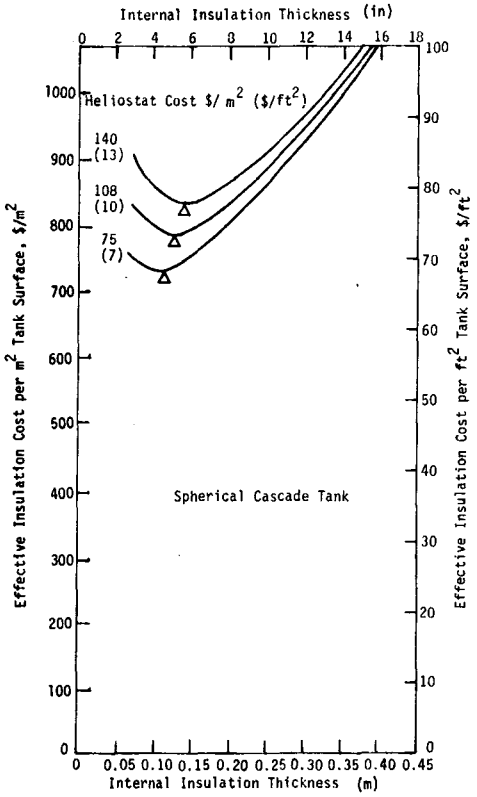

Figure 6-12 Insulation Optimization for Spherical Cascade Tanks

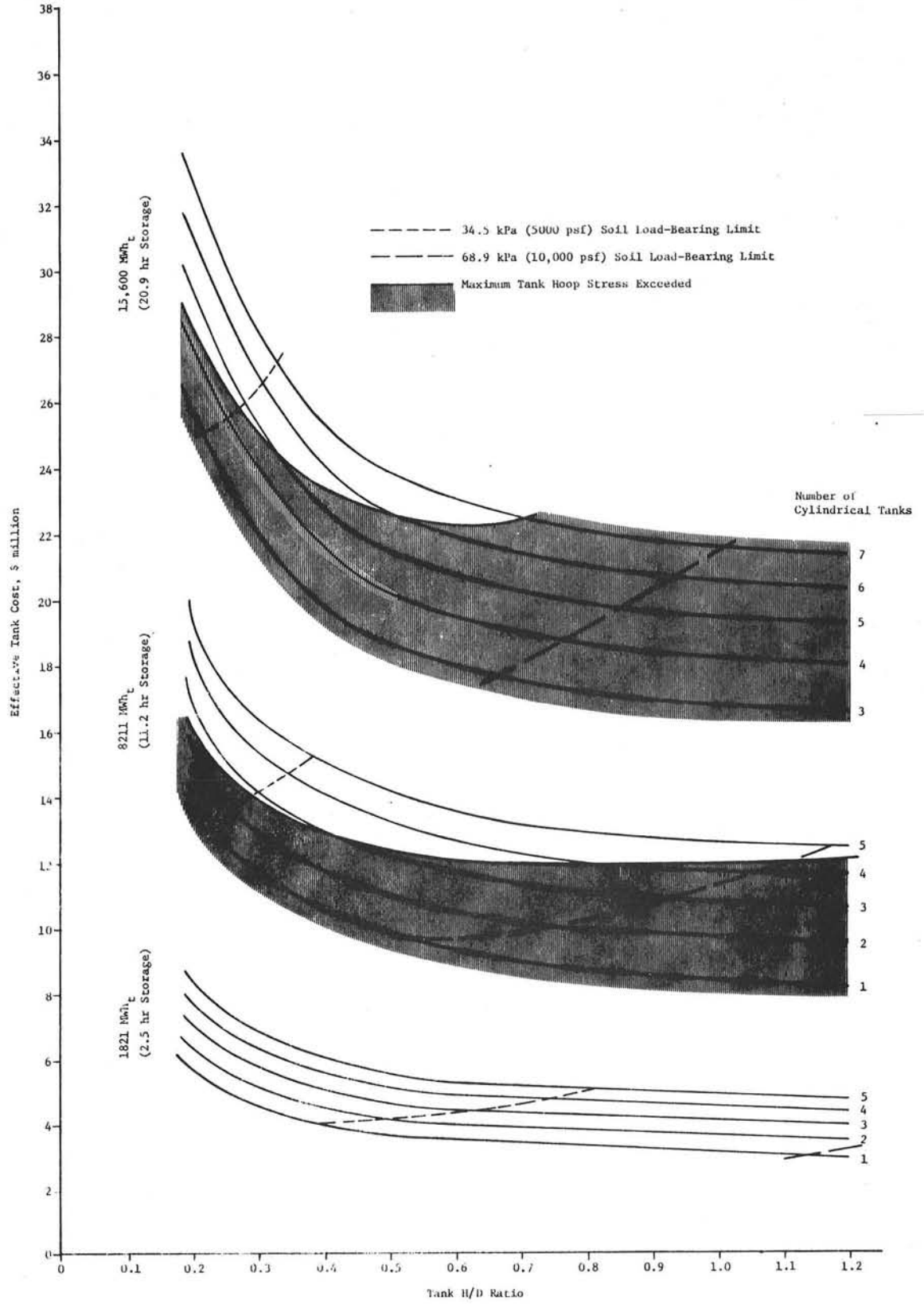

Figure 6-13 Thermocline Tank Cost Parametrics (300 MWe Plant)

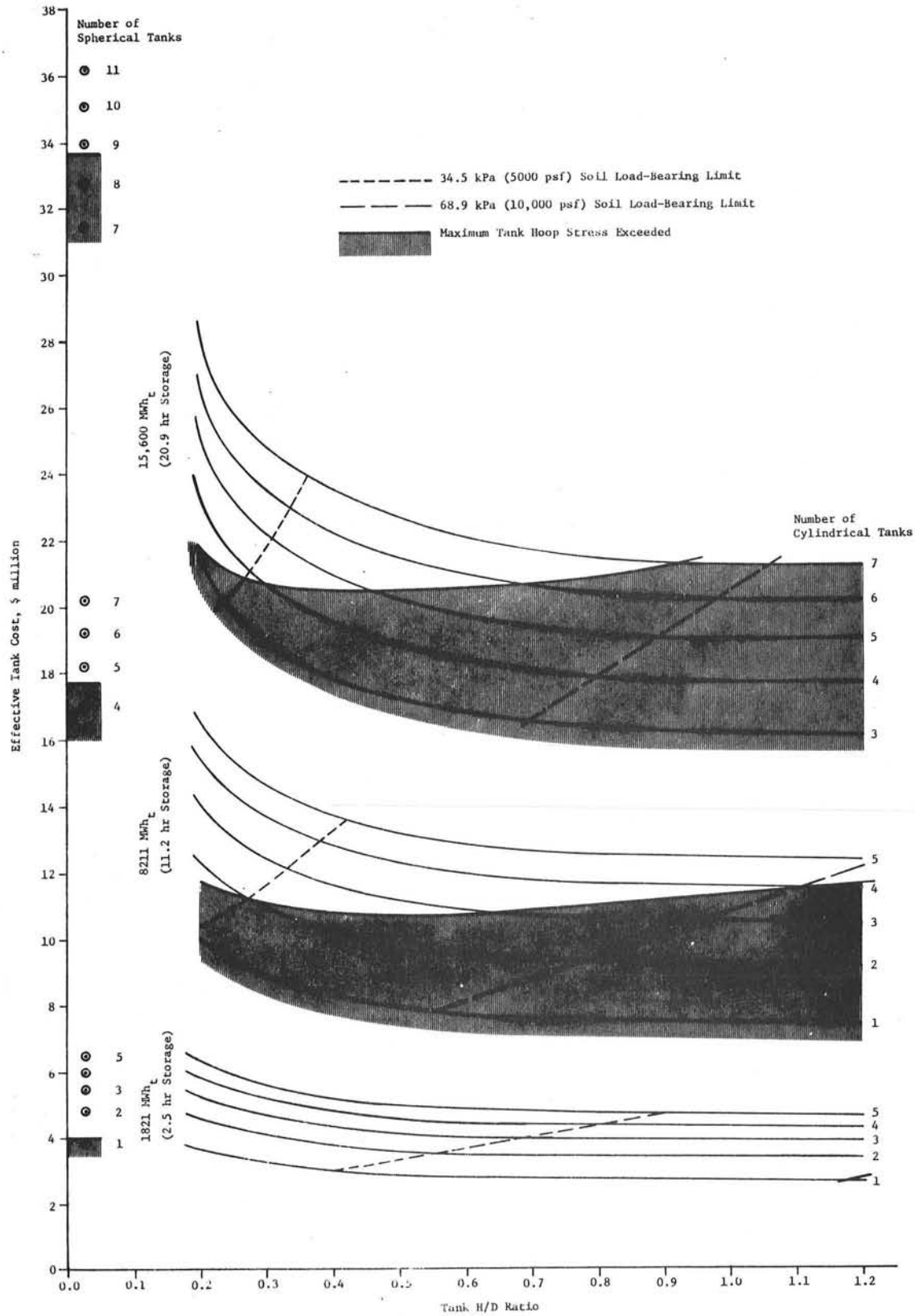

Figure 6-14 Hot Tank Cost Parametrics (300 MWe Plant)

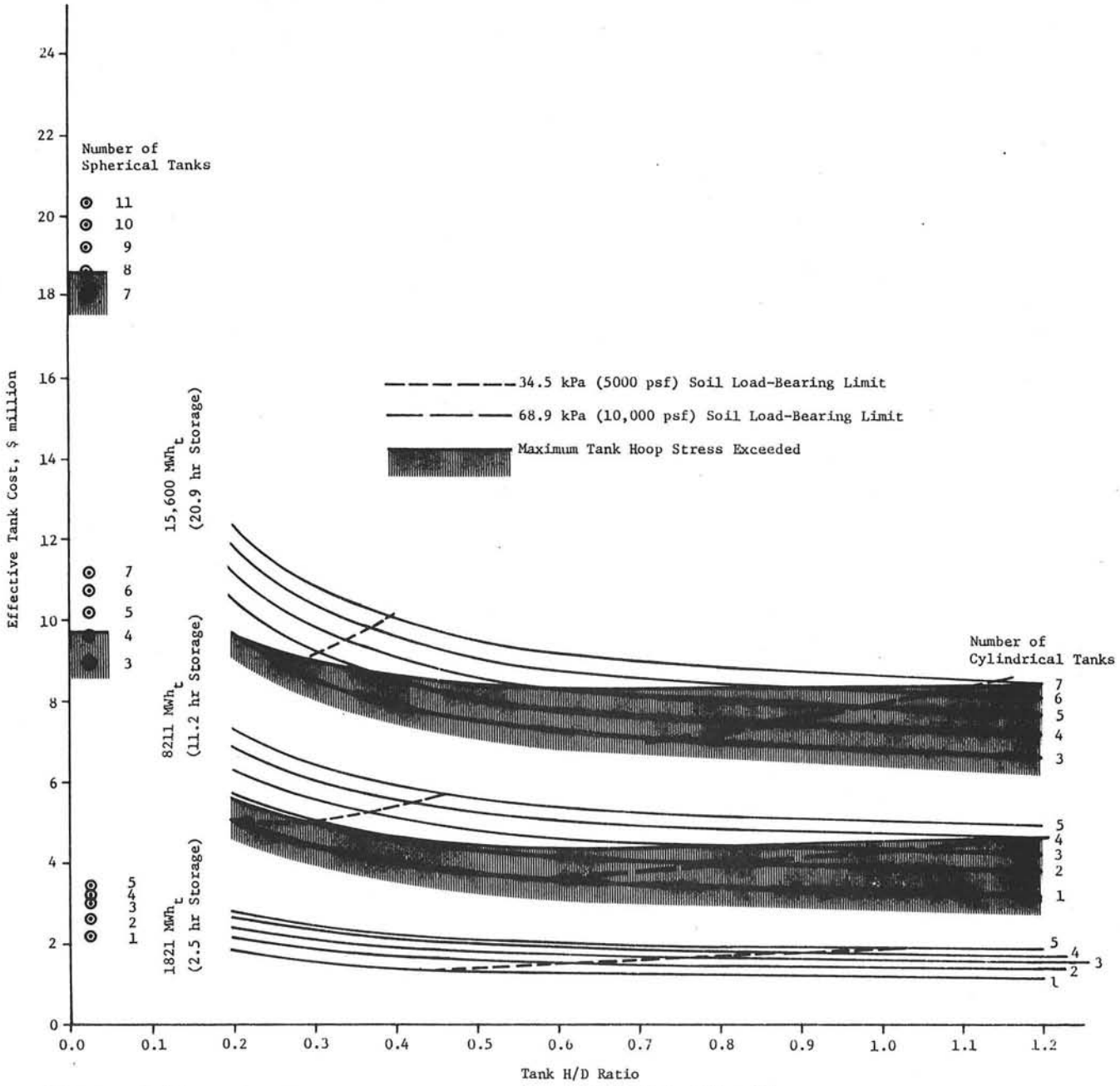

Figure 6-15 Cold Tank Cost Parametrics (300 MWe Plant)

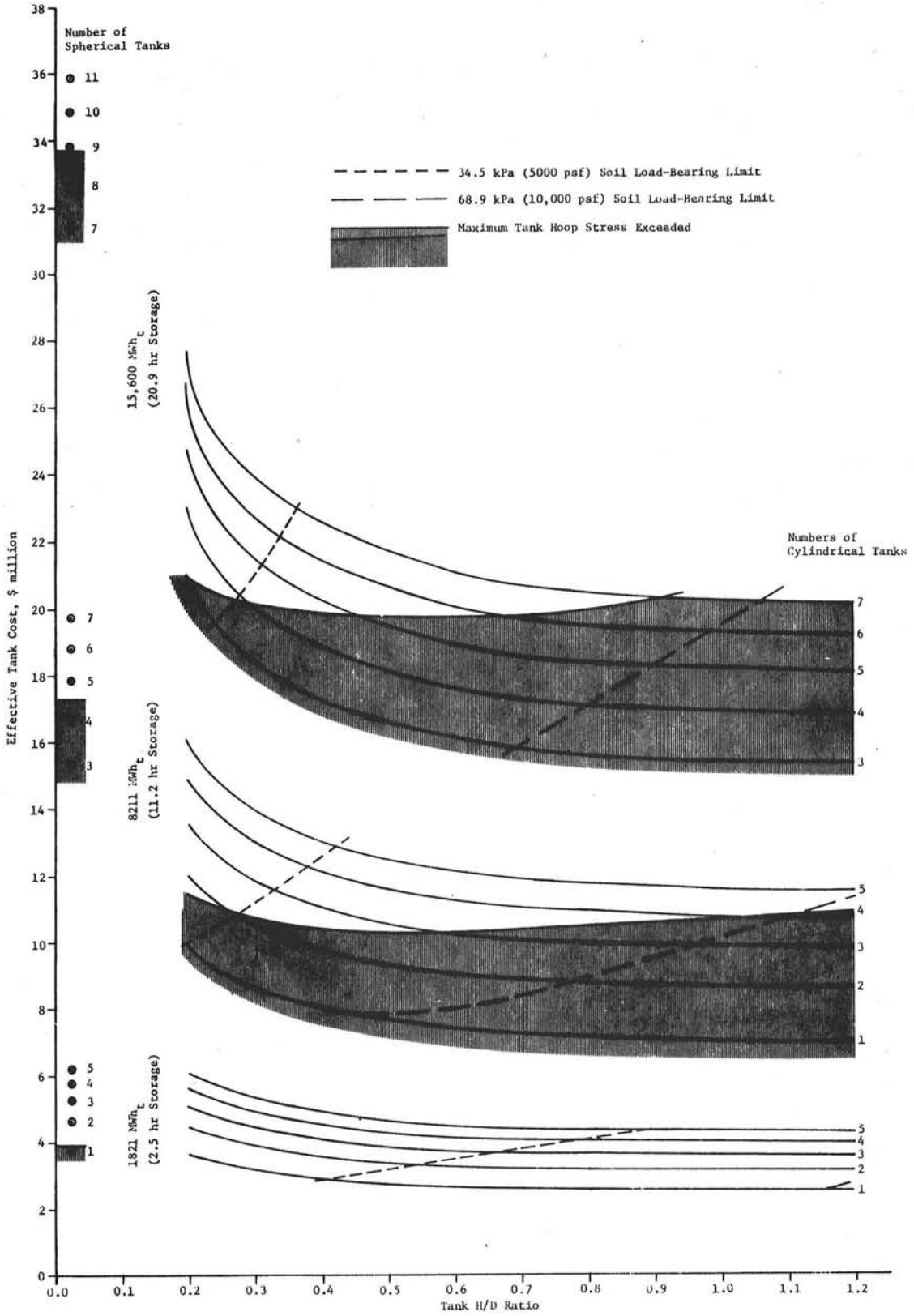

Figure 6-16 Cascade Cost Parametrics

System Parametric Analyses

a. Storage System Type and Storage Size - Table 6-5 and Figure 6-17 compare the effective costs of the three types of storage systems for three different storage capacities. The costs are for optimum configurations for a 300 MWe plant assuming a maximum soil bearing load of 34.5 kPa (5000 psf). Capital cost refers to those components that are actually part of the storage system; effective cost is capital cost plus the cost of the extra heliostats and other components necessary to compensate for the thermal losses.

Figure 6-18 shows this comparison as a function of kWh electrical output from the storage system.

Table 6-5 Storage System Comparison

		Number of Tanks	Tank Height m (ft)	Tank Diameter m (ft)	Effective Tank Cost	Effective System Cost
1821 MWHt (2.5 H)						
Thermocline	Hot	1	12.8 (42.0)	34.6 (113.5)	$ 4.2M	$11.3M
	Drain	1	12.8 (42.0)	28.9 (94.8)	1.0	
Dual Tank	Hot	1	12.8 (42.0)	31.4 (102.9)	3.0	$10.5M
	Cold	1	12.8 (42.0)	28.9 (94.8)	1.4	
Cascade	Hot	1	12.8 (42.0)	31.4 (102.9)	3.0	
	Cascaded	0	-	-	-	$10.5M
	Cold	1	12.8 (42.0)	28.9 (94.8)	1.4	
8211 MWHt (11.2 H)						
Thermocline	Hot	3	12.8 (42.0)	42.0 (137.7)	$14.2M	$35.2M
	Drain	1	12.8 (42.0)	35.3 (115.7)	1.4	
Dual Tank	Hot	2	12.6 (41.2)	47.4 (155.5)	11.3	$36.0M
	Cold	2	12.8 (42.0)	43.1 (141.4)	5.1	
Cascade	Hot	1	12.6 (41.2)	47.4 (155.5)	5.7	
	Cascaded	1	12.4 (40.6)	48.0 (157.4)	5.5	$33.3M
	Cold	1	12.8 (42.0)	43.1 (141.4)	2.5*	
15,600 MWHt (20.9 H)						
Thermocline	Hot	5	12.8 (42.0)	44.9 (147.4)	$26.0M	$62.9M
	Drain	1	12.8 (42.0)	37.5 (123.2)	1.6	
Dual Tank	Hot	4	12.8 (42.0)	45.7 (150.0)	21.1	$65.6M
	Cold	4	12.8 (42.0)	41.8 (137.3)	9.2	
Cascade	Hot	1	12.8 (42.0)	45.7 (150.0)	5.3	
	Cascaded	3	12.8 (42.0)	45.7 (150.0)	15.3	$58.2M
	Cold	1	12.8 (42.0)	41.8 (137.3)	2.3	

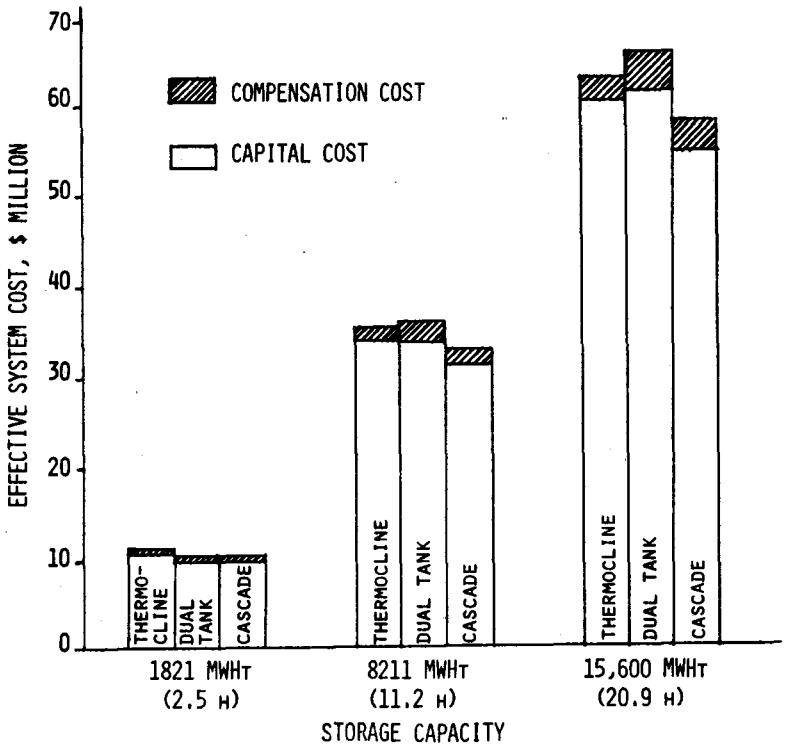

Figure 6-17 Effective Storage System Cost Vs Storage Size (300 MWe Plant)

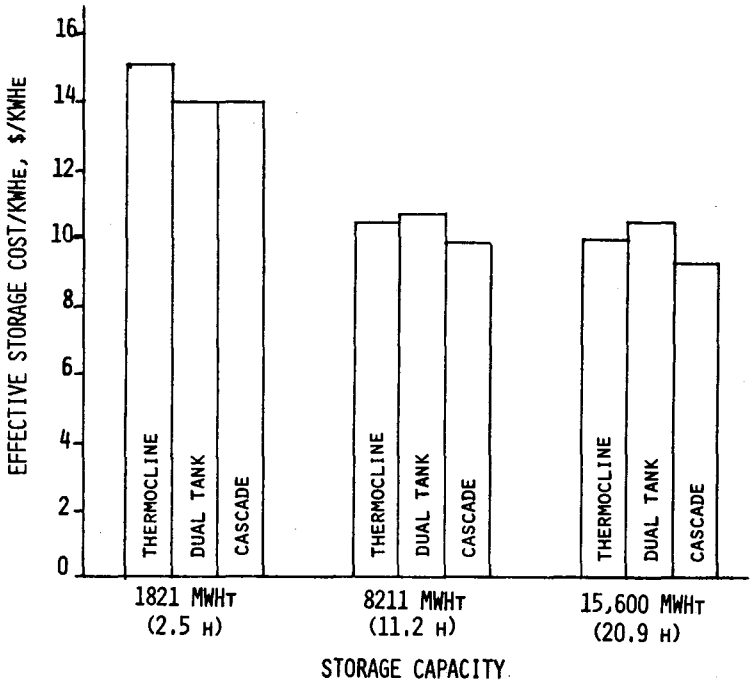

Figure 6-18 Effective Cost of Storage Vs Storage Size (300 MWe Plant)

For small storage capacities where one tank can hold the entire quantity of salt, the dual-tank system is preferred (see case 1 of Table 6-5). Although the thermocline system requires the same number of tanks as the dual-tank system because of the need for a separate drain tank, it is more expensive because of the additional thermocline salt and the larger tank needed to contain it. Because the cascade system requires one hot and one cold tank (no hot/cold tank), it is identical to a dual-tank system at this capacity.

Case 2 of Table 6-5 exemplifies an intermediate storage capacity (about 10,000 MWht and 2 to 3 tank volumes of salt). The cascade system, requiring the same number of internally insulated tanks as the dual-tank system but only one cold tank, starts to show a cost advantage. The savings are small, however--only 8% of the storage system cost and less than a percent of the total plant cost for the 300-MWe plant described in the Advanced Central Receiver Power System, Phase I final report (EG-77-C-03-1724). The additional volume needed for the thermocline salt forces the thermocline system to use three instead of two internally insulated tanks for this particular storage size. Its cost advantage over the dual-tank system is also very small. Because of the technical risks involved in going to either a thermocline or a cascade system and because little is to be gained by doing so, the dual-tank system is also preferred for an intermediate storage capacity.

Large storage capacities, where four or more large tanks are needed to contain the salt, are exemplified by case 3 of Table 6-5. As can be seen in Figure 6-18, the cost of storage for capacities over 10,000 MWht is relatively constant for a dual-tank system and decreases slightly for a thermocline or cascade system. For these large capacities, a significant system cost reduction can be realized with a cascade system because of the need for only one cold tank. This is also true for the thermocline system (the cold tank is a drain tank here), but is somewhat offset by the cost of the thermocline salt and the slightly larger tanks required. The large storage cost reduction possible for large capacities with the cascade system suggests that it may be economically practical to find a solution to the refractory thermal shock and cycling problems. However, in light of current information about refractories, the dual-tank system is still recommended.

Figure 6-19 shows the cost of storage for storage systems other than molten salt when coupled to their respective central receiver plants. The costs of molten salt storage for both internally and externally insulated tanks are also shown. (Storage costs for the nonmolten salt systems were taken from a storage system comparison done by Sandia Labs, Livermore.) It is important to note that this is a comparison of storage costs for storage system/central receiver combinations that have been investigated in considerable detail. While other combinations are possible, only those shown were available for comparison.

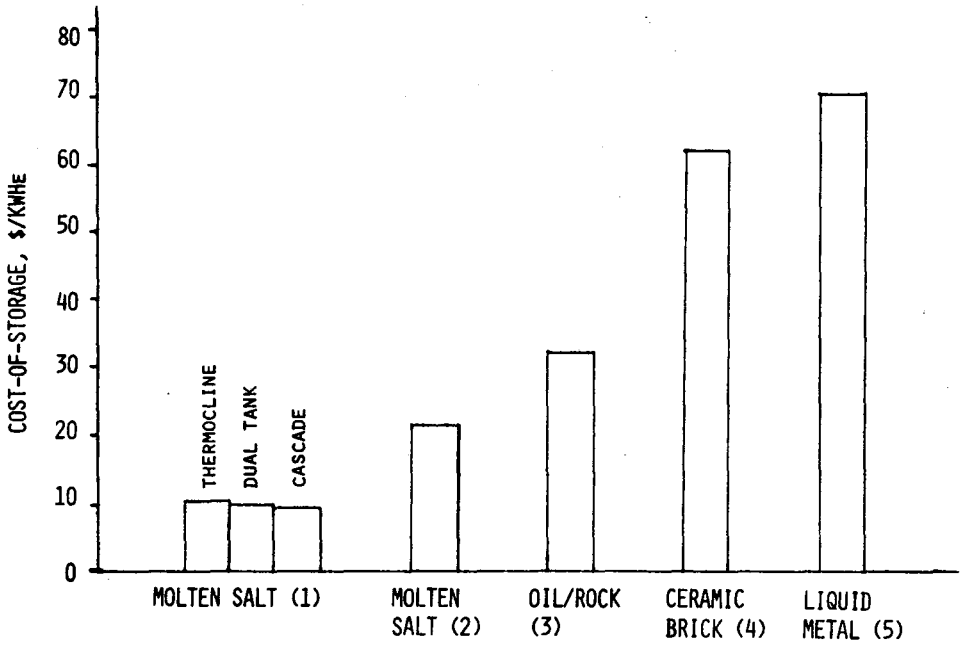

(1) MOLTEN SALT RECEIVER, 300 MWe PLANT, 11 HOURS STORAGE, INTERNALLY INSULATED TANKS
(2) MOLTEN SALT RECEIVER, 300 MWe PLANT, 11 HOURS STORAGE, EXTERNALLY INSULATED DUAL TANKS
(3) WATER/STEAM RECEIVER, 100 MWe PLANT, 6 HOURS STORAGE
(4) GAS COOLED RECEIVER, 100 MWe PLANT, 3 HOURS STORAGE, WELDED STEEL TANKS
(5) LIQUID METAL RECEIVER, 100 MWe PLANT, 3 HOURS STORAGE, EXTERNALLY INSULATED DUAL TANKS

STORAGE COSTS FOR (3), (4), AND (5) WERE SUPPLIED BY SANDIA LABORATORIES, LIVERMORE, FROM A STORAGE SYSTEM COST COMPARISON OF PROPOSED STORAGE SYSTEM/CENTRAL RECEIVER COMBINATIONS.

Figure 6-19 Cost of Storage for Various Storage Systems

As the figure shows, cost of storage for a molten salt system can be cut in half by going to internally insulated carbon steel tanks instead of externally insulated stainless steel ones (see Appendix B for specifics on molten salt storage with stainless steel tanks). Note that the difference in cost between the three molten salt storage concepts is small compared to the gain made by going from externally to internally insulated tanks. This produces the greatest cost reduction for the least technical risk. Using a cascade system over a dual-tank system only yields an additional 5% reduction in storage cost. Because a much greater technical risk is involved, it is not recommended.

b. System Alternatives - By the "nth" commercial plant, the system might be proven enough to drop the tank-draining capability. The cost of the drain tank could then be dropped from the thermocline system. Referring back to Table 6-5, it can be seen that deleting the drain tank makes little difference to the system tradeoffs. For small capacities, deleting the drain tank only brings the cost about even with the dual-tank system, which is preferred by virtue of its lesser technical risk. For intermediate capacities it is cheaper than the dual-tank system but is still more expensive than the cascade system. Here the cost advantage is not deemed large enough to justify using a thermocline system. For large storage capacities, eliminating the drain tank lowers the cost relative to the dual-tank system but it is still more expnsive than the cascade system. Thus if a suitable internal insulation were found that could withstand the thermal shock, the greater cost reduction would be made with the cascade system rather than the thermocline system.

As mentioned earlier, increasing the "bite" into the thermocline transition zone reduces the transition zone thickness and therefore system cost. For a 33 K (60°F) "bite," the zone is reduced to only 1.0 m (3.4 ft) thick and the effective tank cost curves approximate those of a hot or cascade tank (Fig. 6-14 and 6-16). For a storage capacity of 8211 MWht, this would alter Table 6-5 as shown.

8211 MWht (11.2 h)	Number of Tanks	Tank Height, M (ft)	Tank Diameter, M (ft)	Effective Tank Cost, $M	Effective System Cost, $M
Thermocline (Hot)	3	12.8 m (42.0 ft)	40.8 m (133.8 ft)	$12.2 M	$33.2 M

It is important to keep in mind that this analysis does not take into account the lower cycle efficiency associated with the larger "bite." It is not clear at this time how to compensate for the change in efficiency with respect to cost.

Doubling the transition zone "bite" drops the effective cost of the thermocline system down to about that of the cascade system. If this only negligibly affects cycle efficiency and if it is not detrimental to the system downstream of storage, the thermocline system would be more attractive than the cascade system for the larger storage sizes. This is because the thermal shock is not as great in a thermocline tank as in a cascaded tank (this, of course, assumes that there is a suitable internal insulation system that can withstand the thermal shock and cycling).

VII. STORAGE SUBSYSTEM RESEARCH EXPERIMENT (SRE)

A. OBJECTIVES

The design of a storage SRE is described in this chapter. The purpose of the test tank system is to demonstrate fabrication and performance of the major system components and the establish confidence necessary for building a full-size tank system. This study establishes the system and tank design. The objectives of the test are:

1) Demonstrate tank fabrication processes for carbon steel tank, liner, and insulation;

2) Establish leak check method for liner;

3) Demonstrate use of full-size pieces of tank liner and insulation to establish heat losses directly applicable to full-size tanks;

4) Provide data on the pressure cycling of the membrane liner;

5) Simulate tank inflow and outflow;

6) Demonstrate the method of mixing and melting the initial salt when filling the system;

7) Verify stress of liner and tank during system cycling;

8) Verify such design constraints as foundations and tank headers.

B. SRE DESIGN

The selected SRE system design is a dual-tank system with one hot (internally insulated and lined) tank and one cold (externally insulated) tank. This will allow inflow and outflow to be simulated for both types of tanks. A heater and cooler are required to change the molten salt temperature between the tanks (Fig. 7-1).

Both tanks are 4.6 m (15 ft) in diameter and 4.6 m (15 ft) tall. This size was selected so the hot tank could use full-scale liner panels as well as the same insulation thicknesses recommended for the commercial system and yet still keep the heater and cooler requirements within reason. The choice of a 4- or 5-meter tank makes little difference; a 2-meter tank is considered too small.

The cooler is an updraft forced-air heat exchanger with horizontal tubes. A feedback control system controls the heat rejection by modulating the louvers. Heaters and insulation are necessary to permit preheating of the unit above the salt freezing point prior to startup.

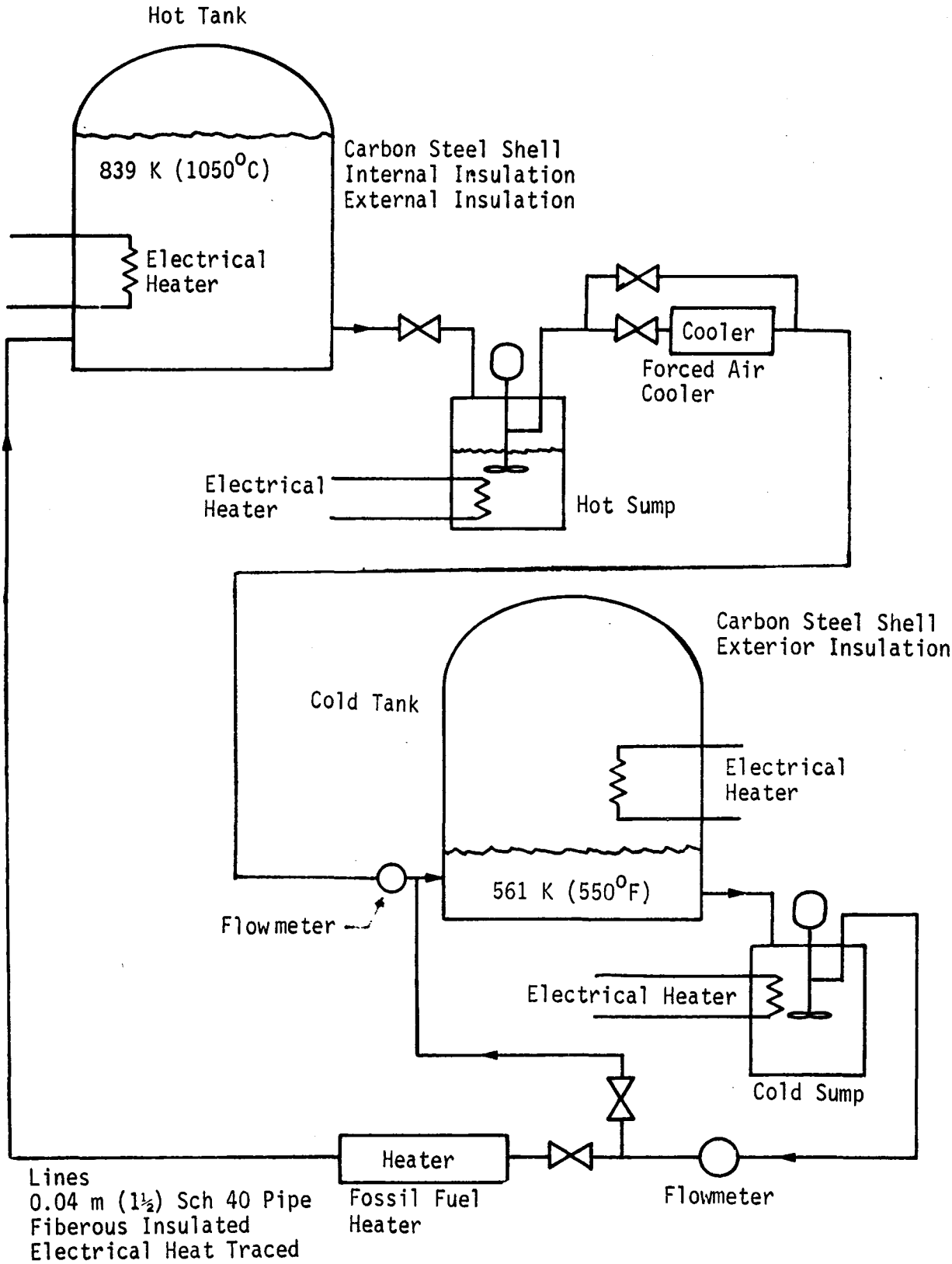

Figure 7-1 SRE Test Schematic

The heater is a vertical cyclindrical unit with coiled heater tubes. Fossil fuel heaters at the bottom of the unit heat the tubes by exhaust gases. These heaters are used commercially in molten salt applications.

The system shown in Figure 7-1 allows for filling the tank in 5 hours and draining the tank in 5 hours to simulate a normal day cycle. The cooler and heater are sized for the maximum flow rate and temperature change. The pumps used are cantilever-type pumps to avoid seal and bearing problems. The pumps are suspended into sumps with heaters to maintain their temperature.

The system is filled by using the cold sump to melt the draw salt. Electrical heaters are used to melt the salt. Partherm 430 (Park Chemical) could be used or sodium nitrate and potassium nitrate could be bought in bulk and mixed in the cold sump. Purchase of the bulk would be cheaper and be more representative of actual system operation.

The lines and cooler are trace-heated to prevent salt from freezing when it is not being pumped. The cooler will have to be heated to prevent freezing during startup and no-flow conditions. Electrical heaters are also placed on the hot and cold tanks to prevent freezing.

It is necessary to perform element tests of the liner. The first series of tests are bending and pressure cycling tests taken to fatigue failure. These tests establish the material thickness and the spacing and size of the expansion fold (knuckle) that should be used. The second series of tests involves making a corner section and building a 1-m^3 section of the tank. Three of these sections are filled with 839 K (1050°F) molten salt and cycled to failure under three different stresses. These tests are expected to give enough data and confidence to build and operate a full-scale tank.

The design requirements of each system element are given in Table 7-1.

Table 7-1 SRE Design Requirements

Hot Tank - 4.6-m dia x 4.6-m high (15-ft dia x 15-ft high)

Tank material - carbon steel

Wall insulation
Internal - 0.23-m (9-in.) Krilite 30 insulating brick
External - 0.08-m (3-in.) fibrous blanket

Floor insulation
Internal - 0.23-m (9-in.) Krilite 30 insulating brick
External - 0.15-m (6-in.) insulating concrete

Roof insulation
Internal - 0.15-m (6-in.) fibrous blanket
External - 0.15-m (6-in.) block insulation

Internal Liner - Stainless steel liner on all inside surfaces

Table 7-1 SRE Design Requirements (continued)

External lagging - protective sheathing top and sides

Heater - 20 kW electrical heater to maintain salt at 553 K (500°F)

Cooling coil under foundation for ground cooling using facility water

Cold Tank - 4.6-m dia x 4.6-m high (15-ft dia x 15-ft high). Same design as hot tank

Tank material - carbon steel

Wall insulation (external) - 0.25-m (10-in.) fibrous blanket

Floor insulation (external) - 0.15-m (6-in.) insulating concrete

Roof insulation (external) - 0.18-m (7-in.) block insulation

External lagging - protective sheathing top and sides

Heater - 20 kW electrical heater to maintain salt at 553 K (500°F)

Cooling coil under foundation for ground cooling using facility water

Hot Sump - 0.76-m dia x 0.76-m high (30-in. dia x 30-in. high)

Tank material - stainless steel

Top and side insulation - 0.15-m (6-in.) fibrous blanket

Floor insulation - 0.15-m (6-in.) insulating concrete

Pump - Cantilever pump, 26 gpm, 79 ft head, stainless steel

Electrical heater - 0.9 kW band heater, exterior of tank

Cold Sump Processors (2) - 0.44-m dia x 0.91-m high (8-ft dia x 3-ft high)

Tank material - carbon steel

Top and side insulation - 0.25-m (10-in.) fibrous blanket

Floor insulation - 0.15-m (6-in.) insulating concrete

Pump - Cantilever pump, 26 gpm, 66-ft head, carbon steel

Electrical heater - 152 kW tubular heater through tank

Table 7-1 SRE Design Requirements (concluded)

Heater - oil-fired air-atomizing furnace. Standard furnace design, usable for molten salt. 2.34-m dia x 7.9-m high (92-in. dia x 26-ft high), stainless steel coil

Cooler - updraft, forced air variable-pitched fans for control; stainless steel coil. Electrical heater provided for initial heating

Lines

Material - 0.04-m (1.5-in.) dia pipe schedule 40, either carbon steel or stainless steel as required

Insulation - 0.05-m (2-in.) thick, either fibrous blanket or calcium silicate

Trace heating - 295-W/m (90-W/ft) heater cable

Heater controls - required for hot tank, cold tank, hot sump, cold sumps (4), lines (6), and cooler

Instrumentation

Thermocouples - 100
Probe thermocouples - 50
Strain gages - 25
Flow measurements - 2
Pressure transducers - 10

C. SCHEDULE

A schedule for the SRE is shown in Figure 7-2. The program, including a one-month test period, will be completed in 13 months. The liner design would have to be selected in the fourth month, well ahead of completion of the liner development testing. We believe this is an acceptable risk. Long-lead procurement of such critical hardware as the cooler, liner material, valves, and pumps would have to be done very early. The schedule risk could be significantly reduced if long-lead procurement and liner development could be started earlier. Also a program duration of 18 months might be more feasible.

D. SYSTEM COST

A budgetary cost estimate of a program for the SRE design, build and test is described in this section. The test phase will encompass one-month. Although this program does not include a longer test time, some consideration should be given to a longer test duration and possible teardown of the system for evaluation.

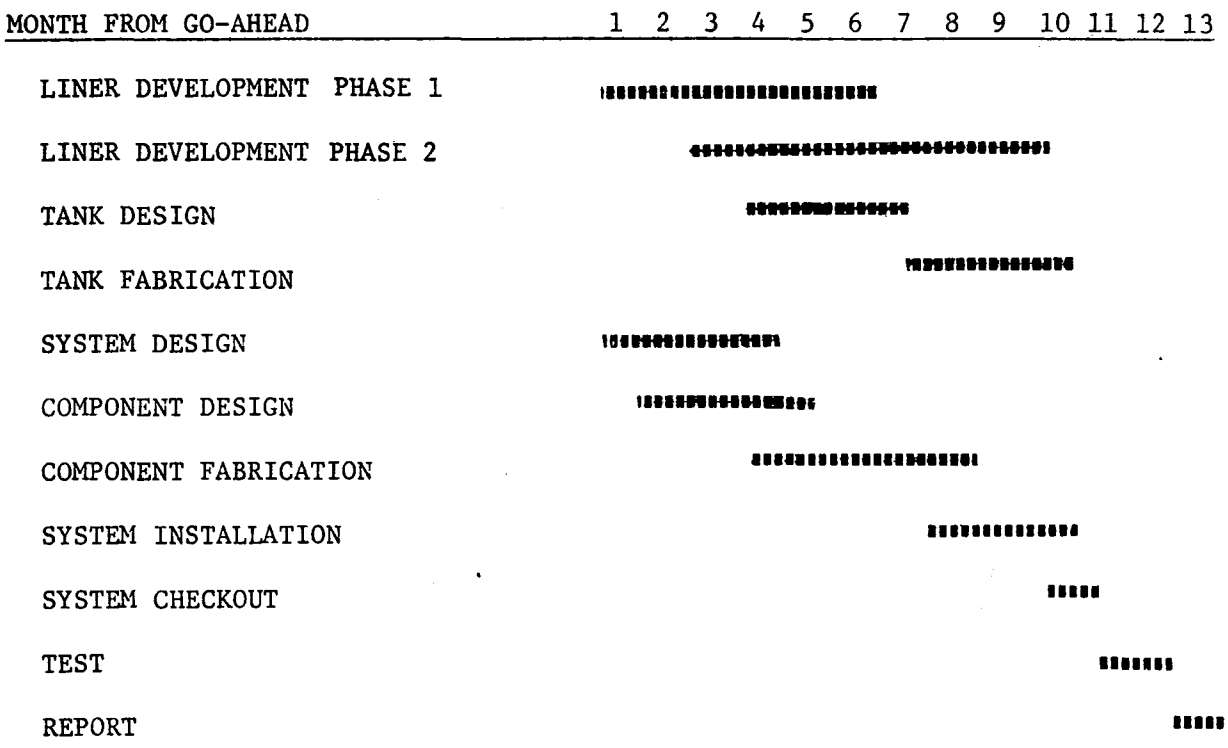

FIGURE 7-2 SRE PROGRAM SCHEDULE

Cost estimates:

Hot tank - total design and fabrication	$ 369,000	(1)
Cold tank - shell design same as hot tank	209,000	(2)
Heater - design and fabricated	123,000	(1)
Cooler - design and fabricated	49,000	(1)
Pumps - two cantilever	22,000	(1)
Valves - six valves	17,000	(3)
Miscellaneous - pipe, structure, insulation, console, etc.	37,000	(2)
Electrical equipment - heater, controller, etc.	59,000	(2)
Instrumentation-thermocouples, gauges, flow meters etc.	15,000	(3)
Engineering	283,000	(2)
Fab/build	130,000	(2)
Site installation	22,000	(2)
Trips and TDY	20,000	(2)
Miscellaneous reports, reproduction, etc.	25,000	(2)
Liner development	362,000	(1)
Salt	96,000	(3)
Total Cost	$1,838,000	

(1) Vender Quotes
(2) Martin Marietta Corporation Estimate
(3) Previous Purchases

APPENDIX A

MATERIAL EVALUATION PHOTOGRAPHS

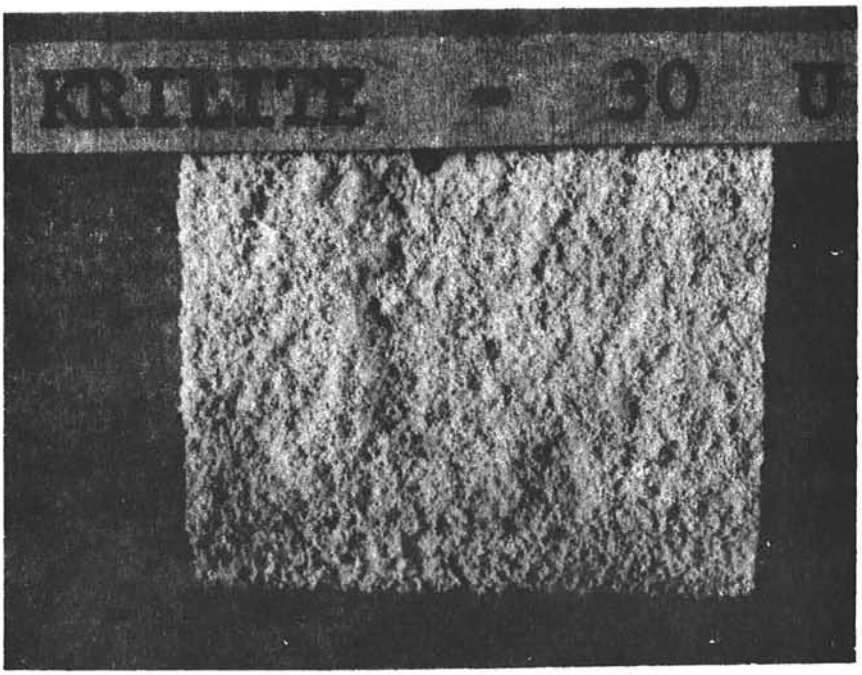

(a) Unexposed

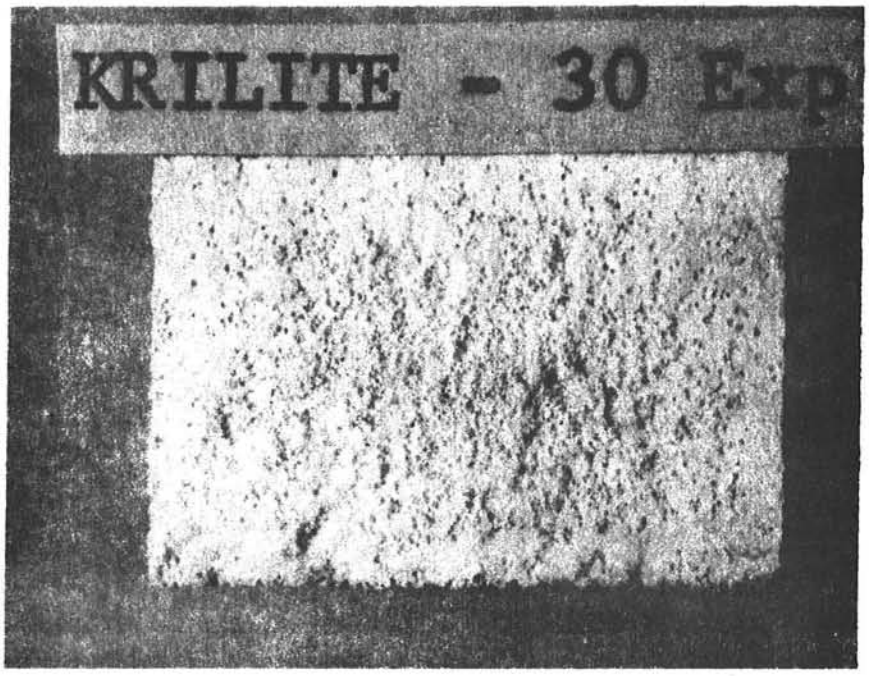

(b) Exposed

Figure A-1
Unexposed and Exposed Surfaces of Insulating Brick KRILITE 30 (3X)

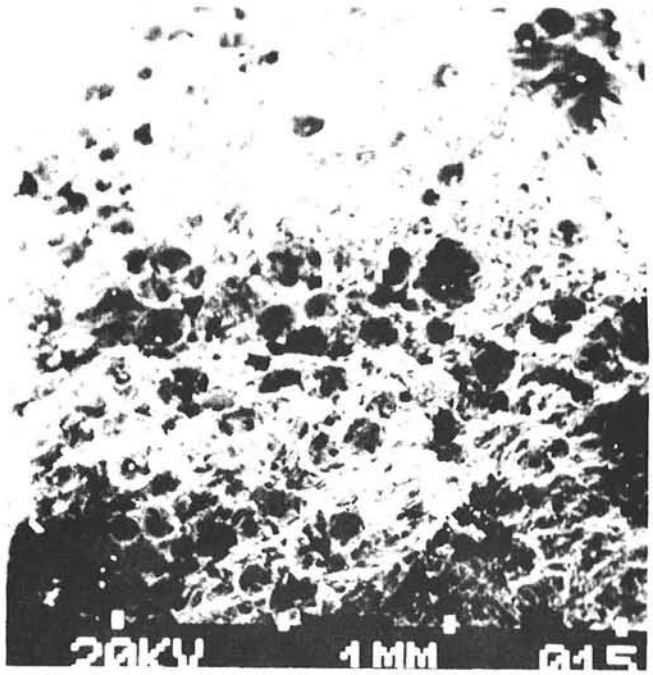

(a) Pore wall rupturing

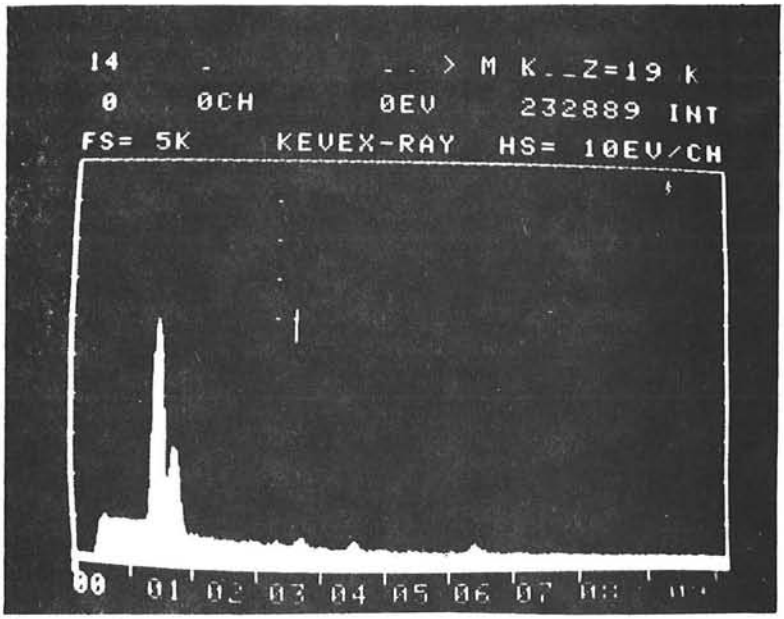

(b) Elemental analysis showing the brick matrix composition Aℓ ans Si.

Figure A-2
Unexposed Krilite 30 - Room Temperature Fracture Surface Showing Pore Wall Rupturing

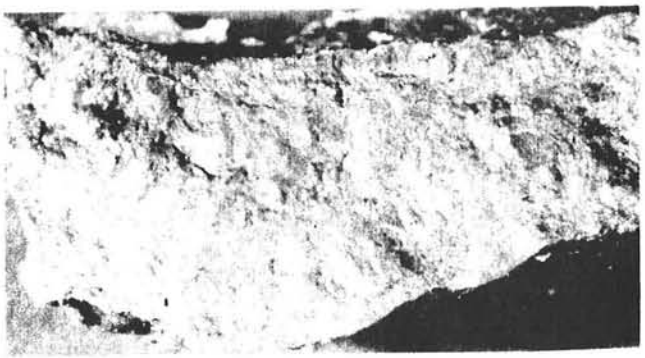

(a) Fracture surface - absence of pore structure

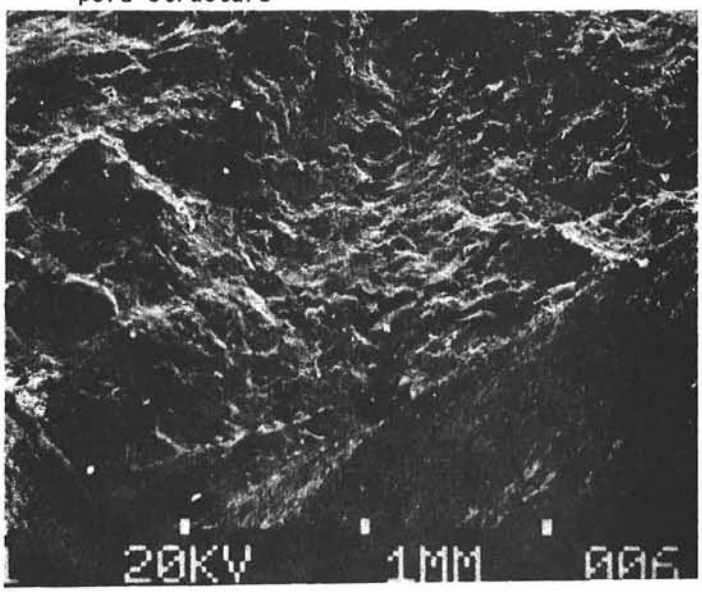

(b) Edge of the fracture surface - absence of pore wall rupturing shown in figure. Transgranular tear ridges with intermittent cleavage facets.

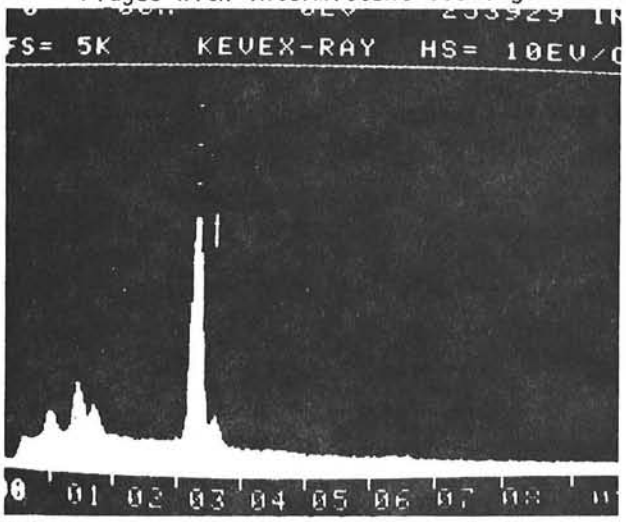

(c) Presence of K and little Na (salt) on the fracture

Figure A-3
Exposed Krilite 30 SEM Evaluation (Room Temerature Fracture Surface)

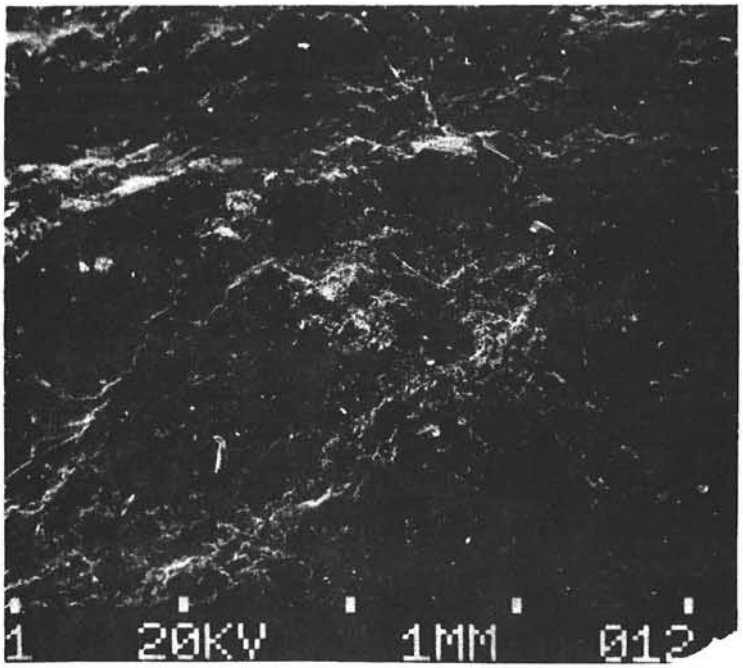

(a) Fracture mode same as Fig. A-3 (b). less cleavage facets.

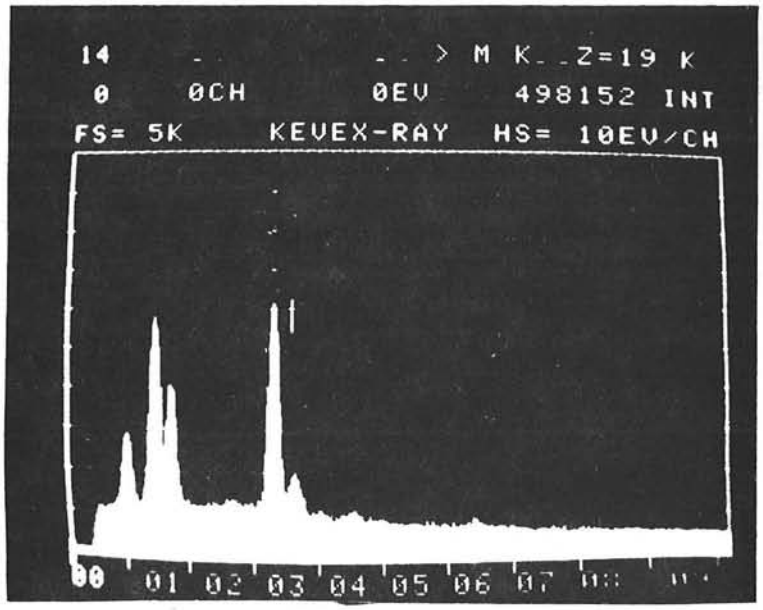

(b) Salt penetration (K. Na) and homogenous blending with brick matrix (Al, Si and Ca) indicating new compound formation.

Figure A-4
Exposed Krilite 30 - SEM Evaluation - Center of the Fracture Surface Shown in Fig. A-3 (a)

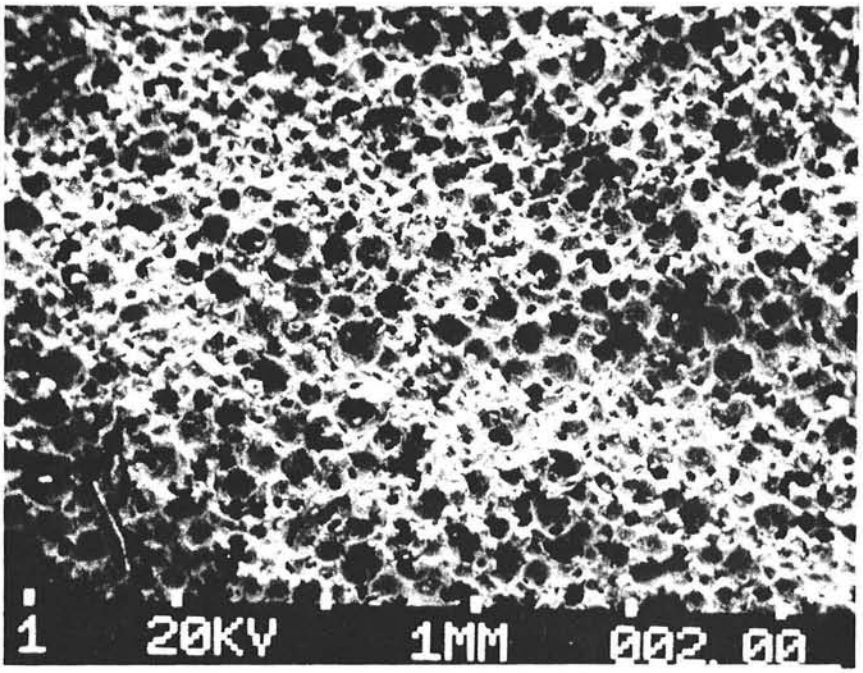

(a) Porewall rupturing same as Fig A-1(a)
Typical all over the fracture surface

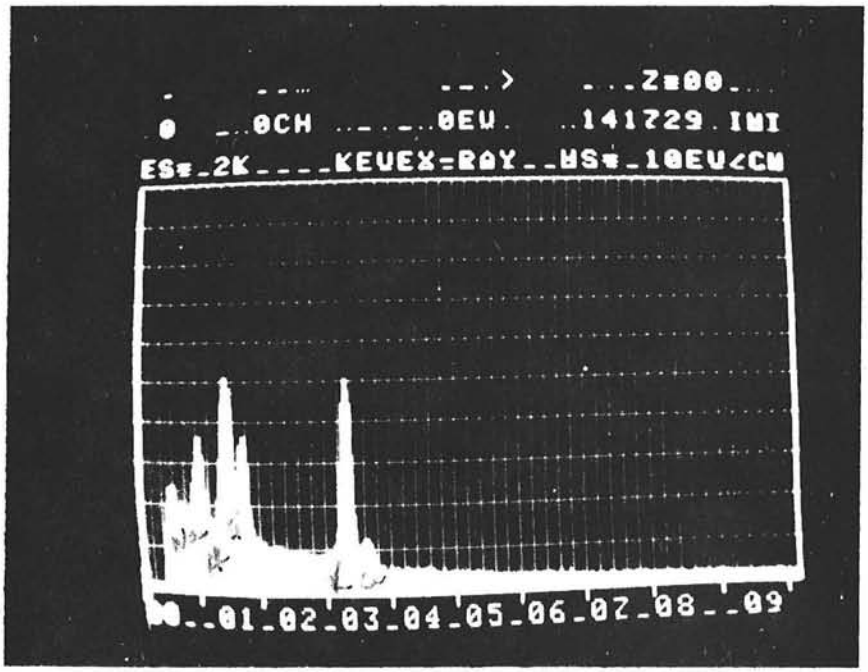

(b) Salt (K, Na) impregnation of
brick matrix (Aℓ, Si, Ca)

(Typical all over the fracture surface)

Figure A-5
Exposed Krilite 30 - High-Temperature Fracture Surface

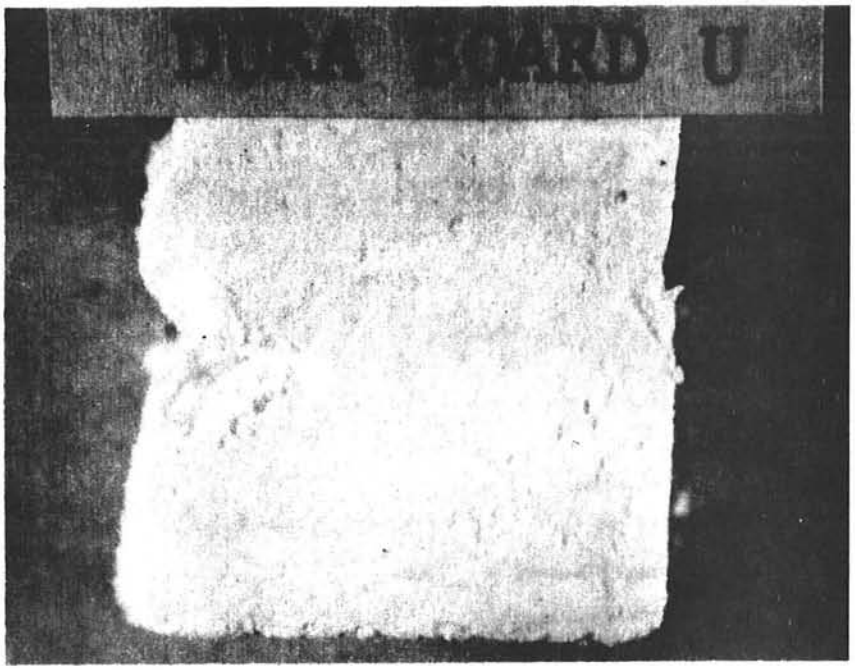

(a) Unexposed

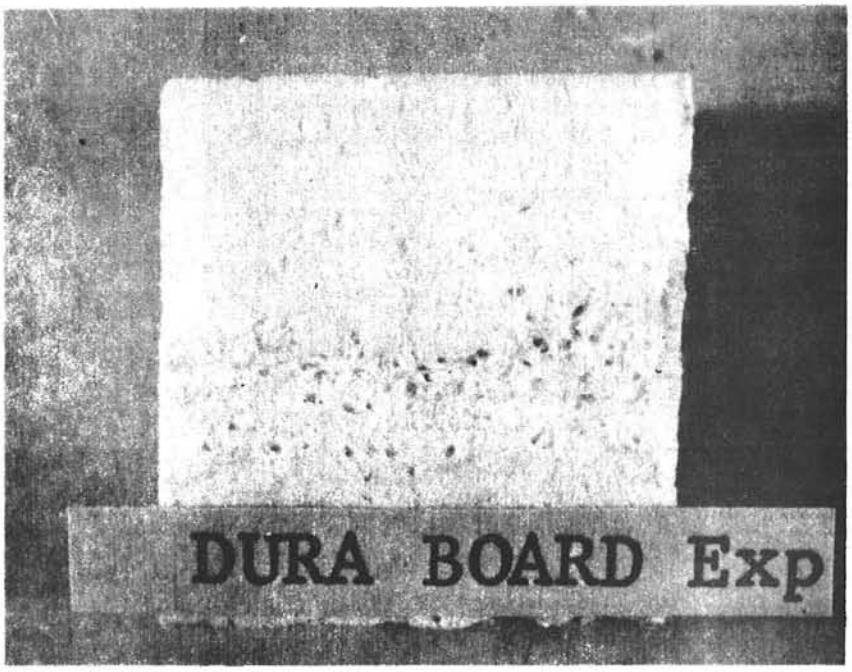

(b) Exposed

Figure A-6
Unexposed and Exposed Surfaces of Fiberboard "Duraboard" (3X)

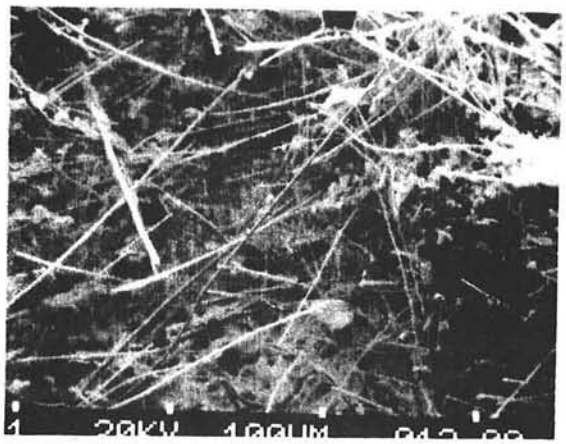

(a) Unexposed fracture surface featureless fracture

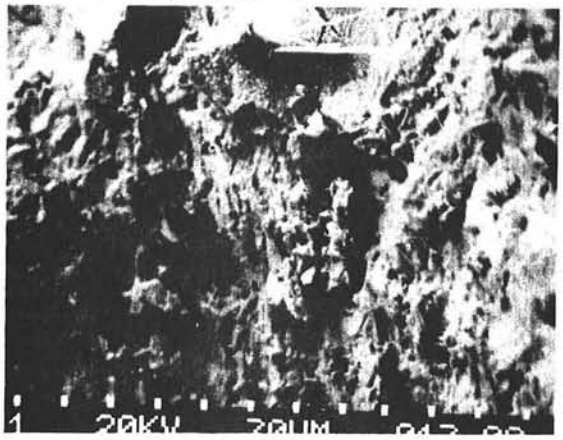

(b) 500 hr exposed fracture surface cleavage type of fracture

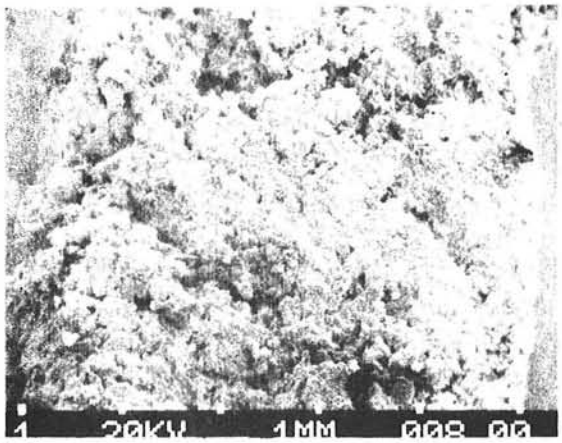

(c) 1000 - Hr exposed fracture surface Transgranular stress corrosion type failure surface completely covered with salt.

Figure A-7
DURABOARD - Unexposed and Exposed Fracture Surfaces - SEM - Room Temperature Fracture

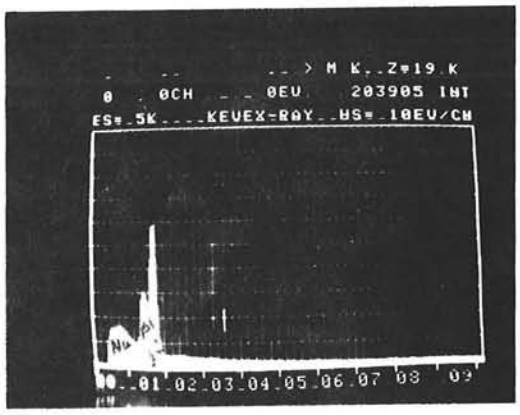

(a) Unexposed - Base Matrix Aℓ, Si

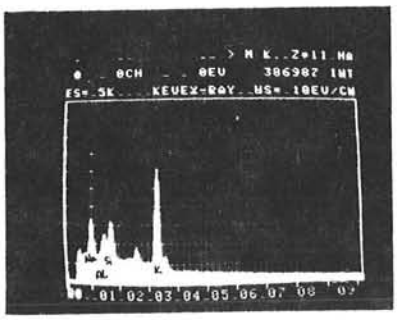

Surface

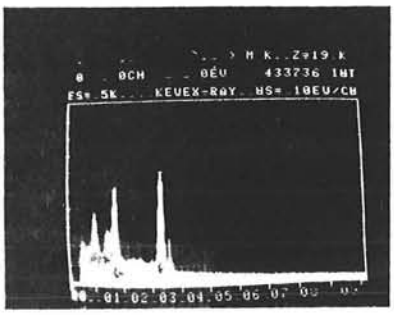

Subsurface

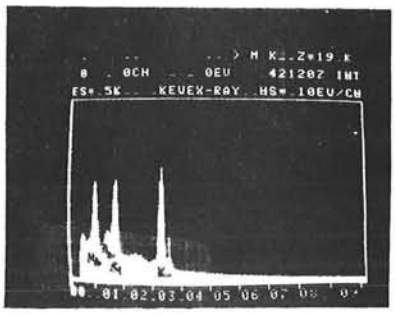

Center of the Specimen

(b) 500-hr exposure

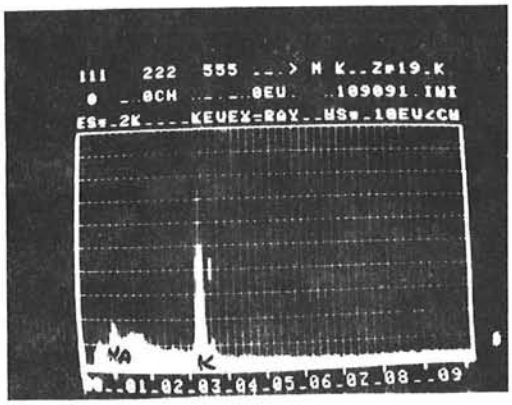

Surface

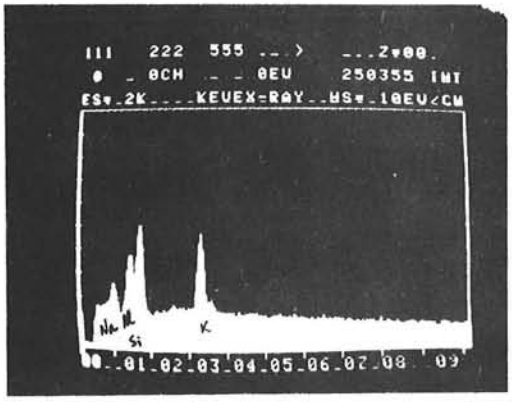

Center

(c) 1000-hr exposure

Figure A-8 Salt Impregnation of Duraboard

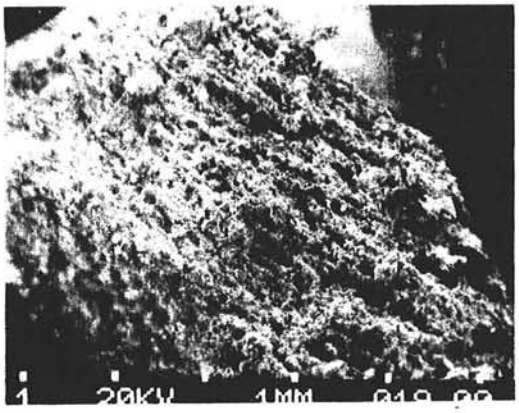

(a) Typical room temperature fracture surface same as (b)

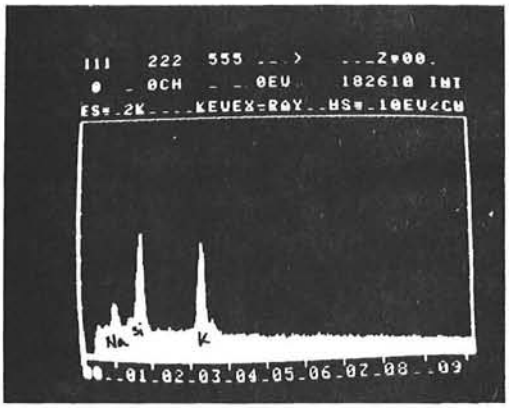

Kevex-ray elemented analysis

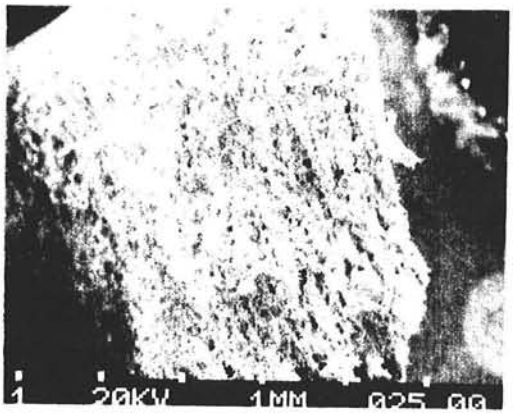

(b) Typical high-temperature fracture surface same as Fig (a)

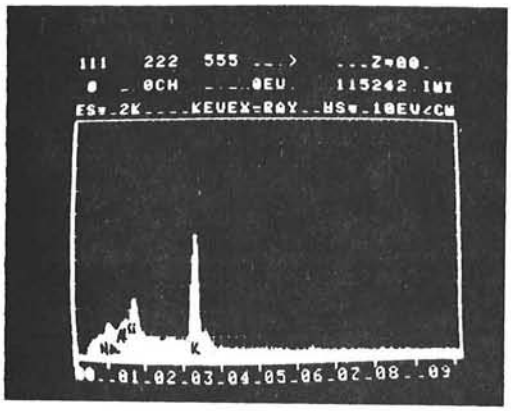

Elemented analysis

Figure A-9
1000 hr Exposed Duraboard Fracture Surfaces, (a) Room Temperature and (b) High Temperature

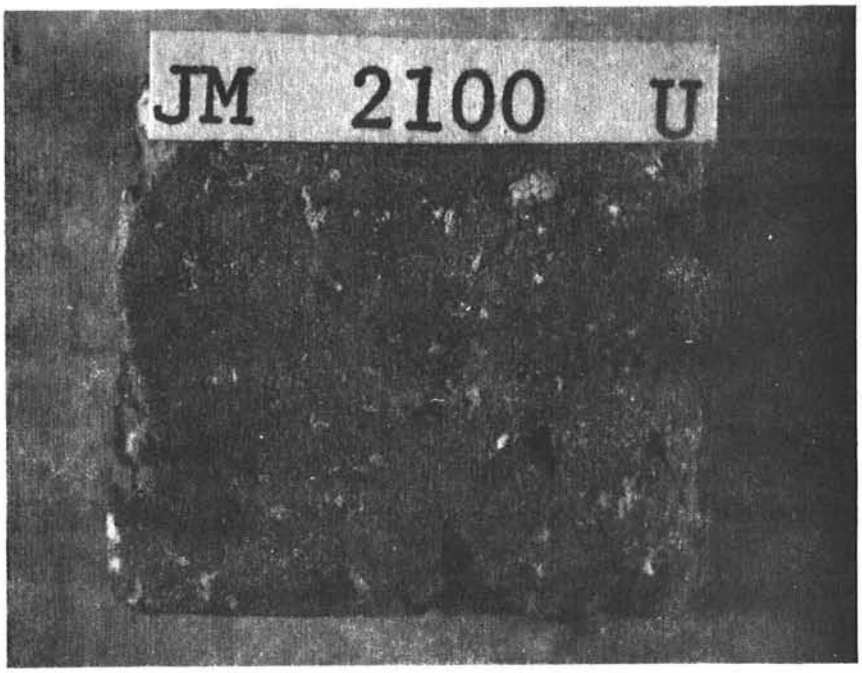

(a) Unexposed

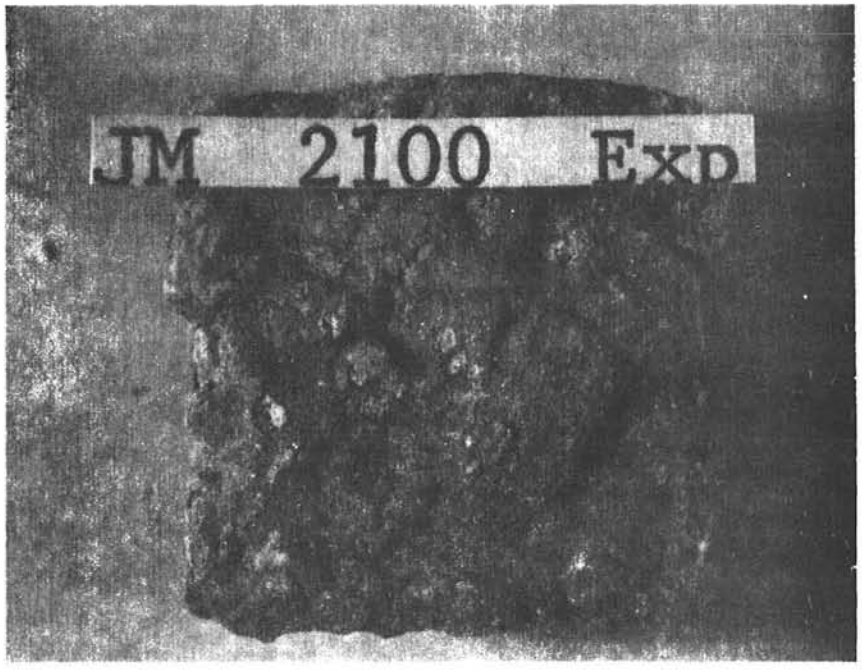

(b) Exposed

Figure A-10
Unexposed and Exposed Surfaces of Insulating Castable JM 2100 (3X)

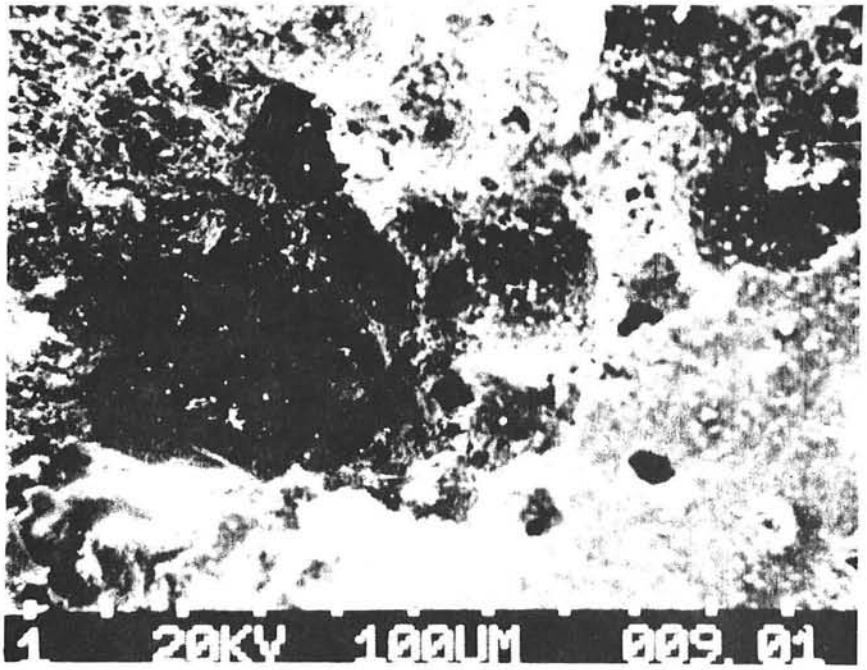

(a) Unexposed fracture due to rupturing of pores

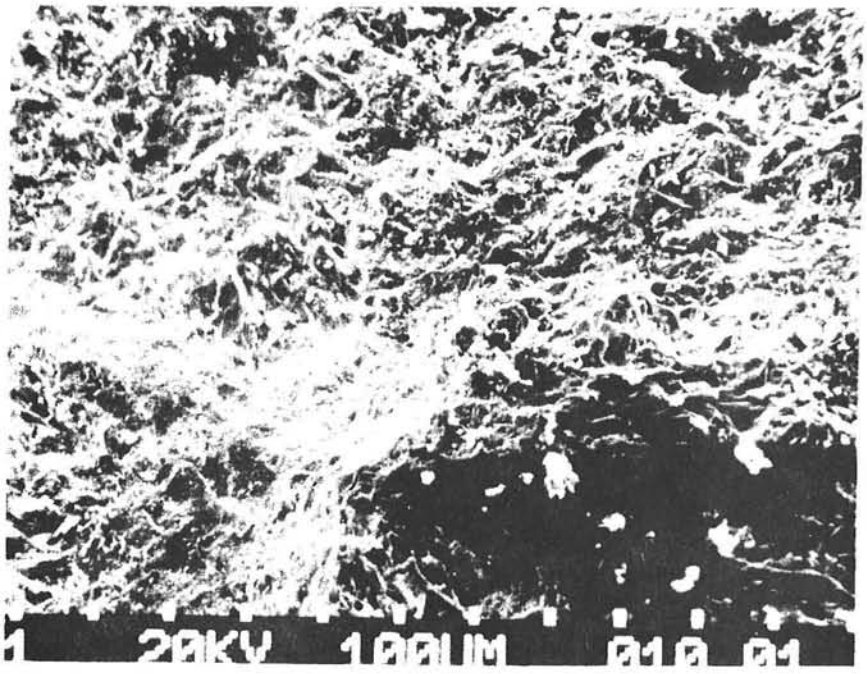

(b) Exposed - intergranular with many cleavage facets

Figure A-11
Unexposed and Exposed Fracture Surfaces - JM 2100 Castable

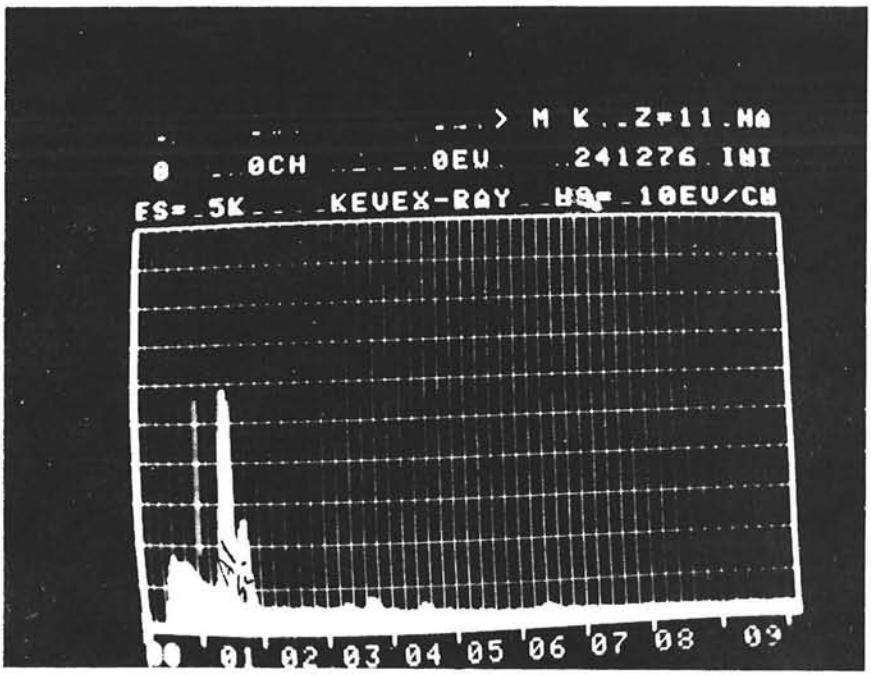

(a) Unexposed - matrix Aℓ, Si

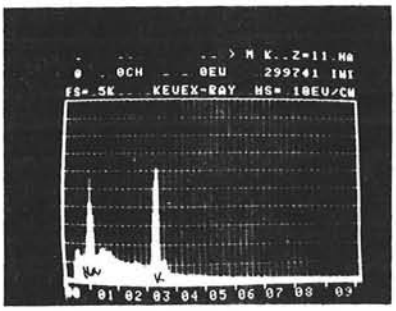

Surface

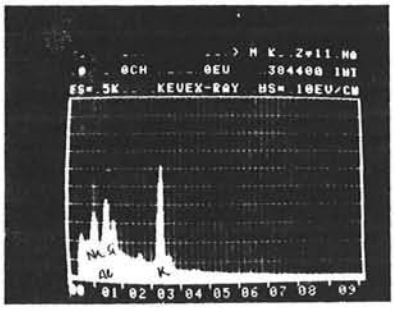

Subsurface

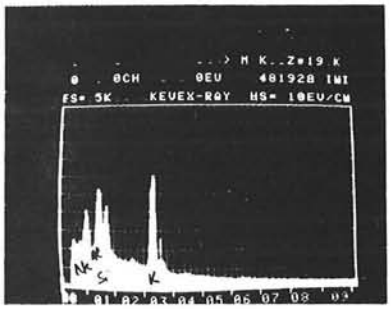

Center

(b) 500-hr exposed - uniform compound formation subsurface and center. Surface covered with salt.

Figure A-12 JM2100 - Salt Impregnation

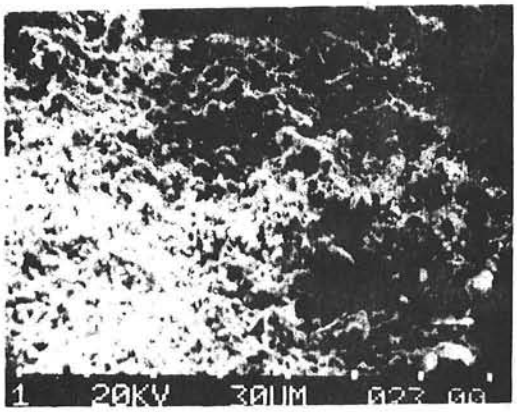

(a) Unexposed stress corrosion type fracture - surface covered with corrosion product

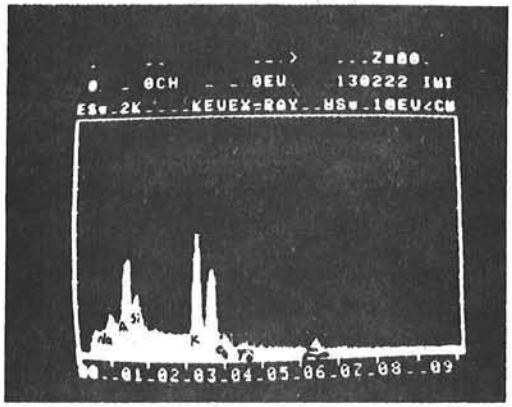

Elemental analysis

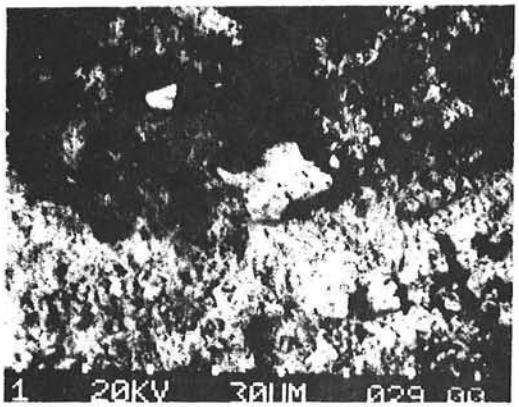

(b) Exposed - fracture same as (a)

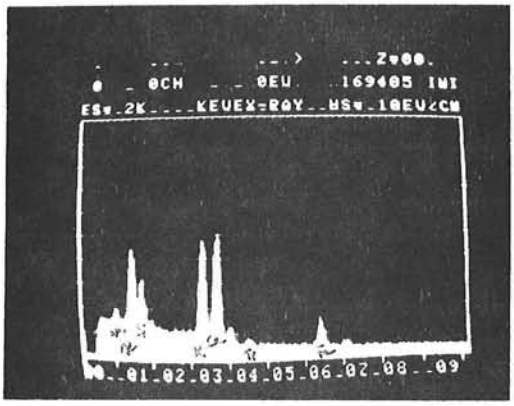

Elemental analysis

Figure A-13
1000-hr Exposed Fracture Surfaces of JM2100, (a) Room Temperature and (b) High Temperature

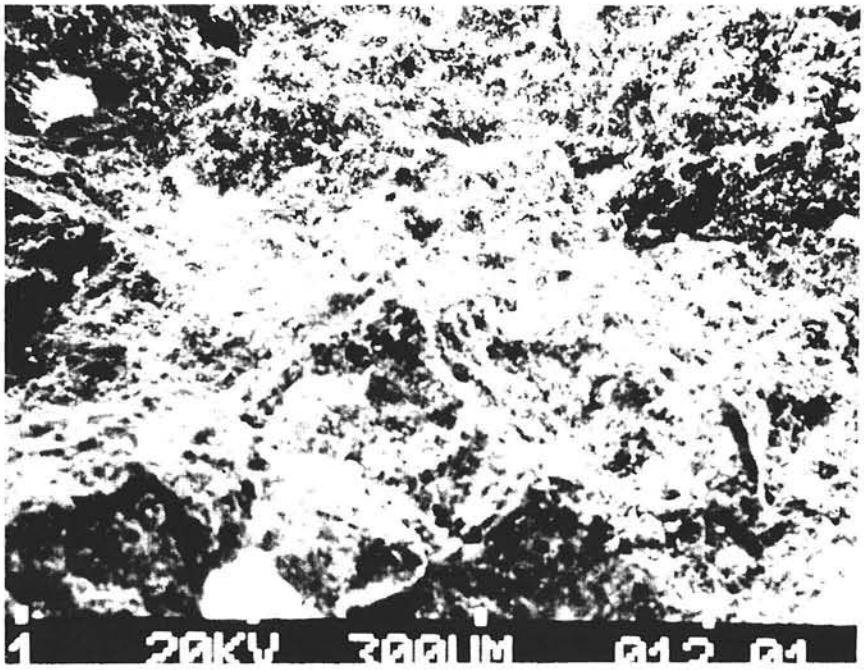

(a) Unexposed fine examples overload type failure

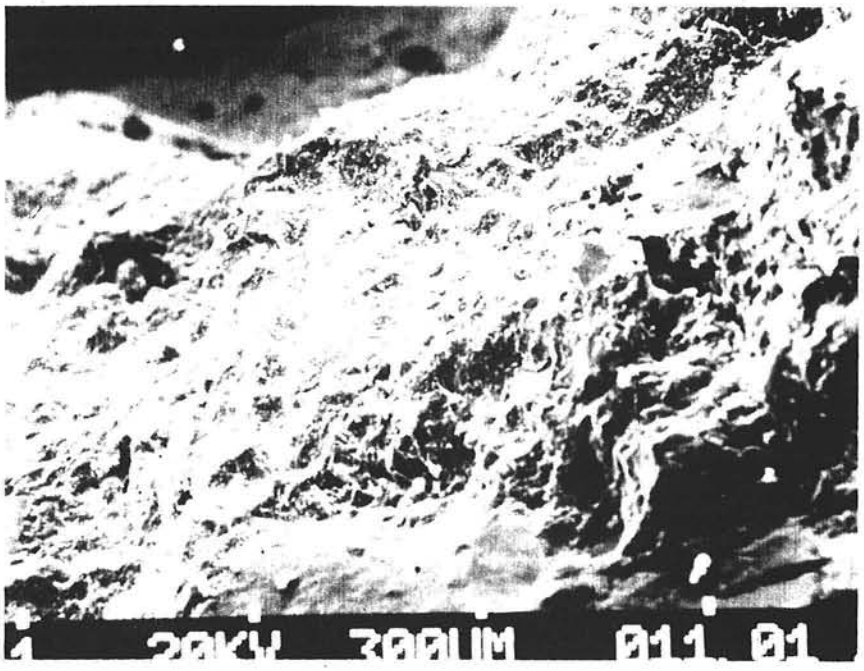

(b) 500-hr exposed surface. Intergranular with some cleavage facets.

Figure A-14
Unexposed and Exposed (500-hr) Fracture Surfaces of JM2800

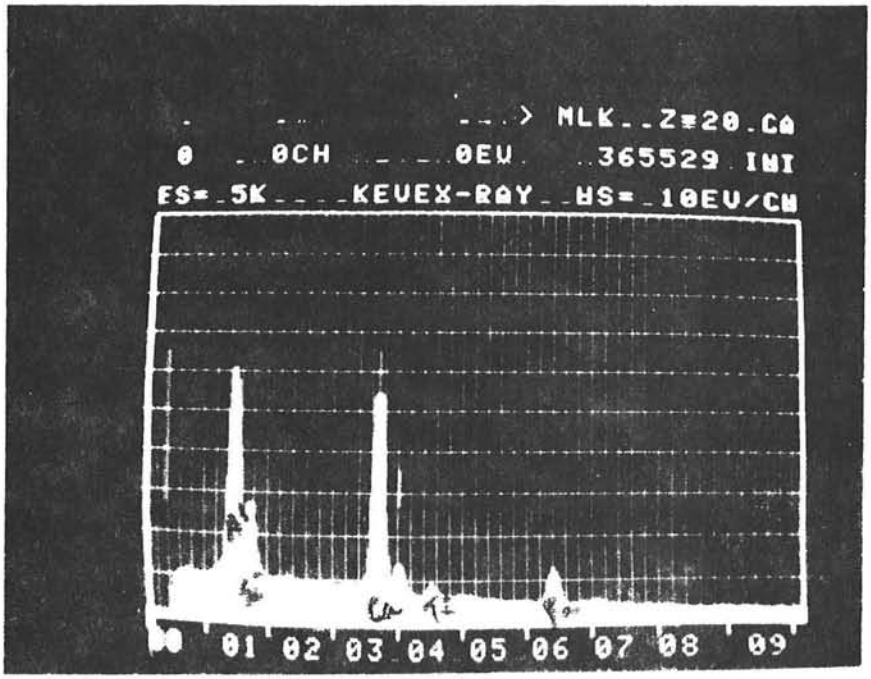

(a) Unexposed - Matrix Aℓ, Si, Ca, Ti and Fe

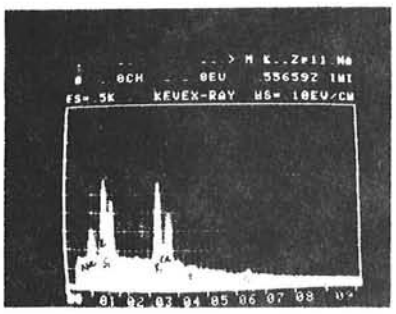

Surface

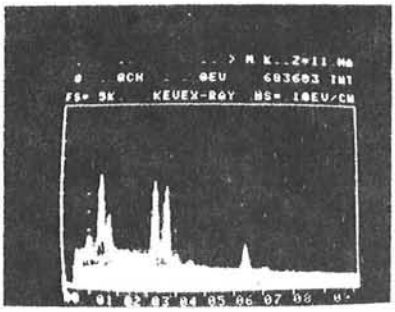

Subsurface

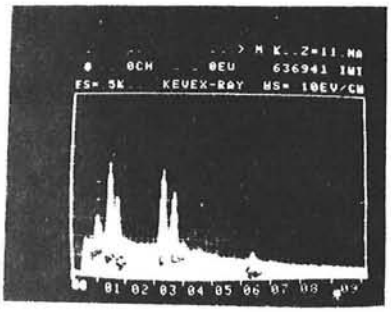

Center

(b) 500-hr exposed specimen - indicating uniform. New compound formation throughout the specimen cross section.

Figure A-15 Salt Impregnation of JM2800 Castable Material

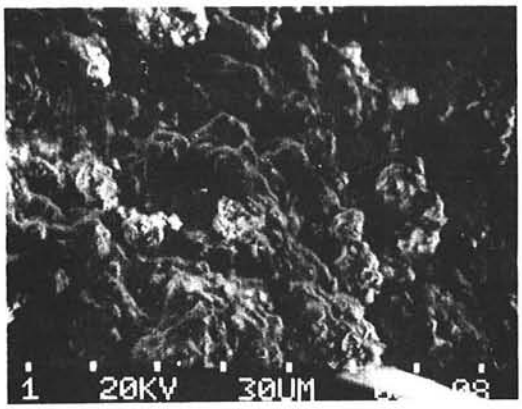

(a) Stress conversion type fracture surface covered with corrosion product

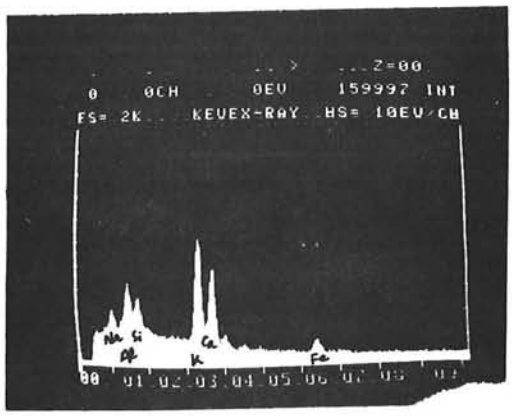

Elemental analysis

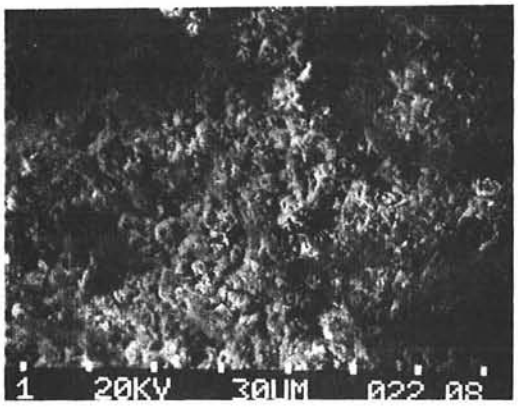

(b) Same as (a) except finer structure

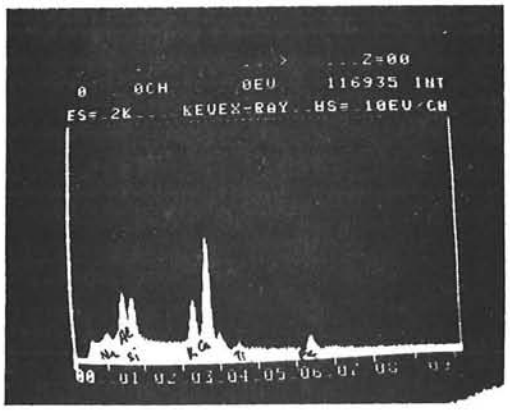

Elemental analysis lower salt concentration than (a)

Figure A-16
1000-hr Exposed Fracture Surfaces of JM2800, (a) Room Temperature and (b) High Temperature

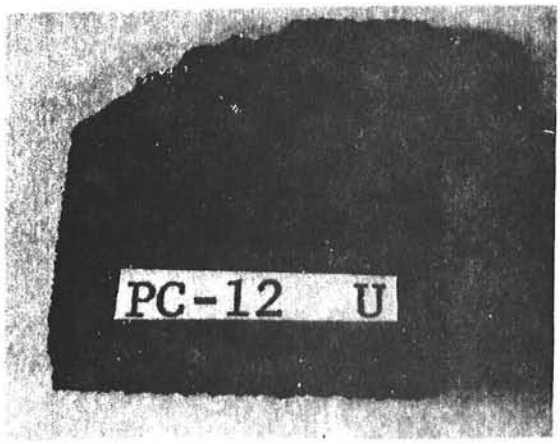

(a) Unexposed

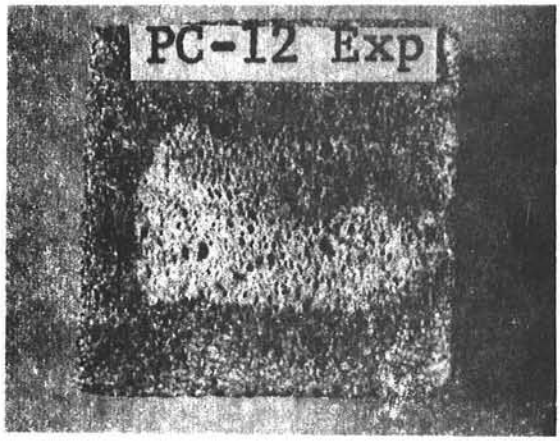

(b) Exposed.

(c) 0.25" below the exposed surface.

Figure A-17
Unexposed and Exposed Surfaces of Foam Glass PC-12, Showing Surface Impregnation with Salt

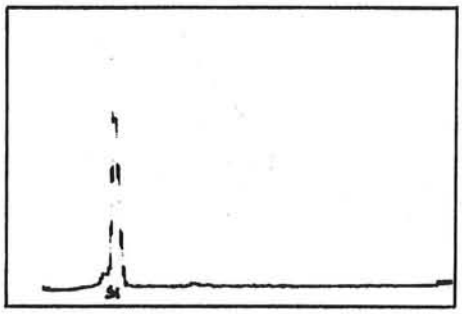

(a) Unexposed sample

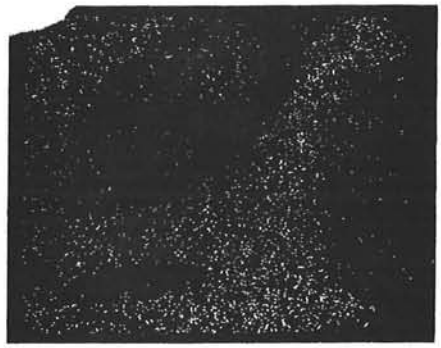

Diffraction pattern

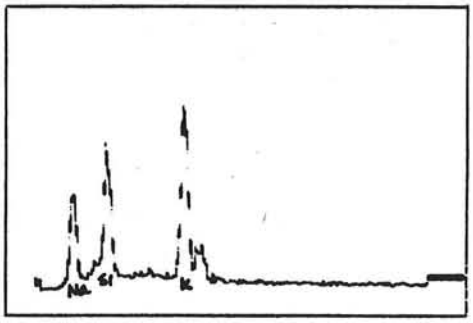

(b) Salt exposed surface

Diffraction pattern

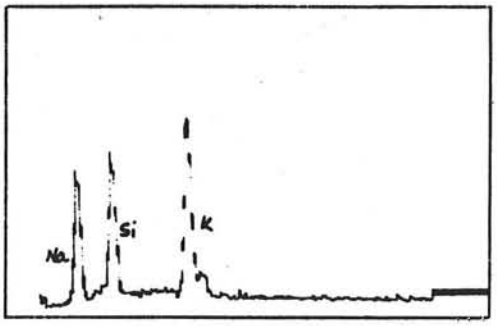

(c) 50μ below the salt exposed surface

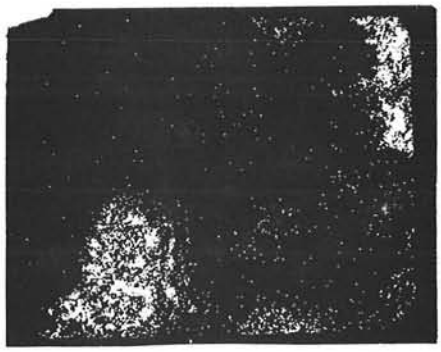

Diffraction pattern

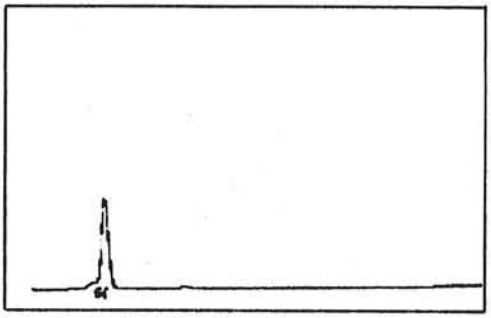

(d) 2000μ below the salt exposed surface

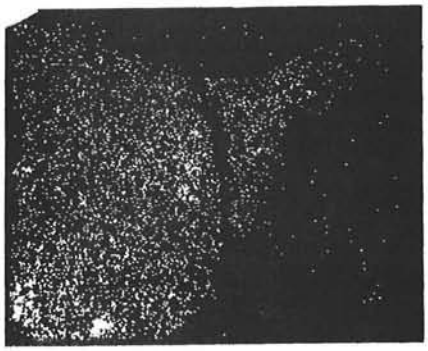

Diffraction pattern

Figure A-18 Electron Microprobe Analysis of Salt Impregnation Depth in PC-12 (Salt Exposed Time - 500 hr) - Potassium Scan - 2000 X

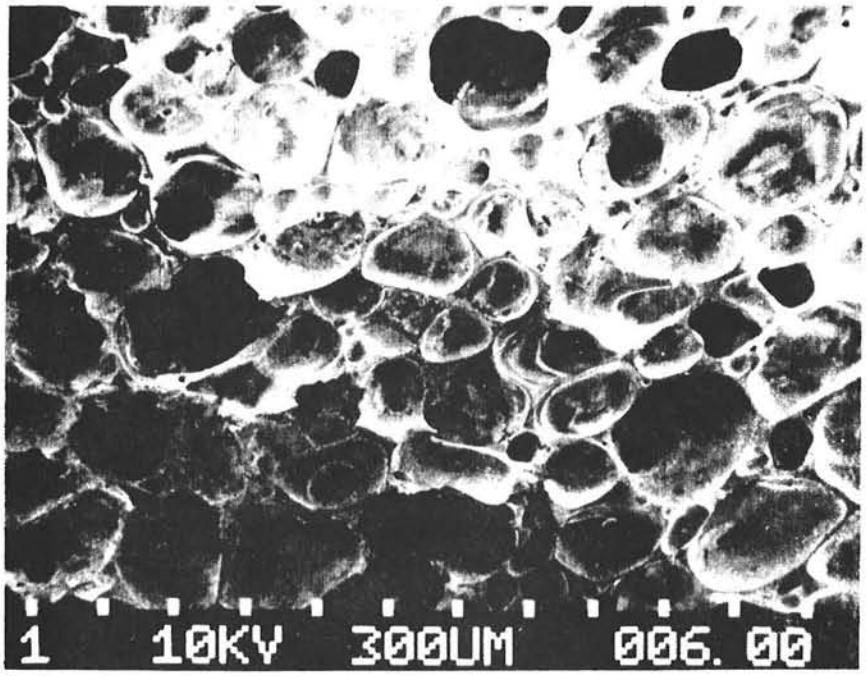

(a) Unexposed - pore rupturing

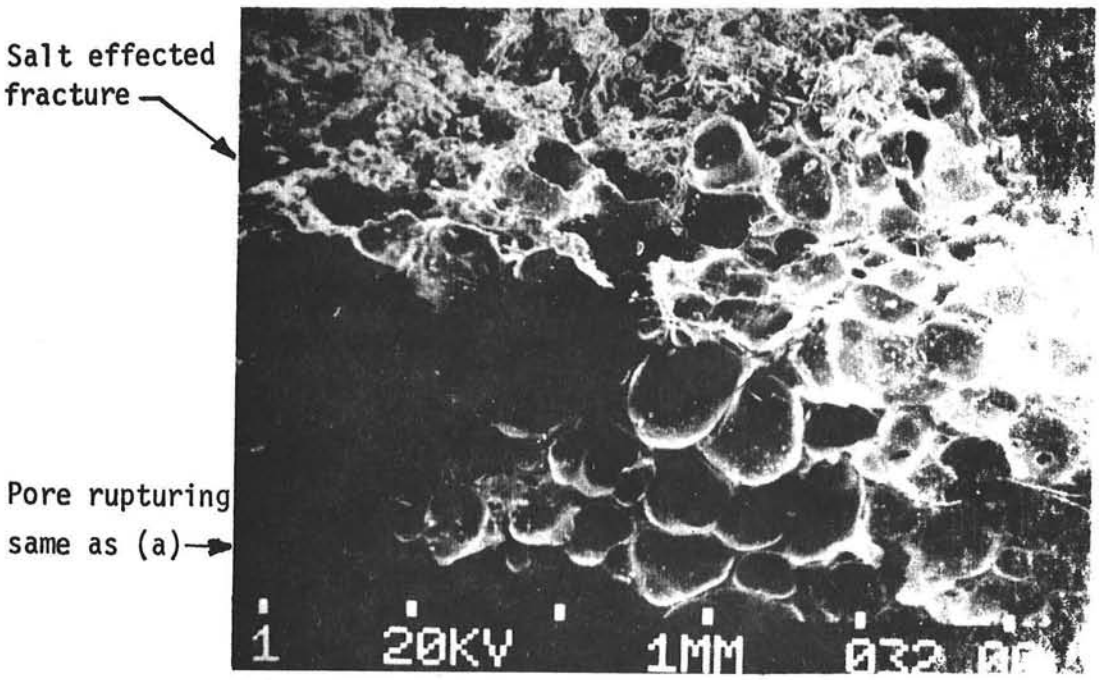

(b) Exposed surface - transgranular fracture at the edge - pore rupturing in center.

Figure A-19

Unexposed and Exposed (500 hr) Fracture Surfaces - PC-12, Showing the Effect of Salt on Fracture Characteristics

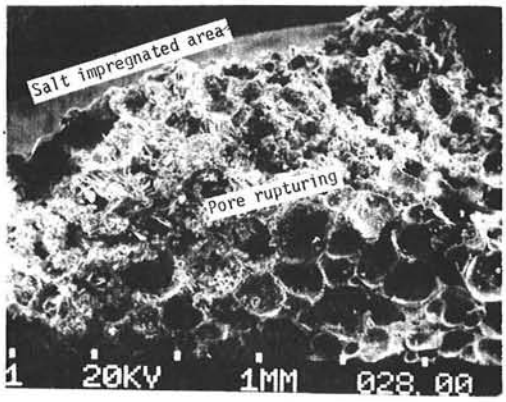

(a) Room temperature

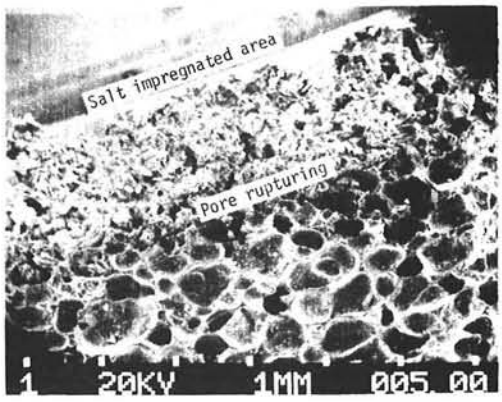

(b) High temperature

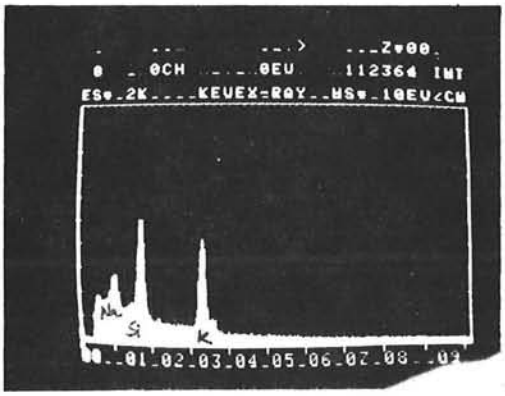

Elemental analysis
of Area A

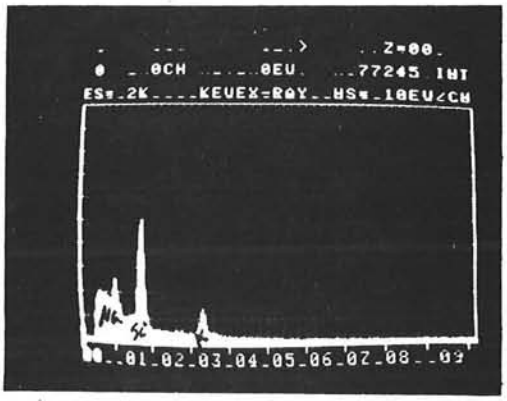

Elemental analysis
of Area A

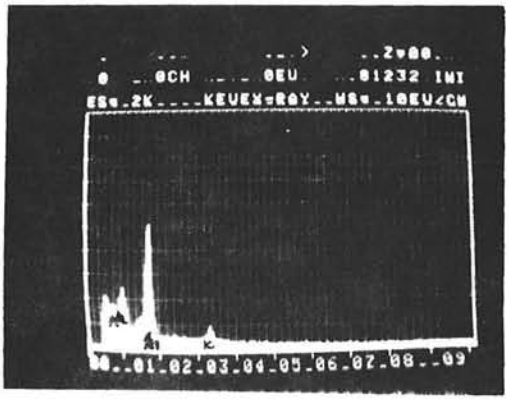

Elemental analysis
of Area B

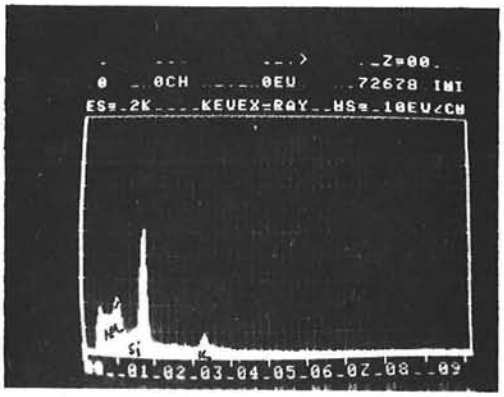

Elemental analysis
of Area B

Figure A-20
PC-12 1000 hr Exposed Fracture Surfaces and Salt Penetration,
(a) Room Temperature and (b) High Temperature, SEM

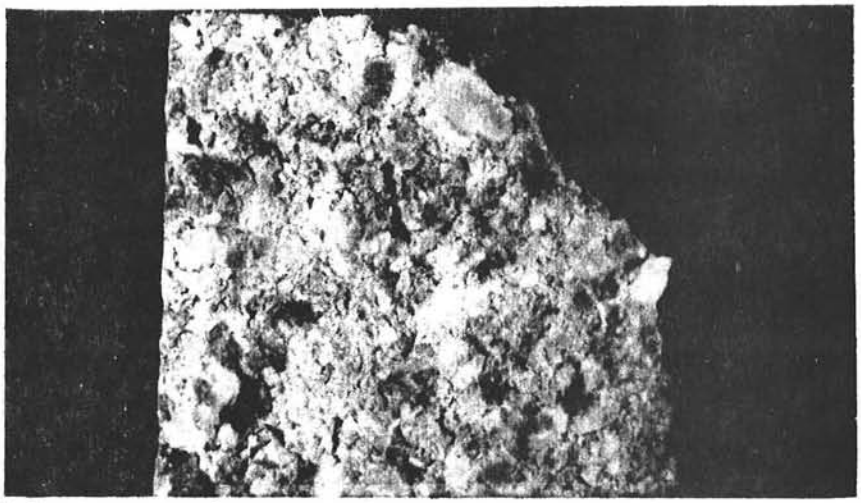

(a) Unexposed

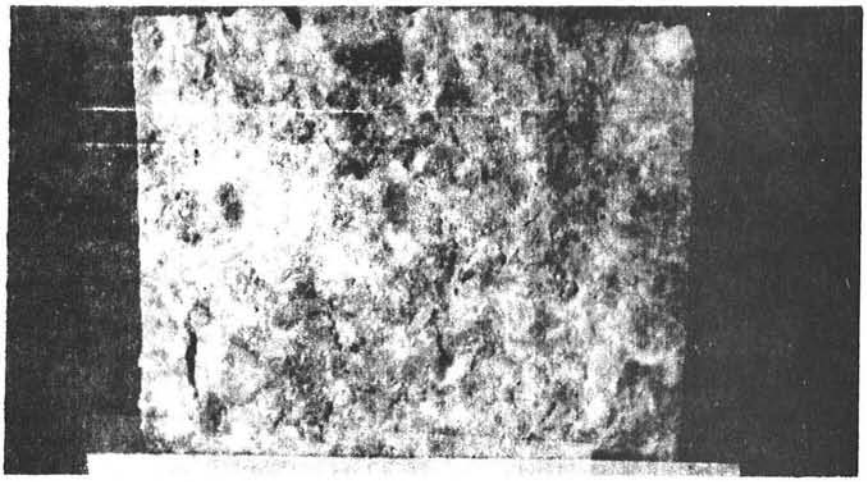

(b) Exposed

Figure A-21 Unexposed and Exposed (500 hr) Surfaces - Maximul 3X.

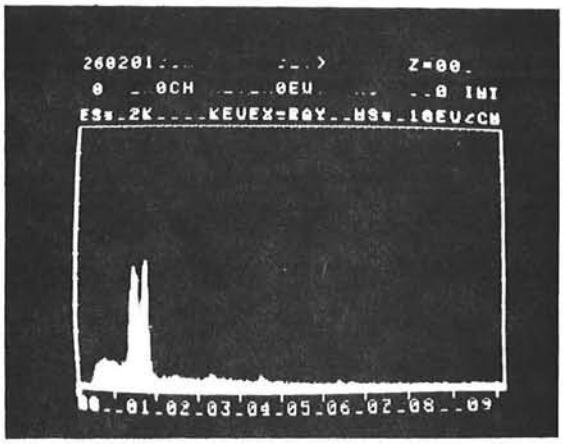

(a) Unexposed

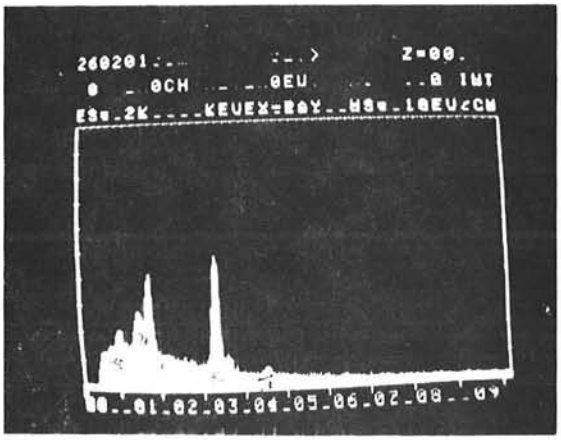

(b) Exposed Surface

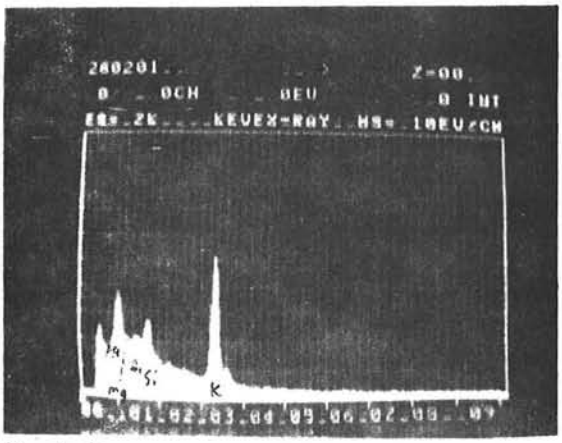

Center

Figure A-22 Maximul - Salt Impregnation - Kevex-ray Analysis

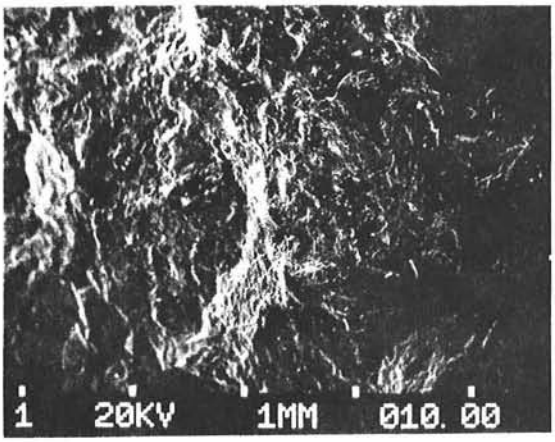

(a) Unexposed - some pore rupturing intergranular type fracture.

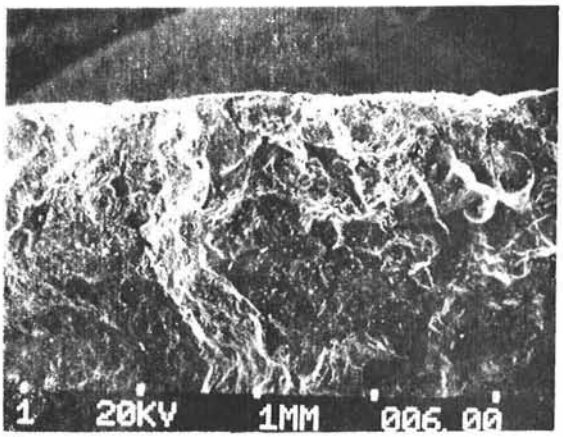

1

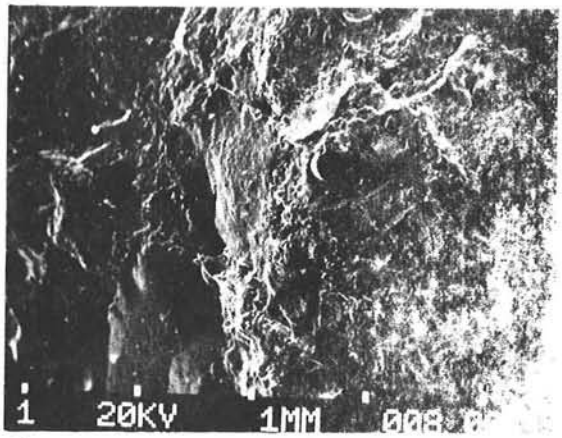

2

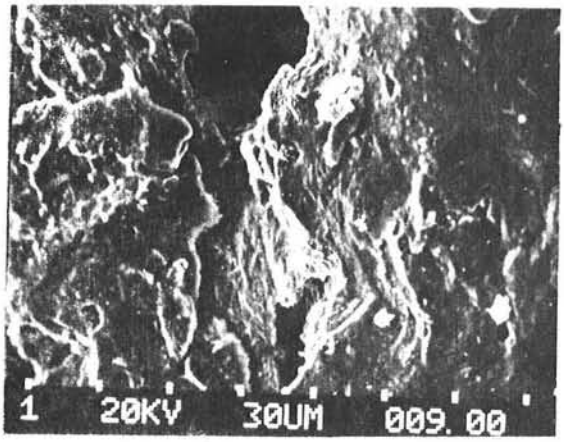

3

(b) Exposed - same as (a) except additional wider intergranular cracks. Cracks filled with salt.

Figure A-23
Maximul - Unexposed and Exposed (1000hr) Fracture Surfaces - SEM

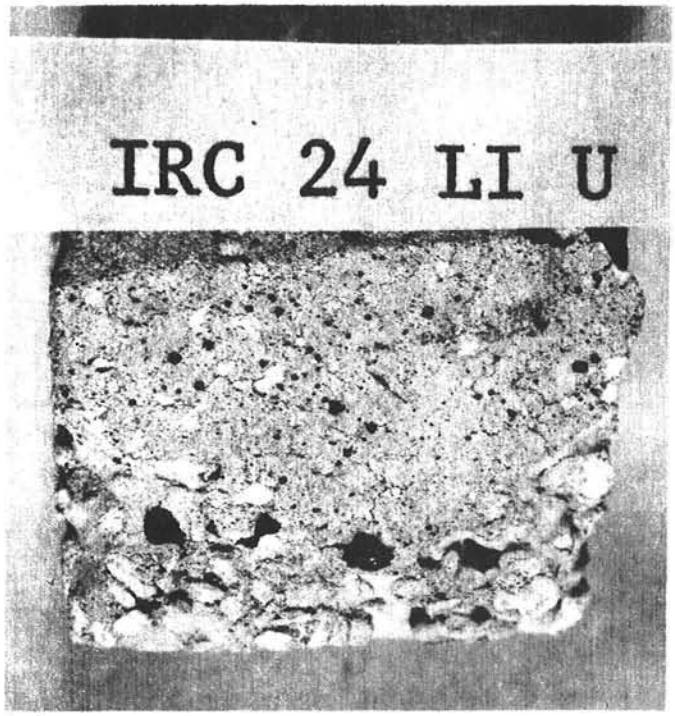

(a) Unexposed

(b) Exposed

Figure A-24
Unexposed and Exposed Surfaces of Insulating Castable **IRC-24LI (3X)**

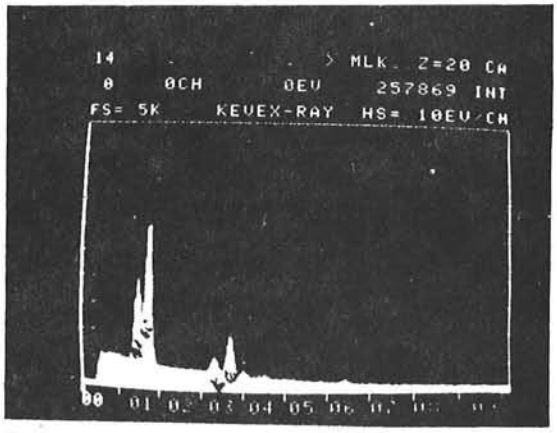

(a) Unexposed sample

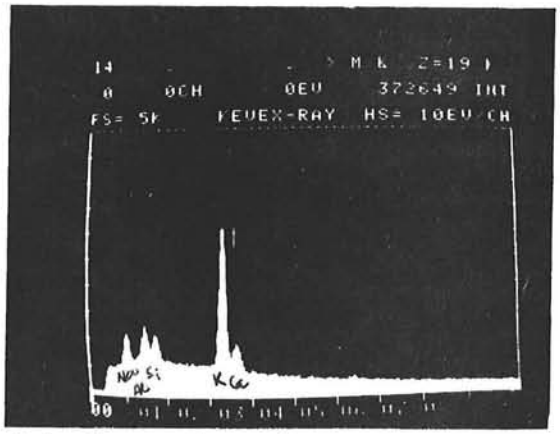

(b) Exposed sample Surface

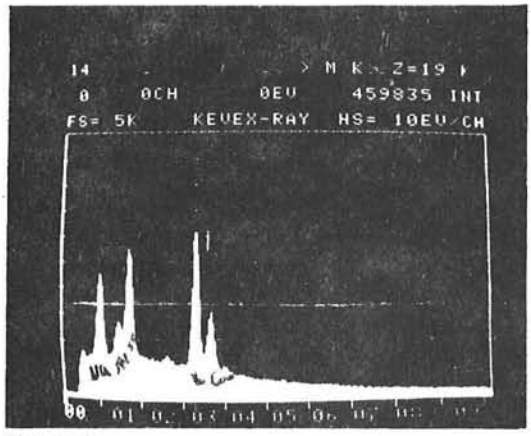

Center

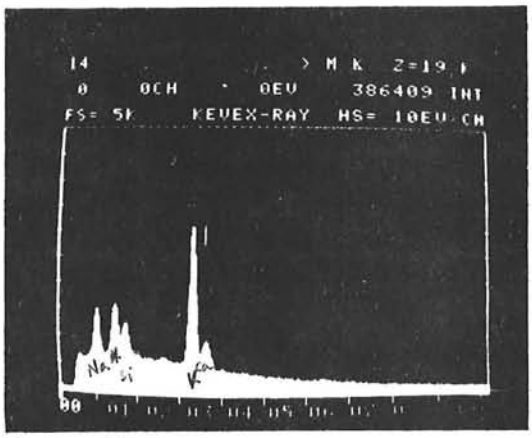

Subsurface

Figure A-25
IRC24LI - Salt Impregnation - (500 hr Exposure).
SEM (Kevex-ray Analysis)

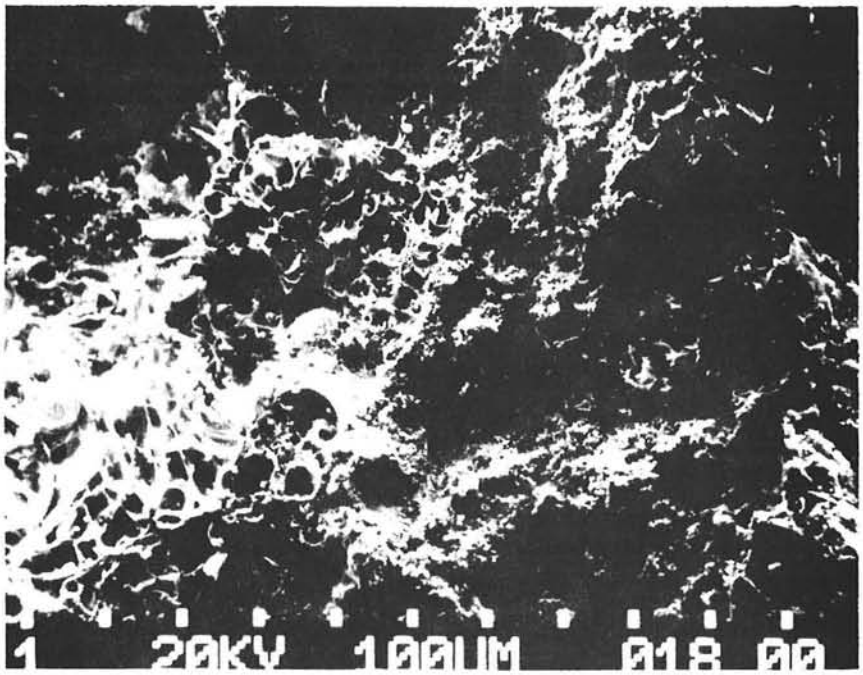

(a) Unexposed - pore rupturing some fine cleavage facets.

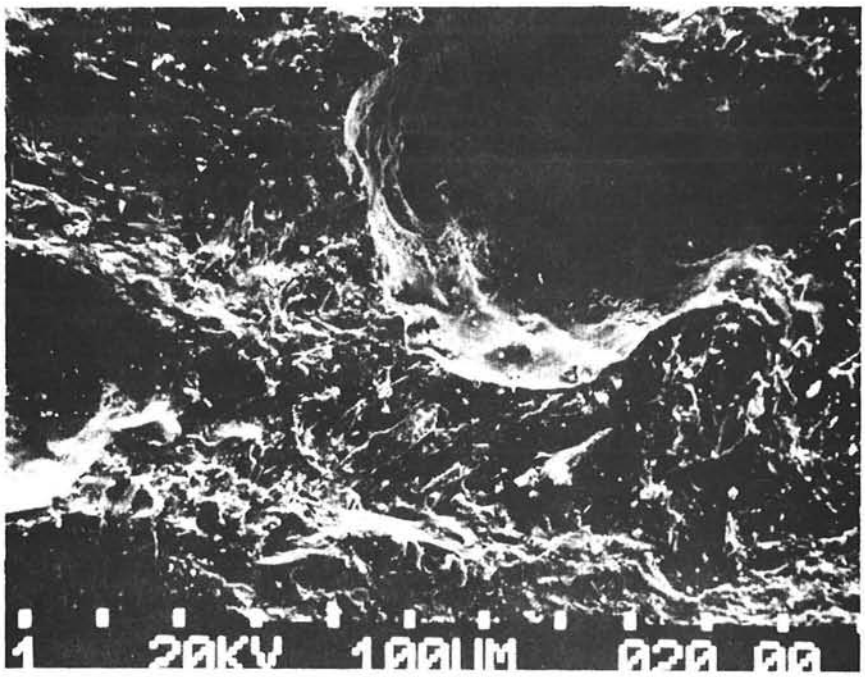

(b) Exposed - rupturing around large voids, elongated cleavage facets.

Figure A-26
IRC24LI - Unexposed and Exposed (500 hr) Fracture Surfaces. SEM.

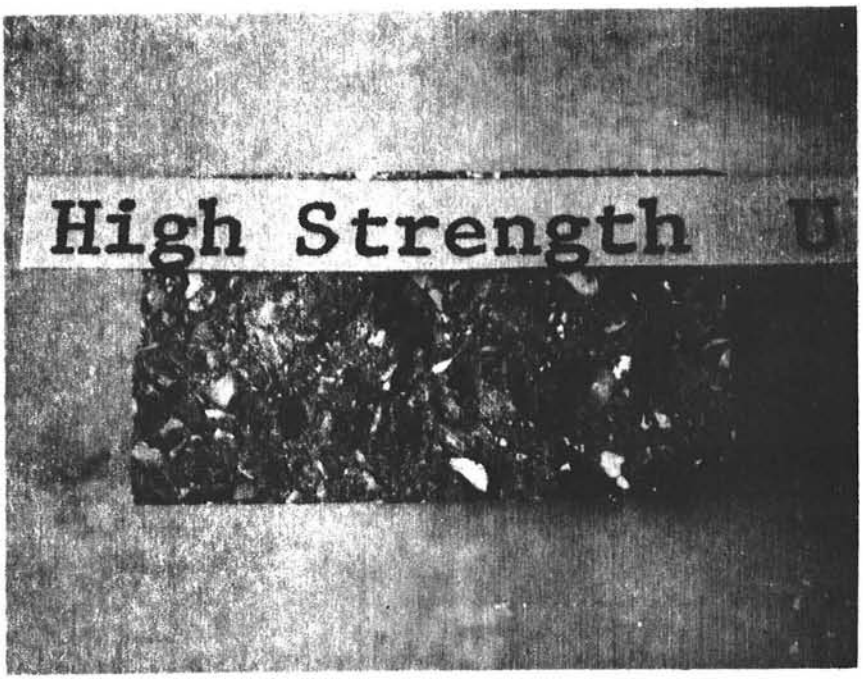

(a) Unexposed

(b) Exposed

Figure A-27 High-Strength. Unexposed and Exposed Surfaces (3X).

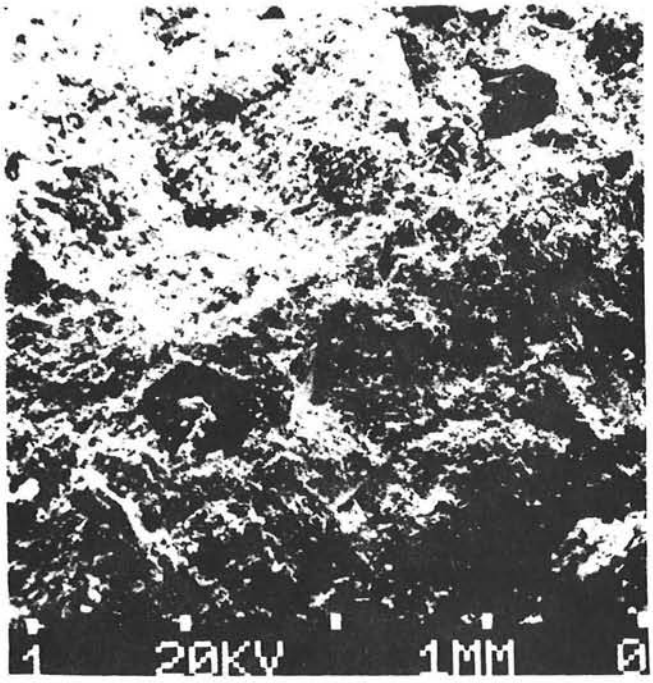

(a) Transgranular overload failure
- areas of fine dimples.

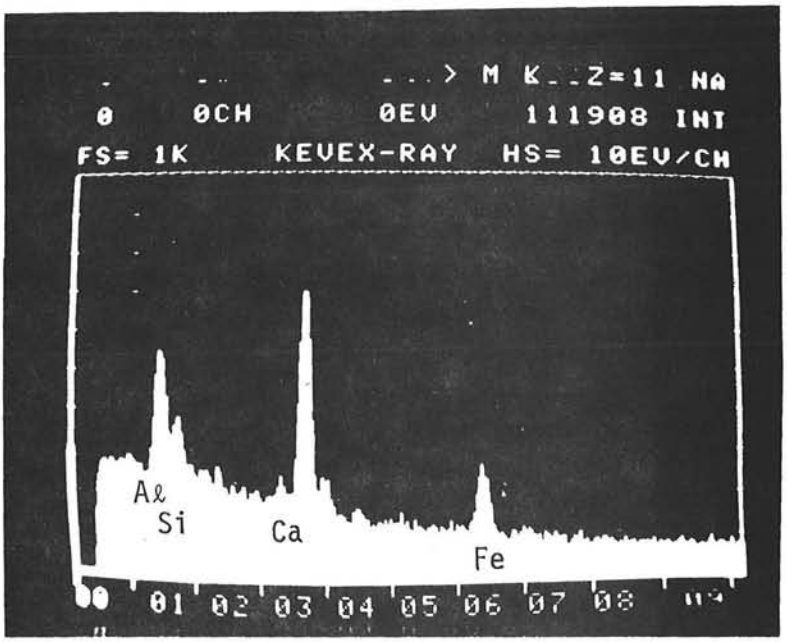

(b) Kevex-ray elemental analysis

Figure A-28 High Strength "Unexposed" Failure Surface

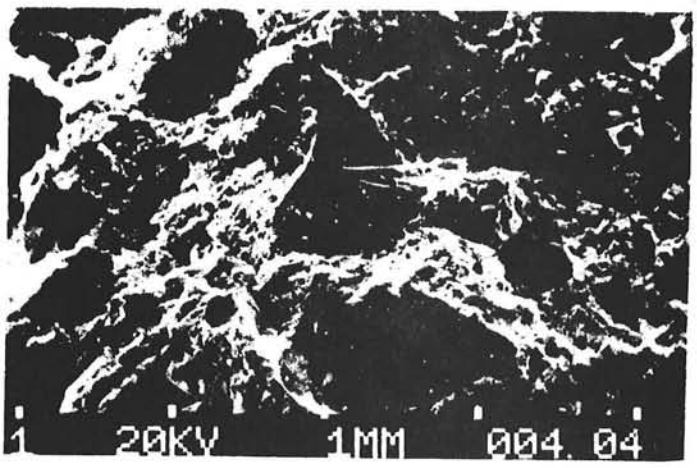

(a) Intergranular type fracture

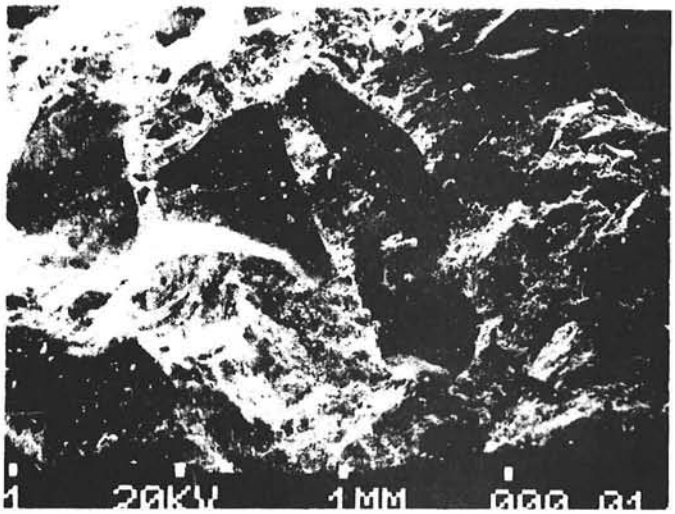

(b) Same as (a), different area

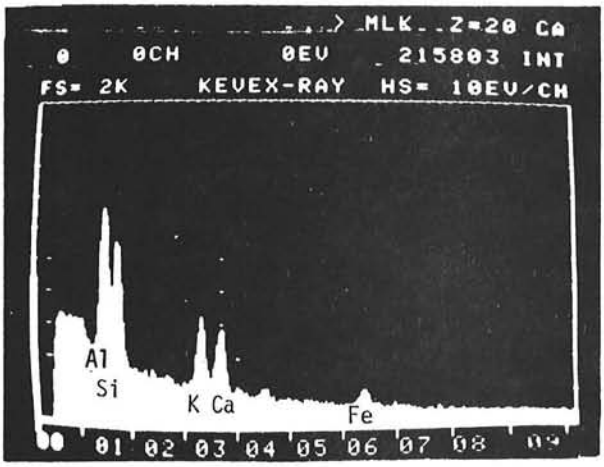

(c) Elemental analysis - salt impregnation and probable new compound formation as compared to Fig. A-28 b

Figure A-29

High Strength Brick - Exposed (500 hr) Fracture Surface Edge of the Fracture - SEM

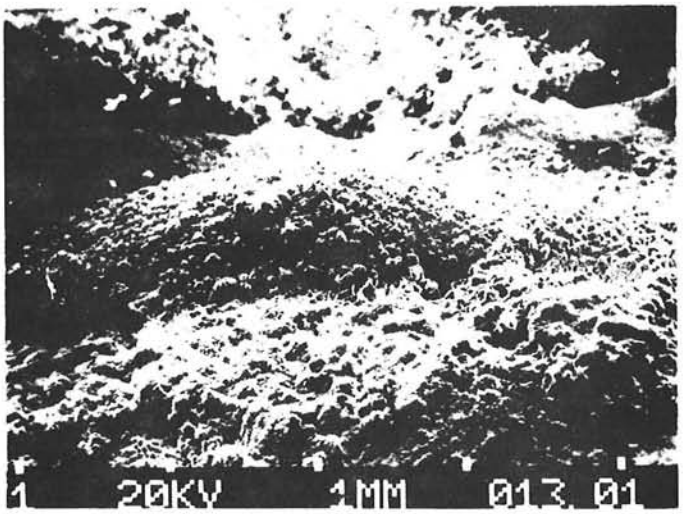

(a) Fracture on salt covered surface - intergranular

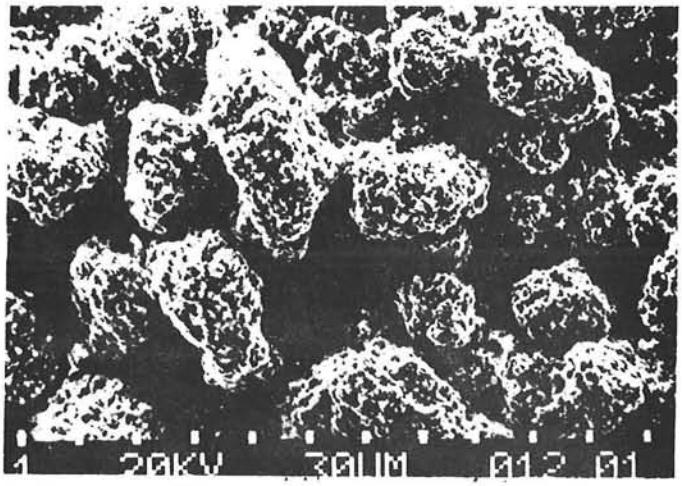

(b) Same as (a), higher magnification - intergranular fracture on salt covered surface

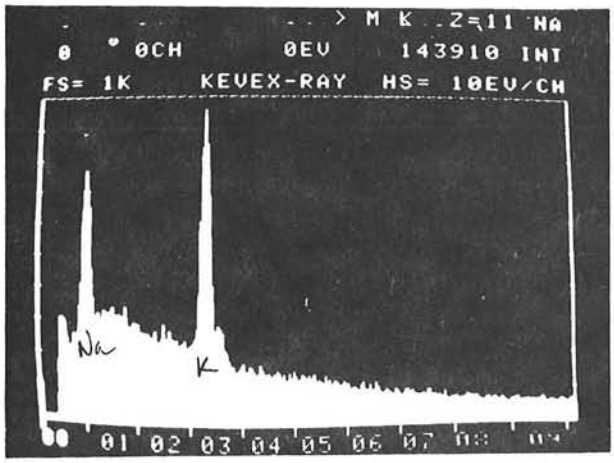

(c) Elemental Analysis

Figure A-30
Same as Fig. A-29 Center of the Fracture Surface - Surface Completely Covered with Salt - No Indication of Compound Formation - Fracture on Salt Covered Areas

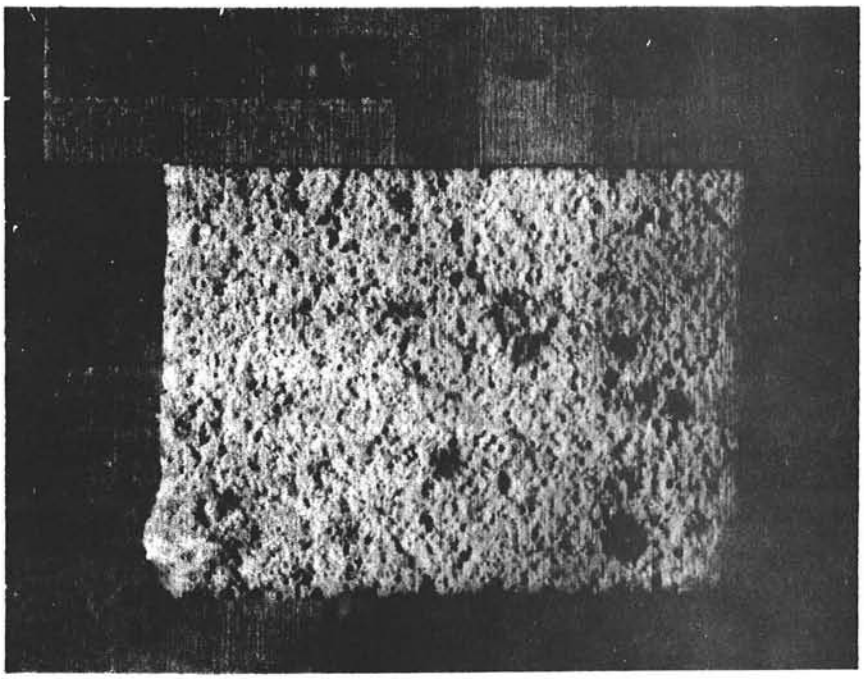

(a) Unexposed

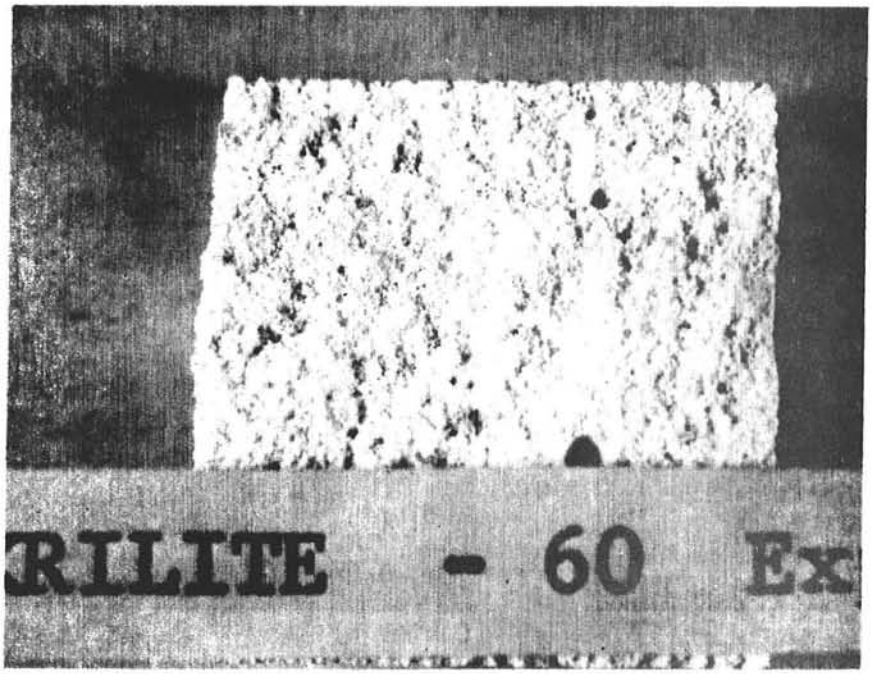

(b) Exposed

Figure A-31
Unexposed and Exposed Surfaces of Insulating Krilite 60 (3X)

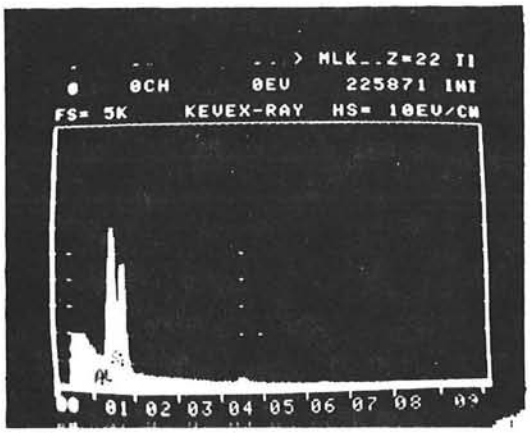

(a) Unexposed

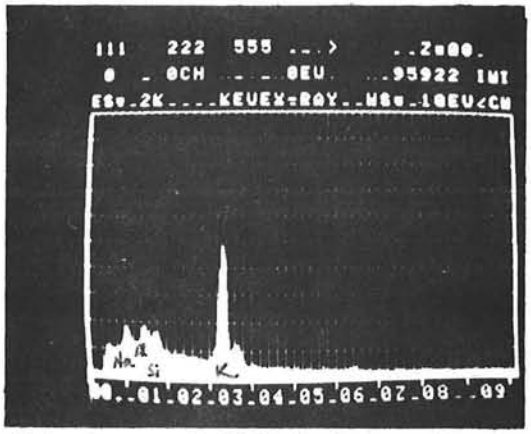

(b) Exposed (500 hr) Surface

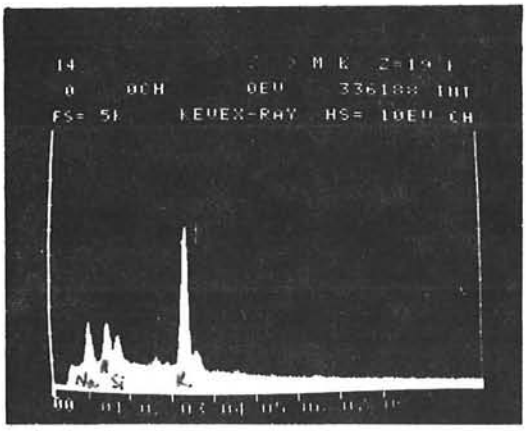

Subsurface

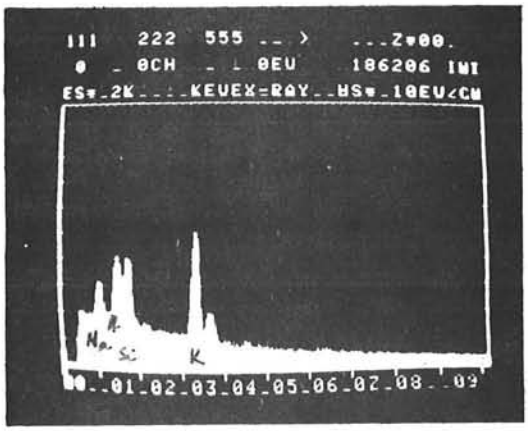

Center

Figure A-32 Krilite 60 - Salt Impregnation - Kevex-ray Analysis

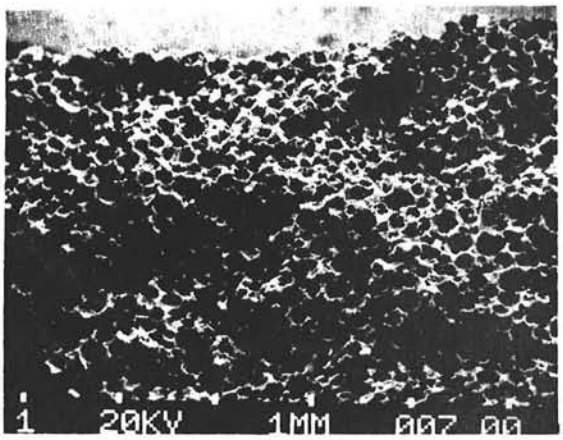

(a) Unexposed - pore rupturing

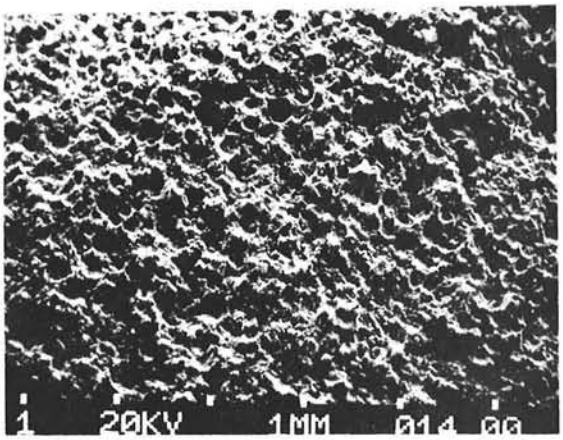

(b) Exposed - room temperature fracture - pores filled with salt

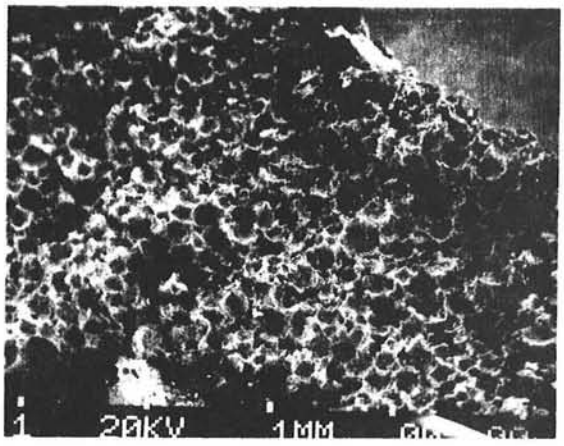

(c) Exposed - high temperature fracture - same as (a)

Figure A-33

Krilite 60 - Unexposed and Exposed (500 hr) Fracture Surfaces - SEM

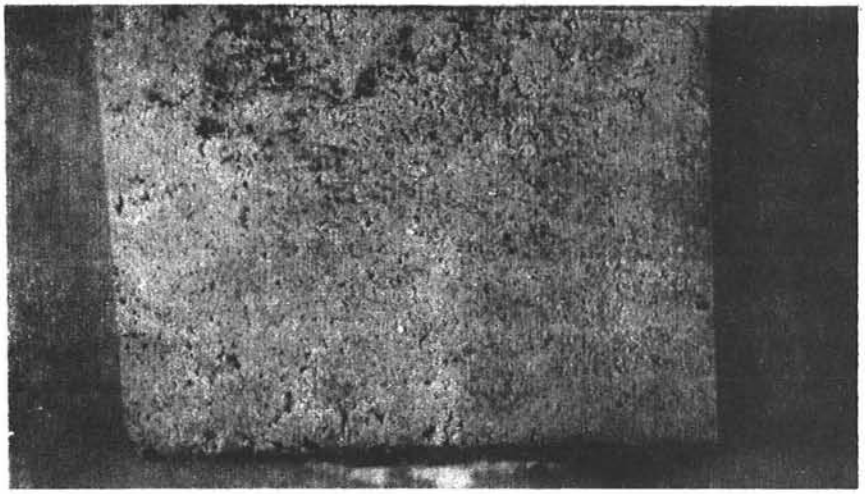

(a) Unexposed

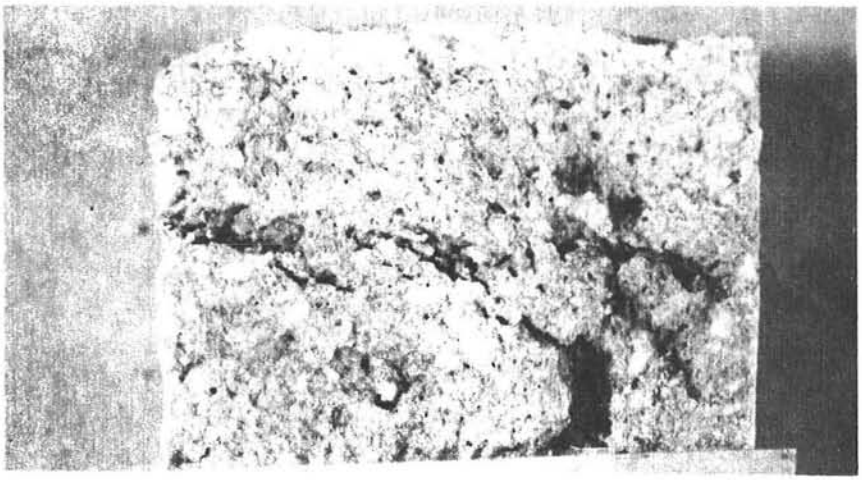

(b) Exposed

Figure A-34
Unexposed and Exposed Surfaces of Fired Castable Coreline (3X)

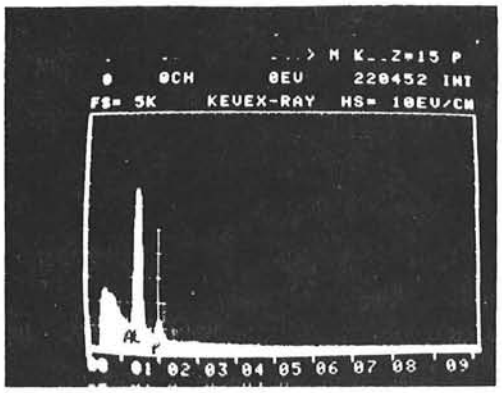

(a) Unexposed

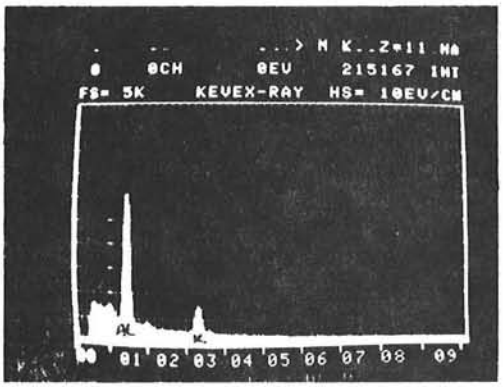

Surface

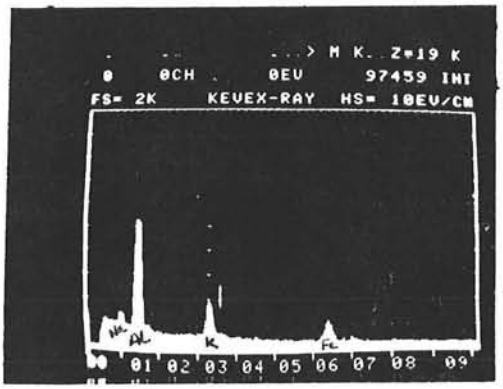

Subsurface

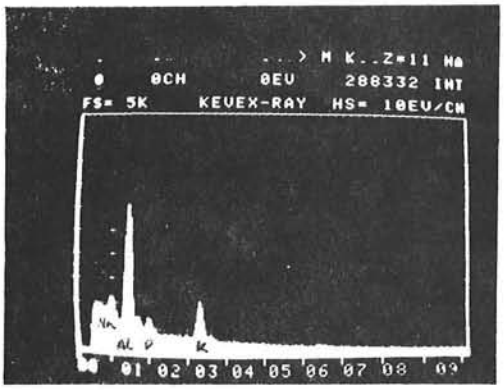

Center

(b) Exposed (500 hr)

Figure A-35
Coreline - Salt Impregnation - Kevex-ray Elemental Analysis

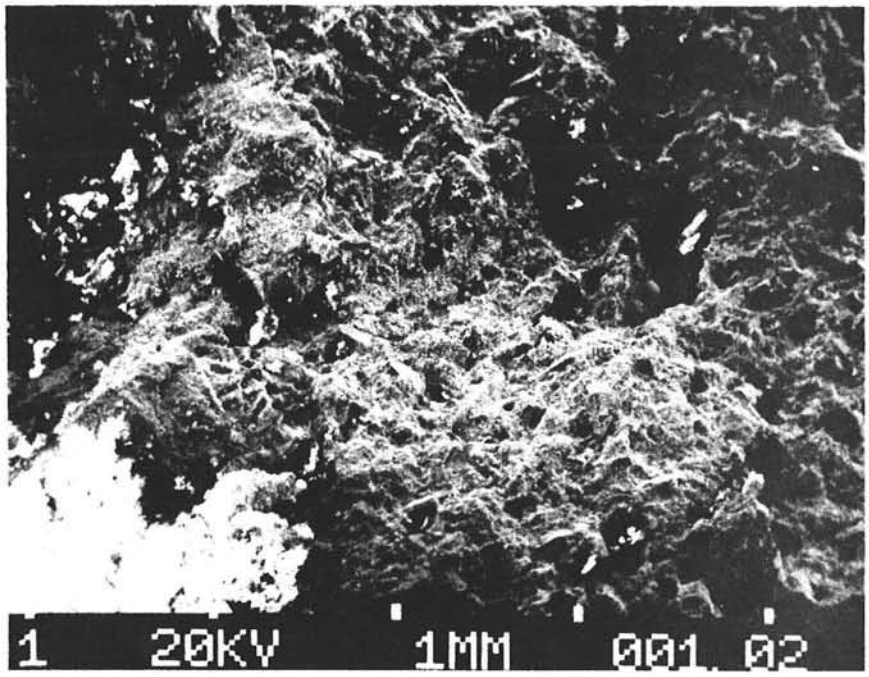

(a) Unexposed transgranular - areas of elongated dimples and some pore rupturing.

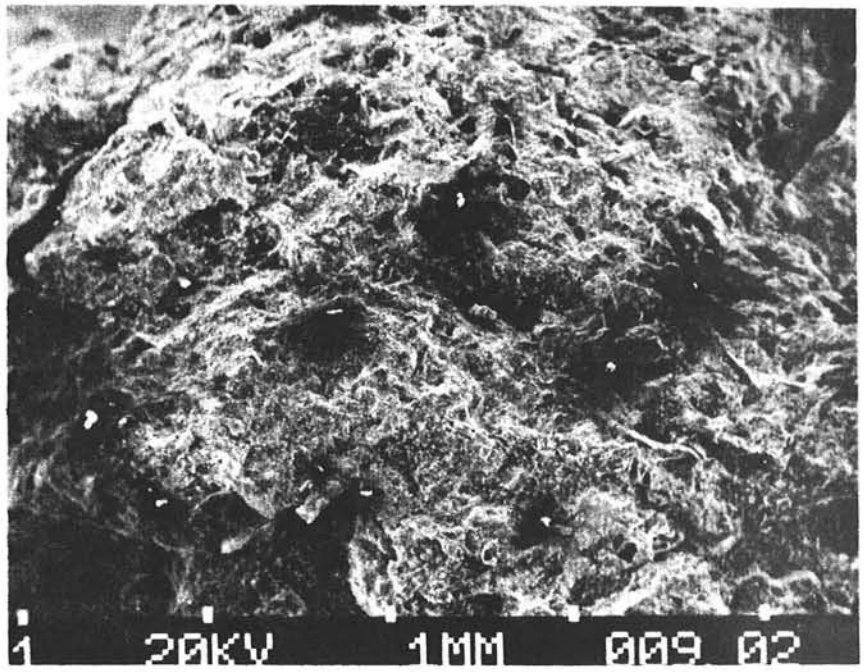

(b) Exposed - same as (a) with added thermal cracking.

Figure A-36
Coreline - Unexposed and Exposed (500 hr) Fracture Surfaces - SEM

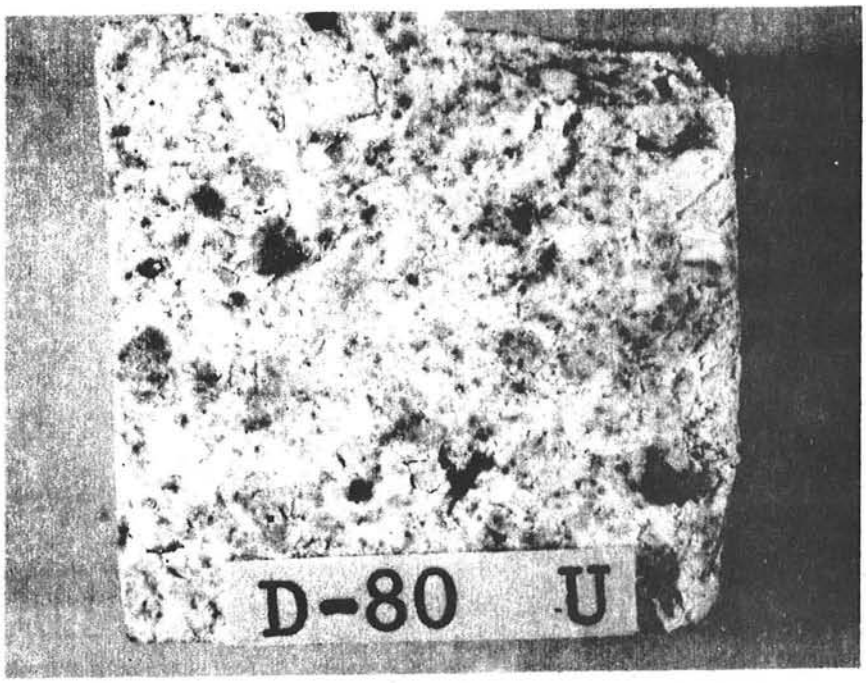

(a) Unexposed

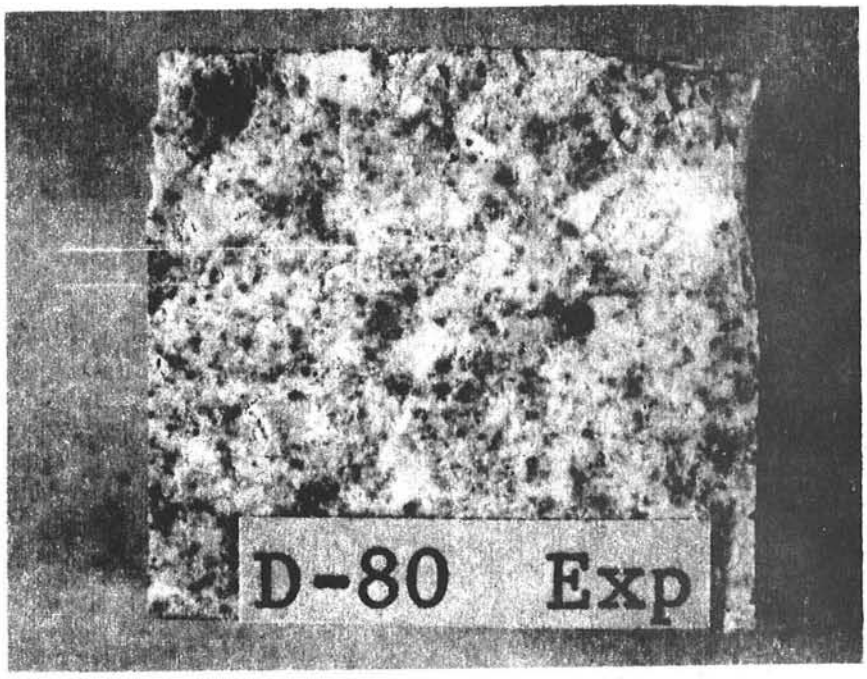

(b) Exposed

Figure A-37
Unexposed and Exposed Surfaces of Dense Brick (D-80) (3X)

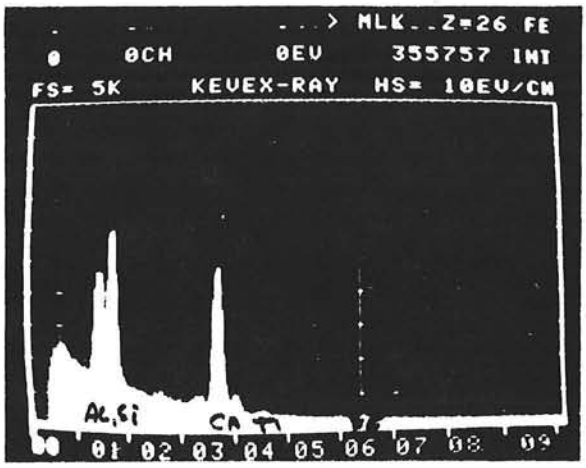

(a) Unexposed

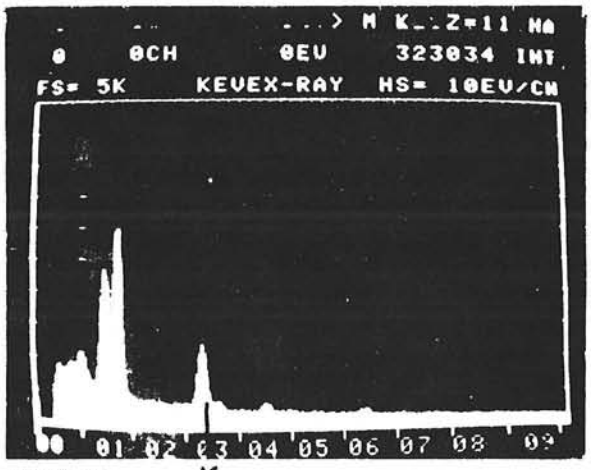

Surface

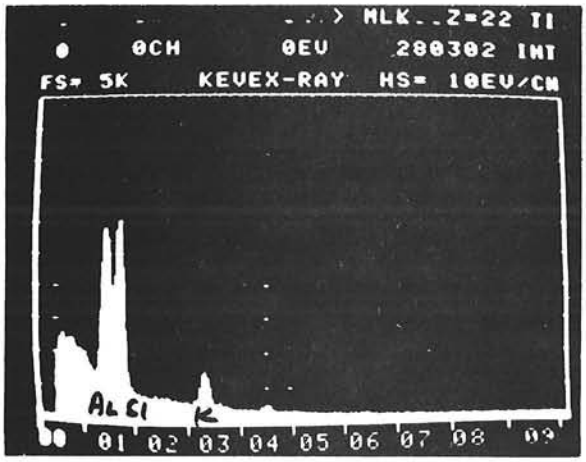

Subsurface

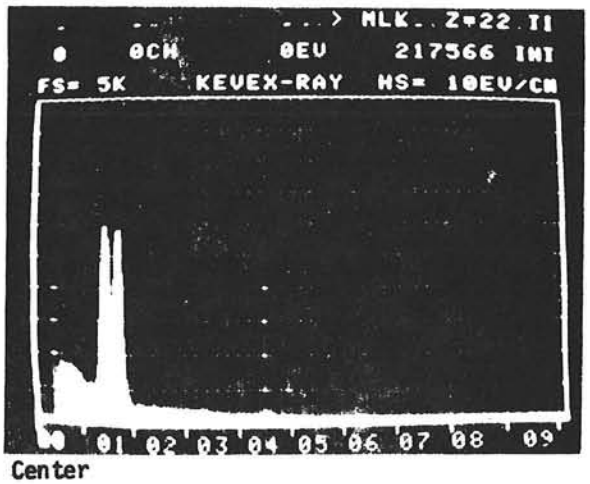

Center

(b) Exposed

Figure A-38

D-80 Kevex-ray Elemental Analysis Showing Salt Impregnation and Leaching Out of "Ca" from the Exposed Sample.

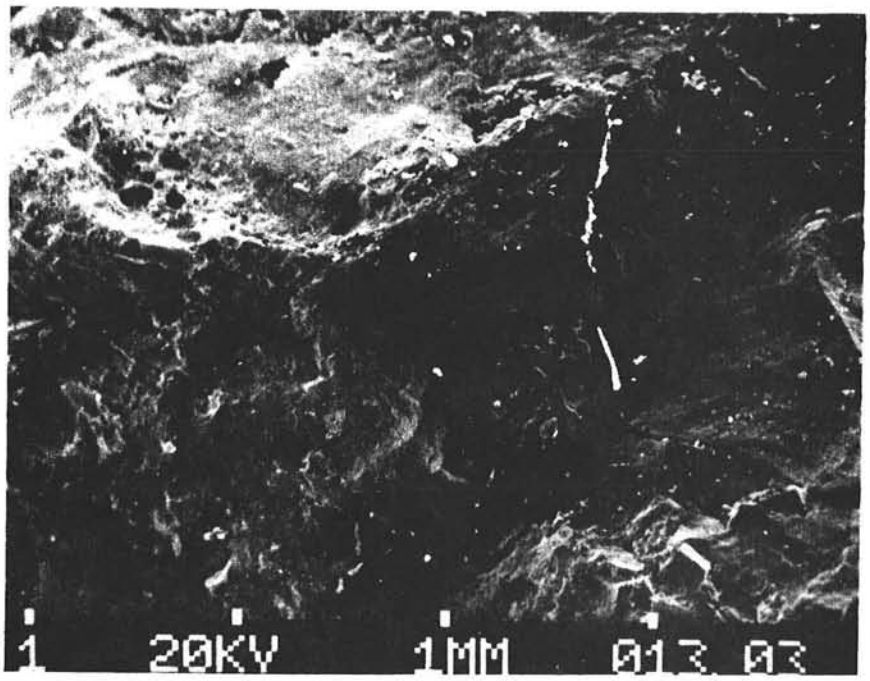

(a) Unexposed - Intergranular fracture with extensive secondary cracking

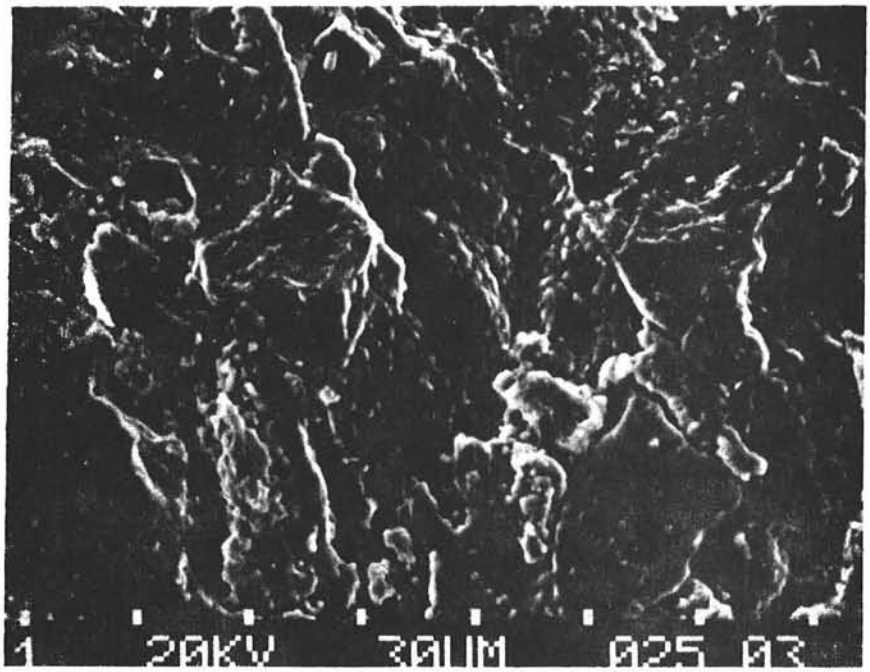

(b) Exposed - Stress Corrosion type extensive intergranular cracking

Figure A-39
D-80 Unexposed and Exposed (500 hr) Fracture Surfaces - SEM

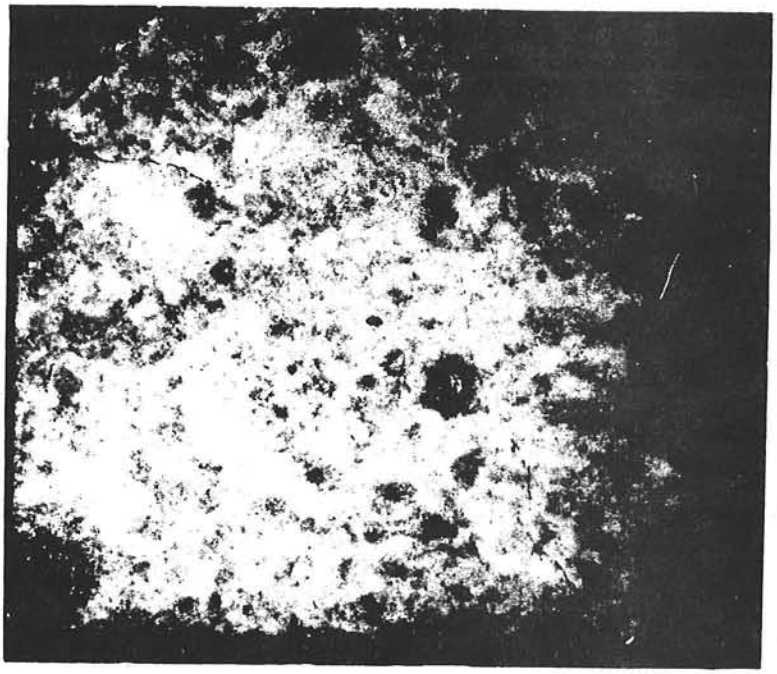

Figure A-40
Exposed Surface Dense Brick VISIL Showing
Thermal Cracking (10X)

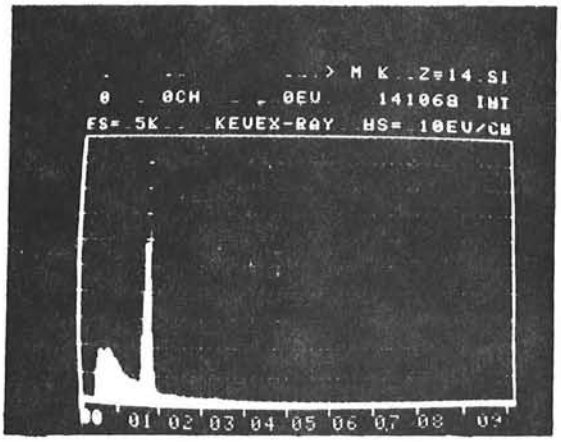

(a) Unexposed sample

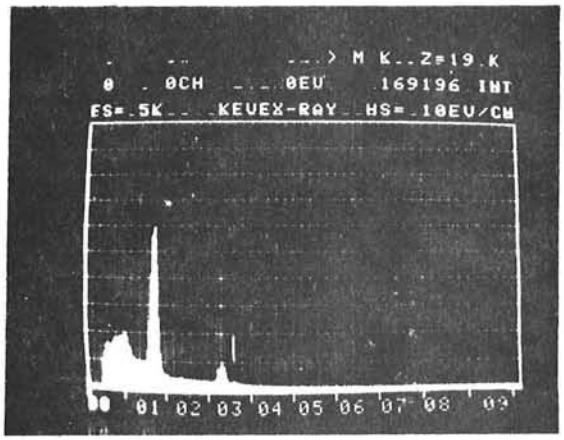

Surface

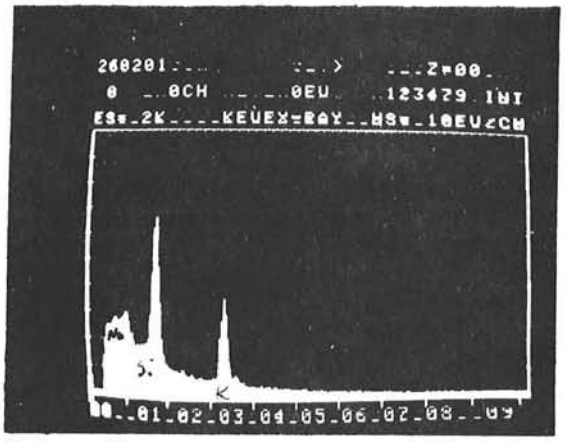

Subsurface

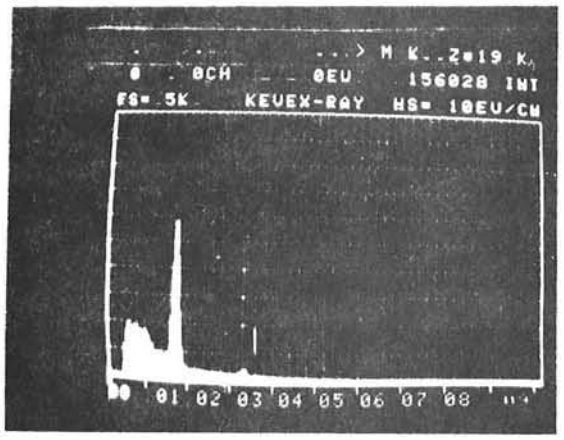

Center

(b) Exposed sample

Figure A-41 VISIL Salt Impregnation - Kevex-ray Elemented Analysis

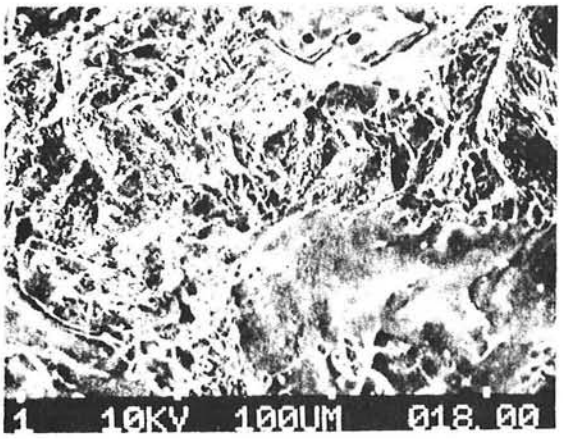

(a) Unexposed - Intergranular cracking combined with large cleavage facets.

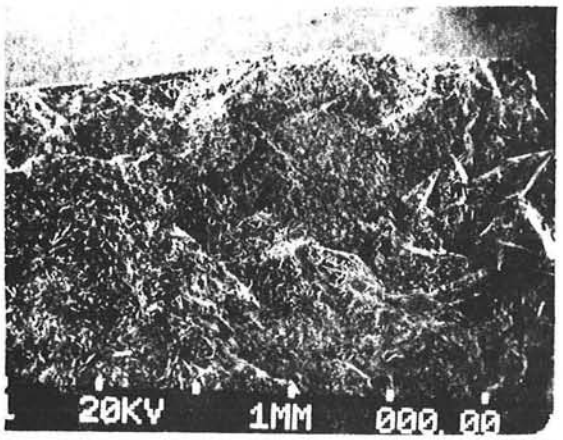

20X

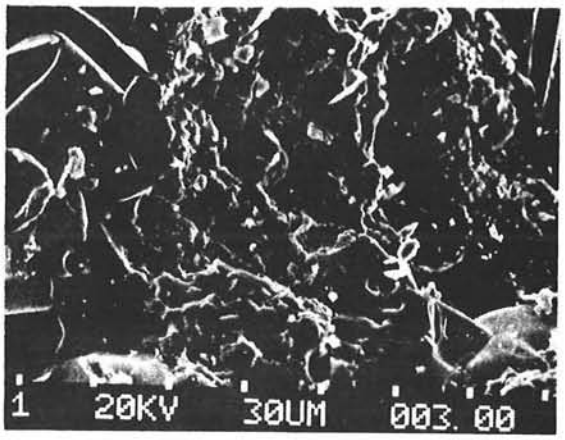

500X

(b) Exposed - Edge of the fracture surface - stress corrosion type intergranular cracking.

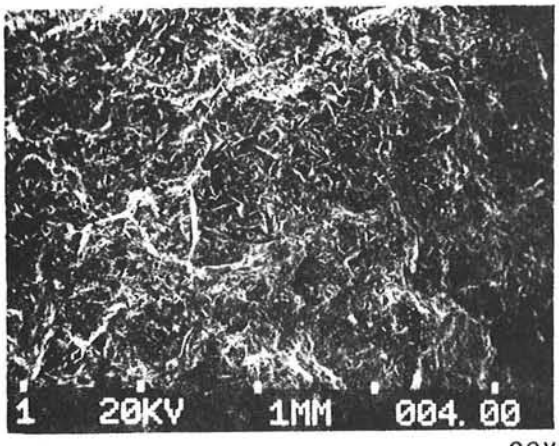

20X

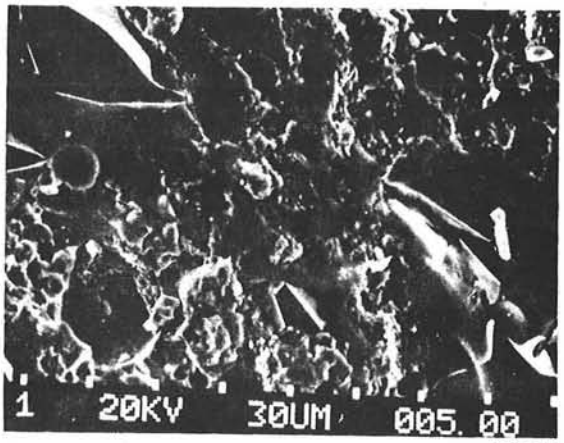

500X

(c) Exposed - Center of the fracture - same as (b)

Figure A-42 VISIL - Unexposed and Exposed (500 hr) Fracture Surfaces

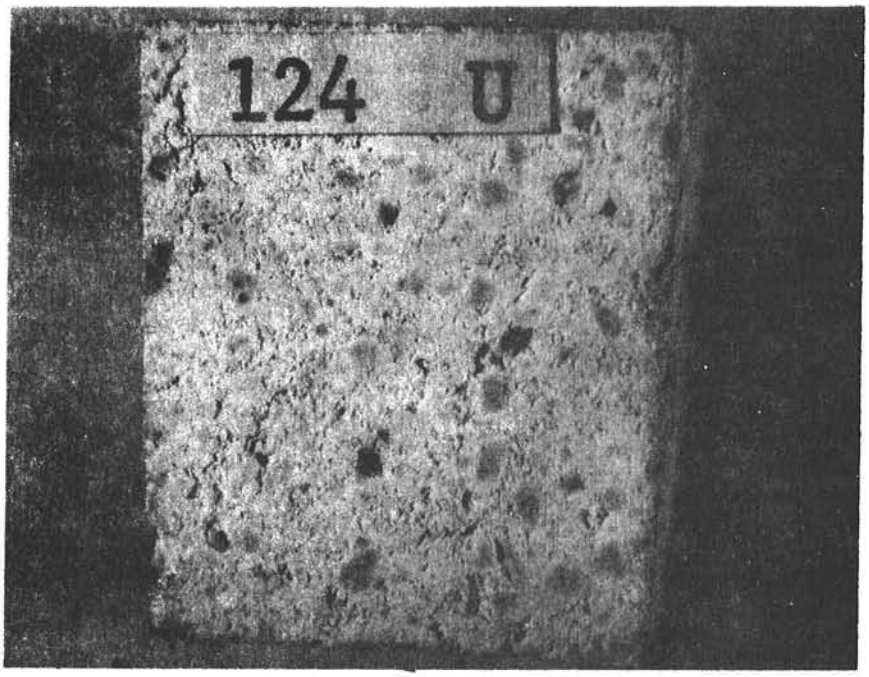

(a) Unexposed

(b) Exposed

Figure A-43
Unexposed and Exposed Surfaces of Dense Brick CS124 (3X)

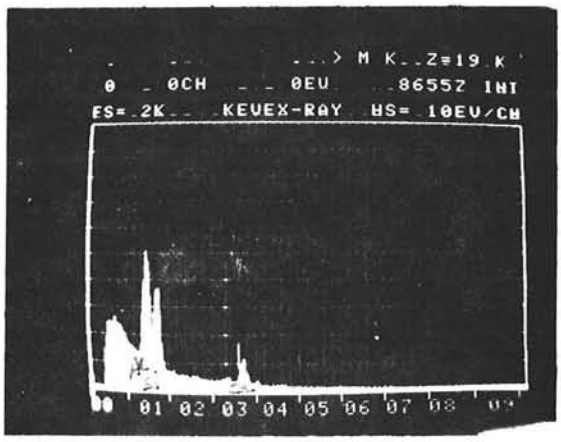

(a) Unexposed

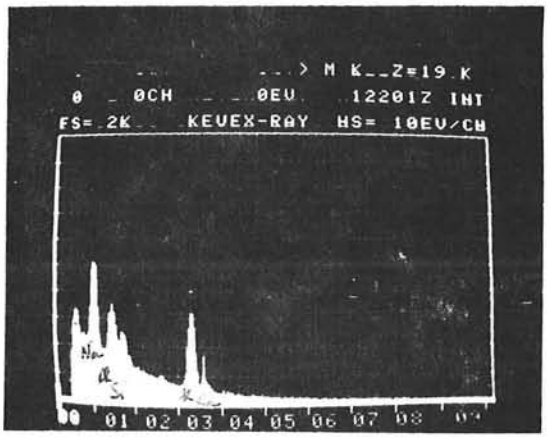

Surface

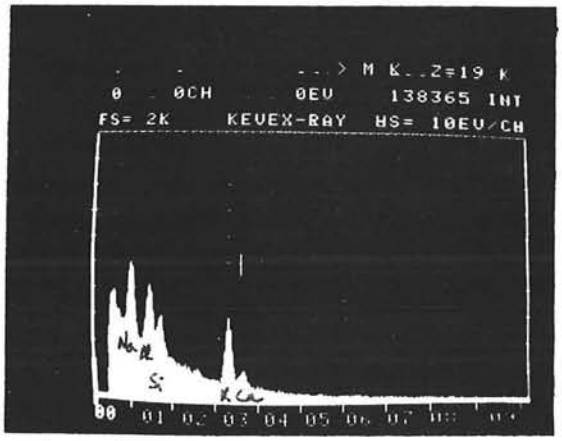

Subsurface

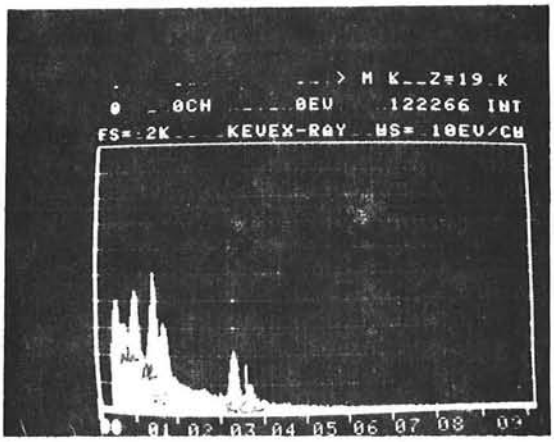

Center

(b) Exposed

Figure A-44
CS124 - Salt Impregnation - Kevex-ray Analysis, also Showing "Leaching Out" of Ca from the Exposed Sample

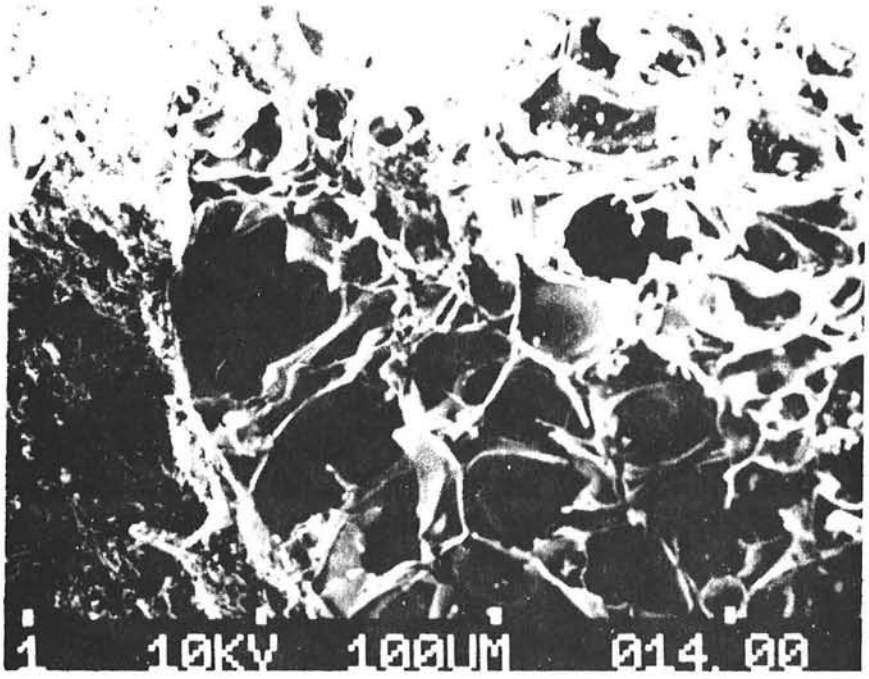

(a) Unexposed sample - pore wall rupturing, intergranular cracking, cleavage facets.

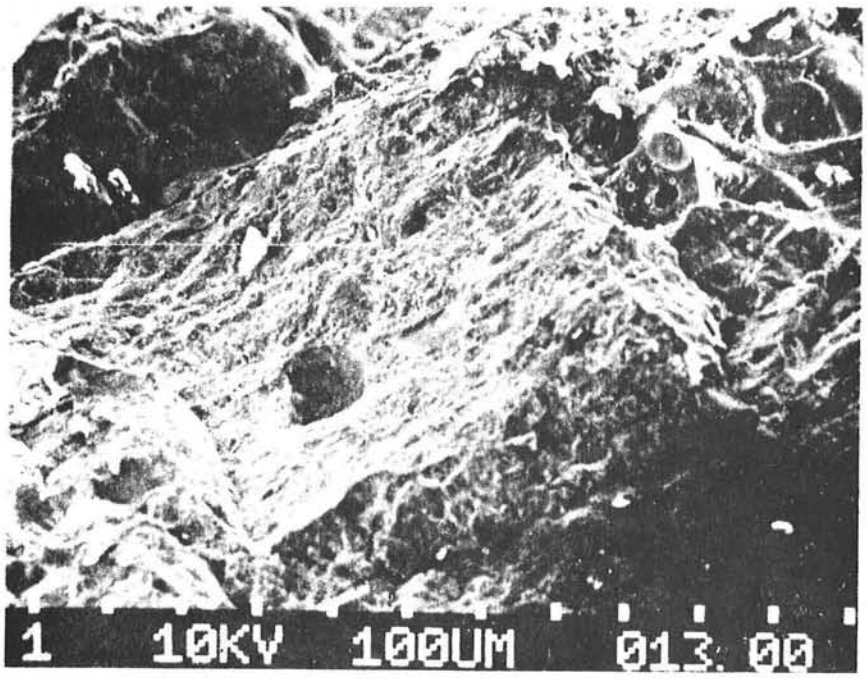

(b) Exposed - same as (a) except no pore wall rupturing extensive thermal cracking.

Figure A-45
CS124 - Unexposed and Exposed (500 hr) Fracture Surfaces - SEM

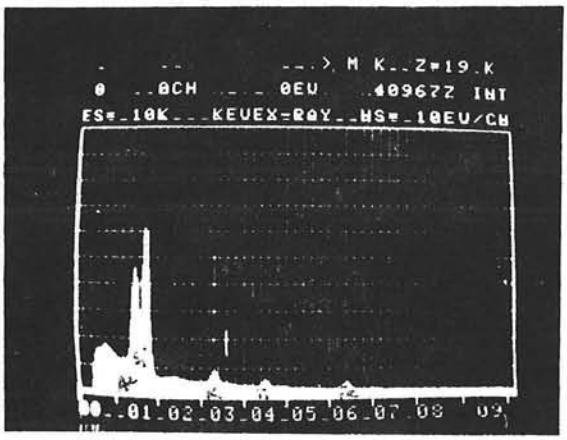

(a) Unexposed

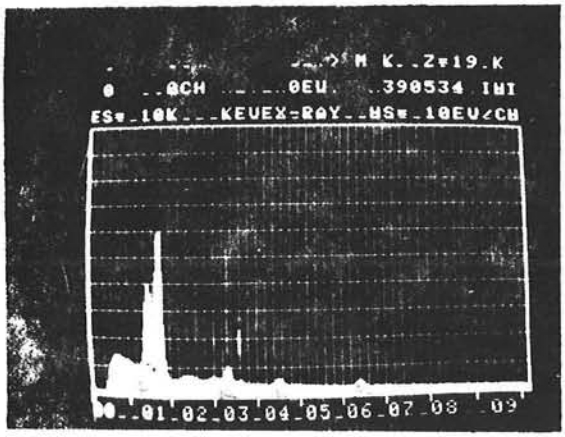

Surface

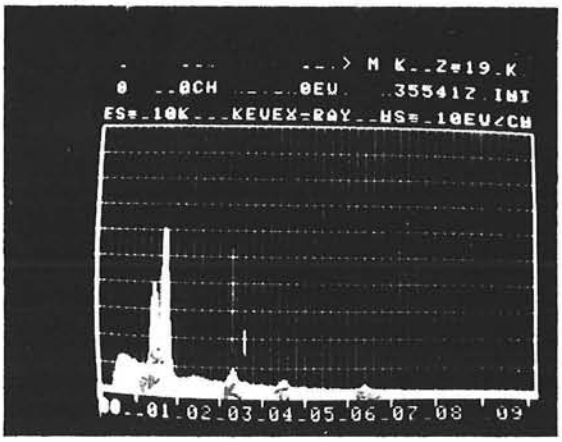

Subsurface

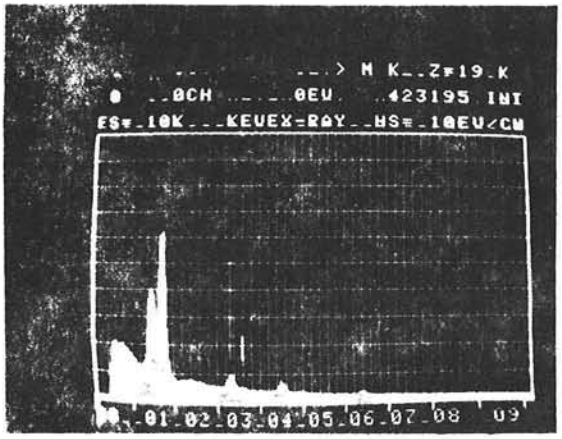

Center

(b) Exposed Sample

Figure A-46
Semiacid (Dense Brick) - Salt Impregnation - Kevex-ray Analysis, Showing No Salt (Na, K) Impregnation.

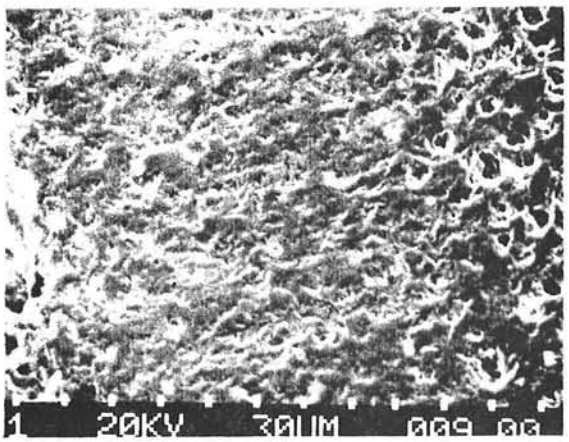

(a) Unexposed - pore rupturing

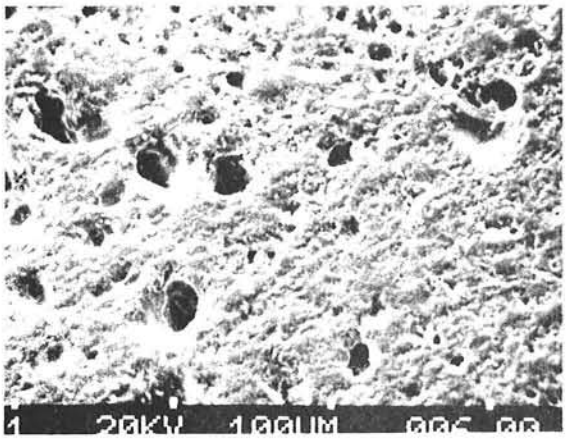

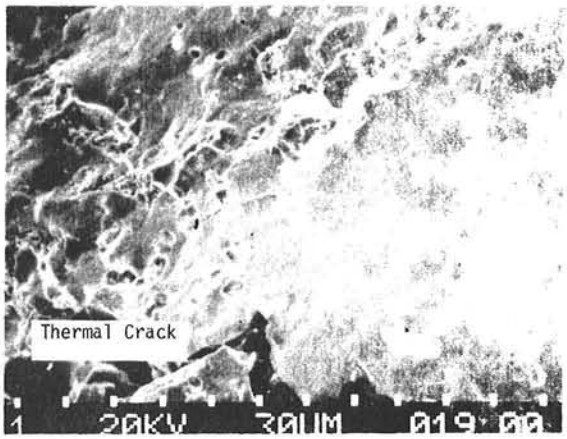

(b) Same fracture mode as (a) the pores enlarged, areas of wide thermal cracks.

Figure A-47
Semiacid (Dense Brick) - Unexposed and Exposed (500 hr) Fracture Surfaces - SEM

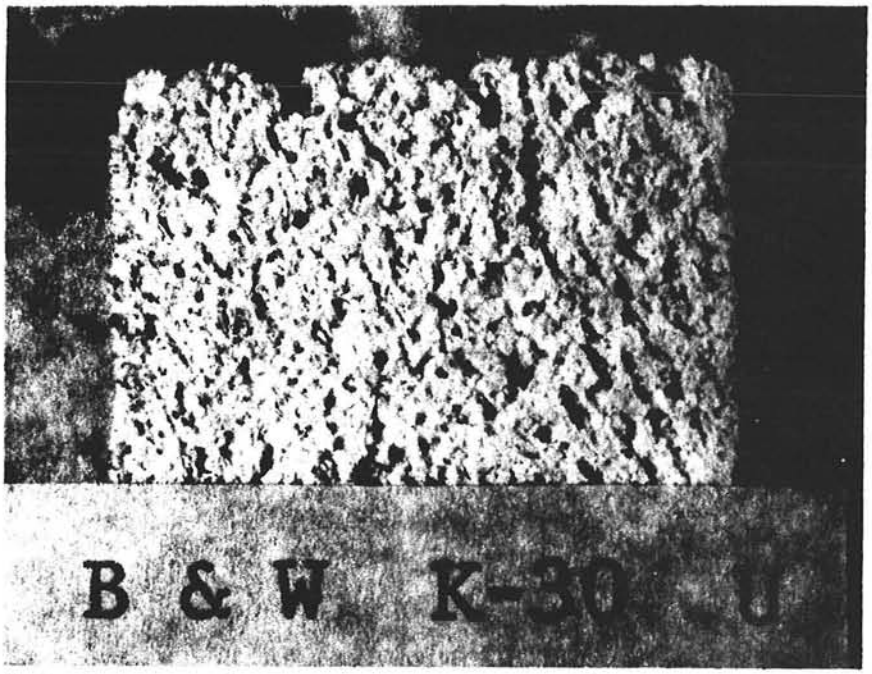

(a) Unexposed

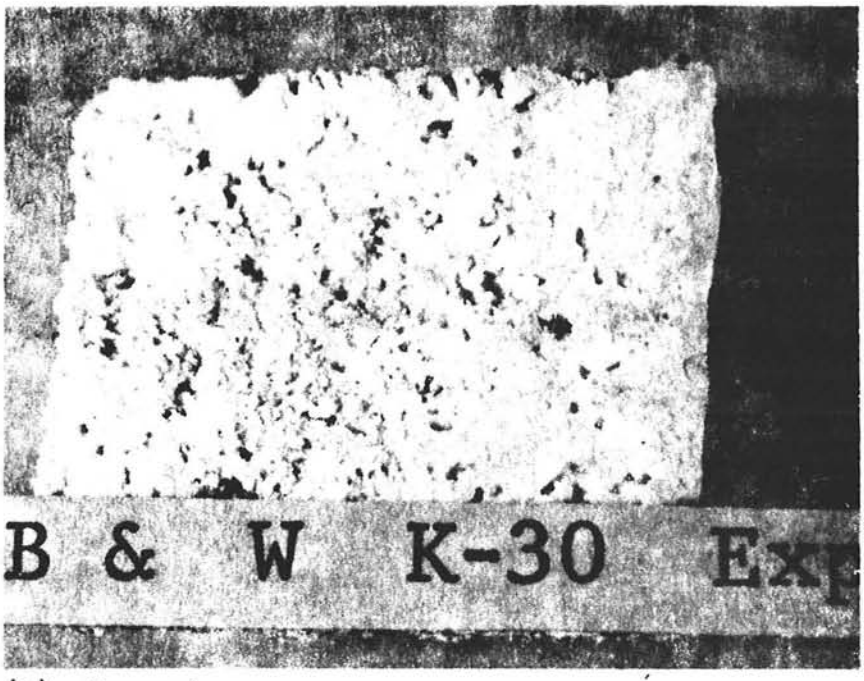

(b) Exposed

Figure A-48
Unexposed and Exposed Surfaces of Insulating Brick K-30 (3X)

APPENDIX B

KAISER REFRACTORIES MATERIAL EVALUATIONS

KAISER
REFRACTORIES

DIVISION OF KAISER ALUMINUM & CHEMICAL CORPORATION

July 9, 1979

Owen Scott
Martin Marietta Corp.
P.O. Box 179
Denver, CO 80201

Dear Mr. Scott:

I hope our last Friday meeting was of value to you in explaining our lab results and in recommending refractories for your application. As we indicated, your application is not a normal refractory situation in that your requirements of essentially zero assimilation of refractory into your bath and a refractory life of at least 30 years are impossible to achieve. You did request that I inform you by letter of our recommendations regarding a safety lining and insulation. I think we essentially concluded that you will need a protective metal skin inside the refractory to prevent nitrate bath contact with the refractory. Our results indicate that if this contact does occur you will assimilate refractory into your bath and that refractory life will most likely not achieve the desired 30 year life period.

In summary, the following would be our recommendations as per our discussion at our laboratory this past Friday.

1. If you require or desire a safety lining behind the metallic lining we would recommend our Maximul super duty brick for this application. The reasons are this brick is the most resistant of those tested to the alkali nitrate bath. It would contain any leakage through the metallic liner for a long period of time and most likely would not contaminate your bath as we assume a leakage would be a one way proposition. The brick should be place using our hi strength phospate bonded HiLo mortar as this would give the greatest resistance to slag attack along mortar joints.

2. A fiber insulating material placed between the metallic liner and safety lining or insulating lining would help protect the lining from mechanical wear against the refractory product. It would also improve the insulating characteristics of the lining due to the fact that fibrous insulating materials have a very low K factor. If you have any movement of the liner in relation to the refractory backup we are sure wear would be a problem because most all refractories are very abrasive.

3. We would recommend an insulating brick be used between the safety lining and structural shell or between the inner lining and the structural shell if a safety lining is not used. An insulating brick has a lower K factor than a castable and would not require the drying procedure a castable would require. In the event of a leak, as you have already noted in your tests, our Krilite insulating product would absorb the bath. The bath would stop at its freezing point as it approaches the shell and would progress only as the temperature increases due to the higher conductivity of the bath saturated insulating product. To improve the insulating characteristics of this portion of the vessel another thickness of fiber could be placed between the insulating brick and the structural shell. The insulating brick should be placed with a standard super duty mortar dipped joint for best structural integrity. Brick would take longer to lay up and would be more costly than the castable but would not require the amount of predrying as would the castable. In either case the structural shell should be vented to vent any moisture loss during initial heat up.

4. Corpatch was only briefly discussed as a possible safety coating to be placed on the insulating lining. Corpatch is a thin putty-consistency material placed in thin coatings. Since it is a phosbonded product it would be resistant to the nitrate attacked but not as resistant as a burned brick product like Maximul. It would also develop some crack patterns during drying which would make it more susceptible to penetration by the bath if a leak should occur. If this material was used it also should be covered with a fiber to protect the metal lining from abrasion.

I am attaching a copy of the lab report which you already have and which we discussed at our lab last week. If you feel you need further discussion of this report please do not hesitate to call myself or Wendy. We are sorry we are not able to contain your bath with conventional refractories for your desired 30 year time period. We will be happy to work with you if we may be of other assistance. I will request additional samples of Maximul be sent to you for further testing per your request.

Very truly yours,

J. E. Allen/gr

J. E. Allen
Technical Services

JEA/gr
Attachments
cc: W. A. Reinking
S. W. Ping
B. D. McKenna

KAISER
REFRACTORIES

CUSTOMER SERVICE REPORT

CSRD 79-78

PRODUCT: Maximul, CS-124, Krilite 30, Krilite 60, Lo-Erode, Hi-Strength and IRC 24 LI

DATE: June 27, 1979

CUSTOMER: Martin-Marietta Aerospace Denver, Colorado

BY: B. D. McKenna CFT 31

APPLICATION: Molten Salt Bath Test

PROJECT: 49765

ABSTRACT

This report transmits W. L. Ping's petrographic analysis of seven K/R products tested by Martin-Marietta Aerospace, Denver, Colorado. Their testing consisted of submerging specimens for 21 days in a molten (1100°F) bath of 60% $NaNO_3$ and 40% KNO_3. The Maximul and CS-124 test specimens had the best resistance to chemical attack and the Krilite 30 and Krilite 60 test specimens had the next best resistance. The Lo-Erode and Hi-Strength specimens were readily attacked by the salt and the IRC 24 LI had the least resistance to deterioration by the molten salt.

BMD/yg

Attachment

CENTER FOR TECHNOLOGY
POST OFFICE BOX 870 · PLEASANTON, CALIFORNIA 94566 · PHONE 415/462-1122

LABORATORY SERVICES REPORT SERIAL NO. P79-181

Subject: Molten Salt Bath Test Specimens from Martin Marietta Aerospace, Denver, Colorado

By: W. L. Ping

Fourteen one-inch refractory cubes from Martin Marietta Aerospace, Denver, Colorado, were submitted for petrographic examination. Seven Kaiser products were submerged in a molten salt bath--60% $NaNO_3$ and 40% KNO_3--at 1100°F for 21 days. Both tested and untested versions of the products were submitted; the compositions tested included Maximul, CS-124 (Krimax), Krilite 30, Krilite 60, Lo Erode, Hi Strength, and IRC 24 LI. An analysis of the alteration mechanisms operative in the tested samples and their relative resistance to the salt attack was requested. A brief description of the alteration experienced by each product is given below:

Maximul and CS-124 (Krimax)

Impregnation of brick structure by KNO_3 and $NaNO_3$. Salts fill brick porosity but do not react with or in any detectable way alter the brick bond structure.

Krilite 30 and Krilite 60

Strong penetration of Krilite pore structure by $NaNO_3$ and KNO_3. Some deterioration of "bubble" structure; at areas where cell walls are thinnest, the molten salt reacted with the refractory mullite to form a nepheline [$\frac{1}{2}((K,Na)_2O \cdot Al_2O_3 \cdot 2SiO_2)$]. The latter was redeposited on intact pore wall surfaces, leaving a break in the formerly continuous cell structure.

Lo Erode and Hi Strength

The calcium aluminate cement bond system of these castables was readily susceptible to chemical attack by the intruding salts. KNO_3 and $NaNO_3$ thoroughly impregnate the castables' pore structures, and apparently form soluble, amorphous complexes with the calcium aluminate bond system. The unused Hi Strength sample showed a bond assemblage of tricalcium aluminate hydrate ($3CaO \cdot Al_2O_3 \cdot 6H_2O$), gibbsite ($Al_2O_3 \cdot 3H_2O$), and gehlenite ($Ca_2Al_2SiO_7$), indicating that the castable had been dried above 100°C but below 200°C. After 21 days of immersion in the 1100°F salt bath, gehlenite was the only detectable crystalline bonding phase; X-ray diffraction indicated a slight increase in the amount of gehlenite, owing to the prolonged 1100°F soak. Polished section examination revealed that the altered matrix bonding phases were strongly leached by the aqueous sample preparation techniques; the absence of mounting epoxy in this "bondless" area indicates that a water

soluble matrix phase was present in the structure during epoxy impregnation of the sample but was subsequently removed during the aqueous grinding and polishing steps. It is likely that these soluble, amorphous reaction complexes are low-melting eutectic phases; they are unquestionably detrimental to the structural integrity and strength of the refractory castable.

The unused Lo Erode showed a similar low temperature matrix bond system, except that it does not contain a gehlenite. Its crystalline bonding phases included tricalcium aluminate hexahydrate and gibbsite; after testing its only crystalline bonding phase was minor calcium dialuminate ($CaAl_4O_7$), and microstructural examination again revealed a thoroughly water leached matrix bond system.

IRC 24 LI

The insulating castable showed the most severe deterioration of any of the seven products. Its high porosity (and hence high internal surface area) structure, combined with the high level of calcium aluminate cement in this product, made it especially susceptible to the molten salt attack. Curiously, the unused specimen displays a phase assemblage characteristic of a fired (cured) piece; it contains no hydrated phases, but instead shows major gehlenite ($Ca_2Al_2SiO_7$) and calcium dialuminate ($CaAl_4O_7$), with minor calcium monoaluminate ($CaAl_2O_4$). The tested specimen shows a penetration of the castable pore structure by both $NaNO_3$ and KNO_3, as well as strong alteration of its bond system. Crystalline reaction products include major nepheline ($Na_2KAl_4Si_4O_{16}$) and secondary sarcolite ($NaCa_4Al_3Si_5O_{19}$); none of the original crystalline bonding phases survived the salt attack. Polished section examination again indicates the presence of water soluble (amorphous) alkali nitrate-calcium aluminate complexes.

* * *

Comments

None of the cement-bonded castables are acceptable choices for this application. Chemically, the calcium aluminate bond system is not compatible with the molten salts, and is readily attacked by them; the calcium aluminate phases are especially susceptible to deterioration in their uncured (i.e., hydrated) state, in which they exist at the outset of service in this application. In general, however, a calcium aluminate cement-bonded product is at its worst in the temperature range in question; at intermediate temperatures, strengths are relatively low, and the bonding phases are still transitional. It is generally not until +2000°F temperatures are reached that the structure attains its optimum stability and strengths.

Insulating refractories, such as the Krilite products, are similarly not recommended for this application. While mullite-glass aggregate grains (i.e., calcined flint) proved quite resistant to attack in the products of this test series which contained them (Maximul, CS-124, Lo Erode, Hi Strength), the mullite-glass "bubble" structure of the Krilite products was deteriorated by the molten salts. This was due to the extremely high internal surface area of the bubble structure; over time, the thinnest portions of the cell walls were destroyed via reaction with the molten salt penetrant. The extremely high porosity and correspondingly high permeability of an insulating refractory result in massive salt penetration; in addition to its detrimental effect on the refractory, the amount of salt absorbed by an entire refractory lining would be quite considerable and would be detrimental to the efficiency of the manufacturing process.

The preferred refractory type for this application is a burned fireclay product, such as the Maximul or the CS-124. Their fired structures are relatively inert to the molten salts at operating temperatures, and their low permeabilities minimize structural penetration; the latter would help control possible freeze-thaw damage incurred during any periods of intermittent operation, as well as limit the internal refractory surface area exposed to the penetrating salts. If a monolithic is, for some reason, required for this application, a phosphate-bonded plastic would be an acceptable candidate. While a fireclay brick would probably be preferable from both performance and cost viewpoints, the plastic should give acceptable results and would not be expected to be subject to the strong deterioration exhibited by the calcium aluminate cement-bonded products. If possible, however, the monolithic should be cured ($\sim$600°C) before any molten salt is introduced.

WLP/ejb

APPENDIX C

EXTERNALLY INSULATED DUAL TANK STORAGE SYSTEM

APPENDIX C: EXTERNALLY INSULATED DUAL TANK STORAGE SYSTEM

This appendix presents the costs for an externally insulated dual tank storage system comparable to the internally insulated systems described in this report. This storage system was the alternate design for the Martin Marietta Advanced Central Receiver Power System, Phase I program. It was considered because it did not require any new technology. The system is sized for 11.2 hours of storage for a 300 MWe plant with a molten salt receiver (8211 MWHt storage). The two hot tanks are stainless steel spheres 34.4 m (113 ft) in diameter. They are supported at the mid-section on pivots to allow for radial expansion. They are insulated externally with 0.15 m (6 in.) of glass fiber insulation with lagging for weather protection. The cold cylindrical tanks are the same as for the internally insulated system.

The cost to build the stainless steel tanks was supplied by Chicago Bridge and Iron Co. (Boston) for tanks of their design. Due to wall thickness and thermal expansion considerations, they considered a spherical stainless steel tank more practical than a cylindrical one. The costs are for a tank of 316 stainless steel.

TABLE C-1

Externally Insulated Dual Tank Molten Salt Storage System Costs

Hot Salt Storage Tanks	$47,800,000
Cold Salt Storage Tanks	2,100,000
External Insulation	1,390,000
Foundations	2,000,000
Other Tank Costs	180,000
Pumps, Valves, Piping	2,220,000
Salt	17,400,000
Total System Capital Cost	$73,070,000
Cost-of-Storage, electrical	$21.75/kWHe

APPENDIX D

BIBLIOGRAPHY

BIBLIOGRAPHY

1. A Deep-Well Solar Irrigation Experiment, R.L. Alvis, Sandia Technology, Vol. 3, No. 1, March 1977.

2. Essais de la Centrale Electrosolaire de 1 MW_{TH}, Laboratorire D'Energetique Solaire, Odeilla, Font Rameu, France.

3. Sensible Heat Storage in Liquids, T.D. Brumleve, Sandia Laboratories, Livermore, SLL-73-0263.

4. Solar Total Energy Test Facility Project Test Results: High-Temperature Thermocline Storage Subsystem, T.D. Harrison, C.E. Hickox, A. Ortega, K. Wally, Sandia Laboratories Livermore, SAND 77-1528.

5. Stratification Enchancement in Liquid Thermal Storage Tanks, R.I. Loehrke, J.C. Holzer, H.N. Gari, M.K. Sharp; Journal Energy Vol. 3, No. 3 Mag - June 1979.

6. Thermocline Degradation in a Packed Bed Thermal Storage Tank, S.B. Margolis, Sandia Laboratories, Livermore SAND 77-8032.

7. Anharmonic Analysis of a Time-Dependent Packed Bed Thermocline, S.B. Margolis, Sandia Laboratories, Livermore SAND 77-8686.

8. Effect of a Conducting Wall on a Stratified Fluid in a Cylinder, Constance W. Miller, University of California, Berkeley, CA.

9. Mass and Energy Transfer in a Hot Liquid Energy Storage System; Warren F. Phillips, Robert A. Pate; Utah State University, Logan, Utah.

10. Free Convection Circulation in a Thermal Energy Storage System Driven by Heat Loss from the Walls; R. Viskanta, N.W. Hale Jr., Purdue University, West Lafayette, Indiana.

UNLIMITED RELEASE

INITIAL DISTRIBUTION:

TIC/UC62

USDOE (5)
Division of Energy Storage Systems
Washington, D. C. 20545
Attn: G. Pezdirtz
J. H. Swisher
J. Gahimer
R. Scheithauer
W. Frier

USDOE
Albuquerque Operations Office
Special Programs Division
P. O. Box 5400
Albuquerque, NM 87115
Attn: D. K. Nowlin

NASA-Lewis Research Center (2)
Cleveland, OH 44101
Attn: A. W. Nice
J. Calogeras

Oak Ridge National Laboratory
Oak Ridge, TN 37830
Attn: D. Eissenberg

USDOE (3)
San Francisco Operations Office
1333 Broadway
Oakland, CA 94612
Attn: J. Blasy
R. Hughey
D. Elliott

USDOE (4)
Division of Solar Technology
Washington D. C. 20545
Attn: G. W. Braun
M. U. Gutstein
G. M. Kaplan
J. E. Rannels

Aerospace Corporation (2)
2350 El Segundo Blvd.
El Segundo, CA 90009
Attn: E. Katz
P. Mathur

JPL (4)
4800 Oak Grove Dr.
Pasadena, CA 91103
Attn: V. Truscello
R. Manvi
D. Young
J. Becker

EPRI (2)
P. O. Box 10412
3412 Hillview Ave.
Palo Alto, CA 94303
Attn: J. Bigger
T. R. Schneider

SERI (4)
1536 Cole Blvd.
Golden, CO 80401
Attn: R. Copeland
K. Touryan
B. Gupta
C. Wyman

C. Winter, 400
A. Narath, 4000
J. H. Scott, 4700
G. E. Brandvold, 4710; Attn: B. W. Marshall, 4713
R. P. Stromberg, 4714
V. L. Dugan, 4720; Attn: J. V. Otts, 4721
J. F. Banas, 4722
J. A. Leonard, 4725
J. K. Galt, 5000
R. S. Claassen, 5800
R. G. Kepler, 5810
M. J. Davis, 5830
N. J. Magnani, 5840; Attn: F. P. Gerstle, Jr., 5844

T. B. Cook, 8000
W. J. Spencer, 8100
W. E. Alzheimer, 8120; Attn: C. S. Hoyle, 8122
R. J. Gallagher, 8124; Attn: W. S. Winters, Jr., 8124
A. N. Blackwell, 8200
B. F. Murphey, 8300
D. M. Schuster, 8310; Attn: R. W. Mar, 8313
J. C. Swearengen, 8316
R. Rinne, 8320
L. Gutierrez, 8400
C. S. Selvage, 8420
R. C. Wayne, 8450
J. Genoni, 8450
P. J. Eicker, 8451
A. C. Skinrood, 8452

T. T. Bramlette, 8452
W. G. Wilson, 8453
L. G. Radosevich, 8453 (2)
Publications Division, 8265, for TIC (2)
Publications Division, 8265/Technical Library Processes Division, 3141
Technical Library Processes Division, 3141 (2)
Library and Security Classification Divsion, 8266 (3)